The Synthesis of Group 9 Complexes for Use as Transfer Hydrogenation Catalysts and Anti-Cancer Agents

Stephanie Jayne Lucas

Submitted in accordance with the requirements for the degree of Doctor of Philosophy

The University of Leeds
School of Chemistry

February 2013

The candidate confirms that the work submitted is her own, except where work which has formed part of jointly-authored publications has been included. The contribution of the candidate and the other authors to this work has been explicitly indicated below. The candidate confirms that appropriate credit has been given within the thesis where reference has been made to the work of others. The reference for the jointly authored paper is stated below:

 S. J. Lucas; R. M. Lord; R. L. Wilson; R. M. Phillips; V. Sridharan; P. C. McGowan *Dalton Trans.* **2012**, *41*, 13800-13802

This copy has been supplied on the understanding that it is copyright material and that no quotation from the thesis may be published without proper acknowledgement.

The right of Stephanie Jayne Lucas to be identified as Author of this work has been asserted by her in accordance with the Copyright, Designs and Patents Act 1988.

Acknowledgements

Abstract

This thesis concerns the synthesis of group 9 Cp* and hydroxyl tethered Cp* based complexes for their use as both anti-cancer agents and transfer hydrogenation catalysts. The successful catalysts were immobilised covalently onto Wang resin for their use as recyclable transfer hydrogenation catalysts in the reduction of benzaldehyde and acetophenone.

Chapter 1 is a current review of transfer hydrogenation using metal-arene complexes and immobilised catalysts.

Chapter 2 describes the synthesis and characterisation of group 9 hydroxyl tethered Cp* based dihalide dimers.

Chapter 3 describes the synthesis and characterisation of group 9 Cp* and hydroxyl tethered Cp* based pyridine dihalide complexes.

Chapter 4 describes the syntheseis and characterisation of group 9 Cp* and hydroxyl tethered Cp* based picolinamide halide complexes.

Chapter 5 describes the synthesis and characterisation of iridium Cp* chloride bidentate complexes, where the bidentate ligand is either an XL or 2L ligand.

Chapter 6 describes the catalytic testing of compounds discussed in Chapters 2-5 for the reduction of benzaldehyde and acetophenone.

Chapter 7 describes the synthesis and characterisation and catalytic activity of immobilised group 9 hydroxyl tethered Cp* based dichloride dimers.

Chapter 8 describes *in vitro* IC_{50} results for select compounds described in Chapters 2-5 against a range of cancer cell lines.

Chapter 9 gives experimental details for processes discussed in Chapters 2-8 and characterisation data for the novel compounds discussed in Chapters 2-5.

Table of Contents

Abbreviations

A2780	human ovarian carcinoma
API	active pharmaceutical ingredient
Ar	aryl group
BINAP	2,2′-bis(diphenylphosphino)-1,1′-binaphthalene
CATHy	Catalytic Asymmetric Transfer Hydrogenation
cf.	*confer* (compare)
Cp	cyclopentadiene
Cp*	pentamethylcyclopentadienyl
CsDPEN	*N*-camphorsulfonyl-1,2-diphenylethylenediamine
DPEN	diphenylethylenediamine
dppf	1,1'-bis(diphenylphosphino)ferrocene
EDX	energy-dispersive X-ray spectroscopy
ee	enantiomeric excess
et. al.	*et alii* (and others)
GC	gas chromatography
HT-29	human colon carcinoma
IC_{50}	half maximal inhibitory concentration
ICP	inductively coupled plasma
IPA	*iso*-propanol
IR	infrared
L	2 electron donor
MCF-7	human breast adeno carcinoma
Me	methyl
MeOH	methanol
MOF	metal-organic framework
MTT	(4,5-Dimethylthiazol-2-yl)-2,5-diphenyltetrazolium bromide
NHC	N-heterocyclic carbene
NMR	nuclear magnetic resonance
PEG	polyethylene glycol
Ph	phenyl
ppm	parts per million

QUINAP	1-(2-diphenylphosphino-1-naphthyl)isoquinoline
SBA	mesoporous silica
t-Boc	N-*tert*-butoxycarbonyl
TEAF	triethlylammonium formate
tert	tertiary
Tf	triflyl
TMS	tetramethylsilane
TOF	turnover frequency
TON	turnover number
tosyl	4-toluenesulfonyl
triflate	trifluoromethanesulfonate
triflic	trifluoromethanesulfonic
Ts	tosyl
TsCYDN	N-(*para*-toluenesulfonyl)-1,2-cyclohexanediamine
TsDPEN	N-1,2-diphenylethylenediamine
v/v	volume/volume
X	1-electron donor
XPS	X-ray photoelectron spectroscopy

Chapter 1　Introduction

1.1 Introduction

This Chapter is a review of prior and current research in the field of transfer hydrogenation and immobilised catalysis. The transfer hydrogenation section will focus on Group 9 Cp* and ruthenium-arene complexes. The immobilisation section will focus on methods of immobilisation and current catalysts, paying particular attention to those used for transfer hydrogenation reactions.

1.2 Transfer Hydrogenation

Transfer hydrogenation is either the addition of H_2 to a substrate using a hydrogen donor molecule, or the removal of H_2 from a substrate using a hydrogen acceptor molecule. In the first case the substrate is an unsaturated compound such as an aldehyde/ketone, imine or alkene and in the second case, an alcohol or amine. The reaction occurs with the use of a metal catalyst which mediates the hydrogen transfer step. It is generally accepted that transfer hydrogenation reactions proceed through an intermediate metal hydride species (**Scheme 1.1**).
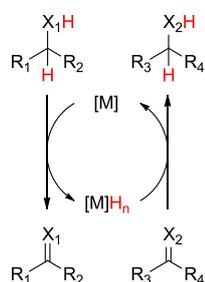
Scheme 1.1 General mechanism for catalytic transfer hydrogenation

In hydrogenations the catalyst removes hydrogen from the hydrogen donor, itself forming a metal hydride species, and then adds this hydrogen across the substrate's unsaturated bond. In reverse dehydrogenation reactions, the hydrogen donor is the substrate and the metal hydride will add hydrogen to a hydrogen acceptor molecule. Transfer hydrogenation offers a milder alternative to conventional methods used to reduce and oxidise substrates, negating the use of hazardous hydrogen gas coupled with milder conditions, safer reagents and no requirement for pressurised vessels.

Catalytic transfer hydrogenation was first demonstrated using a palladium black catalyst to transfer hydrogen from cyclohexene to a variety of organic acceptors.[1] The Meerwein-Ponndorf-Verley reaction was discovered in 1925, which is the

reduction of ketones using the IPA (*iso*-propanol) system (discussed in more detail below), with aluminium alkoxide catalysts.[2-4] Transfer hydrogenation using soluble transition metal catalysts was first realised by Henbest *et al.*[5] who used iridium phosphite complexes to reduce cyclohexanones to their corresponding alcohol. *iso*-Propanol was used as the solvent and the hydrogen donor, becoming oxidised to acetone in the process.

Iron complexes are becoming increasingly popular alternatives to ruthenium and group 9 catalysts, however they will not be discussed in this review.[6,7] Although this review will focus on ketone reductions and alcohol oxidations, examples of other transfer hydrogenation transformations will be discussed, as well as relevant hydrogenation/dehydrogenation reactions, whereby H_2 is used as the hydrogen donor/is released respectively.

1.2.1.1 The IPA System

iso-Propanol is commonly used as a hydrogen donor for reduction systems, whereby it becomes oxidised to acetone (**Scheme 1.2**).
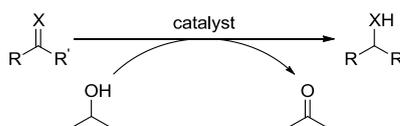
Scheme 1.2 Reduction using the IPA system

As *iso*-propanol is cheap, readily available and fairly safe, it is a desirable reagent. Due to the reversible nature of the system, *iso*-propanol is used in a large excess and hence becomes the solvent. Although the reaction is initially controlled by kinetics, as it is reversible, over time it comes under thermodynamic control. For this reason, yields are not always quantitative and enantiomeric excess (ee) values can be low, depending on the redox potentials of the alcohols/ketones. The IPA system is suitable for aldehyde/ketone and iminium salt reductions but not imine reductions. The reverse oxidation system is often performed in acetone, which behaves as the hydrogen acceptor and becomes reduced to *iso*-propanol. Primary alcohols can be used in place of *iso*-propanol, however the aldehyde by-product can interfere in the reaction.[8] *iso*-Butanol is less active than *iso*-propanol, and other alcohol containing compounds such as glucose and ascorbic acid also work but have to be used in a lower concentration. A base is often required to activate the pre-catalyst.

1.2.1.2 The TEAF system

The combination of formic acid and triethylamine is called TEAF.[9] Formate behaves as the hydrogen donor in this case, itself forming carbon dioxide.
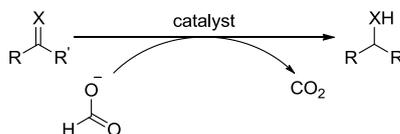
Scheme 1.3 Reduction using the IPA system

The azeotropic molar mixture of 5:2 of formic acid:triethylamine is often used.[10-13] This system is irreversible due to the release of carbon dioxide so the reaction is under kinetic control, overcoming the problems associated with the IPA system and therefore allowing quantitative yields and high ee values. The TEAF system is used to reduce imines along with aldehydes/ketones and iminium salts. Although this system can be very effective, it is not always compatible with the catalyst due to the acidic conditions. In aqueous systems, sodium formate is often used in preference to the TEAF system.

1.2.1.3 Hydrogen Borrowing

Hydrogen borrowing uses the same principles as the above mentioned transfer hydrogenation systems except that the hydrogen donor and acceptor are incorporated into the product, for example in N-alkylations (discussed in section **1.2.7**) whereby the alcohol is initially oxidised, the resulting aldehyde is a reagent for imine formation, then the hydrogen originally removed from the alcohol is used to reduce the imine to the resulting amine. As the catalyst removes hydrogen from the alcohol, then adds it across the imine bond it is said to have "borrowed" it. A base is sometimes required to activate the catalyst, however, due to this mechanism there is no requirement for external hydrogen donors or acceptors, making the process atom efficient. Borrowing hydrogen methods are also used in C-C bond forming reactions (section **1.2.9**).

1.2.2 Aldehyde/Ketone Reduction

1.2.2.1 The Noyori Catalyst and Its Mechanism

In 2001, Noyori won the Nobel Prize for his work on asymmetric transfer hydrogenation of pro-chiral ketones using ruthenium-arene complexes with chiral

diphenylethylamine (DPEN) and amino-alcohol, shown in **Figure 1.1**.[14-16]
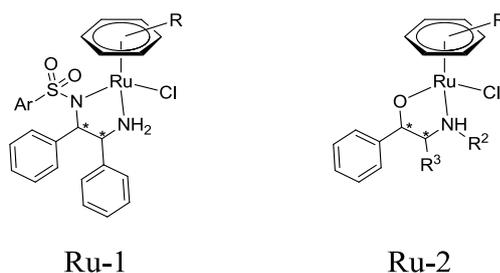
Figure 1.1 Noyori catalysts

Ru-1 type complexes were initially tested as catalysts for ketone transfer hydrogenations using the IPA system (described in section **1.2.1.1**) and the conditions shown in **Scheme 1.4**.[15] The reaction was also performed in the absence of any ligand using ([Ru(mesitylene)Cl$_2$]$_2$), resulting in an 8% conversion of acetophenone to (S)-1-phenylethanol after 15 hours.
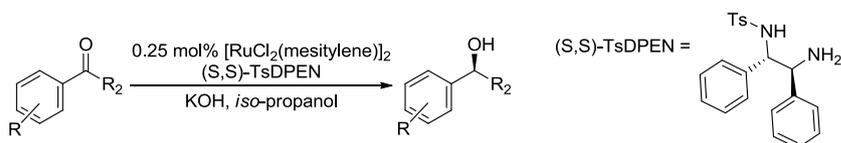
Scheme 1.4 Reduction of acetophenones using a Ru-1 type Noyori catalyst with the IPA system

0.5 mol% of the ruthenium TsDPEN catalyst converted 95% of acetophenone to (S)-1-phenylethanol with 97% ee in 15 hours. When R = 3-Cl or 4-Cl, the acetophenone could also be reduced selectively with a high conversion in a time of 2.5-19 hours, whereas for electron donating groups such as methyl or methoxy groups the selectivities and sometimes conversions were significantly reduced, due to the inherent problems of the IPA system discussed in section **1.2.1.1**.

The same catalyst was later used for the same reaction using the TEAF system (described in section **1.2.1.2**) with the conditions shown in **Scheme 1.5**.[14]
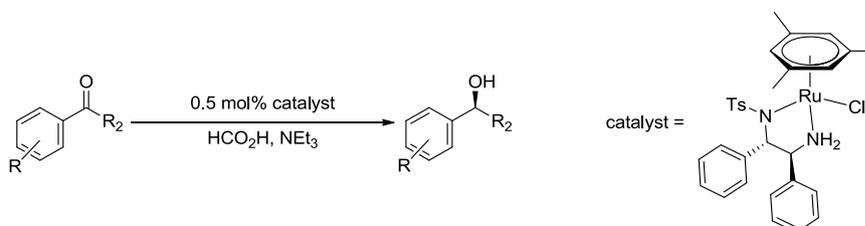
Scheme 1.5 Reduction of acetophenones using a Ru-1 type Noyori catalyst with the TEAF system

0.5 mol% of the ruthenium TsDPEN catalyst converted >99% of acetophenone to (S)-1-phenylethanol with 98% ee in 20 hours. Unlike with the IPA system, the TEAF

system also converted all of the functionalised acetophenones tested, including those with electron donating groups, with at least 96% conversion and at least 95% ee. Since this initial reaction, Xiao has shown that the ideal formic acid:triethylamine ratio for this reaction is 0.2:1, conversely to the azeotropic mixture of 5:2.[17]

A second generation of catalysts were synthesised by Noyori with the general structure of Ru-2 shown in **Figure 1.1**.[16] The replacement of diamine with amino-alcohol ligands increased the catalytic activity for the reduction of acetophenone using the IPA system to the extent that the reaction was complete within 1 hour compared to the previous 15 hours, however with a slightly lower yield and ee of 94 and 92% respectively (reaction shown in **Scheme 1.6**). A similar trend is seen with the substituted acetophenones. These catalysts are incompatible with the TEAF system, presumably because the acidic nature of the TEAF system protonates the alcohol resulting in de-coordination of the ligand.[8] Although the hexamethylbenzene and the amino-alcohol ligand shown in **Scheme 1.6** gave the best combination for the highest yield and enantioselectivity, increased steric bulk on the η^6-arene ring tends to decrease the conversion, and high enantioselectivity is only obtained when an appropriate arene and amino-alcohol ligand are combined.
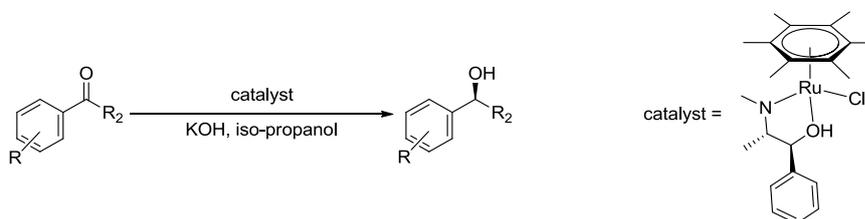
Scheme 1.6 Reduction of acetophenones using a Ru-1 type Noyori catalyst with the TEAF system

Scheme 1.7 shows the proposed mechanism for a ketone reduction based on computational analysis and experimental evidence.[18-21] Reacting the 18 electron pre-catalyst **A** with an equivalent of base leads to the formation of the active 16 electron catalyst, **B**. Addition of *iso*-propanol to **B** forms an 18 electron hydride complex **C**, whereby *cf.* to the starting complex **A**, a hydride has replaced a chloride. The presence of the NH moiety on the bidentate ligand was found to be a crucial factor as, when replacing the H with a Me group, the activity was lost. Interestingly, this mechanism occurs *via* the second coordination sphere, where the substrate does not directly bind to the ruthenium centre, but instead interacts with the δ^+ amine H and the δ^- hydride. Mass spec evidence using similar catalysts reported by Wills supports

the mechanism.[22]
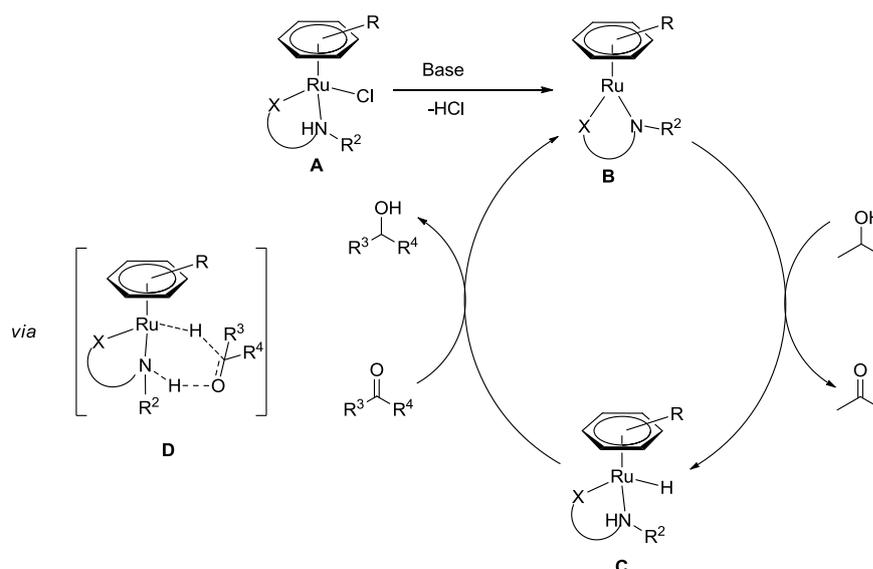
Scheme 1.7 The Noyori mechanism for ketone/aldehyde reduction

Deuterated benzylalcohols can also be prepared selectivity using Noyori catalysts to reduce the corresponding benzaldehyde, with the conditions shown in **Scheme 1.8**.[23] The reaction time varied depending on X, from 0.5 to 14 hours, with a conversion of 90-100% and ee values of 97-99%. The deuterated alcohols were prepared by either reducing the deuterated benzaldehyde using the IPA system (described in section **1.2.1.1**), or the protic benzaldehyde using the TEAF system (described in section **1.2.1.2**) containing deuterated formic acid. The advantage with the TEAF system is that only a stoichiometric amount of deuterated formate is required, whereas in the IPA system a large excess of deuterated *iso*-propanol is essential.
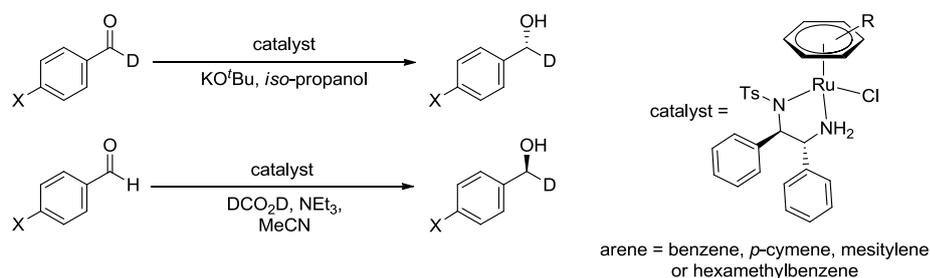
Scheme 1.8 Reduction of benzaldehydes to their deuterated benzylalcohol using a Ru-1 type Noyori catalyst

Noyori's work revolutionised the field of transfer hydrogenation leading to many research groups attempting to optimise the catalytic system, through catalyst design, reaction conditions and reaction scope.

1.2.2.2 Adaptations of Noyori Catalysts

In 1996 Knochel reported the use of simple amino(sulfonamido)cyclohexanes (TsCYDN) as alternatives to the diphenylethylamine (DPEN) ligands featured in the Noyori type Ru-1 catalysts (shown in **Figure 1.1**)[24]
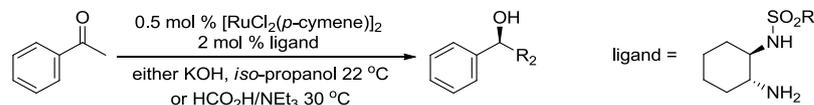
Scheme 1.9 Reduction of acetophenone using $[RuCl_2(p\text{-cymene})]_2$ and amino(sulfonamido)cyclohexanes (CYDN)

These types of ligand form active catalysts with ruthenium, with 1 mol% of the catalyst reducing acetophenone with 96-97% conversion and 89-92% ee after 22 hours using the IPA system (described in section **1.2.1.1**), or >99% conversion and 89-96% ee using the TEAF system at 30 °C. This system is less efficient than the Noyori systems however, as twice as much catalyst is used and the catalyst is less selective.

Knochel also prepared substituted ferrocenes, with either alcohol, amino or amino and phosphine groups on the Cp ring, as ligands for this reaction.[24-26] Although the amino-phosphine and diols were inactive or showed trace activity, the amino functionalised ferrocenes were active ligands for acetophenone reductions, with the conditions shown in **Scheme 1.10**. The most active catalyst is when the ferrocene ligand has R = Ph and R^2 = Me, with 1 mol% of the catalyst reducing 92% of acetophenone with an ee of 71% after 3 hours. Although, this is less selective than the Noyori system, the reaction time is shorter and at room temperature the % ee remains constant throughout the reaction.
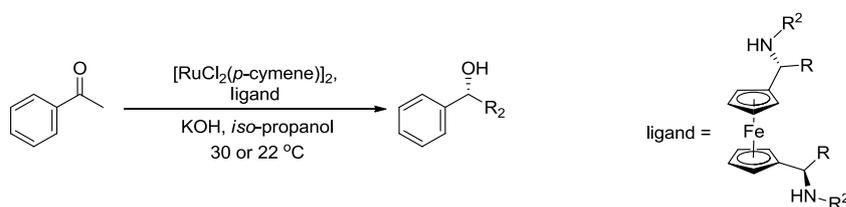
Scheme 1.10 Reduction of acetophenone using $[RuCl_2(p\text{-cymene})]_2$ and amino substituted ferrocene ligands

Exchanging iron in the ligand to ruthenium did not affect the catalytic activity, and replacing R^2 from a methyl to bulkier groups decreased or inhibited the activity. The TEAF system was incompatible with these ligands except when R^2 is a tosyl group. However, this was still inferior to the Noyori system with a conversion and ee

value of 42% and 83% respectively. Knochel also showed that lowering the temperature from ambient to -30 °C had a positive effect on the selectivity, however much longer reaction times were required.

After the first reported example[27,28] both Ikarya and Blacker separately researched the group 9 Cp* analogues to the ruthenium Noyori catalysts, named CATHy catalysts.[29,30] They were prepared the same way, by reacting the [MCp*Cl$_2$]$_2$ dimer with the ligand and base. Ikariya prepared the RhCp*(TsDPEN) complex, along with the RhCp*(TsCYDN) and IrCp*(TsCYDN) complexes (**Figure 1.2**) and compared these to the original Ru-1 type catalyst (**Figure 1.1**) Ru-arene(TsDPEN).
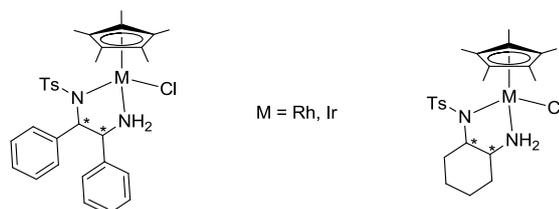
Figure 1.2 MCp* equivalents of the Noyori catalysts, named CATHy catalysts

The RhCp*(TsCYDN) complex showed higher activity than its iridium analogue after 12 hours with a conversion and enantioselectivity of 85% and 97% compared to 36% and 96% respectively. The RhCp*(TsDPEN) catalyst, however, only gave a conversion of 14% with 90% ee after 12 hours compared to 92% and 94% respectively for the ruthenium analogue. The Cp analogues have shown to be less soluble and oxidatively stable than the Cp* catalysts.[8] Bulkier Cp derivatives have also been prepared but offer lower optical inductions or reactivity. In attempting to optimise the catalyst, Blacker has shown that when enlarging the ring between the chelating ligand and the metal from a 5 membered ring, the metal-ligand association is weaker and the ee value decreases.[8]

1.2.2.3 Scale Up of Asymmetric Transfer Hydrogenation of Ketones

Although the Noyori and CATHy systems are suitable and effective for laboratory scale, they required process research and development before scaling up to manufacture.[8] The catalytic loading must be smaller than 0.1 mol% for the catalyst contribution cost to be small. In the IPA system (described in section **1.2.1.1**), laboratory scale reductions require a dilute solution in order to avoid the back reaction and a loss of enantiomeric excess, however this is not economically feasible at industrial scale. Continuous removal of acetone eliminates the back reaction which, fortunately due to the relative boiling points of *iso*-propanol and acetone, can

be achieved through distillation of the acetone.

In the TEAF system (described in section **1.2.1.2**), the decomposition of formic acid to hydrogen and carbon dioxide, or worse carbon monoxide and water, is problematic. This problem seems to be addressed by bubbling through 1% (v/v) oxygen in nitrogen, helping to remove the gases, with the oxygen being shown to increase the catalyst's lifetime. Matching the substrate addition to its reduction rate avoids hydrogen formation. An alternative is to feed the hydrogen donor to the substrate and catalyst in a solvent, which minimises unwanted side reactions but makes the pH harder to control. The pH must be above 3.5 in aqueous systems, since formate is the hydrogen donor. By using aqueous biphasic conditions, the pH can be controlled leading to a robust system. Water has the added bonus of being a high-boiling solvent, minimising losses to the atmosphere, as well as absorbing carbon dioxide as bicarbonate so avoiding the need for gas sparging. Using a solvent is also desirable due to the high viscosity of neat TEAF.

Iridium and rhodium Cp* complexes with the 1,2-aminoindanol ligand were twice as active as the ruthenium *para*-cymene analogues. However, they were less enantioselective and less stable. For example the RhCp*(TsDPEN) catalyst loses activity at temperatures above 40 °C. As there is no apparent relationship between electron withdrawing or electron donating aryl sulfonamide ligands (DPEN ligands) screening has provided the most convenient way to determine the optimal catalyst for a particular substrate, in terms of the metal and ligand, usually by a robot. The DPEN ligands tend to make the most selective catalysts along with being relatively inexpensive and easy to make on a large scale.

CATHy catalysts have been successfully applied to the large scale syntheses of (R)-N-methyl-α-methyl-3',5'-bis(trifluoromethyl)benzylamines, (R)-styrene oxide, diltiazem, duloxetine, (S)-2-(3-nitrophenyl)ethylamine hydrochloride, (R)-1-tetralol and (S)-4-fluorophenylethanol.[31]

1.2.2.4 Further Mechanistic Studies

The catalytic intermediate 16 electron and IrCp*(TsCYDN) hydride species, analogous to the ruthenium intermediates in **Scheme 1.7**, were isolated and characterised by NMR analysis.[32] NMR and CHN analysis for the IrCp*(TsDPEN) intermediates was reported in 1998 along with limited NMR analysis of the rhodium analogue.[28] Some 16 electron intermediates were also isolated by Perutz, however

more interestingly, he demonstrated the coordination of formate to a RhCp*(TsCYDN) complex, contrasting to the traditional Noyori mechanism (**Scheme 1.11**).[33] This coordination is reversible with heat, accompanied by the production of carbon dioxide and hydrogen.
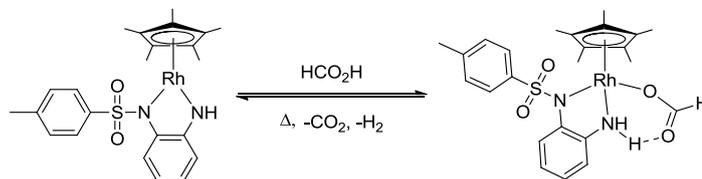
Scheme 1.11 Reversible coordination of formate to a RhCp* Noyori-type intermediate

The same group later reacted the RhCp*(TsDPEN) precursor with formic acid, which resulted in the complete displacement of the chelating ligand and formation of the cationic dimer shown in **Scheme 1.12**.[34]
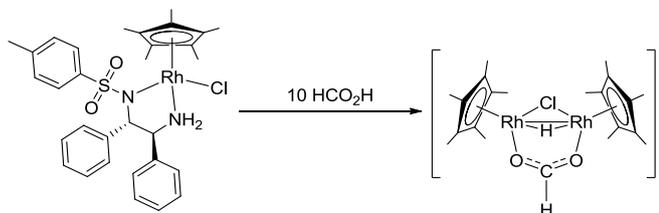
Scheme 1.12 Coordination of formate and removal of TsDPEN from a RhCp* Noyori-complex

In an NMR investigation of the reduction of d_6-acetone by d_{15}-triethylamine/formic acid, catalysed by the RhCp*(TsDPEN) complex in a CD_3CN solvent, the research group confirmed that the rhodium formate dimer was observed. Although this dimer by itself was a very poor catalyst (for imine reduction), the addition of the TsDPEN ligand reformed the same activity and selectivity of the RhCp*(TsDPEN) complex, concluding that although the formate dimer may form, the catalytic activity is not necessarily blocked as the presence of free chiral ligand may allow recovery of activity.[34]

1.2.2.5 Reductions in Water

Industrially, the use of water as a solvent is desirable as it is cheap, safe and environmentally benign.[35] Performing reactions in water may also result in pH-dependence, allowing for fine-tuning of selectivity and limiting side reactions. To circumvent the problem of low solubility of most organic substrates in water, surfactants are usually used such as sodium dodecyl sulfate. The catalyst in these

systems can often be recycled by separating the product containing organic phase from the catalyst containing aqueous phase.

1.2.2.5.1 Achiral Reduction

In 1999 Ogo, Watanabe and co-workers reported a transfer hydrogenation system using the water soluble IrCp* catalyst shown in **Figure 1.3**.[36]
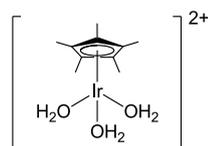
Figure 1.3 The first reported water soluble IrCp* catalyst for carbonyl reductions

The aqua ligands impart water solubility to the metal complex, along with being labile in water which provides vacant sites. They also impart pH dependence, whereby at high pH, the aqua ligands are deprotonated to form hydroxo ligands.

The same research group later improved this design by replacing 2 of the water ligands with bipyridine (bpy), shown in **Figure 1.4**.[37,38] The complex is pH dependant, being significantly more active at low pH values with a peak at pH 2.0. At higher pH values (>6.6) the aqua ligand is deprotonated to a hydroxyl ligand, which is significantly less labile.
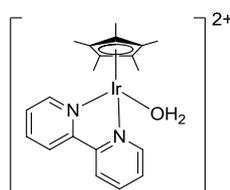
Figure 1.4 Water soluble IrCp* bpy complex
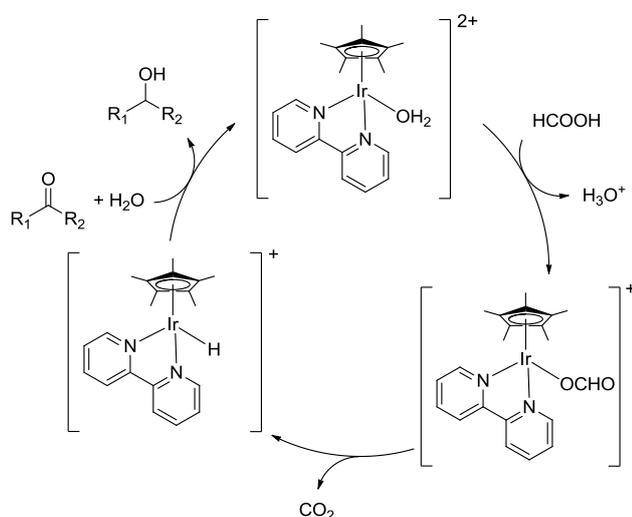
Scheme 1.13 Proposed mechanism for ketone reduction using an IrCp* bpy complex

Süss-Fink reported the synthesis and catalytic activity of ruthenium-arene 1,10-phenanthroline complexes using formic acid as the hydrogen donor.[39]
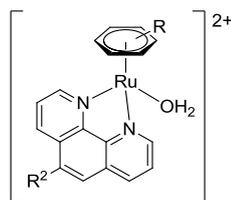
Figure 1.5 Water soluble Ru-arene 1,10-phelanthroline complex

A related system was later reported by Fischmeister, Renaud and co-workers whereby two pyridine ligands are linked by an amine in the *ortho* positions, shown in **Figure 1.6**.[40]
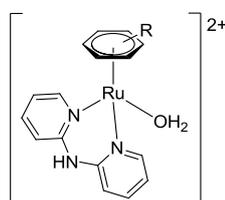
Figure 1.6 Water soluble Ru-arene amine linked pyrdine complex

The water soluble complexes discussed thus far have slow reduction rates, possibly because the mechanism must be different to that of Noyori catalysts (**Scheme 1.7**) due to the absence of the NH moiety.

Xiao has focused a lot of attention on Noyori type catalysis in water.[41] An achiral IrCp* Noyori-type catalyst was active for the reduction of benzaldehyde, shown in **Scheme 1.14**, whereby 1×10^{-4} mol% of catalyst converted > 99% of benzaldehyde to benzyl alcohol in 0.3 hours and 2×10^{-5} mol% of catalyst converted 98% of benzaldehyde to benzyl alcohol in one hour.[42] The reduction rate in water is higher than the IPA or TEAF system (described in section **1.2.1.1** and section **1.2.1.2** respectively).
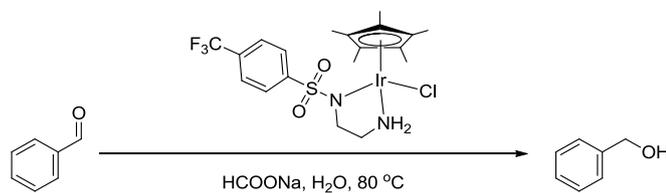
Scheme 1.14 Reduction of benzaldehyde by a water soluble IrCp* Noyori-type catalyst

Interestingly, water soluble substrates were not reduced using this system implying that the catalysis takes place 'on water'.

1.2.2.5.2 Chiral Acetophenone Reduction

Williams investigated the asymmetric transfer hydrogenation of ketones with water soluble Noyori-type catalysts through modification of the TsDPEN and TsCYDN ligands, shown in **Figure 1.7**.[43,44]

A   B
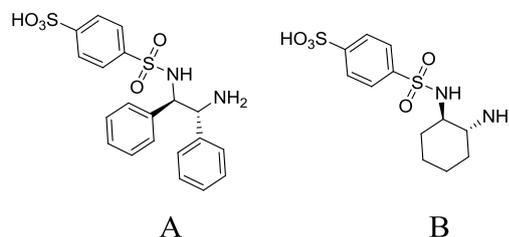
Figure 1.7 Water soluble variations of TsDPEN and TsCYDN ligands

The catalysts were prepared *in situ* and the reaction was performed in a mixture of *iso*-propanol and water. The system was highly selective, however slow reduction rates were seen, with the most active reduction of acetophenone seen when using 1 mol% of the catalyst prepared from [RhCp*Cl$_2$]$_2$, ligand A (in **Figure 1.7**) and potassium *tert*-butoxide, in *iso*-propanol containing 15% water at 22 °C, whereby 94% of acetophenone was reduced to (R)-1-phenylethanol with 95% ee after 18 hours. Using the more reactive 3'-fluoroacetophenone, it was surprisingly found that increasing the water content to 51%, and therefore decreasing the concentration of the reagent *iso*-propanol, significantly increased reduction rates using a catalyst formed from [IrCp*Cl$_2$]$_2$, ligand B (in **Figure 1.7**) and base, demonstrated in **Scheme 1.15**. These reductions, however, still required the use of an organic co-solvent.

% water	% Conversion	% ee
34	82	94
51	94	93
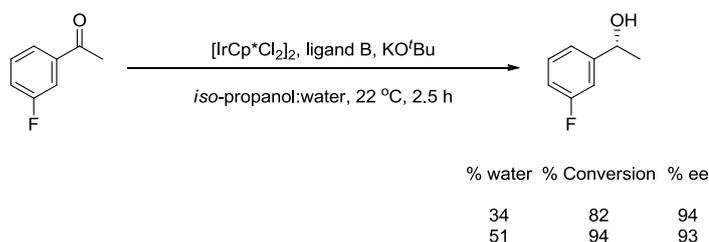
Scheme 1.15 Reduction of 3'-fluoroacetophenone using water soluble Noyori catalysts in the IPA system containing water

The first example of asymmetric transfer hydrogenation of ketones in water with no organic co-solvents was demonstrated by Chung, using a prolinamide ligand with the conditions shown in **Scheme 1.16**.[45,46]
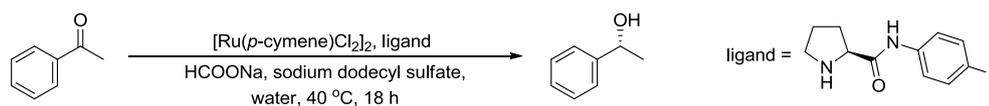
Scheme 1.16 Reduction of acetophenone in water using a Ru-prolinamide catalyst

2.5 $\times$ 10^{-3} mol% of catalyst converted 98.3% of acetophenone to (R)-1-phenylethanol with 68.6% ee after 18 hours. Variable conversions and ee values of 44-99% and 54-94% are seen for substituted acetophenones.

Building on the earlier example by Williams, a more substituted water soluble Noyori-type ligand was reported by Deng, shown in **Figure 1.8**.[47]

C
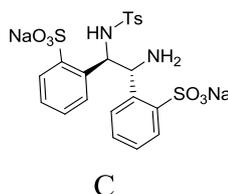
Figure 1.8 A further water soluble variation of TsDPEN

The best activity and selectivity was seen using 1 mol% of the Ru(*p*-cymene) catalyst compared to IrCp* and RhCp*, whereby after 24 hours >99% of acetophenone is converted to (R)-1-phenylethanol with 95% ee (**Scheme 1.17**). Unlike the previous prolinamide complexes, when using the Ru(*p*-cymene) catalyst good conversions and ee values are seen for substituted acetophenone substrates of 88-100% and 81-95% respectively, apart from 2'-methylacetophenone whereby only a 19% conversion is seen after 24 hours, with 80% ee. The catalyst could also be recycled once without a loss of enantioselectivity.

M-arene	% Conversion	% ee
[Ru(*p*-cymene)Cl$_2$]$_2$	>99	95
[RhCp*Cl$_2$]$_2$	92	84
[IrCp*Cl$_2$]$_2$	10	58
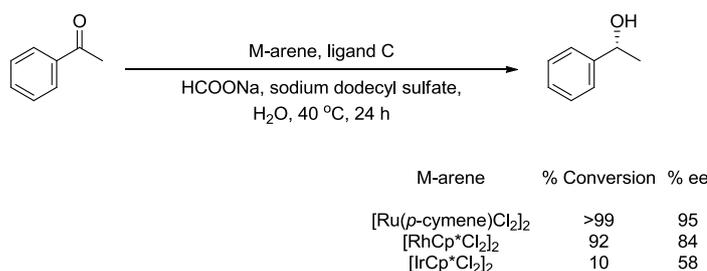
Scheme 1.17 Reduction of acetophenone using a water soluble Noyori-type catalyst in aqueous conditions

Until 2004, there were no reported examples of the original Noyori catalysts being used in aqueous asymmetric transfer hydrogenation systems. This was exploited by Xiao who found that aqueous systems using sodium formate significantly accelerated ketone reduction systems with full conversion and 95% ee after one hour (**Scheme 1.18**) compared to the original TEAF system, where full

conversion required more than 10 hours but had a higher selectivity with 97% ee.[48] The *in situ* formed Ru-TsDPEN catalyst in these conditions is the same as that in the IPA system.[18]
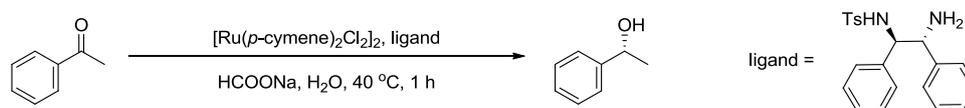
Scheme 1.18 Reduction of acetophenone using a Noyori catalyst in aqueous conditions

Like the Ru(*p*-cymene)TsDPEN complex, Xiao has also shown that a range of Noyori-type catalysts are effective in aqueous systems encompassing ruthenium-arene, and group 9 Cp* complexes with DPEN, TsCYDN and amino-alcohol ligands, with the group 9 complexes being more soluble than the ruthenium ones.[41,49] 1 mol% of the RhCp*(TsCYDN) catalyst converts >99% of acetophenone to (R)-1-phenylethanol in 95% ee in only 15 minutes, which is more active than its iridium and ruthenium-arene analogues, and substantially quicker than the traditional IPA and TEAF systems (systems discussed in sections **1.2.1.1** and **1.2.1.2** respectively and rates discussed in section **1.2.2.1**).[49] In 2005 Süss-Fink developed the TsCYDN systems by preparing a library of Ru-arene complexes with *trans*-1,2-diaminocyclohexane or N-tosylated diamine ligands, and the arene varying in steric bulk.[50] The research group showed that the N-tosylated complexes were more active and selective than their simpler diamine analogues and that hexamethylbenzene gave a more active Ru-arene complex than simply benzene, which was justified in terms of a CH/π attraction model with the arene and π system of the substrate described by Noyori.[51]

Switching from the original TEAF system to sodium formate allows the use of amino-alcohol ligands, although the corresponding catalysts are less active and enantioselective than the diamine analogues. Similarly to previous achiral systems (section **1.2.2.5.1**), as the complexes are more soluble in the organic substrate than water, the catalysis is thought to takes place 'on water'.

When using 1 mol% of M-arene(CsDPEN) catalysts in water, the RhCp* catalyst outperforms the Ru(*p*-cymene) and IrCp* analogues in terms of activity and selectivity, as shown in **Scheme 1.19**. When a lower catalytic loading of 0.1 mol% is introduced, however, the IrCp* catalyst shows much higher activity, with the reaction complete in 2.5 hours compared to 20 for both the RhCp* and Ru(*p*-

cymene) analogues, although with a slightly lower enantioselectivity of 98% ee compared to 99% for RhCp*.

	M-arene	Time / h	% Conversion	% ee
	Ru(p-cymene)	2	99	97
1 mol%	RhCp*	0.7	99	99
	IrCp*	0.7	98	97
	Ru(p-cymene)	20	95	96
0.1 mol%	RhCp*	20	89	99
	IrCp*	2.5	97	98
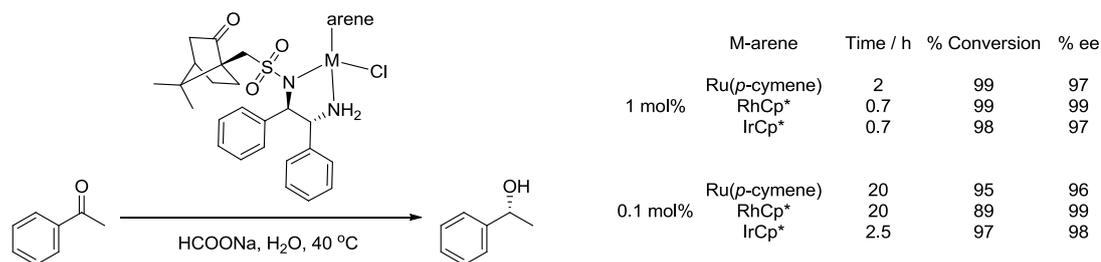
Scheme 1.19 The CsDPEN ligand shows the best selectivity when combined with RhCp*Cl against aqueous ketone reductions

1.2.2.5.3 Proposed Mechanism of Asymmetric Transfer Hydrogenation of Ketones in Water

The Xiao systems with Noyori catalysts discussed in the previous section show pH dependence in the reduction of acetophenone.[52] The higher the pH (controlled using triethylamine and formic acid) the more active the catalyst, with trace activity below pH 3, a shallow increase in the turnover frequency (TOF) up to ~pH 4, then a sharp increase from <10 mol^{-1} h^{-1} to >100 mol^{-1} h^{-1} at pH 5, followed by a more shallow increase to ~pH 7 where the TOF is over 140 mol^{-1} h^{-1}. This is partially attributed to the requirement for HCOO$^-$ as the hydrogen donor, but more importantly and along with other evidence such as an increase in enantioselectivity with increasing pH, Xiao proposes that there are two competing pathways which are pH dependant. At neutral pH the cycle follows the conventional Noyori mechanism, whereas at low pH it is proposed that the diamine is protonated (presumably the secondary amine) and dissociates from the metal to allow coordination of a labile, possibly water, ligand.

An extensive mechanistic study was later published by Xiao, in which the NMR, X-ray crystallography, DFT, and kinetic isotope data all lead to the mechanism shown in **Scheme 1.20**.[53]

Acidic　　　　　　　　　　　　　**Neutral**　　　　　　　　　　**Basic**

where X is either formate or water
(resulting in a cationic species)

Inactive

Scheme 1.20 Proposed mechanism for asymmetric transfer hydrogenation of ketones in aqueous systems for both high and low pH values

In the case of Ru-arene(TsCYDN) complexes, Süss-Fink proposes that chloro ligands may hydrolyse to aqua ligands as the activity of chloro and aqua ligated Ru-arene diamine compounds are comparable under the conditions used (sodium formate, 60 °C, pH 9).[50] In this system the activity was also pH dependent, however enantioselectivity was not, suggesting that the mechanism varies to that in **Scheme 1.20**. In a more extensive study, the same research group showed that using rigid cyclohexane-bearing diamines as ligands resulted in higher enantioselectivity than more flexible pyrollidine-bearing ligands, however the TOF remained the same. All of the systems were pH dependent in terms of TOF with the optimal conversions at pH 9. The enantioselectivity however, was independent of the pH suggesting one reaction mechanism across the pH range.

One of Wills' tethered catalysts (discussed in more detail in the next section) could also be used in aqueous systems achieving very high ee values of 99.5% with the catalyst loadings in line with Xiao's systems.[54]

1.2.2.6 Tethered Catalysts

Noyori-type complexes have been prepared whereby the amino-alcohol/TsDPEN-type ligand is tethered to the arene/Cp* ligand.[54-67] The most promising examples of these types of catalysts have been reported by Wills, where the most active catalyst, shown in **Figure 1.9**, is a ruthenium-arene tethered TsDPEN complex.
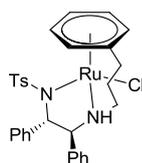
Figure 1.9 Tethered Noyori-type catalyst

Using the TEAF system (described in section **1.2.1.2**), with the conditions shown in **Scheme 1.21**, the reduction of acetophenone was complete using 0.5 mol% of the tethered ruthenium catalyst in 3 hours with 96% ee, whereas the untethered system requires an overnight reaction.
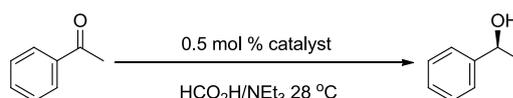
Scheme 1.21 Reduction of acetophenone using a tethered Noyori-type catalyst

Increasing the reaction temperature to 40 °C decreased the reaction time further to *ca.* 100 minutes. It is thought that the tether stabilises the catalyst and its

conformation.

Wills later showed that increasing the tether to a 4 carbon linker further increased the activity, whereby the reduction of 4'-methylacetophenone using the TEAF system at 40 °C was complete in 1.25 hours, compared to 4 or 5 hours with similar 3 carbon linker complexes.[62] Ikariya has developed this system further, by introducing an ether group into the tether (as shown in **Figure 1.9**) which was later reported using a different method by Wills.[56,67] Ether linkages to the backbone of the DPEN ligands had previously been prepared showing moderate selectivity.[64]
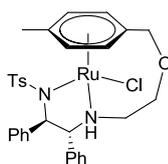
Figure 1.10 Oxo-tethered Noyori-type catalyst

At an extremely low catalytic loading of 2.5×10^{-3} mol%, 75% conversion of acetophenone to (R)-1-phenylethanol with 97% ee was seen after 72 hours in the TEAF system (described in section **1.2.1.2**), compared to 15% conversion and 96% ee to (S)-1-phenylethanol using the analogous all carbon tether (with opposite chirality of the DPEN ligand).

1.2.2.7 Summary of Acetophenone Reduction Systems

A selection of Noyori/CATHy-type catalysts discussed previously have been compared in terms of their activity for the reduction of acetophenone, with the data summarised in **Table 1.1** and **Table 1.2** for the IPA (described in section **1.2.1.1**) and the TEAF (described in section **1.2.1.2**) system respectively.[68] The catalysts chosen all show high activity and selectivity towards the reaction and their structures are shown in **Figure 1.11**.
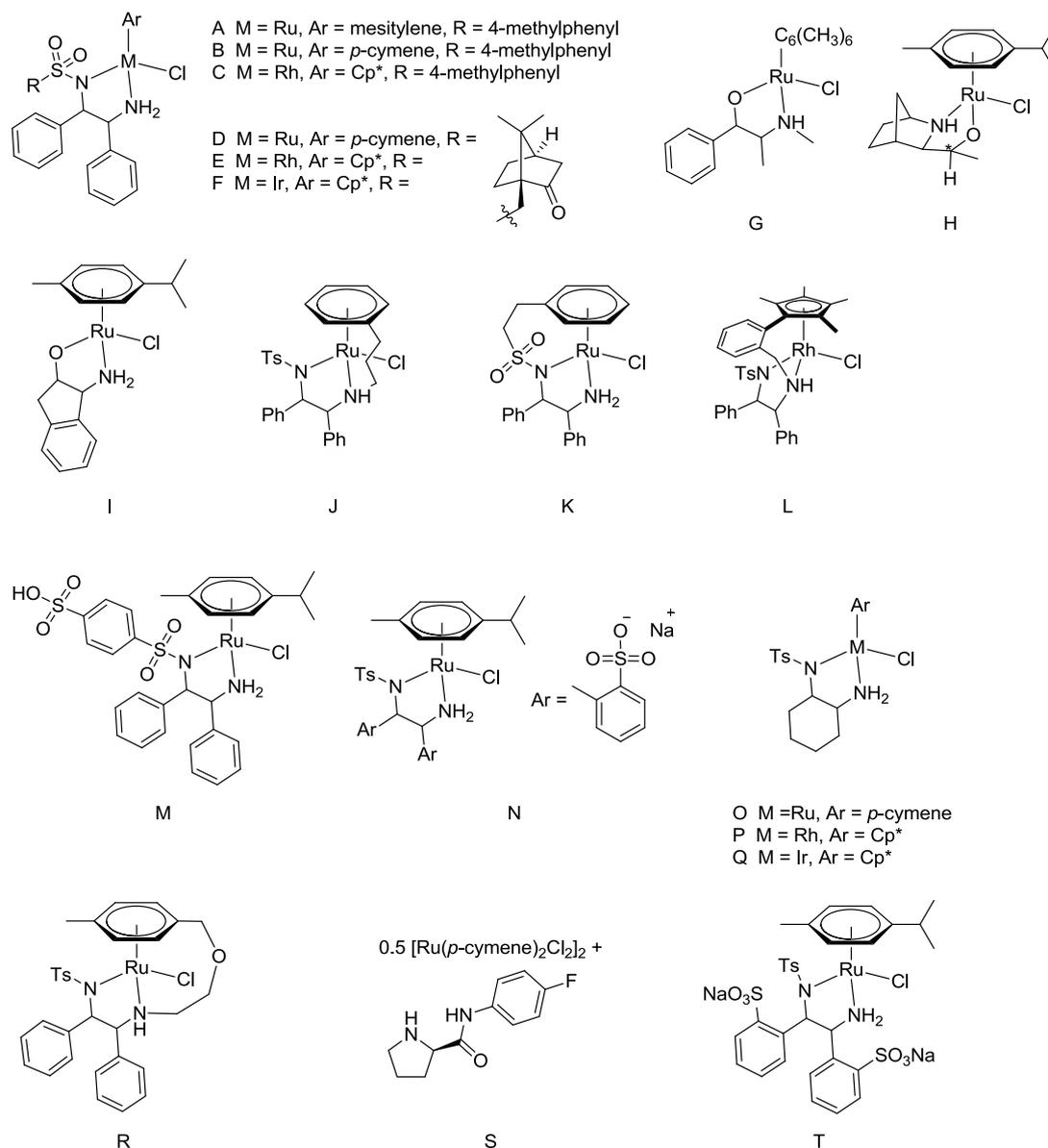
Figure 1.11 Summary of active Noyori/CATHy-type catalysts for the reduction of acetophenone

Catalyst	Amount of catalyst/mol%	Time/hours	Yield/%	% ee
A[14]	0.5	20	>99	98
B[69] sodium formate/water system with no triethylamine. Cetyltrimethylammonium bromide was used as a phase transfer catalyst	1.0-0.0007	4-70	>99-93	95
D[70] sodium formate/water system with no triethylamine	1.0/0.1	2/20	99/95	97/96
E[70] sodium formate/water system with no triethylamine	1.0/0.1	0.7/20	99/89	99
F[70] sodium formate/water system with no triethylamine	1.0/0.1	0.7/2.5	98/97	97/98
L[57]	0.5	10	100	98
J[59]	0.5/0.1	2/79	100/98	96
K[58]	0.5/0.1	1/7	96/83	66/67
N[47] sodium formate/water system with no triethylamine. Dodecyl sulfate was used as a phase transfer catalyst	1	24	>99	95
O[49] sodium formate/water system with no triethylamine.	1.0	2	99	85
P[49] sodium formate/water system with no triethylamine.	1.0	0.25	>99	95
Q[49] sodium formate/water system with no triethylamine.	1.0	1	99	93
R[56]	0.1/0.0025	3/72	>99/75	97
S[46] sodium formate/water system with no triethylamine. Dodecyl sulfate was used as a phase transfer catalyst	0.0025	18	98	69
T[47] sodium formate/water system with no triethylamine. Dodecyl sulfate was used as a phase transfer catalyst	1/0.5	24/48	>99/95	95/93

Table 1.1 Summary of acetophenone reductions using the TEAF/sodium formate system

Catalyst	Amount of catalyst/mol%	Time/hours	Yield/%	% ee
A[15]	0.5	15	95	97
C[27]	1.0	48	80	90
G[16]	0.5	1	94	92
H[71]	0.5	0.7	97	94
I[72]	1.0	1.5	70	91
M[43]	1.0	48	96	94
P[30]	0.5	12	85	97
Q[30]	0.5	12	36	96

Table 1.2 Summary of acetophenone reductions using the IPA system

1.2.2.8 Reduction of Ketones with Additional Functionality

Scheme 1.22 Summary of various alcohols prepared through the reduction of ketones using Noyori catalysts

The range of ketones that can be reduced with Noyori-systems include diaryl, dialkyl, aralkyl, α,β-unsaturated, cyclic, heterocyclic and acyclic ketones, as well as ketones bearing halide, alcohol, ether, thioether, alkene, amine, acid, ester, nitrile, sulfido, sulfone, nitro, and azide substituents, furan, thiophene and quinoline rings.[31] A summary of various chiral alcohols with additional functionality that have been prepared using the reduction of the corresponding ketones with Noyori catalysts is

shown in **Scheme 1.22**.[73] Functional groups at the α or β position to the carbonyl do not interact with the metal centre due to the coordinatively saturated nature of the amine hydrido metal complexes.

Wills demonstrated the use of the Noyori TsDPEN ligated ruthenium catalyst as well as a similar amino-alcohol derivative to be effective for the enantioselective reduction of *tert*-butyloxycarbonyl (t-Boc) protected α-aminoketones, providing a pathway for the synthesis of asymmetric β-amino-alcohols and aziridines, demonstrated in **Figure 1.12**.[74]
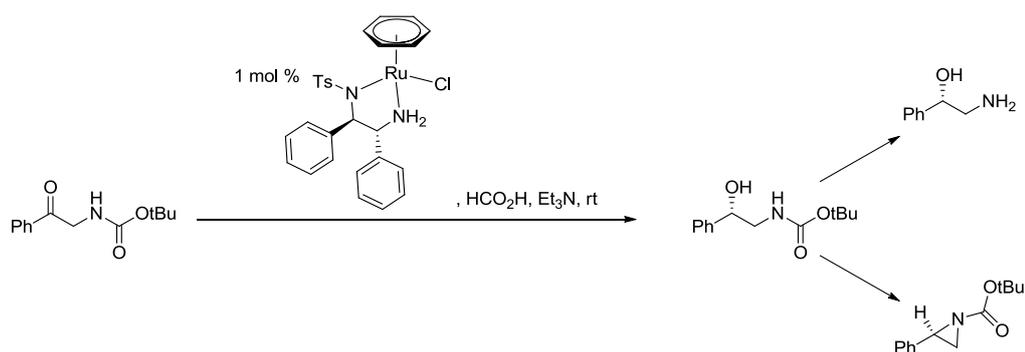
Figure 1.12 Reduction of tBoc-protected α-aminoketones in the synthesis of asymmetric β -amino-alcohols and aziridines

The same research group demonstrated the use of both the Ru *para*-cymene and the analogous rhodium Cp* TsDPEN complexes shown in **Figure 1.13** for the transfer hydrogenation of α,β-unsaturated, α-tosyloxy and α-substituted ketones, with some examples discussed below.[75]
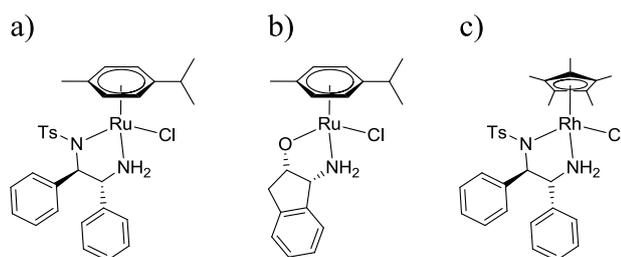
Figure 1.13 a) Ru-*p*-cymene(TsDPEN), **b)** Ru-*p*-cymene(amino-alcohol) and **c)** RhCp*(TsDPEN) catalysts used for the reduction of α,β-unsaturated, α-tosyloxy and α-substituted ketones

Cyclic enones were oxidised to give moderate conversions to the resulting allylic alcohols of 62-80%, depending on the catalyst used (either a or b in **Figure 1.13**) and good to excellent ee values of 72 to >99% (reaction shown in **Scheme 1.23**). No 1,4-reduction product (saturated ketone) was observed when R = Ph or OCH_2Ph, however 20% of the 1,4-reduction by-product was observed when R = $NHCO_2$.

When R is a *tert*-butyl group the catalyst is inactive presumably due to sterics.
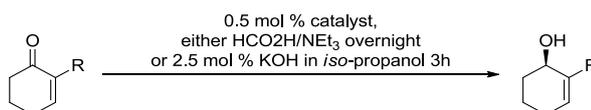
Scheme 1.23 Reduction of cyclic enones

Catalysts **a** and **c** had opposite selectivities for the reduction of 3-(acetylamino)-but-3-en-2-one, whereas catalyst **b** was inactive (**Scheme 1.24**). In both cases, the allylic alcohol was not observed.
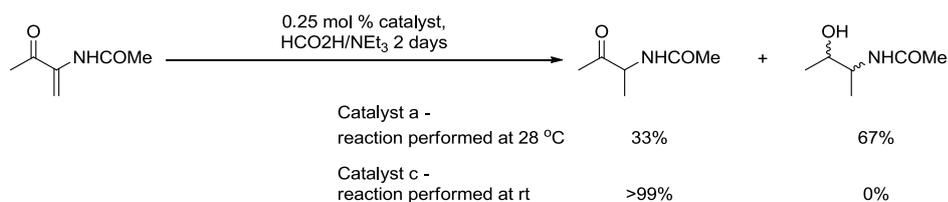
Scheme 1.24 Reduction of 3-(acetylamino)-but-3-en-2-one

1.2.2.9 Hydrogenation Catalysts

Tethered versions of Noyori-type catalysts have been prepared for use as hydrogenation catalysts.[76-78] Ikariya developed ruthenium-arene and group 9 Cp* DPEN complexes whereby the arene/Cp* had a triflylamide tether, with the general structures shown in **Figure 1.14**.[77,78].
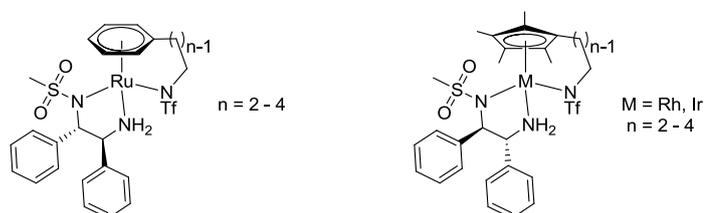
Figure 1.14 Triflylamide tethered Noyori-type catalysts

Although these catalysts were either inactive or showed trace activity for transfer hydrogenation reduction systems, they were highly active hydrogenation catalysts (**Scheme 1.25**), with the most active catalyst being where n = 4 with a yield of between 94-100% depending on the metal and 93% ee.
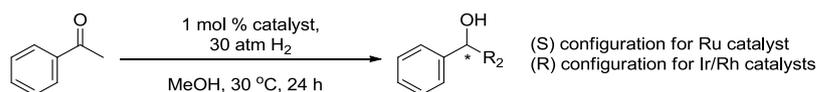
Scheme 1.25 Reduction of acetophenone using triflylamide tethered Noyori-type catalysts

With the smaller chain, where n = 3 the catalytic activity and selectivity decreased, most severely with the ruthenium catalyst, where the yield and ee value

were 20% and 2% respectively. The group 9 catalysts were still moderately active and selective with the shorter chain, where the iridium analogue gave a 53% yield and 86% ee and the rhodium analogue gave a 58% yield with 29% ee. The shortest chain, where n = 2, showed trace activity in the case of ruthenium with <1% yield. The rhodium analogue gave a modest 40% yield and 20% ee, and although the iridium analogue showed similar activity with a 37% yield, it was still highly selective giving 94% ee.

1.2.3 Alcohol Oxidations

The reversibility problem with the IPA system can be used advantageously to resolve a racemic mixture of alcohols, through oxidation of the unwanted alcohol.[79] Using substituted 1-phenylethanols, which were difficult to prepare selectively using the IPA system (see section **1.2.2.1**), the (R)-enantiomers could be selectively resolved from the racemic mixture, with the base-activated Ru-1 type Noyori catalyst in acetone. Acetone acts as the hydrogen acceptor, becoming reduced to *iso*-propanol. 0.2-0.5 mol% of the catalyst resolved the substituted acetophenones in 4.5-40 hours with yields of 43-51% and ee values of 92-99%.
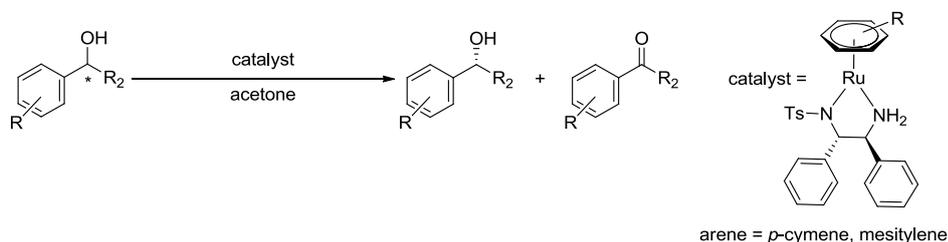
Scheme 1.26 Kinetic resolutions of racemic 1-phenylethanols using a base activated Ru-1 type Noyori catalyst in acetone

Unlike carbonyl reductions, alcohol oxidations result in achiral products, eliminating the need for chiral catalysts. Fujita reported the use of $[IrCp*Cl_2]_2$ as a catalyst at ambient temperature in the oxidation of both primary and secondary alcohols to their respective aldehyde/ketone cleanly.[80] The reaction was performed in acetone, whereby acetone also behaves as a hydrogen acceptor, becoming reduced to *iso*-propanol. This is the reverse of aldehyde/ketone oxidations in *iso*-propanol. Fujita found that addition of K_2CO_3 and a large excess of acetone improved the catalytic activity. The system was most effective for aromatic alcohols, especially with electron-donating groups at the *para*-position, e.g. 4'-methoxybenzyl alcohol where 99% conversion is seen after 6 hours using 0.5 mol% Ir, however moderate

catalytic activity is also observed for non-aromatic alcohols, e.g. octan-1-ol with reflux temperature. It is presumed that the reaction occurs through binding of the substrate to the iridium centre (shown in **Scheme 1.27**), unlike the Noyori-mechanism which occurs in the second coordination sphere.
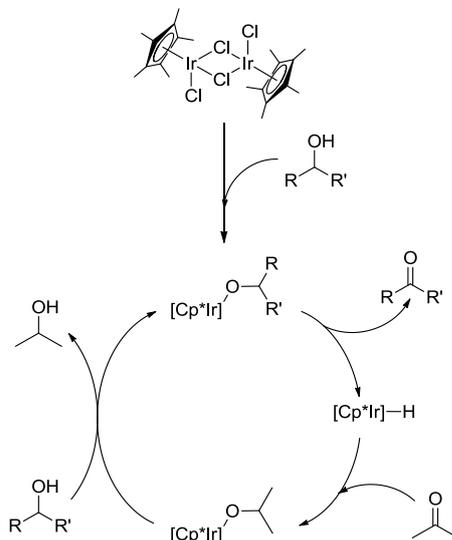
Scheme 1.27 Proposed mechanism for the oxidation of alcohols using [IrCp*Cl$_2$]$_2$ in acetone

Fujita found that the introduction of an N-heterocyclic carbene (NHC) ligand has a significant effect for the Oppenauer-type oxidation of alcohols.[81,82] The NHC ligand behaves as a 2 electron donor breaking up the dimer. Although this resulting neutral complex shows negligible activity, addition of silver triflate in acetonitrile to form a charged species shown in **Figure 1.15**, activates the complex.
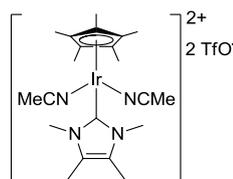
Figure 1.15 Charged IrCp* NHC catalyst for alcohol oxidation

The resulting catalyst is initially 18 times more active than [IrCp*Cl$_2$]$_2$ for the oxidation of 1-phenylethanol to acetophenone. The catalyst requires a base for selective oxidation of alcohols, and oxidation of acid-sensitive alcohols, for example furfuryl alcohol, causes decomposition of starting materials and/or side reactions.

Fujita later found that the introduction of a functionalised Cp* ligand with a basic amino group at the terminus of the tether improved the catalytic activity even further without requiring an external base, as well as expanding the scope of the reaction to include oxidation of acid-sensitive alcohols which were previously unsuccessful

using the Cp* analogue (complex shown in **Figure 1.16**).[83] The charged active species was formed *in situ* with silver triflate.
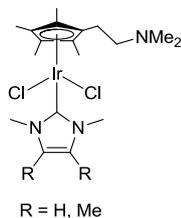
Figure 1.16 Tethered derivative of IrCp* NHC catalyst

1.2.3.1 Oxidant-Free Dehydrogenation

Fujita later developed this transformation to an oxidant-free dehydrogenation using the IrCp* 2-hydroxypyridine complex shown in **Scheme 1.28**, in toluene and in the absence of a base.[84] The mechanism is thought to occur *via* the 2-hydroxypyridine ligand switching between binding in a monodentate and a bidentate fashion, allowing accommodation and subsequent removal of H_2. This is similar to the Noyori catalyst discussed in section **1.2.2.1**, except that the ligand is switching between behaving as an L to an LX ligand, compared with an LX to an X_2 ligand.

0.1 mol% of the iridium catalyst converted 70% of 1-phenylethanol to acetophenone under reflux of toluene after 20 hours, compared to 22% for [IrCp*Cl$_2$]$_2$ and K_2CO_3. High conversions were seen for a range of secondary alcohols, however primary alcohols were not efficiently oxidised by this system (1 mol% of catalyst converted 24% of benzyl alcohol to benzaldehyde in 24 hours). The proposed catalytic mechanism is shown in **Scheme 1.28**.
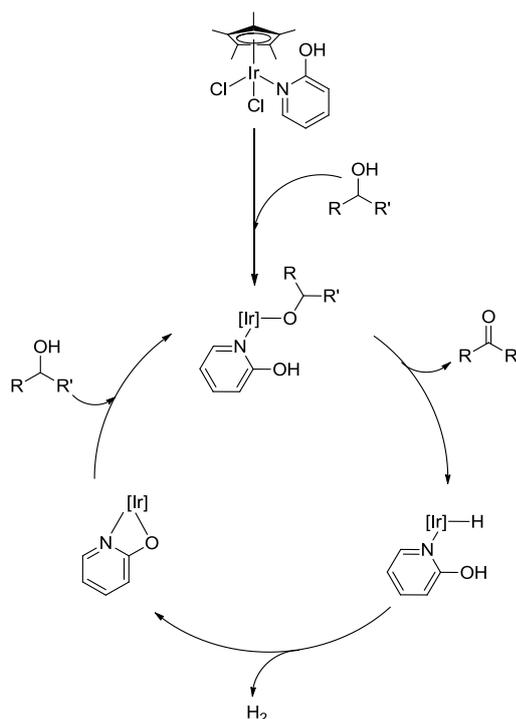
Scheme 1.28 Proposed mechanism for the oxidation of alcohols using a IrCp* 2-hydroxypyridine catalyst in toluene

Both the presence of dihydrogen with acetophenone (observed in an NMR experiment using a sealed NMR tube) and the complex shown in **Figure 1.17** having comparable activity with the monodentate bound 2-hydroxypyridine complex give evidence for the proposed mechanism.
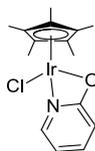
Figure 1.17 Ir Cp* complex with a bidentate bound pyridine ligand

Fujita later showed that an IrCp* complex containing a similar C,N-chelating ligand was an effective catalyst for oxidising both primary and secondary alcohols, shown in **Scheme 1.29**.[85] Various primary alcohols were converted, using 2 mol% Ir, and 5 mol% of sodium methoxide in toluene under reflux/sodium bicarbonate in xylene under reflux for 20 hours, into their aldehydes in a 46-100% yield. The proposed mechanism is shown in **Scheme 1.29,** with NMR evidence for the iridium hydride species.
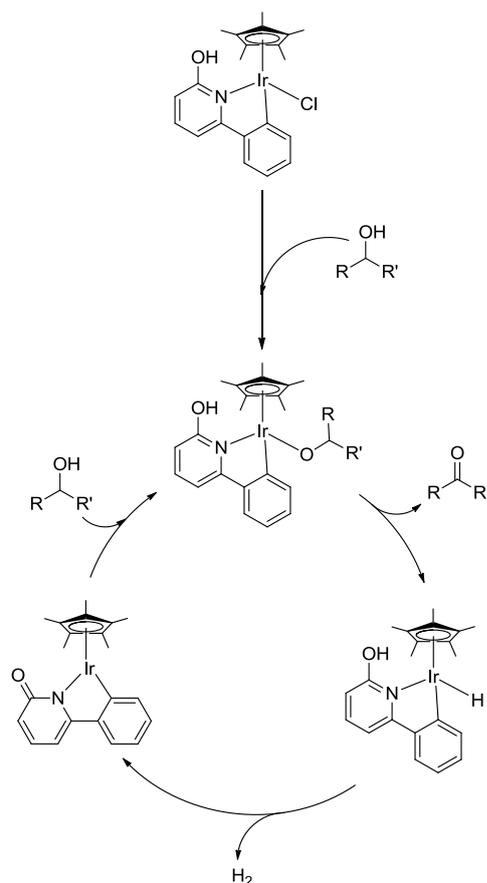
Scheme 1.29 Proposed mechanism for the oxidation of alcohols using an IrCp* complex containing a C,N-chelating ligand

A similar water soluble complex, shown in **Figure 1.18**, was used as a catalyst to oxidise alcohols in water, making the reaction more sustainable than the previous system in toluene.[86]
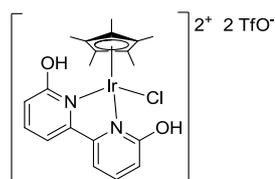
Figure 1.18 Water soluble dicationic IrCp* complex used to oxidise alcohols in water

Making the system even more sustainable and economical, the catalyst could be recycled by adding hexane to the aqueous solution to extract the product, and adding more substrate to the aqueous solution containing the catalyst. The yield for the oxidation of 4'-methoxyl-1-phenylethanol decreased minimally from 98% in run one to 94% after run eight. Also demonstrated, was the reuse of the catalyst for different alcohol substrates.

1.2.4 Imine Reductions

There are many examples of imine reductions using transition metal catalysts,[87,88] and in particular metal arene half sandwich complexes where the metal is iridium, rhodium or ruthenium.[89] A cyclometalated IrCp* catalyst, applicable for imine reductions, is discussed in section **1.2.8** for its use in reductive aminations.[90]

The first example of an imine reduction using a half sandwich complex was demonstrated by Noyori, shortly after the same catalysts had been used for ketone reduction (section **1.2.2.1**). Using the TEAF system (described in section **1.2.1.2**), Ru-1 type catalysts were tested for imine reduction with the conditions shown in **Scheme 1.30**.[91] 0.01-0.5 mol% of the Ru-1 type catalyst in various solvents converted 82-99% of the imine to the corresponding amine with moderate to good ee values of 77-96% in 3-36 hours. Experimental evidence showed that the imine is over a thousand times more reactive than a similar ketone towards this system.
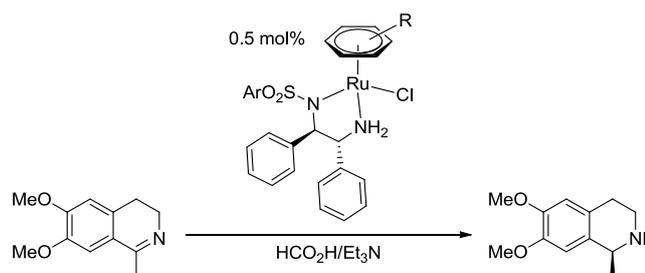
Scheme 1.30 Reduction of imines using Ru-1 type Noyori catalysts in the TEAF system

More recently, Xiao has demonstrated the use of the RhCp*(TsDPEN) complex for quinoline reductions using sodium formate in aqueous solutions, whereby both the C=N and C=C bond are reduced.[92] As with ketone reductions (section **1.2.2.5.2**), the research group found that the catalytic activity was affected by the pH of the system, whereby the optimum was pH 5 for the reduction of 2-methylquinoline. It is thought that the imine is reduced in its protonated iminium form, which is consistent with these findings as the pK_a of the protonated quinoline is 5.4.[31,93-99] As the pK_a of formic acid is 3.6, below this pH the concentration of the reductant, formate, diminishes. The pH was controlled using a 2 M acetic acid/sodium acetate buffer solution. A library of quinolines was then tested using a bulkier DPEN ligand (**Scheme 1.31**). In 6-24 hours the quinolines were reduced to the amines in 80-97% conversion with 96-98% ee depending on the R groups.
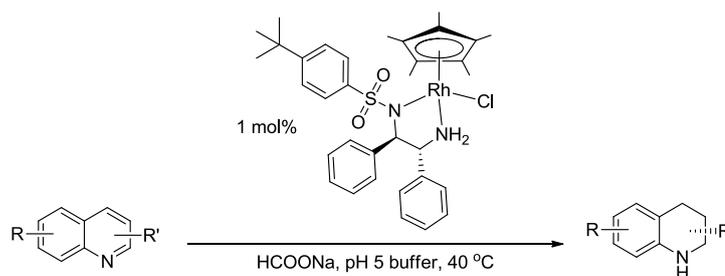
Scheme 1.31 Reduction of imines using Ru-1 type Noyori catalysts in the TEAF system

1.2.5 Amine Oxidations

1.2.5.1 Oxidant-Free Dehydrogenation

The Fujita catalyst discussed in section **1.2.3.1** for oxidant-free alcohol dehydrogenation has also been used for oxidant-free amine dehydrogenation. The 2-hydroxypyridine complex and several derivatives have been tested as catalysts for amine oxidations and the reverse imine reductions, in a recyclable system, with the overall process shown in **Scheme 1.32**. [100] This demonstrated the first homogeneous system for catalytic dehydrogenation and hydrogenation of nitrogen heterocycles.
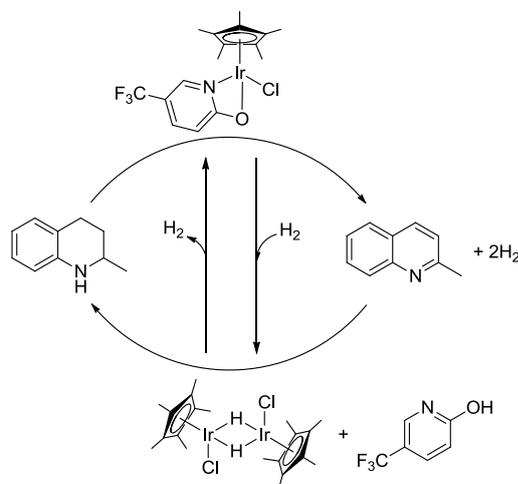
Scheme 1.32 Overall process for the reversible and repetitive catalytic dehydrogenation-hydrogenation

The amine oxidation reaction is performed with 5 mol% Ir in xylene at reflux temperature under an argon atmosphere to form the aromatic imine. To reverse the reaction, the temperature was reduced to 110 °C and the atmosphere of the closed system was replaced with hydrogen. This cycle was repeated 5 times, with a small loss of efficiency from 100% to 98% conversion. Under a hydrogen atmosphere, the dihydro bridged dimeric species shown in **Scheme 1.32** was formed, as determined

by NMR studies. [IrCp*Cl$_2$]$_2$ can also be used to hydrogenate quinoline but using *iso*-propanol as the hydrogen donor/solvent and either CF$_3$CO$_2$H or HClO$_4$ as an additive.[101]

Williams, Blacker and Marsden have demonstrated the use of the SCRAM catalyst ([IrCp*I$_2$]$_2$) in a one pot synthesis to prepare a benzazole from an aldehyde and a hydroxyamino substituted benzene (**Scheme 1.33**).[102] Within this transformation, an amine oxidation occurs, driven by the aromaticity of the final product.
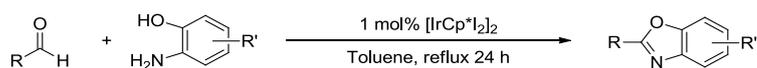
Scheme 1.33 Synthesis of benzazoles using the SCRAM catalyst

1.2.6 Racemisations

The conventional method of asymmetric synthesis is diastereomeric crystallisation, which only allows an optimum of a 50% yield. For this reason, racemisations of optically active centres are attractive transformations as, when combined with a chiral catalyst/enzyme, a dynamic kinetic resolution is implemented whereby a potential 100% conversion of racemic starting materials to an optically pure product can be achieved. Efficient racemisation of optically active alcohols has been widely reported,[103-105]

There have been a few reported examples of catalytic racemisation of amines using ruthenium catalysts, however the catalyst turnover is low, and the high temperatures required are not compatible with some of the other reagents or catalysts.[106-108] In 2007 Blacker reported the racemisation of amines using [IrCp*I$_2$]$_2$, named the SCRAM catalyst, with an example shown in **Scheme 1.34**.[109] The SCRAM catalyst aids the dehydrogenation of the amine, followed by hydrogenation of the resulting imine, losing the initial optical purity. After an hour the % ee was less than 5.
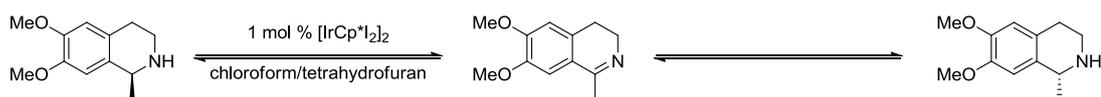
Scheme 1.34 Racemisation of optically active amines using the SCRAM catalyst

The SCRAM catalyst has been combined with a base for methine epimerisation, and crystallisation using (R)-mandelic acid in a semi-continuous dynamic kinetic

resolution to form optically pure (1S,4S)-sertraline (an anti-depressant) from racemic sertralone.[110] First, the (1S,4S) isomer is selectively crystallised from racemic sertraline, the remaining 3 isomers are racemised using base then the SCRAM catalyst and the process is repeated.
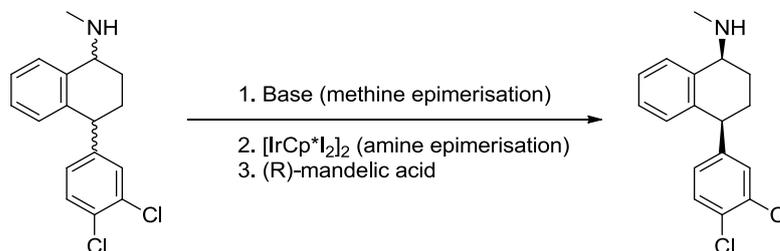
Scheme 1.35 Resolution of racemic tertralone using the SCRAM catalyst

1.2.7 N-Alkylations

1.2.7.1 N-Alkylations of Amines With Alcohols

Conventional syntheses of amines include N-alkylations with alkyl halides,[111-113] and reductive amination with carbonyl compounds.[111,114-116] These traditional methods are undesirable from an environmental standpoint, due to the use of alkyl halides/strong reducing agents as well as the generation of equimolar amounts of wasteful salts as co-products.
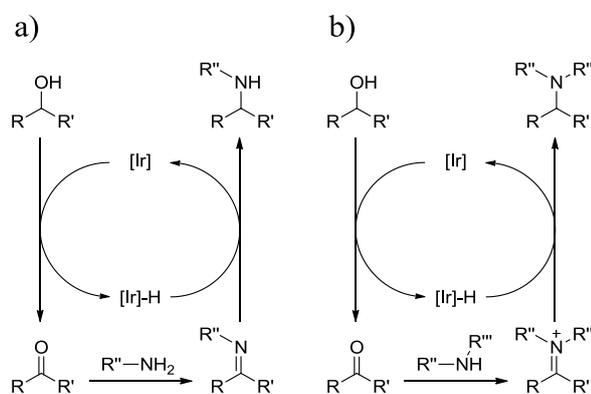
Scheme 1.36 Stepwise N alkylation reaction using a) primary amines and b) secondary amines

N-alkylation reactions comprise of two transfer hydrogenation reactions to form either a secondary or tertiary amine from their constituent alcohols and primary or secondary amine starting materials respectively, eliminating the need for external hydrogen acceptors/donors. The alcohol is a hydrogen donor, becoming oxidised to the corresponding aldehyde/ketone, which reacts with the amine in a reductive amination reaction to form an imine. The catalyst adds hydrogen across the imine,

which is the hydrogen acceptor, to form the resulting amine. The reaction is both atom economical and does not generate harmful by-products whereby, excluding the solvent and base, the only by-product is water. The reaction also employs readily available alcohols, compared to the corresponding halides or carbonyl compounds. The stepwise reaction is shown in **Scheme 1.36**.

Fujita demonstrated the first use of $[IrCp*Cl_2]_2$ as a catalyst for N-alkylation of both primary and secondary amines with primary alcohols, and more importantly secondary alcohols which were incompatible with similar systems.[117,118] Secondary amines were formed in high yields, between 71-98%, from equal amounts of their respective primary amines and primary/secondary alcohols, using 1-3 mol% Ir at 110-130 °C in toluene in the presence of $NaHCO_3$ or K_2CO_3, with the absence of any dialkylated products. Tertiary amines could also be prepared, however due to increased sterics around the starting secondary amine more forcing conditions were sometimes required, e.g. higher catalytic loading/temperatures or a lower yield was observed. Using tertiary alcohols as starting materials resulted in no reaction.

Ammonium salts can also be used as a substrate for N-alkylation reactions catalysed by $[IrCp*Cl_2]_2$, whereby ammonium acetate was the most effective substrate for the trialkylation reactions.[119,120] Interestingly, when ammonium tetrafluoroborate was used as the nitrogen source, high selectivity for the dialkylated product was observed, and complete selectivity when a secondary alcohol substrate was used.

Similarly to the alcohol oxidation reaction discussed in section **1.2.3**, Fujita has demonstrated an N-alkylation reaction in water by using a dicationic Ir Cp* ammine species (shown in **Figure 1.19**) used to catalyse the alkylation of aqueous ammonia with alcohols.[121]
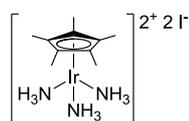
Figure 1.19 Dicationic Ir Cp* ammine complex used as a catalyst for the alkylation of aqueous ammonia

The tertiary amine, tribenzylamine, can be quantitatively formed using 1 mol% Ir at 140 °C for 24 hours. Using less catalyst, shorter reaction times or lower temperatures resulted in a minor dibenzylamine by-product. Presumably due to steric hindrance, when a secondary alcohol is used as a substrate, only the secondary amine

is formed. The catalyst was recycled twice with a slight reduction in yield from 100 to 95%, by firstly extracting the product with an organic solvent then adding more substrate to the aqueous solution.

Williams has demonstrated the use of the SCRAM catalyst ([IrCp*I$_2$]$_2$) without the use of base or any other additives for N-alkylation reactions in water.[122,123] Along with the benefits of using water as a solvent (discussed in section **1.2.2.5**), the absence of base makes the process even more efficient, with the added bonus of the only by-product, water, not contaminating the solvent. The general reactions are shown in **Scheme 1.37**, where the yields for the reaction labelled **a** and **b** vary between 18- 94% and 68-98% respectively.
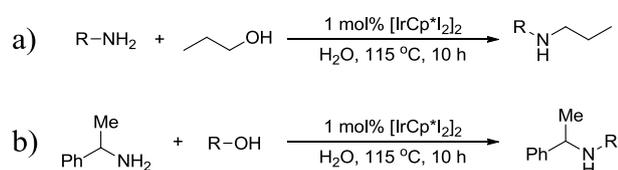
Scheme 1.37 N-alkylation with alcohols using the SCRAM catalyst in aqueous conditions

Williams has also demonstrated the use of ruthenium-arene diphosphine complexes for the N-alkylation of alcohols.[124-127]

1.2.7.2 Formation of N-Heterocycles

By starting with substrates bearing multiple hydroxyl groups cyclic amines can be formed, for example the synthesis of quinolizidine using the water soluble IrCp* complex discussed previously, shown in **Scheme 1.38**.[121]
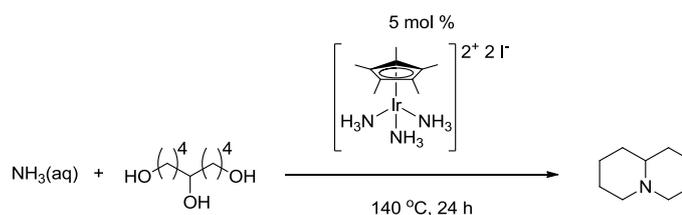
Scheme 1.38 Synthesis of quinolizidine using an N-alkylation reaction with NH$_3$ and a triol

Other N-heterocyclic systems have been synthesised through N-alkylation reactions by starting with amino-alcohol substrates, shown in **Scheme 1.39**.[128] In the case of the indoles, instead of the formation of the imine followed by hydrogenation to the amine, after oxidation of the alcohol an intramolecular nucleophilic attack of the amino group to the resulting aldehyde would occur, followed by a dehydration. The same product is formed when starting with the analogous nitro compounds along

with a trace amount of the amine compound, implying that the amine is an intermediate in the reaction.
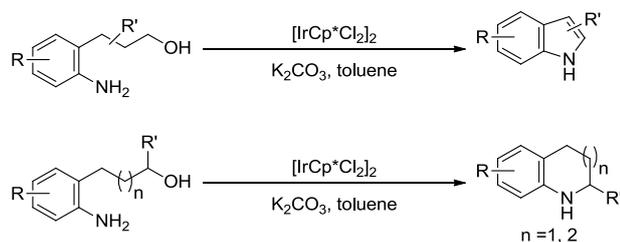
Scheme 1.39 Synthesis of N-heterocycles using aminoalcohol substrates

Saturated cyclic amines can be prepared through N-alkylations of a primary amine with a diol using ruthenium-arene phosphine complexes,[126] as well as [IrCp*Cl$_2$]$_2$ (1-5 mol% Ir) and sodium bicarbonate.[129,130] This can also be achieved by using an ammonia salt as the nitrogen source.[120]

1.2.7.3 Other N-Alkylations

[IrCp*Cl$_2$]$_2$ has been shown to be active for N-alkylations of carbamates,[131] amides,[126,131] and sulfonamides[126,127,132,133] with alcohols. Williams has demonstrated the formation of an amide from an alcohol *via* an N-alkylation reaction.[134]

1.2.8 Reductive Aminations

Reductive aminations are similar to N-alkylations but an aldehyde/ketone is used instead of an alcohol, avoiding the initial alcohol oxidation step. Similarly to N-alkylations, if the substrate contains both the amine and the carbonyl group, an intramolecular reductive amination occurs resulting in the formation of an N-heterocycle. Unlike N-alkylation reactions an external hydrogen donor is necessary to reduce the imine intermediate.
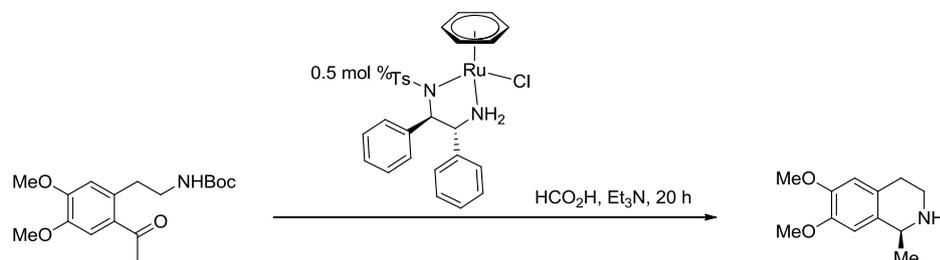
Scheme 1.40 Formation of N-heterocycles *via* intramolecular reductive aminations

This has been demonstrated using several substrate examples by Wills, with one demonstrated in **Scheme 1.40**.[135]

IrCp* picolinamides have also been used for reductive amination reactions, using

ammonium formate as the nitrogen source. Using the conditions shown in **Scheme 1.41**, 0.2 mol% of the picolinamide complex converted 97% of acetophenone to the resulting amine in 5 hours.[136]
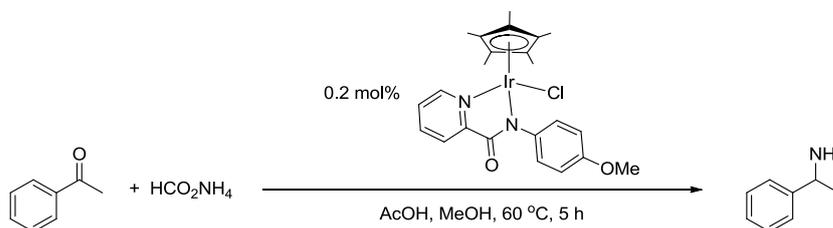
Scheme 1.41 Reductive aminations using an IrCp* picolinamide complex

In 2010, Xiao and co-workers serendipitously discovered that cyclometalated IrCp* complexes bearing ketimine ligands are excellent catalysts for both imine reductions and reductive aminations.[90] During the reduction of ketimines, IrCp*Cl(TsDPEN) was tested as a catalyst giving only moderate conversions, whereas when the catalyst was prepared *in situ* from [IrCp*Cl$_2$]$_2$ and TsDPEN-H, a much higher conversion was seen, though the resulting product was racemic. [IrCp*Cl$_2$]$_2$ was also tested without any additive ligands and the conversion was the same as that obtained with the *in situ* generated catalyst. The research group showed that the ketimine substrate binds to iridium to form the active catalyst in the form of a cyclometalated complex (shown in **Figure 1.20**). The catalysts along with their hydride analogues were characterised by X-ray crystallography.[137]
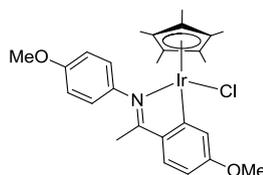
Figure 1.20 IrCp* complex with a cyclometalated ketimine ligand

After a similar catalyst was shown to be effective for aliphatic ketimine reductions, the complex shown in **Figure 1.20** was tested for the reductive amination of aromatic ketones with amines, which show low activity when using boron hydrides,[138] as well as aliphatic ketones with amines and ketones with ammonium formate, with the conditions shown in **Scheme 1.42**.
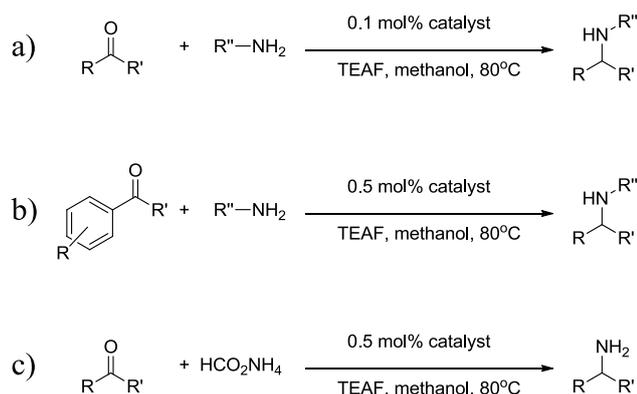
Scheme 1.42 Reductive aminations catalysed by a cyclometalated ketimine IrCp* catalyst

1.2.9 C-C Bond Forming Reactions

Fujita demonstrated the use of $[IrCp*Cl_2]_2$ as a catalyst for the β-alkylation of secondary alcohols with primary alcohols, *via* multiple transfer hydrogenation steps (**Scheme 1.43**).[139]
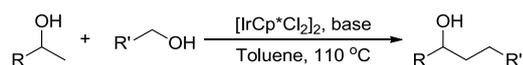
Scheme 1.43 β-alkylation of secondary alcohols with primary alcohols, catalysed by $[IrCp*Cl_2]_2$

Prior to this, the only other example was using a ruthenium catalyst, however large amounts of both a sacrificial hydrogen acceptor (1-dodecene) and a hydrogen donor (dioxane as a solvent) were required.[140] Here, there is no need for sacrificial additives, making the reaction atom economical and environmentally benign (as for the N-alkylation reactions discussed in section **1.2.7**), whereby, disregarding the base and solvent, the by-product is water. The stepwise reaction is similar to the N-alkylation reactions discussed in section **1.2.7**, whereby there is an initial oxidation of the alcohols, followed by a condensation reaction, then a reduction of the double bonds in the intermediate. The condensation reaction here is an aldol condensation between the resulting aldehyde and ketone to form an α,β-unsaturated ketone and the final step consists of two reductions, the C=C and C=O bonds successively to form the resulting secondary alcohol product. The reaction was performed at 110 °C in toluene (similarly to the N-alkylations) with 1-4 mol% Ir, using either sodium hydroxide or sodium *tert*-butoxide as a base, to yield 58-90% of the resulting alcohol after 17 hours, and in some cases a minor product of the corresponding ketone.

Other C-C bond forming reactions including transfer hydrogenation steps have

been reported, for example Williams has combined hydrogen borrowing with a Wittig reaction to couple an alcohol with a ylide to form an alkane *via* the alkene.[141-143]

1.2.10 Other Transfer Hydrogenation Reactions

In the synthesis of N-benzyl-(3-aminomethylglutarimide) derivatives, Wills demonstrated the use of a tethered ruthenium Noyori type catalyst to reduce an alkene bond (**Scheme 1.44**), although the reaction time is 5 days.[144]
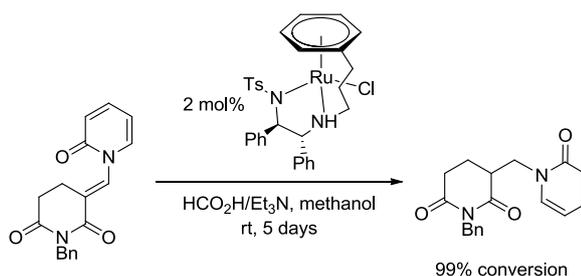
Scheme 1.44 Reduction of an alkene bond, by a tethered ruthenium catalyst to form an N-benzyl-(3-aminomethylglutarimide) derivative

Similarly to N-alkylation reactions, Williams has demonstrated the use of $[IrCp^*Cl_2]_2$ in the synthesis of amides from their corresponding alcohols and hydroxylamine hydrochloride, *via* the oxime.[145]
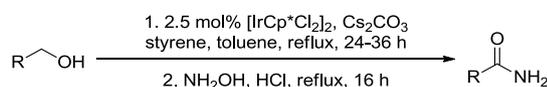
Scheme 1.45 Formation of amides from their primary alcohols and hydroxylamine hydrochloride

1.3 Immobilised Catalysts

Immobilised catalysts or solid supported catalysts aim to bridge the gap between homogeneous and heterogeneous systems by offering the moderate conditions, high activity and selectivity associated with homogeneous systems with the ease of removal and recyclability offered with heterogeneous systems. This is achieved by 'immobilising' a homogeneous catalyst onto a support through either chemical (covalent or non-covalent interactions) or physical methods (encapsulation) discussed below.[146] In order to recycle the catalyst, it can be filtered or decanted from the solution, or in the case of magnetic supports by using a magnet.[147] An added advantage is that the immobilised catalyst can be used in flow reactions

whereby the product is automatically separated from the catalyst avoiding a separation process.

Removal of the catalyst is crucial if the catalyst is used in the synthesis of an active pharmaceutical ingredient (API), where the metal contamination limit is 10 parts per million.[148] In the case of expensive precious metal catalysts, recycling is particularly important for large scale reactions in order to make the procedure commercially viable.

1.3.1 Characterisation of Immobilised Catalysts

Characterisation of solid supported catalysts is problematic as solid state characterisation techniques are less developed than solution phase. Infrared (IR) spectroscopy gives an indication of functional groups in the material, Inductively Coupled Plasma (ICP) analysis determines the amount of metal, however does not provide information on its environment, i.e. if it is in the active form, and solid state NMR can help to provide evidence on environment but is not always conclusive and the peaks are often broad. Energy-dispersive X-ray (EDX) spectroscopy or X-ray photoelectron spectroscopy (XPS) can be used to find the elemental analysis of the sample, with XPS also giving information about the chemical and electronic state of the elements in the material. The main problems with the performance of current immobilised catalysts are reduced activities, inconsistent recyclability, metal leaching and in the case of asymmetric reactions reduced/different selectivities.[146,149]

1.3.2 A Case Study into Factors Affecting the Performance of Immobilised Catalysts

Blümel reported an extensive investigation into covalently immobilised Wilkinson-type catalysts onto silica supports (with the general structure shown in **Figure 1.21**), with respect to ligand lengths, immobilisation method, surface coverage, pore size and recyclability/lifetime.[150]
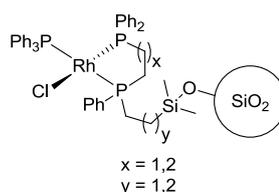
Figure 1.21 Immobilised Wilkinson-type catalyst, through covalent attachment of a chelating phosphine ligand to silica

The research group found that it was necessary to rigorously dry the silica prior to use to prevent crosslinking of the ethoxysilane moieties during the immobilisation, as the wet silica resulted in a catalyst with lower activity. Each catalytic reaction was using 1 mol% Rh (which corresponds to catalytic loading). For three examples of one reaction type (dehydrogenation of 1-dodecene, cyclohexen-1-one and 4-bromostyrene), different catalysts gave the optimum results, and there were no general trends regarding bite angle of the phosphines or the tether length. Due to known deactivation of these catalysts (in a homogeneous state) through dimerisation,[151] the catalytic activity was improved by diluting the catalysts onto the silica surface and keeping the metal centres away from each other. Silica with pores of 100 Å gave more active catalysts than those with smaller pores of 60 Å. Larger pore sizes compromise the mechanical stability of the silica. Non-porous materials have a small surface area, which is disadvantageous for industrial applications as the catalytic loading is small. Immobilised chelating ligands were shown to give more stable catalysts with a longer lifetime compared to monodentate ligands. This is presumably due to reduced metal leaching, although this data was not given.

1.3.3 Types of Immobilisation

1.3.3.1 Covalent

Covalent immobilisation of a catalyst is usually achieved through attachment of a functionalised ligand to the support (shown in **Figure 1.22**). A tether is usually present between the coordinating atoms and the terminus attached to the support to allow flexibility of the catalyst.

Figure 1.22 General design of a covalently immobilised catalyst

The strong covalent linkage should be stable enough towards standard catalytic conditions that no ligand leaching occurs. To avoid metal leaching, there must be a strong bond between the metal and the immobilised ligand. A disadvantage of these systems is achieving the chemical modifications of the catalyst in order to covalently

attach it to a support, *i.e.* adding a functionalised tether, which, along with potentially being difficult to prepare, may alter its catalytic activity.[146] The catalysts often have a loss of efficacy compared to the corresponding homogeneous catalyst due to restricted mobility and therefore an unequally dispersed catalyst throughout the mixture. In the case of chiral catalysts, conformational preferences of the supported complexes may be different to that of the homogeneous anologue which may lead to negative effects on enantioselectivity.[149]

The case study discussed in section **1.3.2** is an example of an effective immobilised catalyst through covalent attachment, with the structure shown in **Figure 1.21** (x = 1 and y = 2).[150] One of the most effective systems was with a low catalytic loading on silica of 4 molecules per 100 nm^2 of surface and with a reaction catalytic loading of 1 mol% for the hydrogenation of 1-dodecene. For the first run the reaction was complete in 30 hours, which is equivalent to its homogeneous counterpart. After the second run the catalyst gradually loses activity up to the 13th run, which is complete in 100 hours.

1.3.3.2 Non-covalent

In comparison to covalent methods, in non-covalent immobilisation the catalyst often does not require any modification. However, they are often not as robust as the attachment is generally weaker.[149] These methods are usually simple and cheap making it attractive for industrial applications. Non-covalent immobilisation may be *via* electrostatic, coordinative or adsorptive methods.

1.3.3.2.1 Electrostatic Interactions

If the catalyst is ionic then the counterion can be exchanged with a charged support, with the most common examples being a cationic catalyst and an anionic support (demonstrated in **Figure 1.23**).
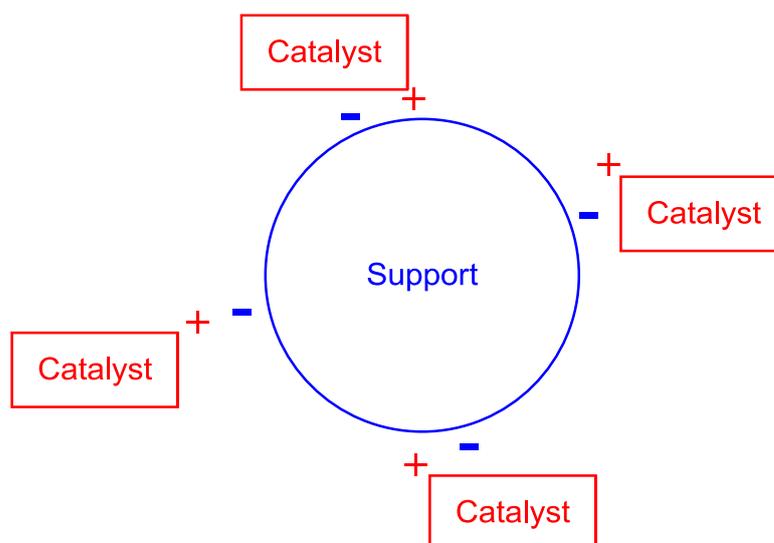
Figure 1.23 General design of an electrostatically immobilised catalyst

Unlike covalent immobilisation, the catalyst does not need to be modified prior to immobilisation, however the catalyst has to be ionic. These systems are prepared either through ion exchange, by replacing the counterion with a charged solid, or through the formation of the complex on a pre-exchanged metal centre.[149] In the first case, a salt will form of the counterion of the complex and oppositively charged counterion of the solid. This salt is either eliminated to the solution or remains on the solid, depending on the solvent used in the exchange process. The more commonly used direct exchange method allows the catalyst to be characterised prior to immobilisation. The choice of exchange solvent is important to achieve the best exchange ratios and hence the higher loading immobilised catalyst. The support is generally a clay but can be an organic, inorganic or hybrid support.

A [(QUINAP)Rh(cod)]$^+$ complex has been immobilised onto a negatively charged clay *via* salt exchange.[152,153]
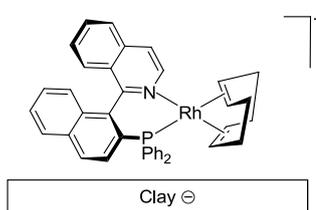
Figure 1.24 Immobilised [(QUINAP)Rh(cod)]$^+$ on clay through electrostatic interactions

The immobilised complex was an active catalyst for the asymmetric hydroboration of styrene, showing comparable activity to the homogeneous system (on the second run), with two successful subsequent recycles.

1.3.3.2.2 Coordinative Bonding

If the support has groups with lone pairs then these can be used to form a coordinative bond to a metal to form an immobilised catalyst. This is achieved either through direct metal-support interaction or with an interposed molecule.[149] There is crossover between coordinative bonding and covalent attachment.

Blümel recently demonstrated the immobilisation of Wilkinson-type rhodium complexes through coordination of an interposed molecule, which itself is attached to a silica support through electrostatic interactions (shown in **Figure 1.25**).[154]
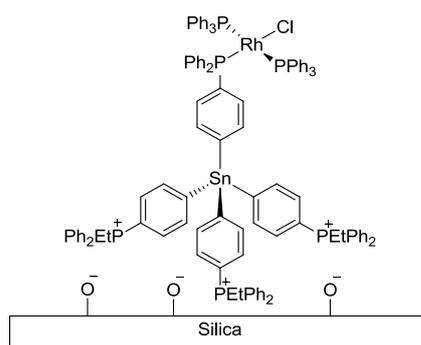
Figure 1.25 Immobilised Wilkinson-type catalyst, through coordinative bonding and electrostatic interactions

The immobilised complex was tested as a catalyst for the hydrogenation of 1-dodecene, using 1 mol% Rh. The catalyst initially converted 1-dodecene to dodecane quantitatively in 24 hours. Prior to the subsequent runs the solution was decanted and the catalyst thoroughly washed with toluene. The catalyst remained active however the reaction time gradually increased through to the 24th run to over 60 hours. The 27th run required over 70 hours for completion and the final 30th run required 100 hours. There were no metal leaching data. The rigid linkers prevent deactivation of the catalyst *via* dimerisation which has been seen when using flexible phosphine linkers.[150,155,156]

1.3.3.2.3 Metal-Organic Frameworks

Ligands with multiple functional groups can be used to bridge metals together to form an extended network. These systems allow a high catalytic loading and more accessible catalytic centres, but require chemical modifications to the catalyst.[149] An example of a metal-organic framework (MOF) is illustrated in **Figure 1.26**, comprising of a ruthenium centre coordinating to a bridged BINAP and chiral diamine ligand.[157]
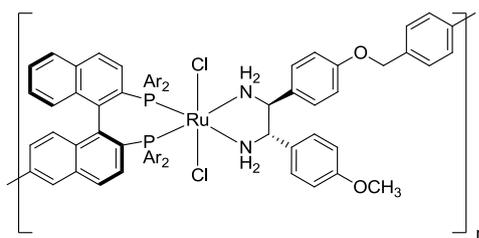
Figure 1.26 A ruthenium MOF used for the enantioselective hydrogenation of ketones

The MOF was used successfully for the enantioselective hydrogenation of aromatic ketones. The catalyst where Ar = 3,5-$(CH_3)_2C_6H_3$ was active for the hydrogenation of a variety of ketones using the conditions shown in **Scheme 1.46**.
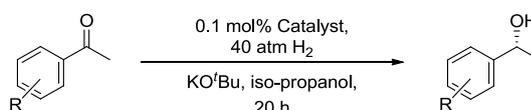
Scheme 1.46 Reduction of acetophenones using a Ru-1 type Noyori catalyst with the IPA system

The catalyst was recyclable for the reduction of acetophenone with the conversion and enantioselectivity reducing from >99-97% and 97.4-95.4% respectively from run one to run seven. There was no detectable ruthenium leaching into the product (<0.1 ppm).

1.3.3.2.4 Adsorption

Immobilisation whereby there is no specific metal-support coordination is considered an adsorption method. Some examples of adsorption are interactions of catalysts to the support through van der Waals interactions or hydrogen bonding. Although this type of bonding is often considered weak, there have been successful recyclable systems, such as an immobilised charged version of an activated rhodium CATHy catalyst attached to Me-SBA-16 shown in **Figure 1.27**.[158] The triflate counterion forms hydrogen bonds to the support, as well as a hydrogen bond to an NH of the TsDPEN ligand.
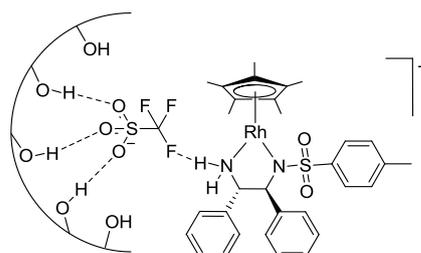
Figure 1.27 Immobilised CATHy-type catalyst onto silica *via* a coordinated triflate counterion

0.2 mol% of the catalyst was active against a range of acetophenone reductions using sodium formate as the hydrogen donor in water and applying ultrasound. After 20 minutes, the acetophenones were reduced in a 96-99% conversion and with 91-97% ee. The catalyst was used 10 times with acetophenone as the substrate, with the end conversion decreasing slightly from almost quantitative to 96% and the ee remaining at 97%. ICP analysis showed that 3.6% of the rhodium had leached out of the supported system after the tenth run.[158]

1.3.3.3 Encapsulation

In an encapsulation system the catalyst is physically trapped within the support matrix (**Figure 1.28**), so there are no requirements for the catalyst to be chemically attracted or attached to its support.
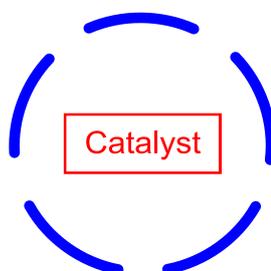
Figure 1.28 General design of an immobilised catalyst *via* encapsulation

This is desirable in terms of the catalyst as it does not have to be chemically modified. However, it can be difficult to prepare the encapsulated system. There are two methods to synthesise encapsulation systems: building the matrix around the catalyst or synthesising the catalyst inside the matrix. In the former instance, the catalyst must be sufficiently stable towards the conditions for building the matrix, whereas for the latter case, the catalyst synthesis must be high yielding as any side products may also become encapsulated and affect the resulting catalytic reaction.

The main problems with encapsulated systems are diffusion based, as the matrix pores must be large enough to allow the substrates to diffuse into the matrix, react with the catalyst and allow the products to leave, yet small enough to trap the catalyst. Another common problem is a different selectivity due to the restricted space. However, this can also be used to its advantage.

Rhodium phosphine complexes have been encapsulated in both inorganic (silica) and hybrid systems and been tested as catalysts for the hydroformylation of 1-hexene.[159] The most active system was seen when incorporating $[RhCl(CO)_2]_2$ with a

phosphine additive (dppf) into a hybrid support (silica with $(EtO)_3Si-Ph-Si(OEt)_3$ as a co-condensation agent). The catalyst was active for 6 runs with turnover numbers (TON) of at least 700 for each run and no leaching was seen by colour, however there were no reported leaching values.

1.3.4 Other Recyclable Systems

There are examples of other recyclable systems which, although they are not strictly immobilised systems, serve the same purpose as the catalyst can easily be separated from the product post reaction. Examples of such reactions are: catalysts which are soluble under the reaction conditions, for example high temperatures, but precipitate upon cooling;[160] biphasic systems (for example if the catalyst is dissolved in an aqueous phase whereas the substrate/product is dissolved in an organic phase);[161] and phase switchable systems where the reaction is performed in a single phase and the catalyst can be switched to another phase post reaction.[162]

1.3.5 Previous Immobilised M-arene Complexes

Many research groups have immobilised Noyori-type catalysts through the diamine/amino-alcohol ligand with varying success.[163-177] **Figure 1.29** shows the various immobilised ligands, along with the immobilised rhodium complex J shown in **Figure 1.27**. As these catalysts are immobilised through the Noyori-type ligand, they are restricted to those specific reactions.
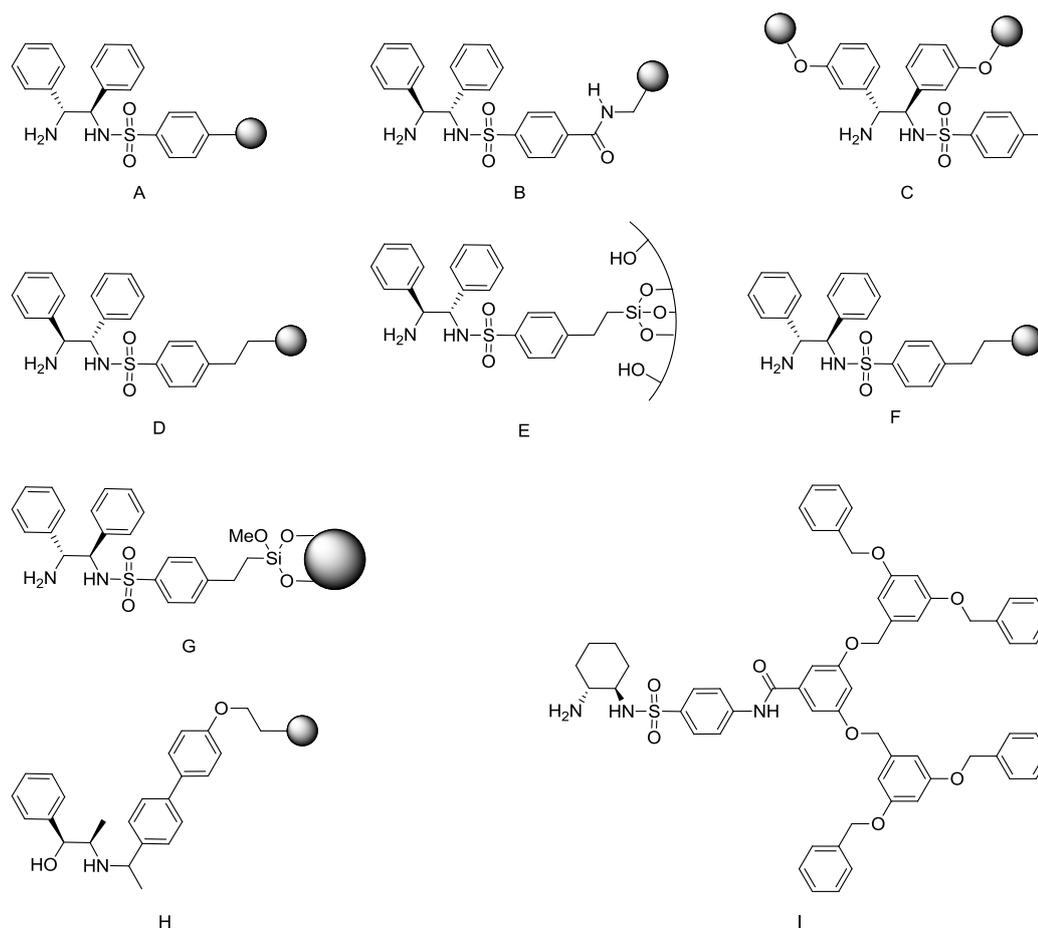
Figure 1.29 Reported immobilised Noyori-type ligands used to complex iridium, rhodium or ruthenium

Table 1.3 highlights immobilised systems for acetophenone reductions with long reaction times and no recycle data.

Catalyst	Metal & ancillary ligands	Support	Catalytic conditions	Catalyst loading/mol%	No. runs	Time/hours	Yield/%	% ee	Leaching/%
A[171]	RuCl(benzene)	polystyrene	KOH, *iso*-propanol	5	1	48	20	64	no data
A[171]	RuCl(benzene)	polystyrene/DVB	KOH, *iso*-propanol	5	4 (no data for runs 2-4)	48	96	31	no data
A[171]	RuCl(*p*-cymene)	polystyrene	KOH, *iso*-propanol	5	1	48	72	40	no data
A[171]	RuCl(*p*-cymene)	polystyrene/DVB	KOH, *iso*-propanol	5	1	48	23	84	no data
E[170] R = H	IrClCp*	SBA-15	^{t}BuOK, methanol, 10 atm H_2, 25 °C	1	1	72	93	90	no data

Table 1.3 Summary of acetophenone reductions using immobilised Noyori/CATHy type catalysts

Table 1.4 highlights more successful systems which have shown moderate-excellent activity upon recycle. The most successful system to date is using the catalyst J (shown in **Figure 1.27** and discussed in section **1.3.3.2.4**) which allows 10 runs for acetophenone reduction with over 95% conversion and 97% ee in only 20 minutes and with minimal leaching of 3.6% rhodium over 10 runs.

Catalyst	Metal & ancillary ligands	Support	Catalytic conditions	Catalyst loading/mol%	No. runs	Time/hours	Yield/%	% ee	Leaching/%
B[164]	RuCl(*p*-cymene)	polystyrene	HCO$_2$H/NEt$_3$, DMF	1	3	18-69	52-80	98-95	no data
B[164]	RuCl(*p*-cymene)	PEG linked polystyrene	HCO$_2$H/NEt$_3$N	1	2	28-72	95-96	97	no data
C[178]	RuCl(*p*-cymene)	PEG	HCO$_2$H/NEt$_3$, 50 °C	1	4	20	99-56	94-82	0.7% (first run only)
A[163]	RuCl(*p*-cymene)	sulfonated polystyrene/DVB	HCOONa, water, 40 °C	1	2	3	100	98-97	no data
B[164]	RuCl(*p*-cymene)	polystyrene	HCO$_2$H/NEt3, dichloromethane	1	3	18-69	52-71	>99-91	no data
H[177]	RuCl(*p*-cymene)	methacrylate polymer	7:3 PEG ester:hydroxyethyl ester copolymer, KOH, *iso*-propanol	4	3	4-14	95-77	81	no data

Catalyst	Metal & ancillary ligands	Support	Catalytic conditions	Catalyst loading/mol%	No. runs	Time/hours	Yield/%	% ee	Leaching/%
F[172]	RuCl(*p*-cymene)	silica	HCO$_2$H/NEt$_3$	1	5	6-44	>99-94	97	30-40
F[169,172]	RuCl(*p*-cymene)	silica	HCO2H/NEt$_3$, 40 °C	1	5	6-44	99-94	97	30-40
G[176]	RhClCp*	silica	HCOONa, water, 40 °C	0.4	12	1 (time not given for the last run)	>99	97-93	3.4%
G[174]	RhClCp*	silica coated Fe$_3$O$_4$	HCOONa, Bu$_4$NBr, water, 40 °C	0.2	10	1	97-92	98-96	no data
I[166]	RhClCp*	-	HCOONa, water, 40∘C	0.5	6	0.66-1.5	>99-97	96-95	no data
J[158]	RhClCp*	SBA-16.	HCOONa, Bu$_4$NBr, water, 41°C	0.2	10	0.33	>99-96	97	3.6%
C[167]	RuCl(*p*-cymene)	PEG	HCOONa, water, 40 °C	1	14	1-48	99-87	92	0.4 % (1st run only)

Table 1.4 Summary of recycled acetophenone reductions immobilised Noyori/CATHy type catalysts

A hydroxyl tethered version of the SCRAM catalyst has previously been prepared and immobilised onto PEG (polyethylene glycol), shown in **Scheme 1.47**.[110] The patented immobilisation method is unique in comparison to the previous Noyori-type ligands as the functionalised Cp* group is immobilised, allowing the use of other ancillary ligands rather than being restricted to the Noyori TsDPEN ligand.[179]
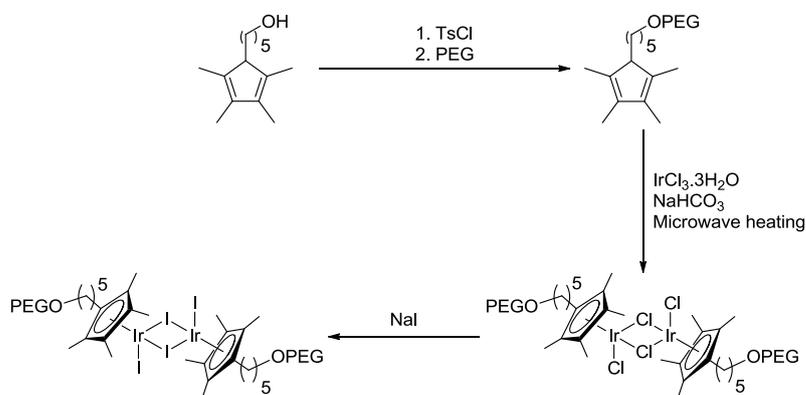
Scheme 1.47 SCRAM catalyst immobilised onto PEG

The PEGylated catalyst was used in a nanoomembrane reactor as part of a semi continuous process to resolve racemic sertraline to (1S,4S) sertraline (similarly to the homogeneous SCRAM catalyst discussed in section **1.2.6**). The initial run was successful however the catalyst showed a loss in activity over two reuses. Although this initial immobilisation attempt had limited success, the method of immobilising through a Cp* based ligand is an attractive one as it allows different ancillary ligands around the iridium, enabling flexible use of the system in a variety of different reactions. The strong η^5 coordination between the Cp ring and the iridium should also prevent metal leaching through ligand dissociation.

1.4 Project Aims

The aims of this project were to:

- Prepare a range of novel iridium and rhodium Cp* complexes (Chapters 3-5) and test them as catalysts against transfer hydrogenation reactions (Chapter 6)

- Synthesise hydroxyl tethered versions of [MCp*X$_2$]$_2$, where M = Ir, Rh and X = Cl, I (Chapter 2) and immobilise the complexes onto a solid support (Chapter 7), as shown in **Figure 1.30**.
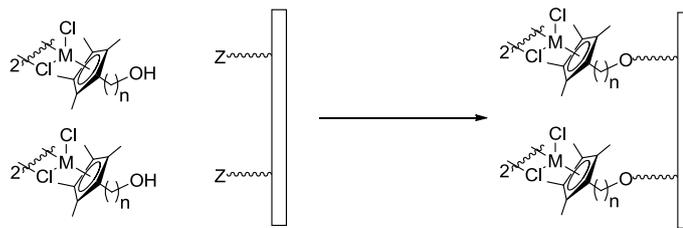
Figure 1.30 Immobilisation strategy of functionalised Cp* Group 9 Complexes onto a solid support

- Test the catalytic activity of the immobilised complexes as transfer hydrogenation catalysts (Chapter 7)

- Test the non-immobilised complexes as anti-cancer agents against a range of cell lines (Chapter 8)

1.5 References

(1)   E. Knoevenagel; B. Bergdolt *Ber. Dtsch. Chem. Ges.* **1903**, *36*, 2857-2860.
(2)   W. Ponndorf *Angew. Chem.* **1926**, *39*, 138-143.
(3)   A. Verley *Bull. Soc. Chim. Fr.* **1925**, *37*, 537.
(4)   H. Meerwein; R. Schmidt *Justus Liebigs Annalen der Chemie* **1925**, *444*, 221-238.
(5)   Y. M. Y. Haddad; H. B. Henbest; J. Husbands; T. R. B. Mitchell *Proc. Chem. Soc.* **1964**, 361.
(6)   K. Junge; K. Schroder; M. Beller *Chem. Commun.* **2011**, *47*, 4849-4859.
(7)   M. Darwish; M. Wills *Catalysis Science & Technology* **2012**, *2*, 243-255.
(8)   A. J. Blacker; P. Thompson In *Asymmetric Catalysis on Industrial Scale*; Wiley-VCH Verlag GmbH & Co. KGaA, **2010**.
(9)   B. T. Khai; A. Arcelli *Tetrahedron Lett.* **1985**, *26*, 3365-3368.
(10)   K. Narita; M. Sekiya *Chem. Pharm. Bull.* **1977**, *25*, 135-140.
(11)   K. Wagner *Angew. Chem., Int. Ed. Engl.* **1970**, *9*, 50-54.
(12)   H. Brunner; W. Leitner *Angew. Chem., Int. Ed. Engl.* **1988**, *27*, 1180-1181.
(13)   H. Brunner; E. Graf; W. Leitner; K. Wutz *Synthesis* **1989**, *1989*, 743-745.
(14)   A. Fujii; S. Hashiguchi; N. Uematsu; T. Ikariya; R. Noyori *J. Am. Chem. Soc.* **1996**, *118*, 2521-2522.
(15)   S. Hashiguchi; A. Fujii; J. Takehara; T. Ikariya; R. Noyori *J. Am. Chem. Soc.* **1995**, *117*, 7562-7563.
(16)   J. Takehara; S. Hashiguchi; A. Fujii; S.-i. Inoue; T. Ikariya; R. Noyori *Chem. Commun.* **1996**, 233-234.
(17)   X. Zhou; X. Wu; B. Yang; J. Xiao *J. Mol. Catal. A: Chem.* **2012**, *357*, 133-140.
(18)   K.-J. Haack; S. Hashiguchi; A. Fujii; T. Ikariya; R. Noyori *Angew. Chem., Int. Ed. Engl.* **1997**, *36*, 285-288.
(19)   R. Noyori; M. Yamakawa; S. Hashiguchi *J. Org. Chem.* **2001**, *66*, 7931-7944.
(20)   D. A. Alonso; P. Brandt; S. J. M. Nordin; P. G. Andersson *J. Am. Chem. Soc.* **1999**, *121*, 9580-9588.

(21) M. Yamakawa; H. Ito; R. Noyori *J. Am. Chem. Soc.* **2000**, *122*, 1466-1478.
(22) J. A. Kenny; K. Versluis; A. J. R. Heck; T. Walsgrove; M. Wills *Chem. Commun.* **2000**, *0*, 99-100.
(23) I. Yamada; R. Noyori *Org. Lett.* **2000**, *2*, 3425-3427.
(24) K. Püntener; L. Schwink; P. Knochel *Tetrahedron Lett.* **1996**, *37*, 8165-8168.
(25) L. Schwink; P. Knochel *Chem. Eur. J.* **1998**, *4*, 950-968.
(26) L. Schwink; T. Ireland; K. Püntener; P. Knochel *Tetrahedron: Asymmetry* **1998**, *9*, 1143-1163.
(27) K. Mashima; T. Abe; K. Tani *Chem. Lett.* **1998**, *27*, 1199-1200.
(28) K. Mashima; T. Abe; K. Tani *Chem. Lett.* **1998**, *27*, 1201-1202.
(29) J. Blacker; B. Mellor, patent number WO9842643 B1, **1997**
(30) K. Murata; T. Ikariya; R. Noyori *J. Org. Chem.* **1999**, *64*, 2186-2187.
(31) H. Zhou; Z. Li; Z. Wang; T. Wang; L. Xu; Y. He; Q.-H. Fan; J. Pan; L. Gu; A. S. C. Chan *Angew. Chem.* **2008**, *120*, 8592-8595.
(32) K. Murata; K. Okano; M. Miyagi; H. Iwane; R. Noyori; T. Ikariya *Org. Lett.* **1999**, *1*, 1119-1121.
(33) A. J. Blacker; E. Clot; S. B. Duckett; O. Eisenstein; J. Grace; A. Nova; R. N. Perutz; D. J. Taylor; A. C. Whitwood *Chem. Commun.* **2009**, 6801-6803.
(34) A. J. Blacker; S. B. Duckett; J. Grace; R. N. Perutz; A. C. Whitwood *Organometallics* **2009**, *28*, 1435-1446.
(35) U. M. Lindström *Chem. Rev.* **2002**, *102*, 2751-2772.
(36) S. Ogo; N. Makihara; Y. Watanabe *Organometallics* **1999**, *18*, 5470-5474.
(37) S. Ogo; N. Makihara; Y. Kaneko; Y. Watanabe *Organometallics* **2001**, *20*, 4903-4910.
(38) T. Abura; S. Ogo; Y. Watanabe; S. Fukuzumi *J. Am. Chem. Soc.* **2003**, *125*, 4149-4154.
(39) J. Canivet; L. Karmazin-Brelot; G. Süss-Fink *J. Organomet. Chem.* **2005**, *690*, 3202-3211.
(40) C. Romain; S. Gaillard; M. K. Elmkaddem; L. Toupet; C. Fischmeister; C. M. Thomas; J.-L. Renaud *Organometallics* **2010**, *29*, 1992-1995.
(41) X. Wu; J. Xiao *Chem. Commun.* **2007**, 2449-2466.
(42) X. Wu; J. Liu; X. Li; A. Zanotti-Gerosa; F. Hancock; D. Vinci; J. Ruan; J. Xiao *Angew. Chem., Int. Ed.* **2006**, *45*, 6718-6722.
(43) C. Bubert; J. Blacker; S. M. Brown; J. Crosby; S. Fitzjohn; J. P. Muxworthy; T. Thorpe; J. M. J. Williams *Tetrahedron Lett.* **2001**, *42*, 4037-4039.
(44) T. Thorpe; J. Blacker; S. M. Brown; C. Bubert; J. Crosby; S. Fitzjohn; J. P. Muxworthy; J. M. J. Williams *Tetrahedron Lett.* **2001**, *42*, 4041-4043.
(45) H. Y. Rhyoo; H.-J. Park; Y. K. Chung *Chem. Commun.* **2001**, *0*, 2064-2065.
(46) H. Y. Rhyoo; H.-J. Park; W. H. Suh; Y. K. Chung *Tetrahedron Lett.* **2002**, *43*, 269-272.
(47) Y. Ma; H. Liu; L. Chen; X. Cui; J. Zhu; J. Deng *Org. Lett.* **2003**, *5*, 2103-2106.
(48) X. Wu; X. Li; W. Hems; F. King; J. Xiao *Org. Biomol. Chem.* **2004**, *2*, 1818-1821.
(49) X. Wu; D. Vinci; T. Ikariya; J. Xiao *Chem. Commun.* **2005**, 4447-4449.
(50) J. Canivet; G. Labat; H. Stoeckli-Evans; G. Süss-Fink *Eur. J. Inorg. Chem.* **2005**, *2005*, 4493-4500.
(51) M. Yamakawa; I. Yamada; R. Noyori *Angew. Chem., Int. Ed.* **2001**, *40*, 2818-2821.
(52) X. Wu; X. Li; F. King; J. Xiao *Angew. Chem., Int. Ed.* **2005**, *44*, 3407-3411.

(53)   X. Wu; J. Liu; D. Di Tommaso; J. A. Iggo; C. R. A. Catlow; J. Bacsa; J. Xiao *Chem. Eur. J.* **2008**, *14*, 7699-7715.

(54)   D. S. Matharu; D. J. Morris; G. J. Clarkson; M. Wills *Chem. Commun.* **2006**, 3232-3234.

(55)   D. J. Morris; A. M. Hayes; M. Wills *J. Org. Chem.* **2006**, *71*, 7035-7044.

(56)   T. Touge; T. Hakamata; H. Nara; T. Kobayashi; N. Sayo; T. Saito; Y. Kayaki; T. Ikariya *J. Am. Chem. Soc.* **2011**, *133*, 14960-14963.

(57)   D. S. Matharu; D. J. Morris; A. M. Kawamoto; G. J. Clarkson; M. Wills *Org. Lett.* **2005**, *7*, 5489-5491.

(58)   J. Hannedouche; G. J. Clarkson; M. Wills *J. Am. Chem. Soc.* **2004**, *126*, 986-987.

(59)   A. M. Hayes; D. J. Morris; G. J. Clarkson; M. Wills *J. Am. Chem. Soc.* **2005**, *127*, 7318-7319.

(60)   D. J. Cross; I. Houson; A. M. Kawamoto; M. Wills *Tetrahedron Lett.* **2004**, *45*, 843-846.

(61)   F. K. Cheung; A. M. Hayes; J. Hannedouche; A. S. Y. Yim; M. Wills *J. Org. Chem.* **2005**, *70*, 3188-3197.

(62)   F. K. Cheung; C. Lin; F. Minissi; A. L. Crivillé; M. A. Graham; D. J. Fox; M. Wills *Org. Lett.* **2007**, *9*, 4659-4662.

(63)   F. K. Cheung; A. M. Hayes; D. J. Morris; M. Wills *Org. Biomol. Chem.* **2007**, *5*, 1093-1103.

(64)   F. K. Cheung; M. A. Graham; F. Minissi; M. Wills *Organometallics* **2007**, *26*, 5346-5351.

(65)   J. E. D. Martins; D. J. Morris; B. Tripathi; M. Wills *J. Organomet. Chem.* **2008**, *693*, 3527-3532.

(66)   F. K. Cheung; A. J. Clarke; G. J. Clarkson; D. J. Fox; M. A. Graham; C. Lin; A. L. Criville; M. Wills *Dalton Trans.* **2010**, *39*, 1395-1402.

(67)   V. Parekh; J. A. Ramsden; M. Wills *Catalysis Science & Technology* **2012**, *2*, 406-414.

(68)   T. Ikariya; A. J. Blacker *Acc. Chem. Res.* **2007**, *40*, 1300-1308.

(69)   F. Wang; H. Liu; L. Cun; J. Zhu; J. Deng; Y. Jiang *J. Org. Chem.* **2005**, *70*, 9424-9429.

(70)   X. Li; J. Blacker; I. Houson; X. Wu; J. Xiao *Synlett* **2006**, *2006*, 1155-1160.

(71)   D. A. Alonso; S. J. M. Nordin; P. Roth; T. Tarnai; P. G. Andersson; M. Thommen; U. Pittelkow *J. Org. Chem.* **2000**, *65*, 3116-3122.

(72)   M. J. Palmer; J. A. Kenny; T. Walsgrove; A. M. Kawamoto; M. Wills *J. Chem. Soc., Perkin Trans. 1* **2002**, 416-427.

(73)   T. Ikariya; K. Murata; R. Noyori *Org. Biomol. Chem.* **2006**, *4*, 393-406.

(74)   A. M. Kawamoto; M. Wills *J. Chem. Soc., Perkin Trans. 1* **2001**, 1916-1928.

(75)   P. Peach; D. J. Cross; J. A. Kenny; I. Mann; I. Houson; L. Campbell; T. Walsgrove; M. Wills *Tetrahedron* **2006**, *62*, 1864-1876.

(76)   M. Ito; N. Tejima; M. Yamamura; Y. Endo; T. Ikariya *Organometallics* **2010**, *29*, 1886-1889.

(77)   M. Ito; Y. Endo; N. Tejima; T. Ikariya *Organometallics* **2010**, *29*, 2397-2399.

(78)   M. Ito; Y. Endo; T. Ikariya *Organometallics* **2008**, *27*, 6053-6055.

(79)   S. Hashiguchi; A. Fujii; K.-J. Haack; K. Matsumura; T. Ikariya; R. Noyori *Angew. Chem., Int. Ed. Engl.* **1997**, *36*, 288-290.

(80)   K. Fujita; S. Furukawa; R. Yamaguchi *J. Organomet. Chem.* **2002**, *649*, 289-292.

(81) F. Hanasaka; K. Fujita; R. Yamaguchi *Organometallics* **2005**, *24*, 3422-3433.
(82) F. Hanasaka; K. Fujita; R. Yamaguchi *Organometallics* **2004**, *23*, 1490-1492.
(83) F. Hanasaka; K. Fujita; R. Yamaguchi *Organometallics* **2006**, *25*, 4643-4647.
(84) K. Fujita; N. Tanino; R. Yamaguchi *Org. Lett.* **2006**, *9*, 109-111.
(85) K. Fujita; T. Yoshida; Y. Imori; R. Yamaguchi *Org. Lett.* **2011**, *13*, 2278-81.
(86) R. Kawahara; K. Fujita; R. Yamaguchi *J. Am. Chem. Soc.* **2012**, *134*, 3643-6.
(87) J.-H. Xie; S.-F. Zhu; Q.-L. Zhou *Chem. Rev.* **2010**, *111*, 1713-1760.
(88) N. Fleury-Brégeot; V. de la Fuente; S. Castillón; C. Claver *ChemCatChem* **2010**, *2*, 1346-1371.
(89) C. Wang; B. Villa-Marcos; J. Xiao *Chem. Commun.* **2011**, *47*, 9773-9785.
(90) C. Wang; A. Pettman; J. Bacsa; J. Xiao *Angew. Chem., Int. Ed.* **2010**, *49*, 7548-7552.
(91) N. Uematsu; A. Fujii; S. Hashiguchi; T. Ikariya; R. Noyori *J. Am. Chem. Soc.* **1996**, *118*, 4916-4917.
(92) C. Wang; C. Li; X. Wu; A. Pettman; J. Xiao *Angew. Chem., Int. Ed.* **2009**, *48*, 6524-6528.
(93) H. Zhou; Z. Li; Z. Wang; T. Wang; L. Xu; Y. He; Q.-H. Fan; J. Pan; L. Gu; A. S. C. Chan *Angew. Chem., Int. Ed.* **2008**, *47*, 8464-8467.
(94) J. B. Aberg; J. S. M. Samec; J.-E. Backvall *Chem. Commun.* **2006**, 2771-2773.
(95) M. Rueping; A. P. Antonchick; T. Theissmann *Angew. Chem., Int. Ed.* **2006**, *45*, 3683-3686.
(96) J. E. D. Martins; G. J. Clarkson; M. Wills *Org. Lett.* **2009**, *11*, 847-850.
(97) C. P. Casey; T. B. Clark; I. A. Guzei *J. Am. Chem. Soc.* **2007**, *129*, 11821-11827.
(98) D. G. Blackmond; M. Ropic; M. Stefinovic *Org. Process Res. Dev.* **2006**, *10*, 457-463.
(99) M. P. Magee; J. R. Norton *J. Am. Chem. Soc.* **2001**, *123*, 1778-1779.
(100) R. Yamaguchi; C. Ikeda; Y. Takahashi; K. Fujita *J. Am. Chem. Soc.* **2009**, *131*, 8410-2.
(101) K. Fujita; C. Kitatsuji; S. Furukawa; R. Yamaguchi *Tetrahedron Lett.* **2004**, *45*, 3215-3217.
(102) A. J. Blacker; M. M. Farah; M. I. Hall; S. P. Marsden; O. Saidi; J. M. J. Williams *Org. Lett.* **2009**, *11*, 2039-2042.
(103) J. H. Koh; H. M. Jeong; J. Park *Tetrahedron Lett.* **1998**, *39*, 5545-5548.
(104) M. Ito; A. Osaku; S. Kitahara; M. Hirakawa; T. Ikariya *Tetrahedron Lett.* **2003**, *44*, 7521-7523.
(105) G. Csjernyik; K. Bogár; J.-E. Bäckvall *Tetrahedron Lett.* **2004**, *45*, 6799-6802.
(106) A. Oku; T.-a. Yokoyama; T. Harada *Tetrahedron Lett.* **1983**, *24*, 4699-4702.
(107) J. S. M. Samec; A. H. Éll; J.-E. Bäckvall *Chem. Eur. J.* **2005**, *11*, 2327-2334.
(108) A. H. Ell; J. S. M. Samec; C. Brasse; J.-E. Backvall *Chem. Commun.* **2002**, 1144-1145.
(109) A. J. Blacker; M. J. Stirling; M. I. Page *Org. Process Res. Dev.* **2007**, *11*, 642-648.
(110) A. J. Blacker; S. Brown; B. Clique; B. Gourlay; C. E. Headley; S. Ingham; D. Ritson; T. Screen; M. J. Stirling; D. Taylor; G. Thompson *Org. Process Res. Dev.* **2009**, *13*, 1370-1378.
(111) B. M. Smith; J. March *Advanced Organic Chemistry*; 5th ed.; Wiley: New York, NY, **2001**.

(112)   R. N. Salvatore; A. S. Nagle; K. W. Jung *J. Org. Chem.* **2002**, *67*, 674-683.
(113)   J. L. Romera; J. M. Cid; A. A. Trabanco *Tetrahedron Lett.* **2004**, *45*, 8797-8800.
(114)   S. Bhattacharyya *J. Org. Chem.* **1995**, *60*, 4928-4929.
(115)   A. F. Abdel-Magid; K. G. Carson; B. D. Harris; C. A. Maryanoff; R. D. Shah *J. Org. Chem.* **1996**, *61*, 3849-3862.
(116)   T. Mizuta; S. Sakaguchi; Y. Ishii *J. Org. Chem.* **2005**, *70*, 2195-2199.
(117)   K. Fujita; Z. Li; N. Ozeki; R. Yamaguchi *Tetrahedron Lett.* **2003**, *44*, 2687-2690.
(118)   K. Fujita; Y. Enoki; R. Yamaguchi *Tetrahedron* **2008**, *64*, 1943-1954.
(119)   R. Yamaguchi; Z. Mingwen; S. Kawagoe; C. Asai; K. Fujita *Synthesis* **2009**, *7*, 1220-1223.
(120)   R. Yamaguchi; S. Kawagoe; C. Asai; K. Fujita *Org. Lett.* **2007**, *10*, 181-184.
(121)   R. Kawahara; K. Fujita; R. Yamaguchi *J. Am. Chem. Soc.* **2010**, *132*, 15108-11.
(122)   O. Saidi; A. J. Blacker; G. W. Lamb; S. P. Marsden; J. E. Taylor; J. M. J. Williams *Org. Process Res. Dev.* **2010**, *14*, 1046-1049.
(123)   O. Saidi; A. J. Blacker; M. M. Farah; S. P. Marsden; J. M. J. Williams *Chem. Commun.* **2010**, *46*, 1541-1543.
(124)   M. H. S. A. Hamid; J. M. J. Williams *Chem. Commun.* **2007**, 725-727.
(125)   M. H. S. A. Hamid; J. M. J. Williams *Tetrahedron Lett.* **2007**, *48*, 8263-8265.
(126)   A. J. A. Watson; A. C. Maxwell; J. M. J. Williams *J. Org. Chem.* **2011**, *76*, 2328-2331.
(127)   M. H. S. A. Hamid; C. L. Allen; G. W. Lamb; A. C. Maxwell; H. C. Maytum; A. J. A. Watson; J. M. J. Williams *J. Am. Chem. Soc.* **2009**, *131*, 1766-1774.
(128)   K. Fujita; K. Yamamoto; R. Yamaguchi *Org. Lett.* **2002**, *4*, 2691-2694.
(129)   K. Fujita; T. Fujii; R. Yamaguchi *Org. Lett.* **2004**, *6*, 3525-3528.
(130)   K. Fujita; Y. Enoki; R. Yamaguchi *Org. Synth.* **2006**, *83*, 217-221.
(131)   K. Fujita; A. Komatsubara; R. Yamaguchi *Tetrahedron* **2009**, *65*, 3624-3628.
(132)   M. Zhu; K. Fujita; R. Yamaguchi *Org. Lett.* **2010**, *12*, 1336-9.
(133)   D. Balcells; A. Nova; E. Clot; D. Gnanamgari; R. H. Crabtree; O. Eisenstein *Organometallics* **2008**, *27*, 2529-2535.
(134)   A. J. A. Watson; A. C. Maxwell; J. M. J. Williams *Org. Lett.* **2009**, *11*, 2667-2670.
(135)   G. D. Williams; R. A. Pike; C. E. Wade; M. Wills *Org. Lett.* **2003**, *5*, 4227-4230.
(136)   M. Watanbe; J. Hori; K. Murata, patent number US 2010/0234596 A1, **2010**
(137)   C. Wang; H.-Y. T. Chen; J. Bacsa; C. R. A. Catlow; J. Xiao *Dalton Trans.* **2013**, *42*, 935-940.
(138)   T. C. Nugent; M. El-Shazly *Adv. Synth. Catal.* **2010**, *352*, 753-819.
(139)   K. Fujita; C. Asai; T. Yamaguchi; F. Hanasaka; R. Yamaguchi *Org. Lett.* **2005**, *7*, 4017-4019.
(140)   C. S. Cho; B. T. Kim; H.-S. Kim; T.-J. Kim; S. C. Shim *Organometallics* **2003**, *22*, 3608-3610.
(141)   M. G. Edwards; J. M. J. Williams *Angew. Chem., Int. Ed.* **2002**, *41*, 4740-4743.
(142)   P. J. Black; M. G. Edwards; J. M. J. Williams *Eur. J. Org. Chem.* **2006**, *2006*, 4367-4378.
(143)   G. Cami-Kobeci; J. M. J. Williams *Chem. Commun.* **2004**, *0*, 1072-1073.

(144) A. A. Bisset; A. Shiibashi; J. L. Desmond; A. Dishington; T. Jones; G. J. Clarkson; T. Ikariya; M. Wills *Chem. Commun.* **2012**, *48*, 11978-11980.
(145) N. A. Owston; A. J. Parker; J. M. J. Williams *Org. Lett.* **2006**, *9*, 73-75.
(146) P. McMorn; G. J. Hutchings *Chem. Soc. Rev.* **2004**, *33*, 108-122.
(147) X. Zheng; L. Zhang; J. Li; S. Luo; J.-P. Cheng *Chem. Commun.* **2011**, *47*, 12325-12327.
(148) A. J. Blacker In *The Handbook of Homogeneous Hydrogenation*; Wiley-VCH Verlag GmbH, **2008**.
(149) J. M. Fraile; J. I. García; J. A. Mayoral *Chem. Rev.* **2008**, *109*, 360-417.
(150) C. Merckle; J. Blümel *Top. Catal.* **2005**, *34*, 5-15.
(151) U. Schubert; K. Rose *Transition Met. Chem.* **1989**, *14*, 291-294.
(152) A. M. Segarra; F. Guirado; C. Claver; E. Fernandez *Tetrahedron: Asymmetry* **2003**, *14*, 1611-1615.
(153) A. M. Segarra; R. Guerrero; C. Claver; E. Fernández *Chem. Eur. J.* **2003**, *9*, 191-200.
(154) B. Beele; J. Guenther; M. Perera; M. Stach; T. Oeser; J. Blümel *New J. Chem.* **2010**, *34*, 2729-2731.
(155) C. Merckle; J. Blümel *Adv. Synth. Catal.* **2003**, *345*, 584-588.
(156) C. Merckle; S. Haubrich; J. Blümel *J. Organomet. Chem.* **2001**, *627*, 44-54.
(157) Y. Liang; Q. Jing; X. Li; L. Shi; K. Ding *J. Am. Chem. Soc.* **2005**, *127*, 7694-7695.
(158) Y. Xu; T. Cheng; J. Long; K. Liu; Q. Qian; F. Gao; G. Liu; H. Li *Adv. Synth. Catal.* **2012**, *354*, 3250-3258.
(159) J. D. Ribeiro de Campos; R. Buffon *New J. Chem.* **2003**, *27*, 446-451.
(160) Y. Brunsch; A. Behr *Angew. Chem., Int. Ed.* **2012**, *52*, 1586-1589.
(161) Y. Yang; N. Priyadarshani; T. Khamatnurova; J. Suriboot; D. E. Bergbreiter *J. Am. Chem. Soc.* **2012**, *134*, 14714-14717.
(162) M. Mokhadinyana; S. L. Desset; D. B. G. Williams; D. J. Cole-Hamilton *Angew. Chem., Int. Ed.* **2012**, *51*, 1648-1652.
(163) Y. Arakawa; N. Haraguchi; S. Itsuno *Tetrahedron Lett.* **2006**, *47*, 3239-3243.
(164) D. J. Bayston; C. B. Travers; M. E. C. Polywka *Tetrahedron: Asymmetry* **1998**, *9*, 2015-2018.
(165) Y.-C. Chen; T.-F. Wu; J.-G. Deng; H. Liu; X. Cui; J. Zhu; Y.-Z. Jiang; M. C. K. Choi; A. S. C. Chan *J. Org. Chem.* **2002**, *67*, 5301-5306.
(166) L. Jiang; T.-F. Wu; Y.-C. Chen; J. Zhu; J.-G. Deng *Org. Biomol. Chem.* **2006**, *4*, 3319-3324.
(167) X. Li; X. Wu; W. Chen; F. E. Hancock; F. King; J. Xiao *Org. Lett.* **2004**, *6*, 3321-3324.
(168) P. N. Liu; J. G. Deng; Y. Q. Tu; S. H. Wang *Chem. Commun.* **2004**, 2070-2071.
(169) P.-N. Liu; P.-M. Gu; J.-G. Deng; Y.-Q. Tu; Y.-P. Ma *Eur. J. Org. Chem.* **2005**, *2005*, 3221-3227.
(170) G. Liu; J. Wang; T. Huang; X. Liang; Y. Zhang; H. Li *J. Mater. Chem.* **2010**, *20*, 1970-1975.
(171) R. ter Halle; E. Schulz; M. Lemaire *Synlett* **1997**, 1257-1258.
(172) P. N. Liu; P. M. Gu; F. Wang; Y. Q. Tu *Org. Lett.* **2003**, *6*, 169-172.
(173) X. Li; W. Chen; W. Hems; F. King; J. Xiao *Org. Lett.* **2003**, *5*, 4559-4561.
(174) Y. Sun; G. Liu; H. Gu; T. Huang; Y. Zhang; H. Li *Chem. Commun.* **2011**, *47*, 2583-2585.
(175) N. Haraguchi; K. Tsuru; Y. Arakawa; S. Itsuno *Org. Biomol. Chem.* **2009**, *7*,

69-75.

(176)   H. Zhang; R. Jin; H. Yao; S. Tang; J. Zhuang; G. Liu; H. Li *Chem. Commun.* **2012**, *48*, 7874-7876.

(177)   S. Bastin; R. J. Eaves; C. W. Edwards; O. Ichihara; M. Whittaker; M. Wills *J. Org. Chem.* **2004**, *69*, 5405-5412.

(178)   X. Li; W. Chen; W. Hems; F. King; J. Xiao *Tetrahedron Lett.* **2004**, *45*, 951-953.

(179)   J. Blacker; K. Treacher; T. Screen, patent number WO 2009/093059 A2, **2009**

Chapter 2   Functionalised Cp* Based Ligands and Their Metal Complexes

2.1 Introduction

This Chapter is concerned with the synthesis and characterisation of hydroxyl tethered Cp* based ligands and their complexation to both rhodium and iridium to form tethered versions of $[MCp*X_2]_2$, where M = Ir, Rh and X = Cl, I. The hydroxyl group provides a linker to attach the dimer onto a solid support, which can then be used as a recyclable immobilised catalyst (discussed in Chapter 7). The addition of these hydroxyl tethers also gives rise to interesting anti-cancer activity of the complexes (discussed in Chapter 8).

Tethered hydroxyl Cp* based ligands were first prepared and complexed onto rhodium and iridium by Blacker *et al.*[1,2] The iridium iodide dimer **2.13** was immobilised onto polyethylene glycol and used as a racemisation catalyst in a semi-continuous process to resolve racemic sertraline (discussed in more detail in Chapter 1).[2] Iridium and rhodium complexes with amine tethered Cp* based ligands have been reported.[3,4] Triflylamide tethered Cp* based ligands have also been reported and tested as catalysts for the asymmetric hydrogenation of acetophenone.[5]

A list of compounds discussed in this Chapter is shown in **Figure 2.1**, with full experimental details described in Chapter 9. Compounds **2.2**, **2.6**, **2.10** and **2.13** have been prepared previously.[1,2]

		M = Rh, X = Cl	M = Ir, X = Cl	M = Ir, X = I
2.1	n = 3	**2.5** n = 3	**2.9** n = 3	**2.13** n = 5
2.2	n = 5	**2.6** n = 5	**2.10** n = 5	
2.3	n = 9	**2.7** n = 9	**2.11** n = 9	
2.4	n = 14	**2.8** n = 14	**2.12** n = 14	
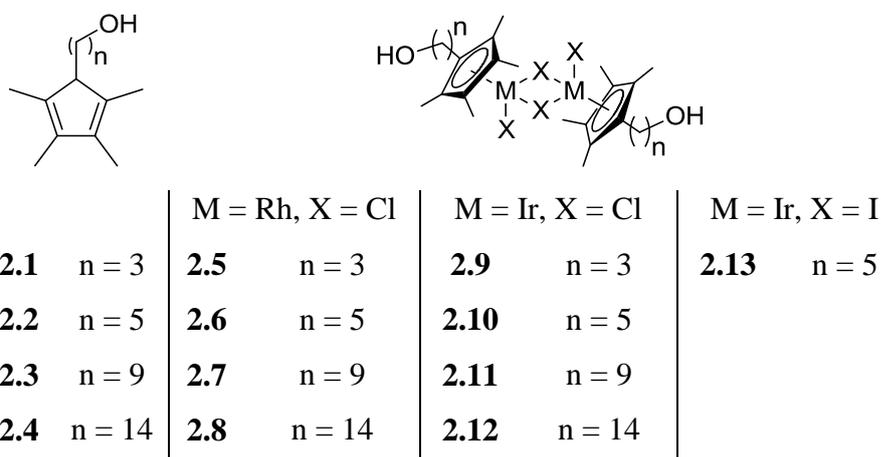
Figure 2.1 List of compounds discussed in Chapter 2

2.2 Synthesis of Hydroxyl Tethered Cp* Based Ligands

The ligands **2.1**-**2.4** were prepared according to **Scheme 1.1**. 2-Bromo-2-butene was reacted with lithium under dry conditions. The lactone with n+1 carbons was added to the resulting lithiated alkene, followed by HCl to give the hydroxyl tethered

ligand with n carbons in the tether.
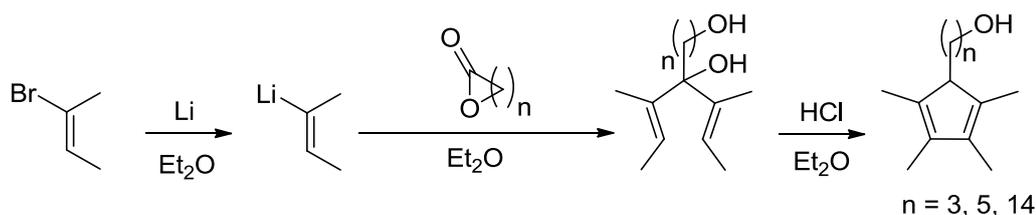
Scheme 1.1 General synthesis of hydroxyl tethered ligands **2.1**-**2.4**

The lactone with n = 9 is not commercially available, so the 9 carbon tethered ligand **2.3** was prepared according to **Scheme 1.2**. The alcohol group on methyl 10-hydroxydecanoate is sensitive to the lithiation step in the ligand synthesis, so was initially protected with a TMS group. The resulting ester was used in the place of the lactone. The TMS group was removed in the acidification step, eliminating the need for an extra step to deprotect the hydroxyl.
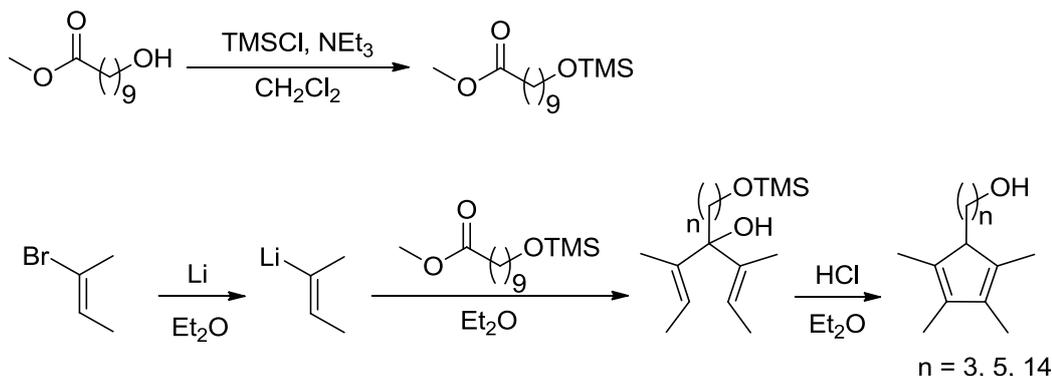
Scheme 1.2 Synthesis of **2.3**

2.3 Synthesis of Hydroxyl Tethered Cp* Based Rhodium Chloride Dimers

The rhodium dimers **2.5**-**2.8** were prepared by refluxing $RhCl_3.3H_2O$ with ligands **2.1**-**2.4** respectively, in methanol overnight.
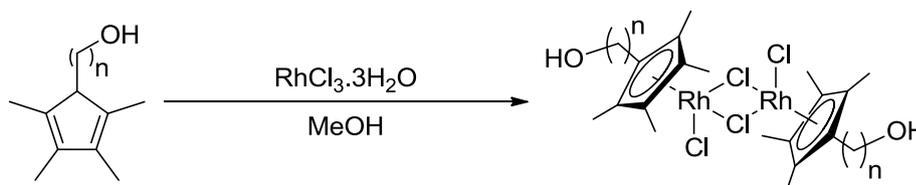
Scheme 1.3 General synthesis of rhodium dimers **2.5-2.8**

The resulting deep red solution was evaporated to dryness and the crude product recrystallised using a dichloromethane/hexane solvent system, to give the dimers as

orange/red powders. The dimers were characterised by ^{1}H and ^{13}C{^{1}H} NMR, elemental analysis and in the cases of **2.5**, **2.6** and **2.7**, single crystal X-ray crystallography.

2.3.1 NMR Characterisation of Rhodium Dimers

Upon complexation of the Cp* based ligands to rhodium, the ^{1}H NMR simplifies due to a loss of regioisomerism, and loss of the proton on the allylic carbon (~1.0 ppm), shown in **Figure 1.2**.
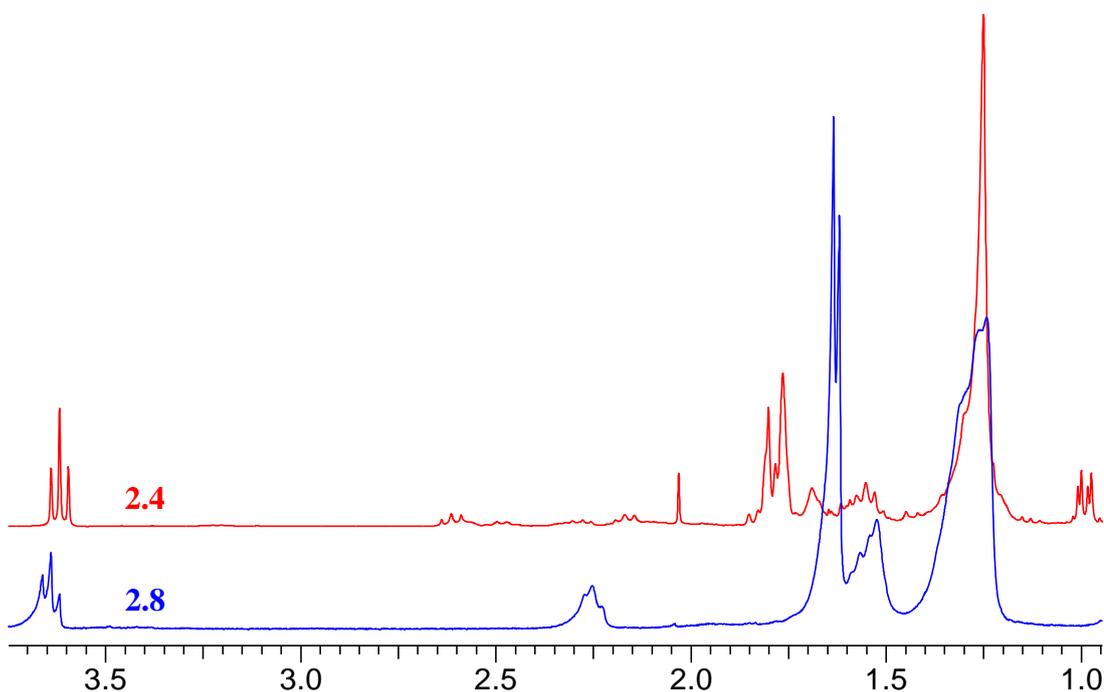
Figure 1.2 NMR spectra of starting ligand **2.4** and its resulting rhodium complex **2.8**

The CH$_2$ protons adjacent to the OH appear as either a triplet or a broad singlet between 3.63 and 3.66 ppm (depending on the chain length) in the ^{1}H NMR spectrum. The CH$_2$ protons adjacent to the functionalised Cp* ring appear as a multiplet between 2.2 and 2.4 ppm. The peaks for the protons of other CH$_2$ groups in the chain vary between 1.2 and 1.8 ppm, and the CH$_3$ protons on the functionalised Cp* ring appear between 1.61 and 1.65 ppm. In the ^{13}C{^{1}H} NMR spectra of the rhodium dimers **2.5**-**2.8**, ^1J coupling is seen between the functionalised Cp* carbons and the spin active ^{103}Rh, appearing as 3 doublets between 94 and 96 ppm with a splitting of 9-10 Hz (shown in **Figure 1.3**). The CH$_2$ adjacent to the OH appears at about 63 ppm. The other CH$_2$ groups appear between 20 and 33 ppm, and the CH$_3$ groups on the functionalised Cp* ring appear at 9.4 ppm.
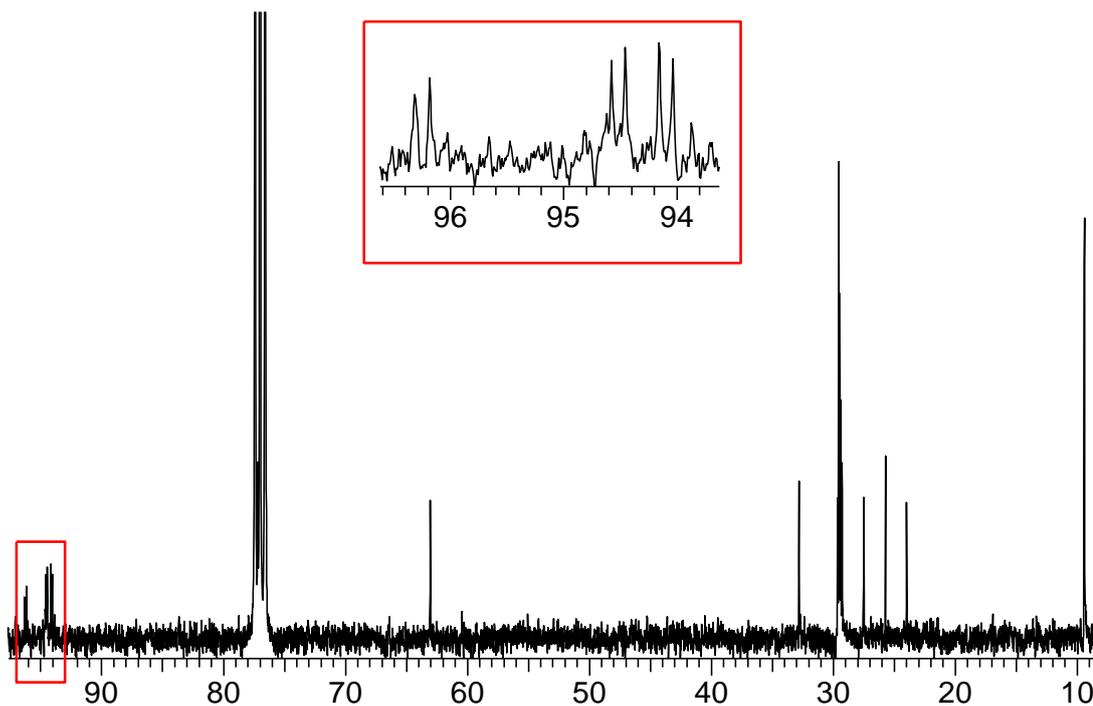
Figure 1.3 ^{13}C{^{1}H} NMR spectra of rhodium complex **2.8** with an expansion to show the functionalised Cp* peaks

2.3.2 X-ray Crystallography Data for Rhodium Dimers

The three dimers **2.5**, **2.6** and **2.7** all crystallise in a monoclinic cell and contain half a molecule in the asymmetric unit. The rhodium centres have a pseudo-octahedral geometry whereby the functionalised Cp* ring occupies three coordination sites and the three chlorides occupy a coordination site each. In all three cases there is a hydrogen bond between the hydroxyl tether and a terminal chloride ligand, with **2.5** and **2.7** showing the same hydrogen bond arrangement (**Figure 1.4**)

a)

b)
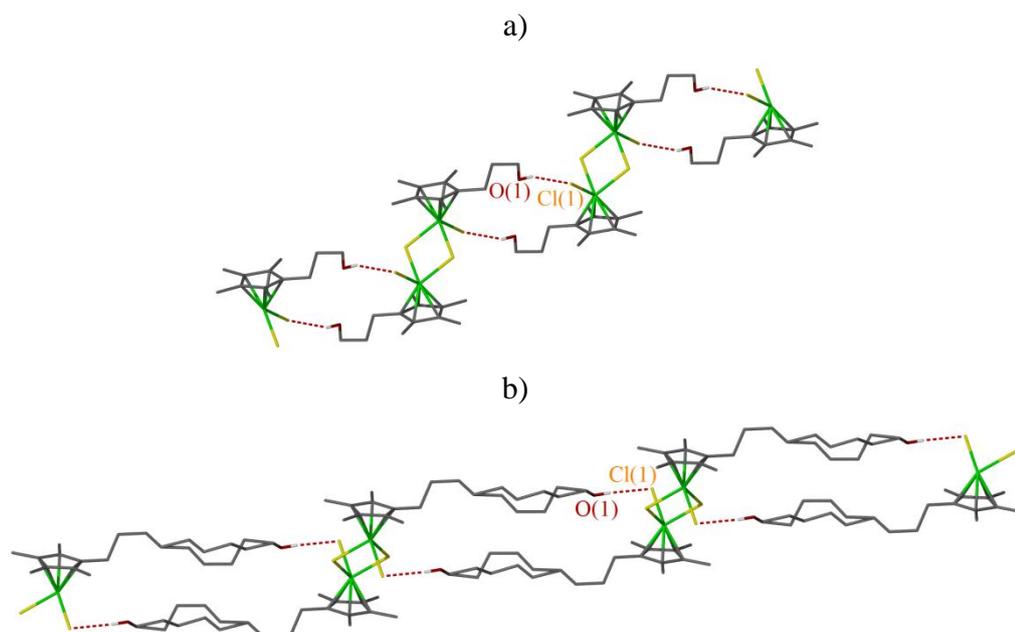
Figure 1.4 Packing diagram of compounds **a) 2.5** and **b) 2.7** to show intermolecular hydrogen bonding between the hydroxyl group and terminal chloride

2.3.2.1 X-ray Crystallography Data for Compound 2.5

Red crystals of compound **2.5** suitable for X-ray crystallography were obtained *via* layer diffusion of hexane into a dichloromethane solution. The structural solution was performed in the space group *P2₁/n*. The molecular structure is shown in **Figure 1.5** and selected bond lengths and angles are shown in **Table 1.1**. There is a hydrogen bond between the OH and Cl(1) of an adjacent molecule with a O(1)..Cl(1) distance of 3.234(2) Å, and symmetry operation of 2-x,-y,1-z, shown in **Figure 1.4**.
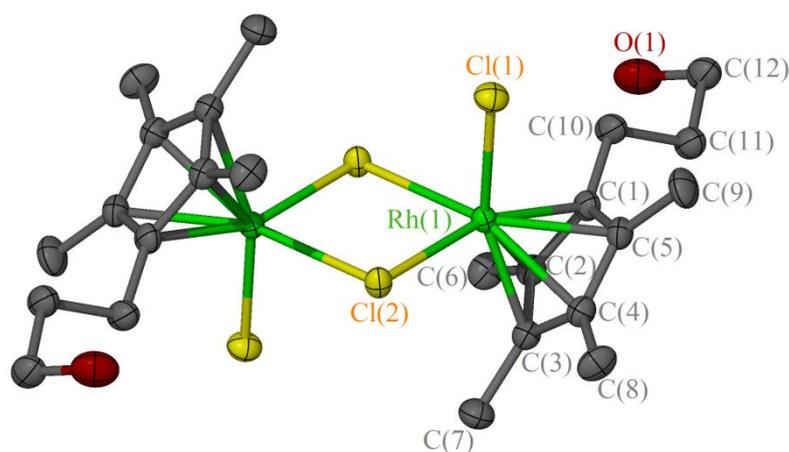
Figure 1.5 A crystal structure of compound **2.5**, displacement ellipsoids are at the 50% probability level. Hydrogen atoms are omitted for clarity.

Bond	Distance (Å)	Bond	Angle (°)
Rh(1)-Cl(1)	2.4341(7)	Cl(1)-Rh(1)-Cl(2)	89.70(2)
Rh(1)-Cl(2)	2.4775(6)	Cl(1)-Rh(1)-Cl(2)[a]	90.51(2)
Rh(1)-Cl(2')[a]	2.4857(6)	Cl(2)-Rh(1)-Cl(2)[a]	83.20(2)
Rh(1)-C$_g$	1.7739(11)	Rh(1)-Cl(2)-Rh(1)[a]	96.80(2)

[a] = 1-x,1-y,1-z

Table 1.1 Selected bond lengths and bond angles for compound **2.5**

2.3.2.2 X-ray Crystallography Data for compound 2.6

Red crystals of compound **2.6** suitable for X-ray crystallography were obtained *via* vapour diffusion from a dichloromethane/pentane solvent system. The structural solution was performed in the space group *P2₁/n*. The molecular structure is shown in **Figure 1.6** and selected bond lengths and angles are shown in **Table 1.2**.
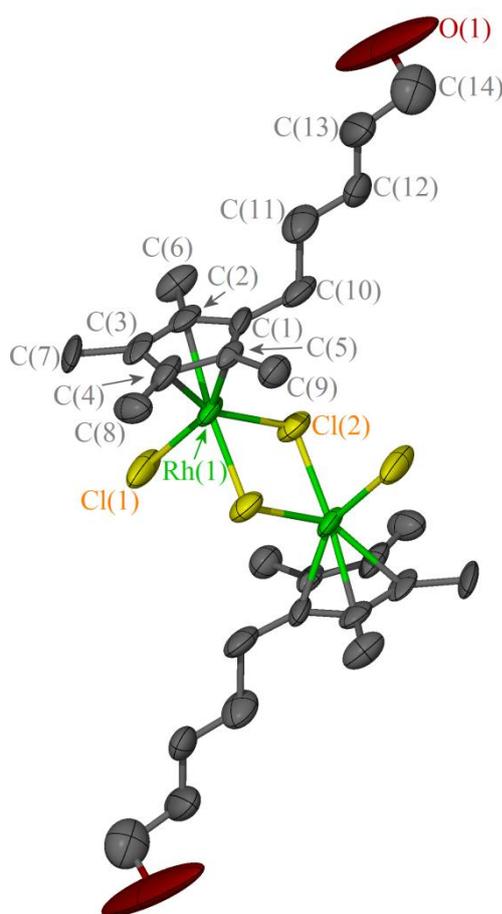
Figure 1.6 A crystal structure of compound **2.6**, displacement ellipsoids are at the 50% probability level. Hydrogen atoms are omitted for clarity.

Bond	Distance (Å)	Bond	Angle (°)
Rh(1)-Cl(1)	2.445(5)	Cl(1)-Rh(1)-Cl(2)	89.4(2)
Rh(1)-Cl(2)	2.468(6)	Cl(1)-Rh(1)-Cl(2)[(a)]	89.56(17)
Rh(1)-Cl(2')[(a)]	2.480(4)	Cl(2)-Rh(1)-Cl(2)[(a)]	84.20(16)
Rh(1)-C$_g$	1.784(8)	Rh(1)-Cl(2)-Rh(1)[(a)]	95.80(18)

[(a)] = -x,-y,1-z

Table 1.2 Selected bond lengths and bond angles for compound **2.6**

The equivalent iridium iodide analogue, reported by Blacker *et al*, crystallised in a triclinic $P\,\bar{1}$ cell with three molecules in the asymmetric unit and similar bond angles.[2]

2.3.2.3 X-ray Crystallography Data for compound 2.7

Red crystals of compound **2.7** suitable for X-ray crystallography were obtained *via* vapour diffusion from a dichloromethane/pentane solvent system. The structural solution was performed in the space group *C2/c*. The asymmetric unit contains a molecule of dichloromethane with half a molecule of **2.7**. The molecular structure is shown in **Figure 1.7** and selected bond lengths and angles are shown in **Table 1.3**. The chain shows disorder with the atoms C14-C17 split into two parts (A and B), both with 50% occupancy.
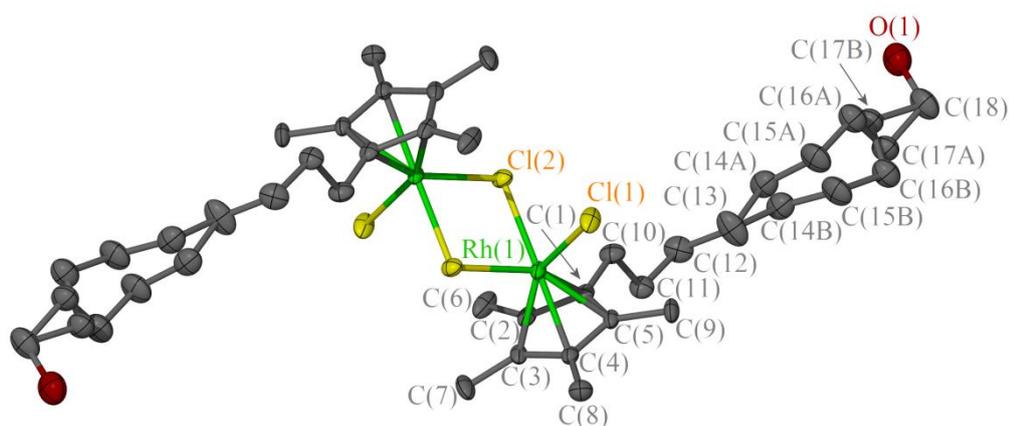
Figure 1.7 A crystal structure of compound **2.7**, displacement ellipsoids are at the 50% probability level. Hydrogen atoms are omitted for clarity.

Bond	Distance (Å)	Bond	Angle (°)
Rh(1)-Cl(1)	2.4353(8)	Cl(1)-Rh(1)-Cl(2)	90.15(2)
Rh(1)-Cl(2)	2.4693(7)	Cl(1)-Rh(1)-Cl(2)$^{(a)}$	89.88(3)
Rh(1)-Cl(2')$^{(a)}$	2.4776(9)	Cl(2)-Rh(1)-Cl(2)$^{(a)}$	83.48(2)
Rh(1)-C$_g$	1.7691(11)	Rh(1)-Cl(2)-Rh(1)$^{(a)}$	96.52(3)

$^{(a)}$ = 1/2-x,1/2-y,1-z

Table 1.3 Selected bond lengths and bond angles for compound **2.7**

Packing diagrams of compound **2.7** are shown in **Figure 1.8**. As can be seen when looking down the b axis, the dimer packs in layers resulting in hydrophobic regions of alkyl chains. There is a void between the alkyl tethers which is filled by dichloromethane molecules. **Figure 1.4** shows the hydrogen bond between the hydroxyl group on the functionalised Cp* tether (O14) and a terminal chloride on an adjacent molecule (Cl1) with a O(1)..Cl(1) distance of 3.322(3) Å and symmetry operation of -x,1-y,-z.
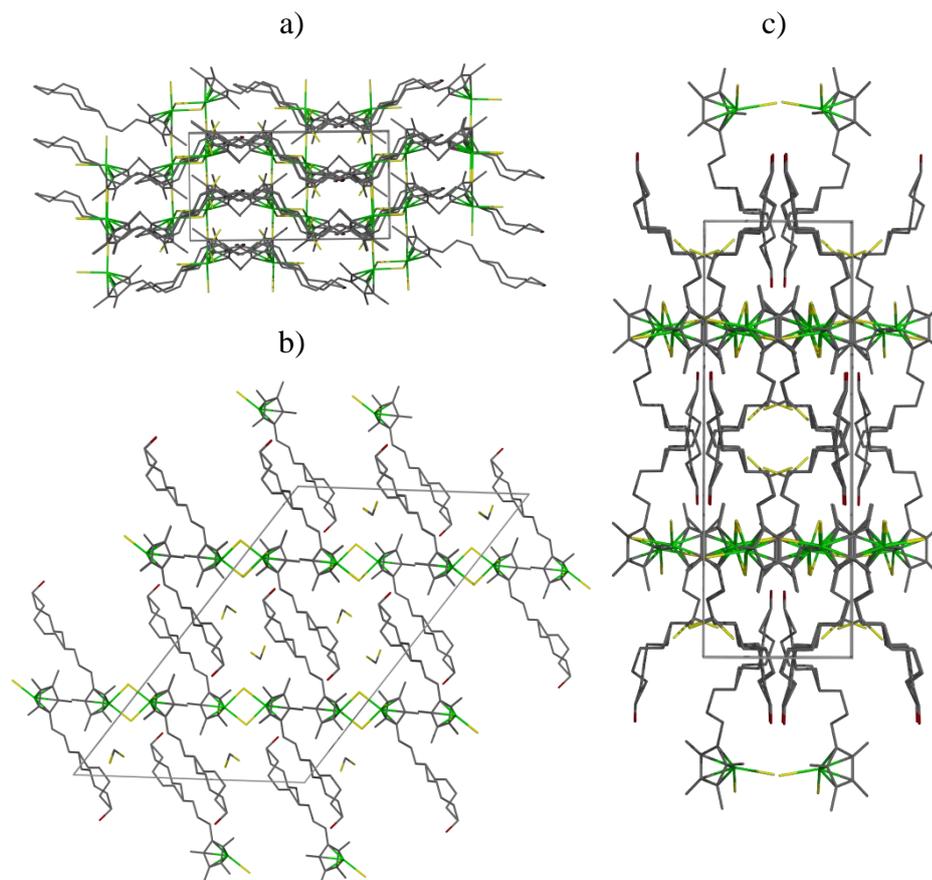
Figure 1.8 Packing diagram of compound **2.7**, shown down a) the a axis, b) the b axis and c) the c axis. Hydrogen atoms omitted for clarity

2.4 Synthesis of Hydroxyl Tethered Cp* Based Iridium Chloride Dimers

The iridium chloride dimers **2.9**-**2.12** were prepared by applying microwave heating to $IrCl_3.3H_2O$ with $NaHCO_3$ and ligands **2.1**-**2.4** respectively in methanol for 10 minutes. The resulting red solution was diluted with dichloromethane and, after an aqueous work up, the crude product was dissolved in dichloromethane and precipitated with hexane to give the dimers as orange powders. The dimers were characterised by ^{1}H NMR, ^{13}C{^{1}H} NMR and CHN analysis.
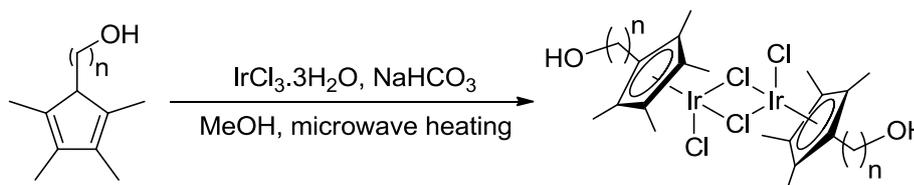
Scheme 1.4 General synthesis of iridium dimers **2.9**-**2.12**

2.4.1 NMR Characterisation of Iridium Chloride Dimers

As expected, the ^{1}H NMR spectra of the iridium dimers (**Figure 1.9**) are similar to their rhodium analogues **2.5**-**2.8**, except the chemical shifts appear slightly more upfield, for example the methyl protons appear between 1.58-1.62 ppm *cf.* 1.61-1.65 ppm for the rhodium analogues.
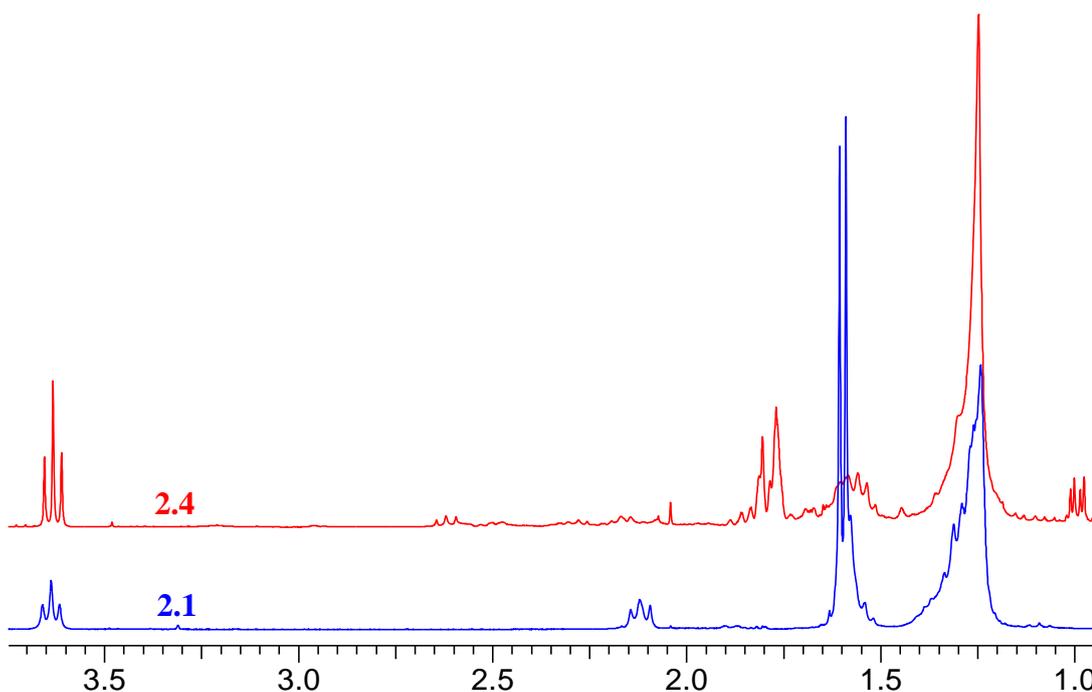
Figure 1.9 ^{1}H NMR spectra of ligand **2.4** and its resulting iridium complex **2.12**

The CH$_2$ protons adjacent to the OH appear as a triplet between 3.64 and 3.66 ppm. The CH$_2$ protons adjacent to the functionalised Cp* ring shift upfield *cf.* their rhodium analogues appearing between 2.1-2.3 ppm *cf.* 2.2-2.4 ppm. The peaks for the protons of other CH$_2$ groups in the chain vary between 1.2 and 1.8 ppm. As for the rhodium analogues, three peaks are seen in the ^{13}C{^{1}H} NMR spectra for the iridium dimers. These appear between 86-88 ppm *cf.* 94-96 ppm for the rhodium analogues. The other carbon peaks seem relatively unaffected compared to their rhodium analogues.

2.5 Synthesis of Hydroxyl Tethered Cp* Based Iridium Iodide Dimers

The iridium iodide dimer **2.13** was prepared by performing a halide exchange reaction using sodium iodide and the iridium chloride dimer **2.10** (**Scheme 1.5**) as shown previously by Blacker *et al.*[2] The reaction was performed in acetone as the insolubility of the NaCl formed drives the reaction to completion. There is a noticeable shift of the methyl groups on the functionalised Cp* ring from 1.6 to 1.9 ppm indicating full conversion. The product formed is a deep red powder *cf.* the starting orange powder. As compound **2.13** has been previously reported, it will not be discussed any further here.
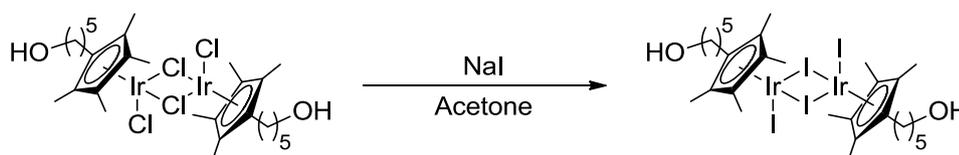
Scheme 1.5 Synthesis of the iridium iodide dimer **2.13**

2.6 Conclusion

Four tethered hydroxyl tethered Cp* based ligands have been prepared and complexed onto both rhodium and iridium to form tethered versions of [RhCp*Cl$_2$]$_2$ and [IrCp*Cl$_2$]$_2$ respectively. The rhodium dimers were prepared in the same manner as [RhCp*Cl$_2$]$_2$ by heating the ligand with RhCl$_3$. More forcing conditions, involving microwave heating, were required to form the iridium chloride dimers. As for [IrCp*Cl$_2$]$_2$, a halide exchange reaction can be performed to transform the iridium chloride dimer into its iodide analogue. These tethered dimers can be immobilised onto a solid support for use as recyclable catalysts, with the results discussed in

Chapter 7. They have been used as starting materials to form monomeric complexes, discussed in Chapter 3 and Chapter 4. The tether also has an interesting effect on the anti-cancer activity, with preliminary results shown in Chapter 8.

2.7 References

(1)   J. Blacker; K. Treacher; T. Screen, patent number WO 2009/093059 A2, **2009**
(2)   A. J. Blacker; S. Brown; B. Clique; B. Gourlay; C. E. Headley; S. Ingham; D. Ritson; T. Screen; M. J. Stirling; D. Taylor; G. Thompson *Org. Process Res. Dev.* **2009**, *13*, 1370-1378.
(3)   T. Reiner; D. Jantke; A. Raba; A. N. Marziale; J. r. Eppinger *J. Organomet. Chem.* **2009**, *694*, 1934-1937.
(4)   M. Ito; N. Tejima; M. Yamamura; Y. Endo; T. Ikariya *Organometallics* **2010**, *29*, 1886-1889.
(5)   M. Ito; Y. Endo; N. Tejima; T. Ikariya *Organometallics* **2010**, *29*, 2397-2399.

Chapter 3 Synthesis of Group 9 Cp* and Functionalised Cp* Pyridine Halide Complexes

3.1 Introduction

This Chapter is concerned with the synthesis and characterisation of iridium/rhodium Cp* and hydroxyl tethered Cp*-based pyridine halide complexes. These complexes have been prepared for use as homogeneous catalysts for transfer hydrogenation reactions, with their catalytic activity discussed in Chapter 5. It is generally thought when using $[MCp*X_2]_2$ (where M = Ir or Rh and X = Cl or I) in transfer hydrogenation reactions that the dimer is a precatalyst and that the active catalyst is a monomeric species.

Group 9 Cp* pyridine complexes have been previously reported,[1-10] with some used as catalysts.[11-17] Fujita reported 2-hydroxypyridine iridium Cp* complexes and found them to be active catalysts for the dehydrogenation of secondary alcohols to their corresponding ketones,[18] as well as reversible dehydrogenation-hydrogenation reactions of nitrogen heterocycles (discussed in more detail in Chapter 1).[19]

3.1	R = H	**3.7**	n = 3, R = H	**3.14**	**3.15**	R = H
3.2	R = 3'-F	**3.8**	n = 5, R = H		**3.16**	R = 3'-Cl
3.3	R = 3'-Cl	**3.9**	n = 14, R = H		**3.17**	R = 3'-Br
3.4	R = 3'-Br	**3.10**	n = 5, R = 3'-Cl			
3.5	R = 3'-I	**3.11**	n = 5, R = 3'-Br			
3.6	R = 4'-NMe$_2$	**3.12**	n = 5, R = 3'-I			
		3.13	n = 5, R = 4'-Me			
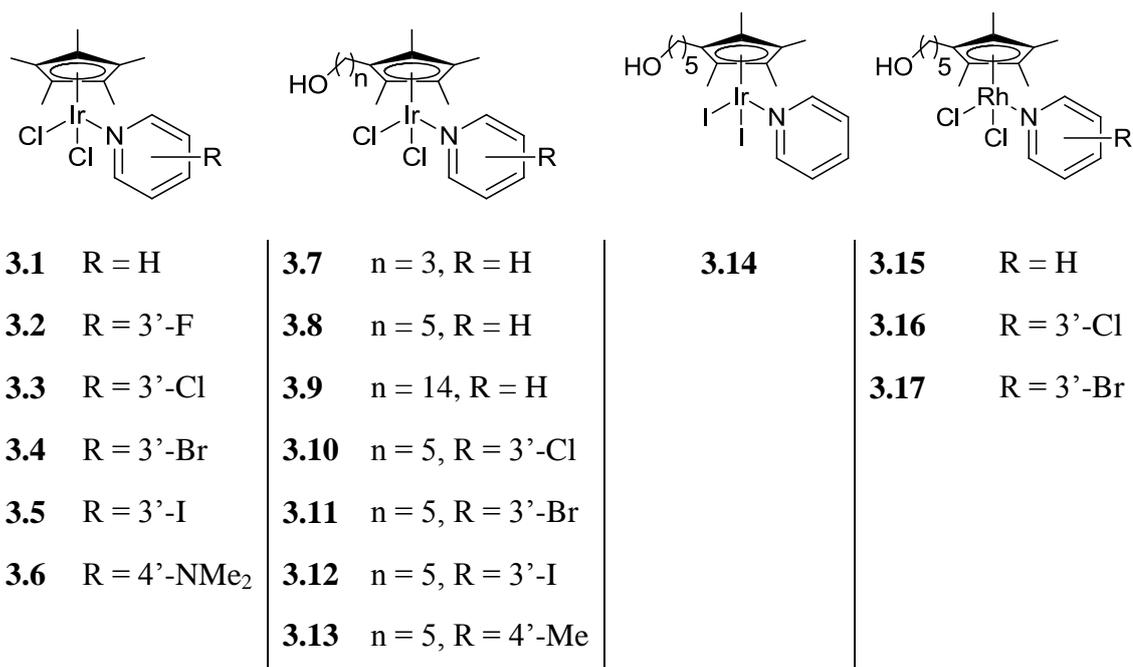
Figure 3.1 List of compounds discussed in Chapter 3

A list of compounds discussed in this Chapter is shown in **Figure 3.1**, with full experimental details described in Chapter 9. All of the pyridine complexes were prepared by reacting the corresponding dimer with the functionalised pyridine. Compound **3.1** has been previously reported, so its synthesis and characterisation will not be discussed here.[20]

All complexes were characterised by ^1H and $^{13}C\{^1H\}$ NMR, elemental analysis

(compound **3.12** and **3.13** are not analatically pure) and in the cases of compounds **3.2**, **3.3**, **3.6**-**3.8**, **3.11**, and **3.15**-**3.17** single crystal X-ray crystallography. There is a general shift in the ^{1}H NMR spectrum of the pyridine proton peaks downfield indicating complexation.

3.2 Synthesis of Iridium Cp* Dichloride Pyridine Complexes

The iridium Cp* pyridine complexes **3.2**-**3.5** were prepared according to **Scheme 3.1**, by stirring [IrCp*Cl$_2$]$_2$ with 2 equivalents of the functionalised pyridine in tetrahydrofuran overnight. The resulting yellow suspension was filtered and recrystallised using vapour diffusion from a dichloromethane/pentane solvent system. Compound **3.6** was prepared by stirring [IrCp*Cl$_2$]$_2$ with 2 equivalents of the functionalised pyridine in dichloromethane overnight.
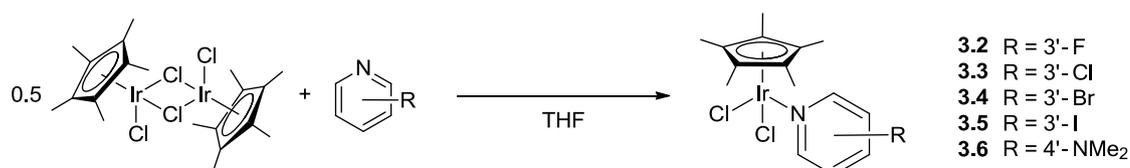
Scheme 3.1 General synthesis of iridium Cp* dichloride pyridine complexes

3.2.1 NMR Characterisation of Iridium Cp* Pyridine Monomers

Upon complexation of the pyridine to [IrCp*Cl$_2$]$_2$, the pyridine peaks shift downfield and the CH$_3$ groups on the Cp* ring shift upfield from 1.59 to 1.55 in the case of **3.2** and to 1.54 in the cases of **3.3**-**3.6** (shown in **Figure 3.3** for compound **3.2**). The chemical shifts of the pyridine proton f increases, going from **3.5**-**3.2** (protons assigned in **Figure 3.2**).
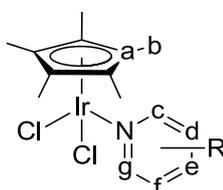
Figure 3.2 Labelled diagram for iridium Cp* pyridine complexes

The reverse trend is seen for the chemical shift of the protons at positions c, e and g. In comparison to the unsubstituted pyridine complex **3.1**, addition of the electron donating NMe$_2$ group, results in an upfield shift of the c (equivalent to g) and d (equivalent to f) protons in the ^{1}H NMR spectrum (demonstrated in **Figure 3.4**).
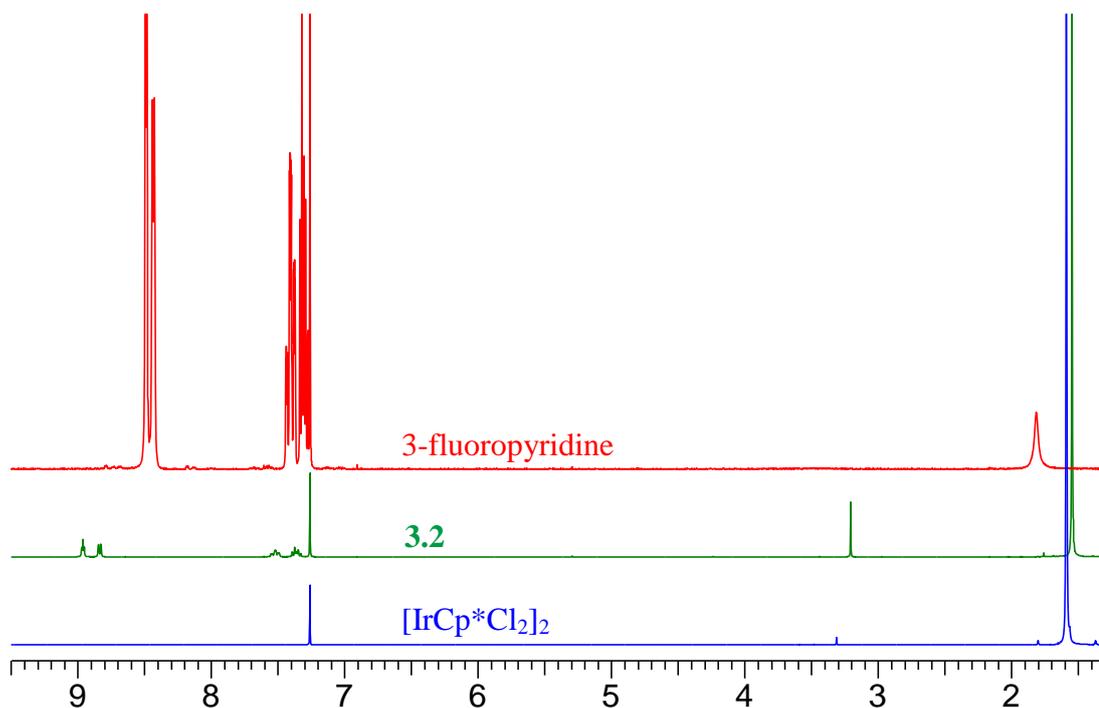
Figure 3.3 Comparison of the ^{1}H NMR spectra of compound **3.2** compared to its precursors, [IrCp*Cl$_2$]$_2$ and 3-fluoropyridine
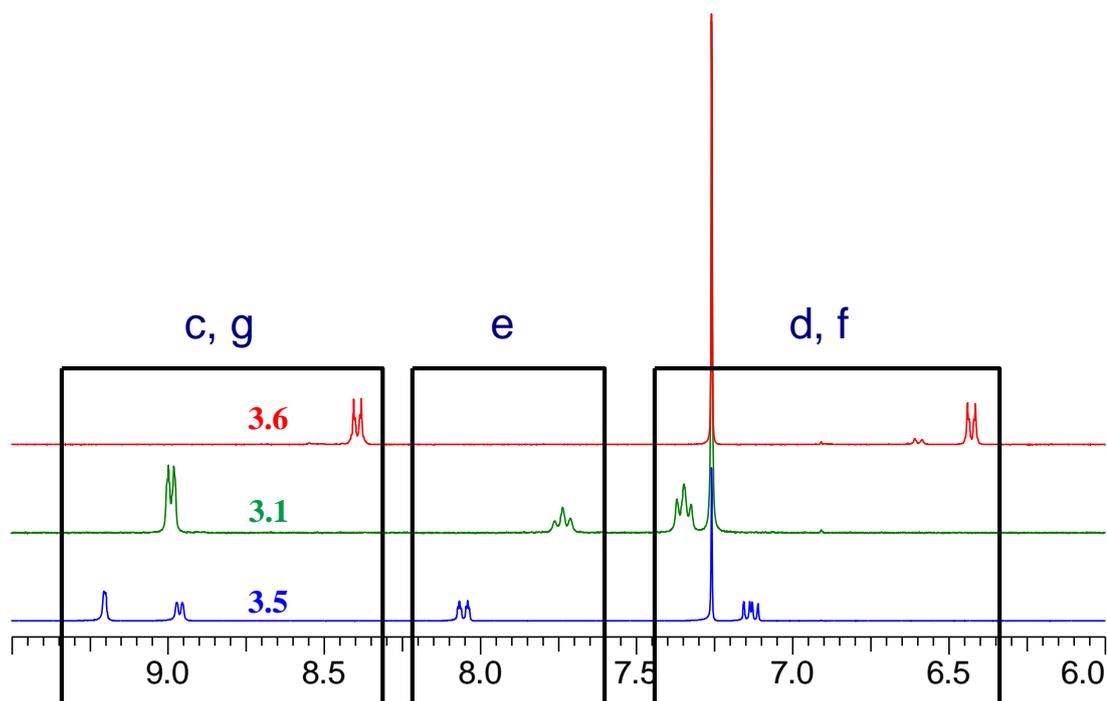
Figure 3.4 Comparison of the ^{1}H NMR spectrum of the aromatic regions of **3.1**, **3.5** and **3.6**

3.2.2 X-ray Crystallography Data for Iridium Cp* Pyridine Monomers

Single crystals of compounds **3.2**, **3.3** and **3.6** were obtained *via* vapour diffusion from a dichloromethane/pentane solvent system giving yellow crystals in the case of compound **3.2** and orange crystals of compounds **3.3** and **3.6**. In all cases the iridium centres have pseudo octahedral geometries whereby the Cp* occupies three coordination sites and the two chlorides and pyridine occupy a coordination site each. Although compounds **3.2** and **3.3** are in different space groups, they pack similarly, most easily seen when viewed from the a axis (**Figure 3.5**), with the molecules packing in anti parallel layers. The molecules have similar bond lengths apart from the Ir-Cl bonds which are 2.4267(5) Å for compound **3.2** and 2.4227(6)/ 2.4111(6) for compound **3.3**. Compound **3.3** is more largely distorted away from pseudo octahedral geometry than compound **3.2** with the angles between the chlorides and nitrogen ranging from 86-88° (compared to 87-91° for compound **3.2**), presumably due to the extra steric bulk from the chloride on the pyridine ring.
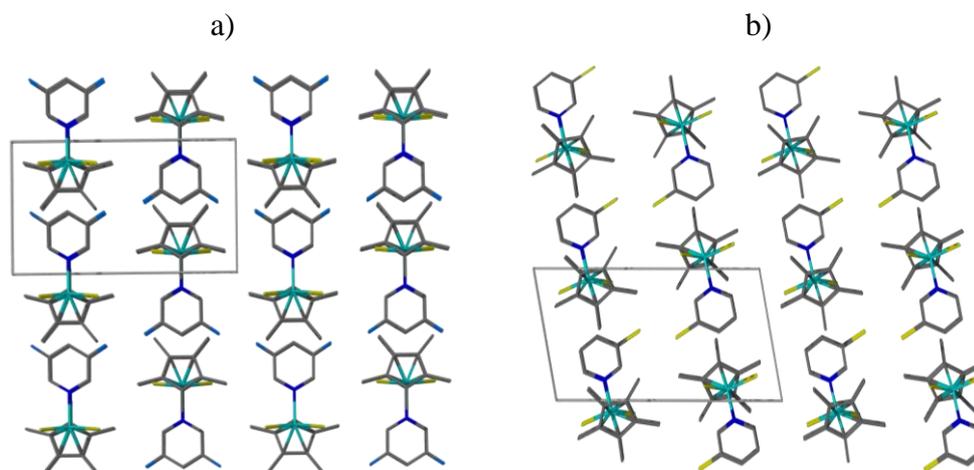
Figure 3.5 a) Compounds **3.2** and **b) 3.3** viewed down the a axis

3.2.2.1 X-ray Crystallography Data for Compound 3.2

Compound **3.2** was solved in a monoclinic cell and structural solution was performed in the space group *P2₁/m*. The molecular structure is shown in **Figure 3.6** and selected bond lengths and angles in **Table 3.1**. There is half a molecule in the asymmetric unit, where the symmetry generated half of the molecule is a reflection of the asymmetric unit (with the symmetry operation x, ½-y, z) and the fluoride is disordered over two positions.
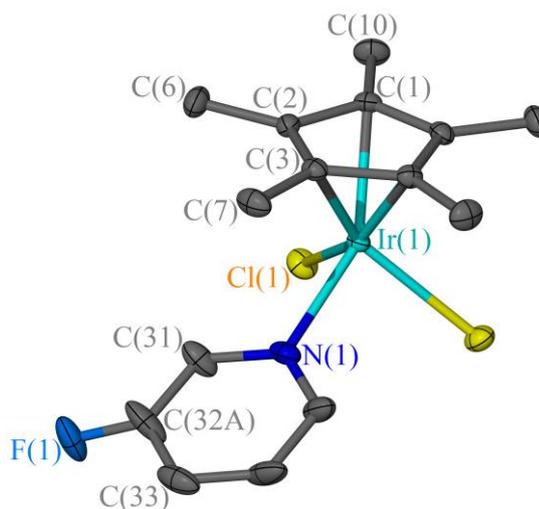
Figure 3.6 A crystal structure of compound **3.2,** displacement ellipsoids are at the 50% probability level. Hydrogen atoms are omitted for clarity

Bond	Distance (Å)	Bond	Angle (°)
Ir(1)-Cl(1)	2.4267(5)	Cl(1)-Ir(1)-Cl(1)(a)	90.67(2)
Ir(1)-N(1)	2.1412(16)	Cl(1)-Ir(1)-N(1)	87.15(4)
Ir(1)-Cg	1.7788(8)	N(1)-Ir(1)-Cl(1)(a)	87.15(4)
		Cg-Ir(1)-Cl(1)	126.31
		Cg-Ir(1)- N(1)	126.69

x, ½-y, z

Table 3.1 Selected bond lengths and bond angles for compound **3.2**

3.2.2.2 X-ray Crystallography Data for Compound 3.3

Compound **3.3** was solved in a triclinic cell and structural solution performed in the space group $P\bar{1}$. The molecular structure is shown in **Figure 3.7** and selected bond lengths and angles in **Table 3.2**. There is one molecule in the asymmetric unit.

Bond	Distance (Å)	Bond	Angle (°)
Ir(1)-Cl(1)	2.4227(6)	Cl(1)-Ir(1)-Cl(2)	87.49(2)
Ir(1)-Cl(2)	2.4111(6)	Cl(1)-Ir(1)-N(1)	87.79(5)
Ir(1)-N(1)	2.1407(18)	Cl(2)-Ir(1)-N(1)	85.97(6)
Ir(1)-C_g	1.7840(10)	C_g-Ir(1)-Cl(1)	127.59(3)
		C_g-Ir(1)-Cl(2)	127.73(3)
		C_g-Ir(1)-N(1)	126.56(6)

Table 3.2 Selected bond lengths and bond angles for compound **3.3**
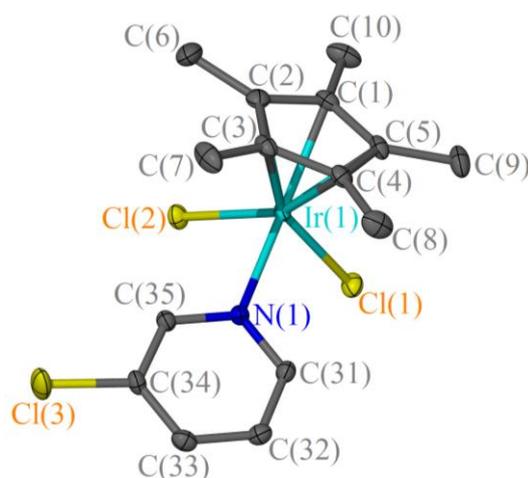
Figure 3.7 A crystal structure of compound **3.3,** displacement ellipsoids are at the 50% probability level. Hydrogen atoms are omitted for clarity

3.2.2.3 X-ray Crystallography Data for Compound 3.6

Compound **3.6** crystallised in a monoclinic cell and structural solution was performed in the space group $P2_1/c$. There are two molecules in the asymmetric unit. The molecular structure is shown in **Figure 3.8** and selected bond lengths and angles are shown in **Table 3.3**.

Bond	Distance (Å)	Bond	Angle (°)
Ir(1)-Cl(1)	2.4382(8)	Cl(1)-Ir(1)-Cl(2)	88.26(3)
Ir(1)-Cl(2)	2.4302(9)	Cl(1)-Ir(1)-N(1)	87.63(6)
Ir(1)-N(1)	2.144(2)	Cl(2)-Ir(1)-N(1)	85.82(7)
Ir(1)-C_g	1.7991(12)	C_g-Ir(1)-Cl(1)	126.33(4)
		C_g-Ir(1)-Cl(2)	128.39(5)
		C_g-Ir(1)-N(1)	126.85(7)
Ir(1A)-Cl(1A)	2.4434(8)	Cl(A)-Ir(1A)-Cl(2A)	89.24(2)
Ir(1A)-Cl(2A)	2.4292(8)	Cl(1A)-Ir(1A)-N(1A)	86.38(7)
Ir(1A)-N(1A)	2.142(2)	Cl(2A)-Ir(1A)-N(1A)	87.16(6)
Ir(1A)-C_{gA}	1.7885(12)	C_{gA}-Ir(1A)-Cl(1A)	126.19(4)
		C_{gA}-Ir(1A)-Cl(2A)	127.33(4)
		C_{gA}-Ir(1A)-N(1A)	127.30(7)

Where A refers to the second molecule in the asymmetric unit

Table 3.3 Selected bond lengths and angles for compound **3.6**
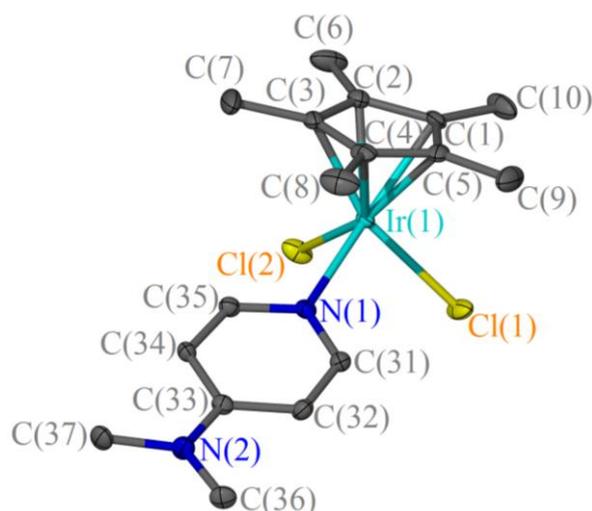
Figure 3.8 A crystal structure of compound **3.6,** displacement ellipsoids are at the 50% probability level. Hydrogen atoms are omitted for clarity

3.3 Synthesis of Iridium Hydroxyl Tethered Cp* Based Dihalide Pyridine Complexes

Complexes **3.7**-**3.14** were prepared according to **Scheme 3.2** where, for the unsubstituted pyridine complexes **3.7**-**3.9**, pyridine was used as the solvent, or, for the substituted pyridine complexes **3.10**-**3.13**, two equivalents of the pyridine was stirred with [IrCp*Cl$_2$]$_2$ in dichloromethane overnight.
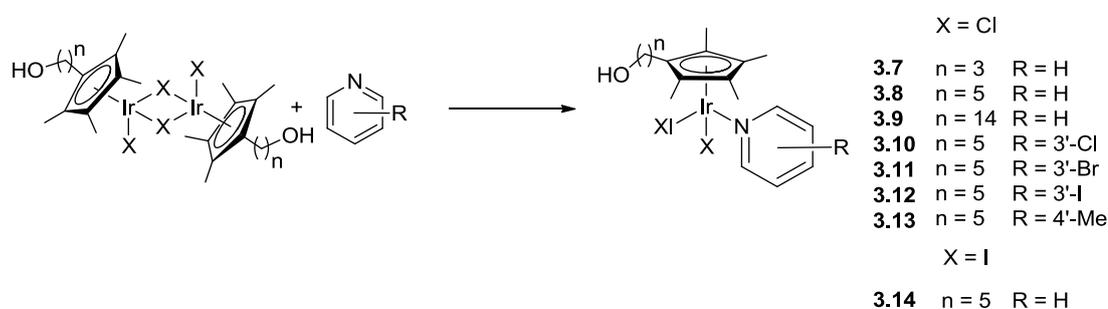
Scheme 3.2 General synthesis of iridium hydroxyl tethered Cp* based dihalide pyridine monomers

3.3.1 NMR Characterisation of Iridium Hydroxyl Tethered Cp* Based Pyridine Monomers

The peaks for the 3'-halopyridine protons of compounds **3.10**-**3.12** in the ^{1}H NMR are similar to those of the Cp* analogues discussed in section **3.2.1**. The chemical shift of proton f decreases upon increasing the tether length from 3 carbons (2.11 ppm) to 5 or 14 carbons (both 2.03 ppm). Proton g's chemical shift also decreases upon increasing the tether length, but by a lesser extent, from 3 carbons

(3.66 ppm) to 5 or 14 carbons (3.64 ppm) as the protons become less affected by the functionalised Cp* ring. These peaks show little change upon addition of substituents onto the pyridine ring. The pyridine protons labelled as c in **Figure 3.9** increase slightly from 8.96 ppm for the 3 carbon tethered complex **3.7** to 8.98 for the 14 carbon tethered complex **3.9**. The other two pyridine protons, d and e, show reverse trends. The pyridine peaks in the $^{13}C\{^1H\}$ NMR show little deviation amongst the varied tether lengths. The shift for carbon g (CH$_2$ adjacent to the OH) increases from 62.0 ppm for **3.7** (where n = 3), to 62.6 ppm for compound **3.8** (where n = 5) and 63.1 ppm for compound **3.9** (where n = 14).
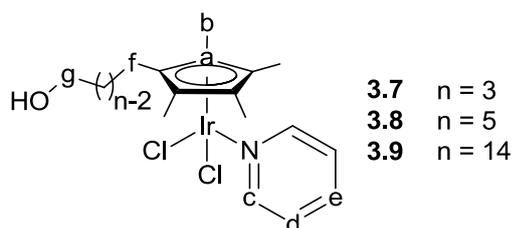
Figure 3.9 Labelled diagram for iridium hydroxyl tethered Cp* based dichloride pyridine complexes
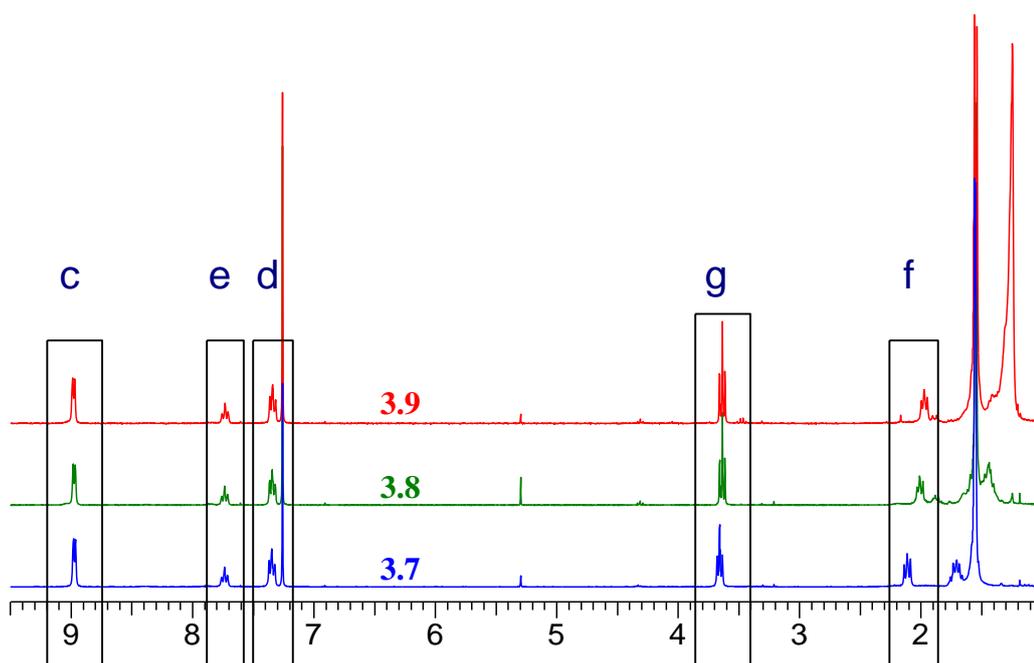
Figure 3.10 Comparison of the ^1H NMR spectra of variable tethered complexes **3.7**, **3.8** and **3.9**

3.3.2 X-ray Crystallography Data for Iridium Hydroxyl Tethered Cp* Based Pyridine Monomers

Single crystals of compounds **3.7**, **3.8**, **3.11** and **3.13** were obtained using vapour diffusion systems. The asymmetric unit for all of compounds contained one molecule. As with the previous compounds, the iridium centres have pseudo octahedral geometries whereby the hydroxyl tethered Cp* based ligand occupies three coordination sites and the two chlorides and pyridine occupy a coordination site each. The tether groups face the opposite side to the pyridine ligand, presumably due to sterics, forming hydrophobic layers where the chains stack. The addition of the hydroxyl tethers gives the potential for the terminal hydroxyl group to hydrogen bond with chloride ligands of adjacent molecules. This can be seen in **Figure 3.11 b)** for compound **3.11**. Compound **3.7** packs similarly to compounds **3.2** and **3.3** (**Figure 3.5**), whereby the molecules pack in alternate layers. The longer, 5 carbon tethered complexes **3.8** and **3.11**, whose structural solutions were both solved in the orthorhombic *Pbca* space group, pack in two parallel followed by two anti-parallel layers when viewed down the a axis, as shown in **Figure 3.11**.

a)   b)
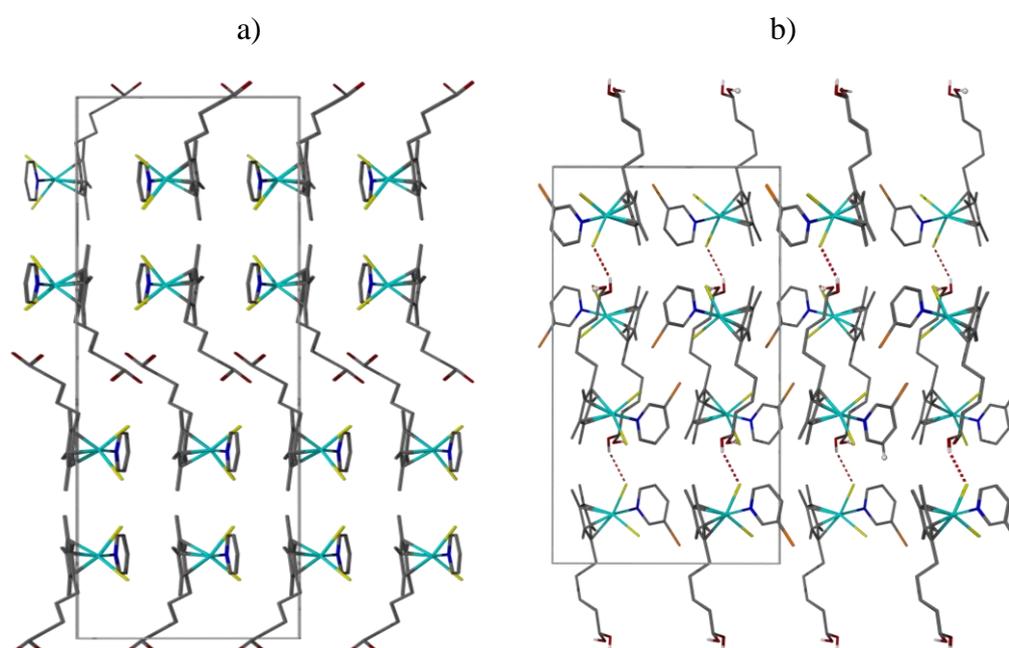
Figure 3.11 Packing diagrams of **a) 3.8** and **b) 3.11** viewed down the a axis

3.3.2.1 X-ray Crystallography Data for Compound 3.7

Yellow crystals of compound **3.7** suitable for X-ray crystallography were obtained *via* vapour diffusion from a dichloromethane/pentane solvent system. Compound **3.7** crystallised in a triclinic cell and structural solution was performed in

the space group $P\bar{1}$. The molecular structure is shown in **Figure 3.11** and selected bond lengths and angles are shown in **Table 3.4**.
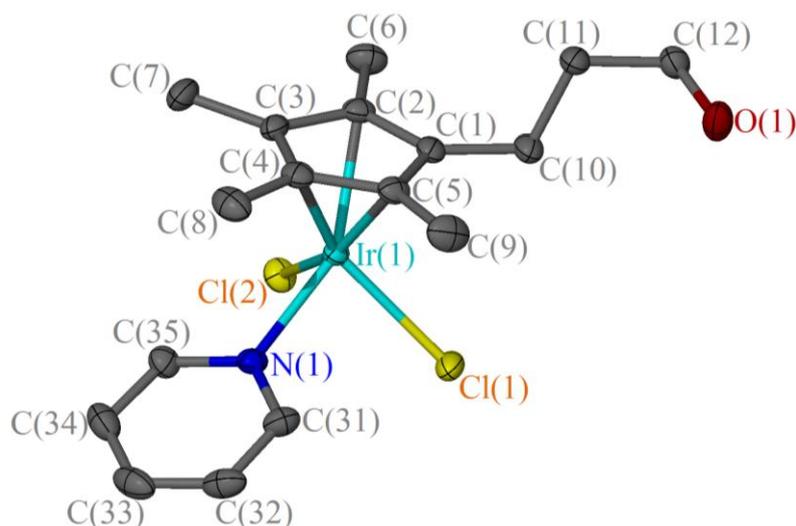
Figure 3.12 A crystal structure of compound **3.7,** displacement ellipsoids are at the 50% probability level. Hydrogen atoms are omitted for clarity

Bond	Distance (Å)	Bond	Angle (°)
Ir(1)-Cl(1)	2.4431(8)	Cl(1)-Ir(1)-Cl(2)	89.30(3)
Ir(1)-Cl(2)	2.4335(8)	Cl(1)-Ir(1)-N(1)	86.01(7)
Ir(1)-N(1)	2.135(2)	Cl(2)-Ir(1)-N(1)	87.02(7)
Ir(1)-C_g	1.7856(14)	C_g-Ir(1)-Cl(1)	126.58(4)
		C_g-Ir(1)-Cl(2)	127.71(4)
		C_g-Ir(1)-N(1)	126.80(8)

Table 3.4 Selected bond lengths and angles for compound **3.7**

3.3.2.2 X-ray Crystallography Data for Compound 3.8

Yellow crystals of compound **3.8** suitable for X-ray crystallography were obtained *via* vapour diffusion from a dichloromethane/diisopropylether solvent system. Compound **3.8** crystallised in an orthorhombic cell and structural solution was performed in the space group *Pbca*. The molecular structure is shown in **Figure 3.13** and selected bond lengths and angles are shown in **Table 3.5**. The oxygen is disordered over two positions with half occupancy each, and the hydrogens attached to C(14) are also disordered.
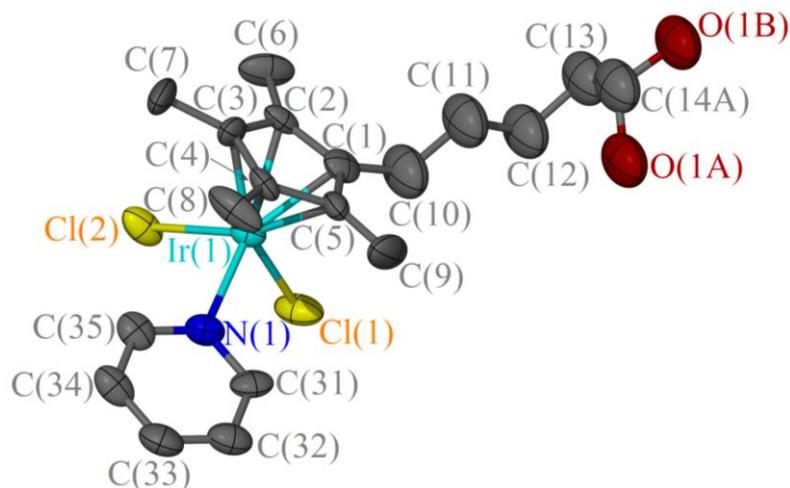
Figure 3.13 A crystal structure of compound **3.8**, displacement ellipsoids are at the 50% probability level. Hydrogen atoms are omitted for clarity

Bond	Distance (Å)	Bond	Angle (°)
Ir(1)-Cl(1)	2.433(6)	Cl(1)-Ir(1)-Cl(2)	87.81(19)
Ir(1)-Cl(2)	2.431(5)	Cl(1)-Ir(1)-N(1)	85.04(19)
Ir(1)-N(1)	2.185(6)	Cl(2)-Ir(1)-N(1)	87.41(19)
Ir(1)-C_g	1.804(3)	C_g-Ir(1)-Cl(1)	127.64(18)
		C_g-Ir(1)-Cl(2)	126.75(17)
		C_g-Ir(1)-N(1)	128.21(17)

Table 3.5 Selected bond lengths and angles for compound **3.8**

3.3.2.3 X-ray Crystallography Data for Compound 3.11

Yellow crystals of compound **3.11** suitable for X-ray crystallography were obtained *via* vapour diffusion from a dichloromethane/pentane solvent system. Compound **3.11** crystallised in an orthorhombic cell and structural solution was performed in the space group *Pbca*. The molecular structure is shown in **Figure 3.14** and selected bond lengths and angles are shown in **Table 3.6**. The alkyl chain is disordered over the atoms assigned as C13, C14 and O1 where positions A and B have occupancies of 83% and 17% respectively.
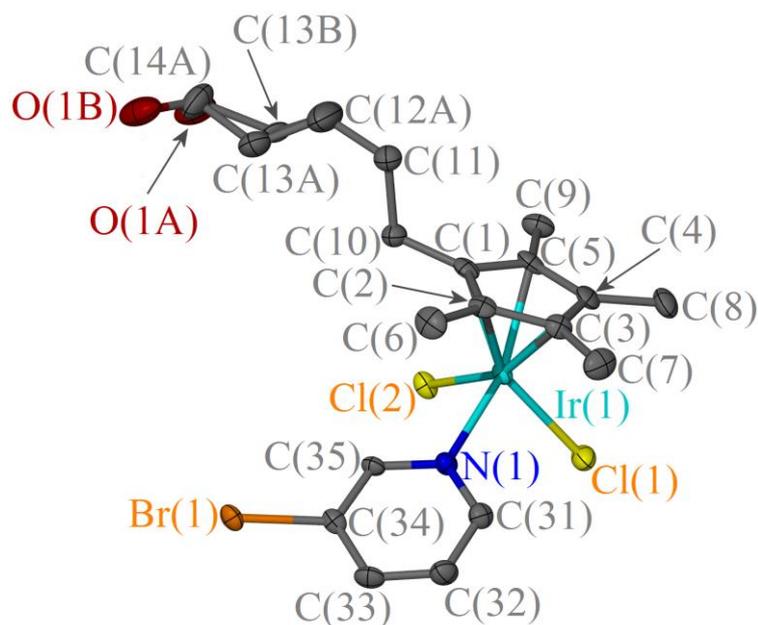
Figure 3.14 A crystal structure of compound **3.11**, displacement ellipsoids are at the 50% probability level. Hydrogen atoms are omitted for clarity

Bond	Distance (Å)	Bond	Angle (°)
Ir(1)-Cl(1)	2.4049(13)	Cl(1)-Ir(1)-Cl(2)	95.61(14)
Ir(1)-Cl(2)	2.4048(12)	Cl(1)-Ir(1)-N(1)	86.73(12)
Ir(1)-N(1)	2.118(4)	Cl(2)-Ir(1)-N(1)	86.44(12)
Ir(1)-C_g	1.769	C_g-Ir(1)-Cl(1)	127.57
		C_g-Ir(1)-Cl(2)	126.15
		C_g-Ir(1)-N(1)	128.43

Table 3.6 Selected bond lengths and angles for compound **3.11**

3.3.2.4 X-ray Crystallography Data for Compound 3.13

Yellow crystals of compound **3.13** suitable for X-ray crystallography were obtained *via* layer diffusion from a dichloromethane/hexane solvent system. Compound **3.13** crystallised in a monoclinic cell and structural solution was performed in the space group *P2₁/c*. The molecular structure is shown in **Figure 3.15** and selected bond lengths and angles are shown in **Table 3.7**.
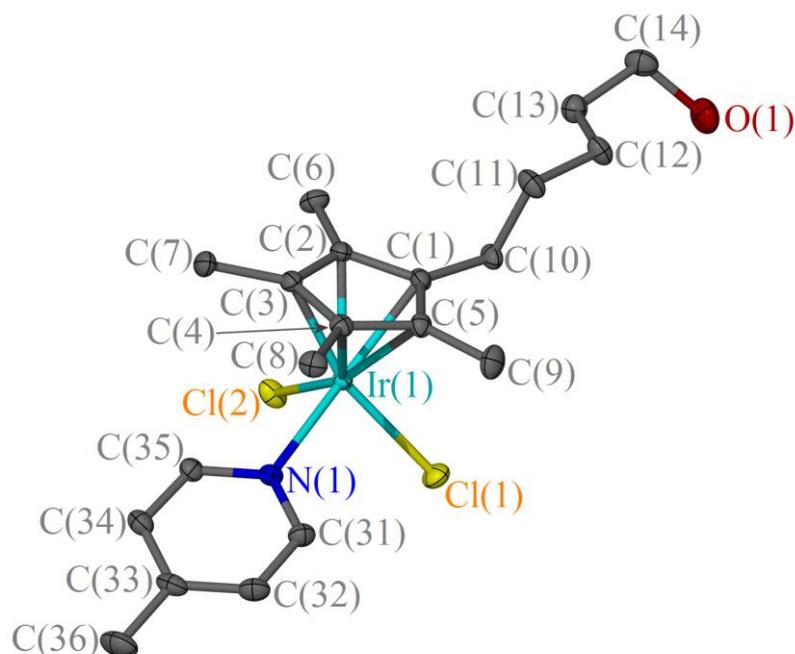
Figure 3.15 A crystal structure of compound **3.13**, displacement ellipsoids are at the 50% probability level. Hydrogen atoms are omitted for clarity

Bond	Distance (Å)	Bond	Angle (°)
Ir(1)-Cl(1)	2.4133(5)	Cl(1)-Ir(1)-Cl(2)	88.00(2)
Ir(1)-Cl(2)	2.4300(5)	Cl(1)-Ir(1)-N(1)	88.22(5)
Ir(1)-N(1)	2.1292(16)	Cl(2)-Ir(1)-N(1)	85.64(4)
Ir(1)-C_g	1.7768(8)	C_g-Ir(1)-Cl(1)	127.40(3)
		C_g-Ir(1)-Cl(2)	128.49(3)
		C_g-Ir(1)-N(1)	125.53(5)

Table 3.7 Selected bond lengths and angles for compound **3.13**

3.4 Synthesis of Rhodium Hydroxyl Tethered Cp* Based Dichloride Pyridine Complexes

Complexes **3.15**-**3.17** were prepared according to **Scheme 3.3**, where for the unsubstituted pyridine complex **3.15**, the rhodium dimer **2.6** prepared in Chapter 2, was stirred in pyridine. The substituted pyridine complexes **3.16** and **3.17** were prepared by stirring **2.6** with two equivalents of the corresponding pyridine in dichloromethane overnight.
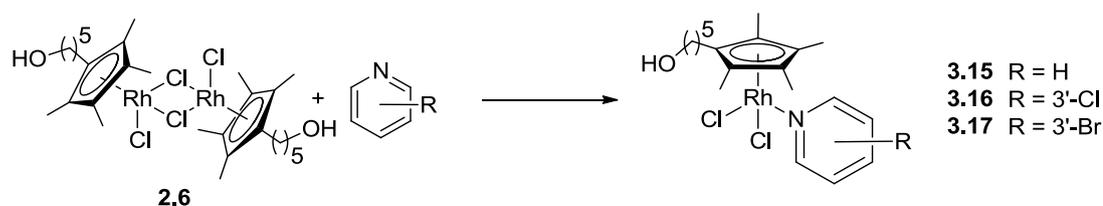
Scheme 3.3 General synthesis of rhodium hydroxyl tethered Cp* based dihalide pyridine monomers

3.4.1 NMR Characterisation of Rhodium Hydroxyl Tethered Cp* Based Pyridine Monomers

The peaks for the rhodium complexes **3.15**, **3.16** and **3.17** are much broader than their iridium analogues, with most peaks appearing as broad singlets. The peaks for the 3'-halopyridine protons of compounds **3.16** and **3.17** in the ^{1}H NMR spectra are similar to that of the Cp* iridium analogues discussed in section **3.2.1**. In comparison to the ^{1}H NMR spectrum of its iridium analogue **3.8**, most of the protons for the rhodium unsubstituted pyridine complex **3.15**, shift downfield, demonstrated in **Figure 3.17**. The peak for proton g (assigned in **Figure 3.16**) remains at 3.64 ppm for both complexes, presumably because the protons are too far away from the metal to be significantly affected by it.
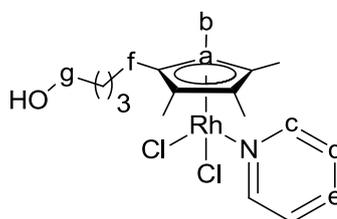
Figure 3.16 Labelled diagram for rhodium hydroxyl tethered Cp* based dichloride pyridine complex **3.15**
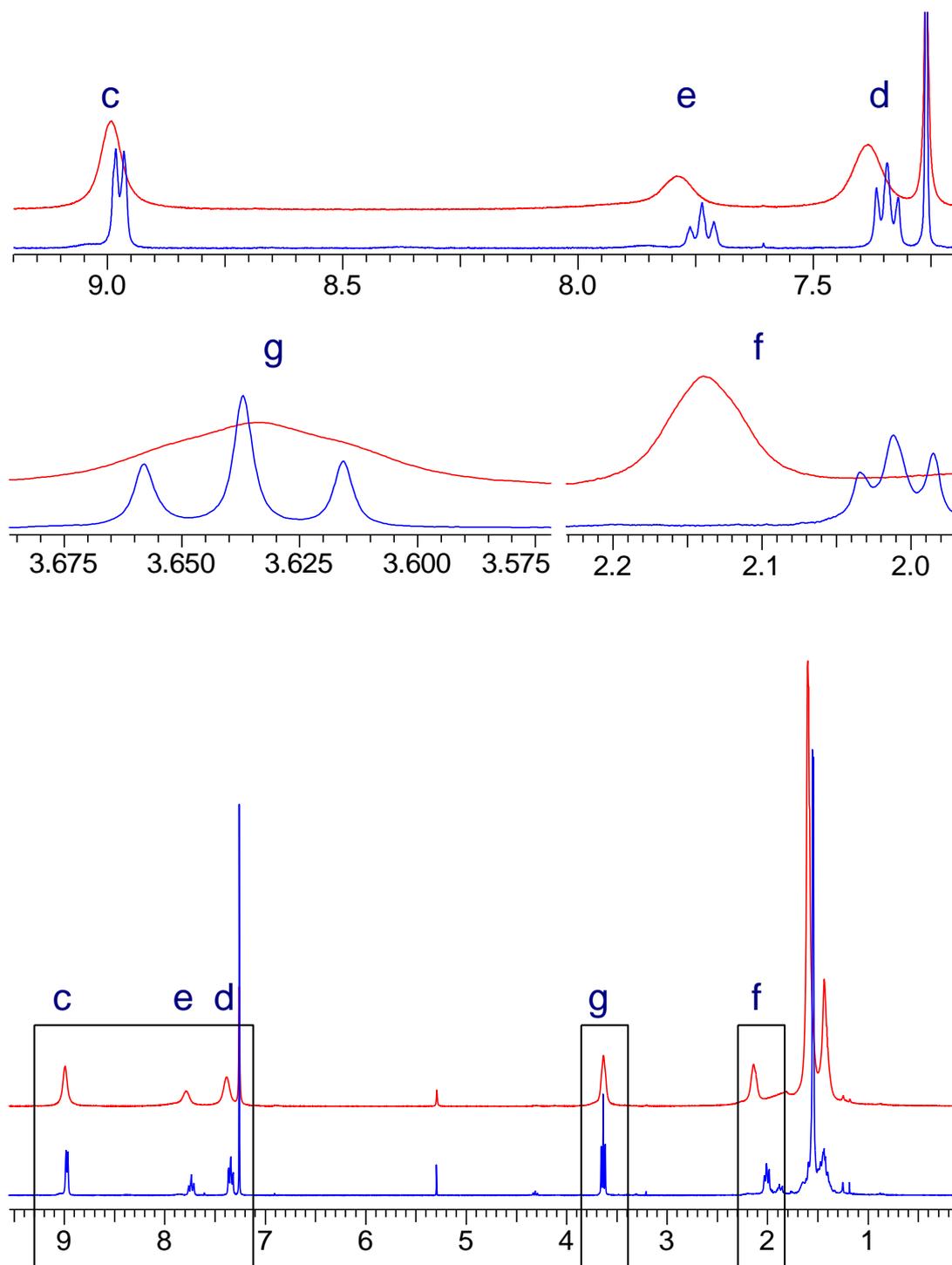
Figure 3.17 Comparison of the ^{1}H NMR spectra of iridium and rhodium tethered pyridine complexes **3.8 and 3.15**

3.4.2 X-ray Crystallography Data for Rhodium Hydroxyl Tethered Cp* Based Pyridine Monomers

Single crystals of compounds **3.15** and **3.16** were obtained using vapour diffusion systems of chloroform/pentane and dichloromethane/pentane respectively. The

asymmetric unit for both compounds contained one molecule. As with the iridium compounds, the rhodium centres have pseudo octahedral geometries whereby the hydroxyl tethered Cp* based ligand occupies three coordination sites and the two chlorides and pyridine occupy a coordination site each and the tethers face the opposite side to the pyridine ligand. Intermolecular hydrogen bonds are seen between the hydroxyl and terminal chloride of compound **3.15** (assigned as O1 and Cl1 in **Figure 3.21**) with an O(1)..Cl(1) distance of 3.2028(18). The intermolecular bonding is similar to that seen for compound **3.7**, demonstrated in **Figure 3.18**.

a)   b)
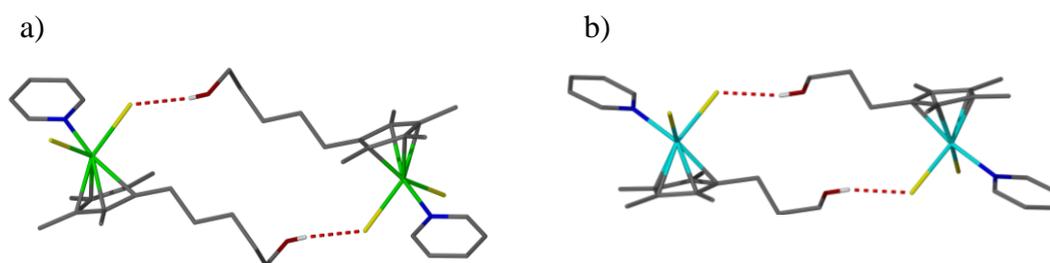
Figure 3.18 Packing diagram of compounds **a) 3.15** and **b) 3.7** showing intermolecular hydrogen bonding between a terminal chloride and hydroxyl group

Compound **3.15** packs in alternate layers similarly to compound **3.7** (and compounds **3.2** and **3.3**, shown in **Figure 3.5**), whereby the molecules pack in alternate layers, as shown viewed down the a axis in **Figure 3.19**. Their structural solutions were both solved in the triclinic $P\bar{1}$ space group.

a)   b)
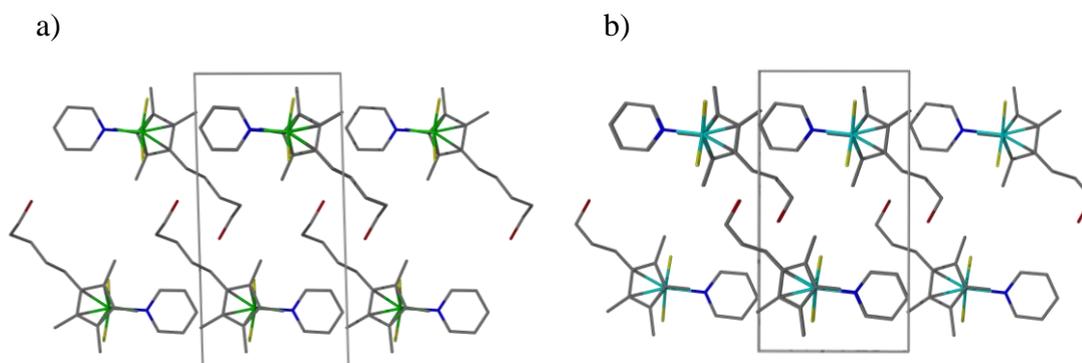
Figure 3.19 Packing diagrams of compounds **a) 3.15** and **b) 3.7** viewed down the a axis

Compound **3.16** packs similarly to both compounds **3.8** and **3.11**, in two parallel followed by two anti-parallel layers when viewed down the a axis, as shown in **Figure 3.20**. Their structural solutions were all solved in the orthorhombic *Pbca* space group.
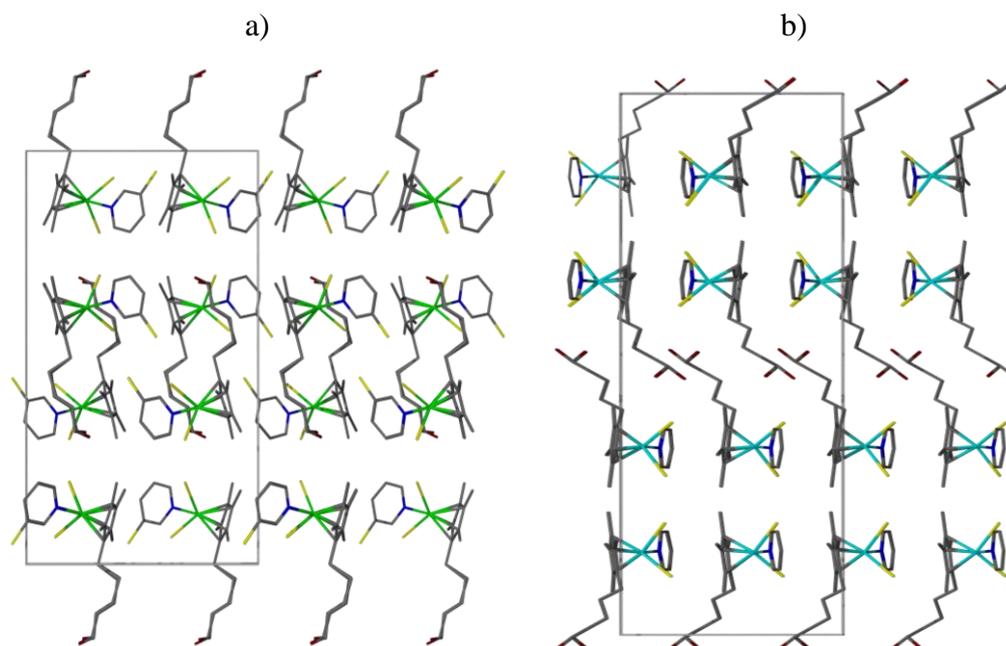
Figure 3.20 Packing diagrams of compounds **a) 3.16** and **b) 3.8** viewed down the a axis

3.4.2.1 X-ray Crystallography Data for Compound 3.15

Red crystals of compound **3.15** were grown, with its molecular structure shown in **Figure 3.21** and selected bond lengths and angles are shown in **Table 3.8**.
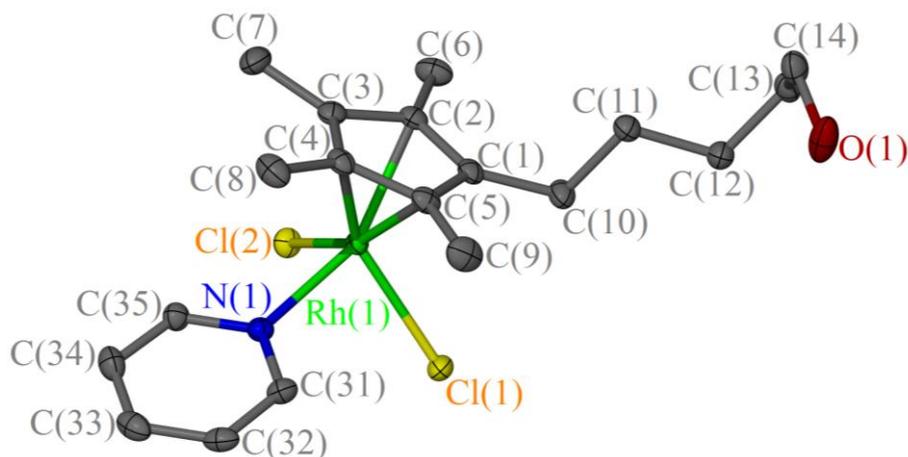

Figure 3.21 A crystal structure of compound **3.15,** displacement ellipsoids are at the 50% probability level. Hydrogen atoms are omitted for clarity

Bond	Distance (Å)	Bond	Angle (°)
Rh(1)-Cl(1)	2.4502(6)	Cl(1)-Rh(1)-Cl(2)	90.53(2)
Rh(1)-Cl(2)	2.4393(5)	Cl(1)-Rh(1)-N(1)	86.91(4)
Rh(1)-N(1)	2.1505(15)	Cl(2)-Rh(1)-N(1)	89.08(4)
Rh(1)-C_g	1.7894(8)	C_g-Rh(1)-Cl(1)	125.96(3)
		C_g-Rh(1)-Cl(2)	126.16(3)
		C_g-Rh(1)-N(1)	126.08(5)

Table 3.8 Selected bond lengths and angles for compound **3.15**

3.4.2.2 X-ray Crystallography Data for Compound 3.16

Orange plates of compound **3.16** were grown, with its molecular structure shown in **Figure 3.22** and selected bond lengths and angles are shown in **Table 3.9**.
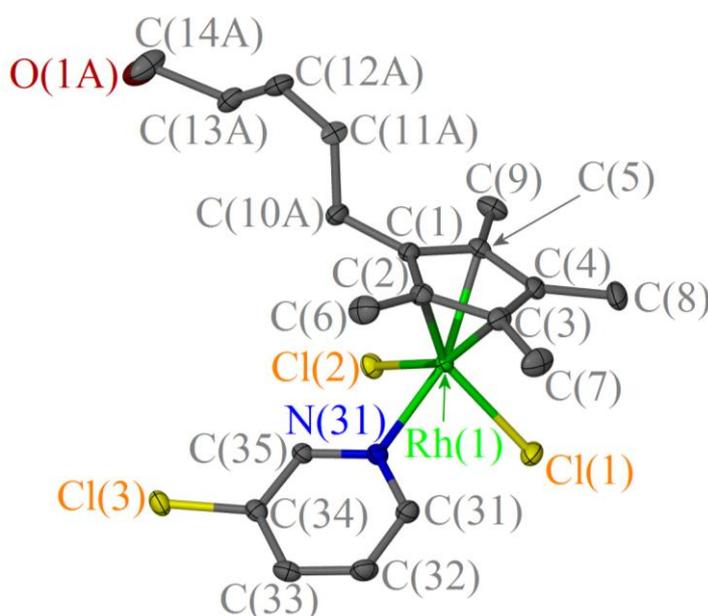
Figure 3.22 A crystal structure of compound **3.16**, displacement ellipsoids are at the 50% probability level. Hydrogen atoms are omitted for clarity

Bond	Distance (Å)	Bond	Angle (°)
Rh(1)-Cl(1)	2.4446(7)	Cl(1)-Rh(1)-Cl(2)	90.07(2)
Rh(1)-Cl(2)	2.4398(7)	Cl(1)-Rh(1)-N(1)	88.28(5)
Rh(1)-N(1)	2.1567(19)	Cl(2)-Rh(1)-N(1)	87.84(5)
Rh(1)-C_g	1.782	C_g-Rh(1)-Cl(1)	126.23
		C_g-Rh(1)-Cl(2)	124.76
		C_g-Rh(1)-N(1)	127.50

Table 3.9 Selected bond lengths and angles for compound **3.16**

3.5 Conclusion

A series of Group 9 Cp* and functionalised Cp* halide pyridine complexes have been synthesised from their corresponding metal halide Cp* or Cp* based dimers and pyridines. They were synthesised using various methods depending on the metal and the ligands. These complexes have been prepared for use as transfer hydrogenation catalysts, discussed in Chapter 6. Some of these complexes have also been tested as anti-cancer agents, with the results discussed in Chapter 8.

3.6 References

(1)   N. A. Bailey; E. H. Blunt; G. Fairhurst; C. White *J. Chem. Soc., Dalton Trans.* **1980**, 829-836.
(2)   T. Cadenbach; C. Gemel; R. Schmid; R. A. Fischer *J. Am. Chem. Soc.* **2005**, *127*, 17068-17078.
(3)   S. Cayemittes; T. Poth; M. J. Fernandez; P. G. Lye; M. Becker; H. Elias; A. E. Merbach *Inorg. Chem.* **1999**, *38*, 4309-4316.
(4)   F. P. Fanizzi; G. J. Sunley; J. A. Wheeler; H. Adams; N. A. Bailey; P. M. Maitlis *Organometallics* **1990**, *9*, 131-136.
(5)   R. H. Fish; E. Baralt; H. S. Kim *Organometallics* **1991**, *10*, 1965-1971.
(6)   J. Gil-Rubio; J. Guerrero-Leal; M. Blaya; J. Vicente; D. Bautista; P. G. Jones *Organometallics* **2011**, *31*, 1287-1299.
(7)   M. Kotera; Y. Sekioka; T. Suzuki *Inorg. Chem.* **2007**, *47*, 3498-3508.
(8)   S. Liu; H. Wang; P.-C. Zhang; L.-H. Weng; X.-F. Hou *Organometallics* **2008**, *27*, 713-717.
(9)   W. Rigby; P. M. Bailey; J. A. McCleverty; P. M. Maitlis *J. Chem. Soc., Dalton Trans.* **1979**, 371-381.
(10)   Y. Sekioka; S. Kaizaki; J. M. Mayer; T. Suzuki *Inorg. Chem.* **2005**, *44*, 8173-8175.
(11)   S. Ogo; R. Kabe; H. Hayashi; R. Harada; S. Fukuzumi *Dalton Trans.* **2006**, 4657-4663.
(12)   L. Byeong-No; Y. Duck-Joo; B. Young-Hun, patent number EP1034842, **2000**
(13)   L. Byeoung-No; Y. Duck-Joo; B. Young-Hun, patent number JP2000281695, **2000**
(14)   C. M. Yung; M. B. Skaddan; R. G. Bergman *J. Am. Chem. Soc.* **2004**, *126*, 13033-13043.
(15)   A. M. Royer; T. B. Rauchfuss; D. L. Gray *Organometallics* **2010**, *29*, 6763-6768.
(16)   S. Ogo; N. Makihara; Y. Kaneko; Y. Watanabe *Organometallics* **2001**, *20*, 4903-4910.
(17)   N. D. Schley; J. D. Blakemore; N. K. Subbaiyan; C. D. Incarvito; F. D'Souza; R. H. Crabtree; G. W. Brudvig *J. Am. Chem. Soc.* **2011**, *133*, 10473-10481.
(18)   K.-i. Fujita; N. Tanino; R. Yamaguchi *Org. Lett.* **2006**, *9*, 109-111.

(19)   R. Yamaguchi; C. Ikeda; Y. Takahashi; K. Fujita *J. Am. Chem. Soc.* **2009**, *131*, 8410-2.
(20)   M. Puebla *Optica Pura y Aplicada* **1987**, *20*, 201-219.

Chapter 4   Synthesis of Group 9 Cp* and Functionalised Cp* Picolinamide Halide Complexes

4.1 Introduction

This Chapter discusses the synthesis and characterisation of novel 18 electron air-stable piano stool iridium and rhodium Cp* and hydroxyl tethered Cp* based halide complexes incorporating picolinamide ligands synthesised previously within the McGowan group.[1,2] Many iridium/rhodium picolinamide compounds have been reported previously[3-15], used in applications such as luminescence[16-21] and catalysis.[22,23] Iridium Cp* picolinamide complexes have been previously prepared, where they were used as reductive amination catalysts, discussed in Chapter 1.[23] The picolinamides bind to the iridium through the two nitrogens as an LX donor, whereas for analogous ruthenium-arene compounds the picolinamides bind through the pyridyl nitrogen and either the amide nitrogen or oxygen depending on the nature of the picolinamide substituents.[1,2] The complexes discussed in this Chapter are shown in **Figure 4.1**.

4.1	R = H	**4.14**
4.2	R = 4'-F	
4.3	R = 2', 4'- diF	
4.4	R = 2', 5'- diF	
4.5	R = 2'-Cl	
4.6	R = 3'-Cl	
4.7	R = 2', 4'- diCl	
4.8	R = 2', 5'- diCl	
4.9	R = 4'-Ac	
4.10	R = 4'-NO$_2$	
4.11	R = 2'-OMe	
4.12	R = 2'-OMe, 4'-NO$_2$	
4.13	R = 2', 4', 6'-triMe	

4.16	R = 3'-Cl	**4.18**	R = 2'-Cl
4.17	R = 4'-NO$_2$	**4.19**	R = 3'-Cl
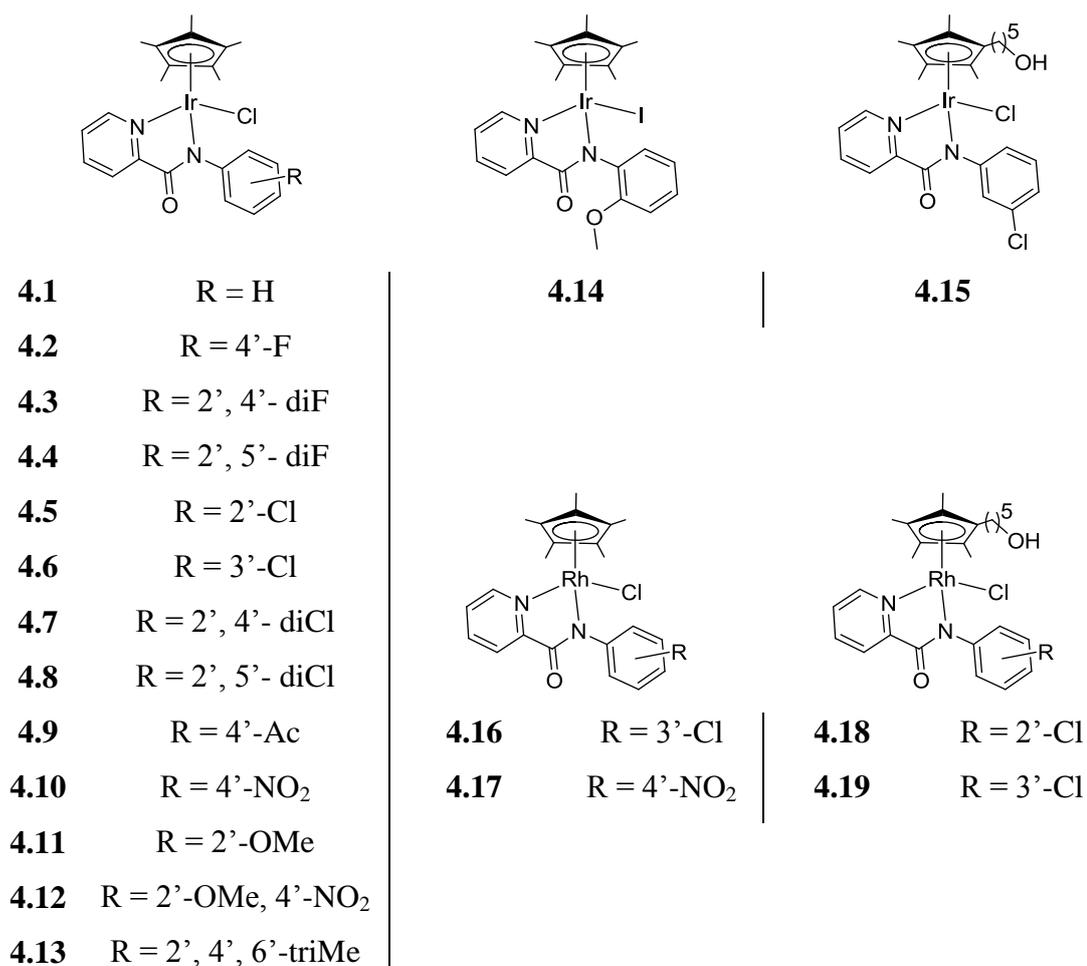
Figure 4.1 List of compounds discussed in Chapter 4

The products were characterised by ^{1}H, and ^{13}C{^{1}H} NMR spectroscopy, elemental analysis and mass spectrometry. In addition single crystals of compounds **4.6**, **4.7**, **4.9**, **4.10**, **4.12**-**4.15** and **4.19** were obtained. There is a characteristic peak in the mass spectra due to the molecular ion minus a halide ligand. The synthetic procedures used depended on the identity of the metal and the functionalised Cp* ligand, thus are discussed separately for the relevant compounds.

4.2 General Characteristics of Picolinamide Complexes

4.2.1 NMR data

Upon complexation, there is a general shift in the ^{1}H NMR spectrum of the picolinamide proton peaks downfield and the methyl groups upfield, along with removal of the amide proton peak.
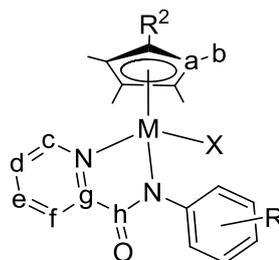
Figure 1.2 Labelled diagram for metal Cp* or Cp* based picolinamide complexes
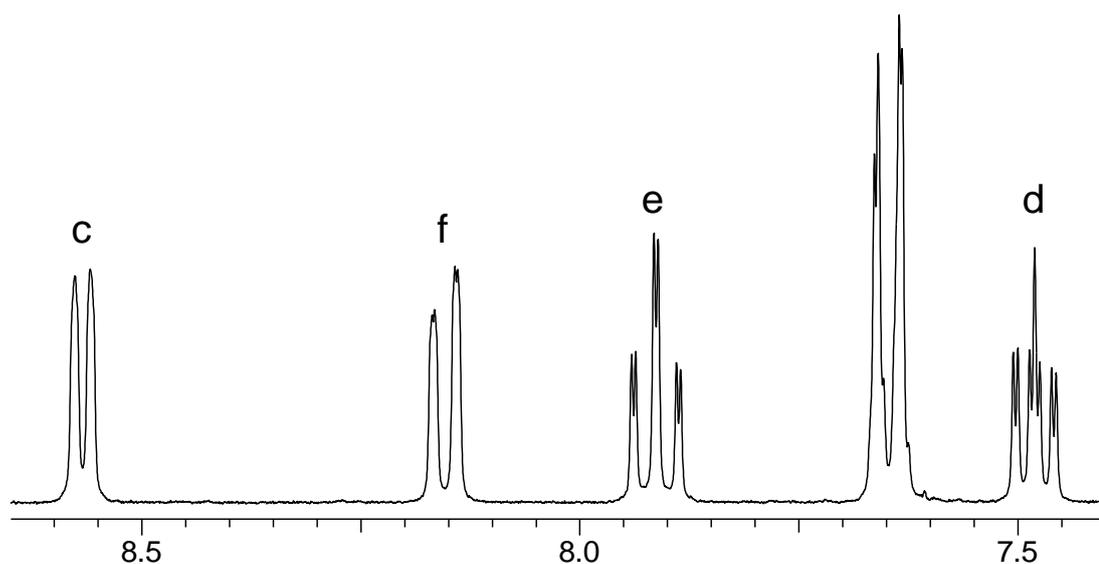
Figure 1.3 ^{1}H NMR of pyridyl protons in **4.1** (unassigned peak corresponds to a proton in the aniline ring)

In the ^{1}H NMR spectrum, proton c (defined in **Figure 1.2**) has the highest chemical shift with a d-ddd splitting pattern, depending on the resolution. The peak appears at 8.57 ppm in the case of the unsubstituted picolinamide complex **4.1** (shown in **Figure 1.3**), between 8.53 and 8.56 ppm when there are electron donating substituents, and between 8.58 and 8.64 when there are electron withdrawing substituents on the picolinamide. Proton f appears as a ddd (8.10-8.22 ppm). Proton e has a vtd splitting pattern (7.81-8.01 ppm) as similar coupling is observed with protons d and f. The peak for the d proton appears between 7.41-7.63, with a ddd splitting.

In the ^{13}C{^{1}H} NMR the highest peak observed is carbon h appearing at 165.8-170.0 ppm (shown in **Figure 1.4** for **4.1**). The highest pyridyl peak is the quarternary carbon g (154.2-155.8 ppm), followed by c (148.8-151.3 ppm), e (138.3-139.3 ppm), d (126.9-128.5 ppm), then f (123.8-127.1 ppm). The quarternary Cp/Cp* peak a is observed between 86.5-87.6 where M = Ir, and 94.7-97.3 where M = Rh (as a doublet with a $^1J(^{13}$C-^{103}Rh) coupling of 8.0-8.1 Hz). The methyl carbon b appears between 8.4 and 9.1 ppm.
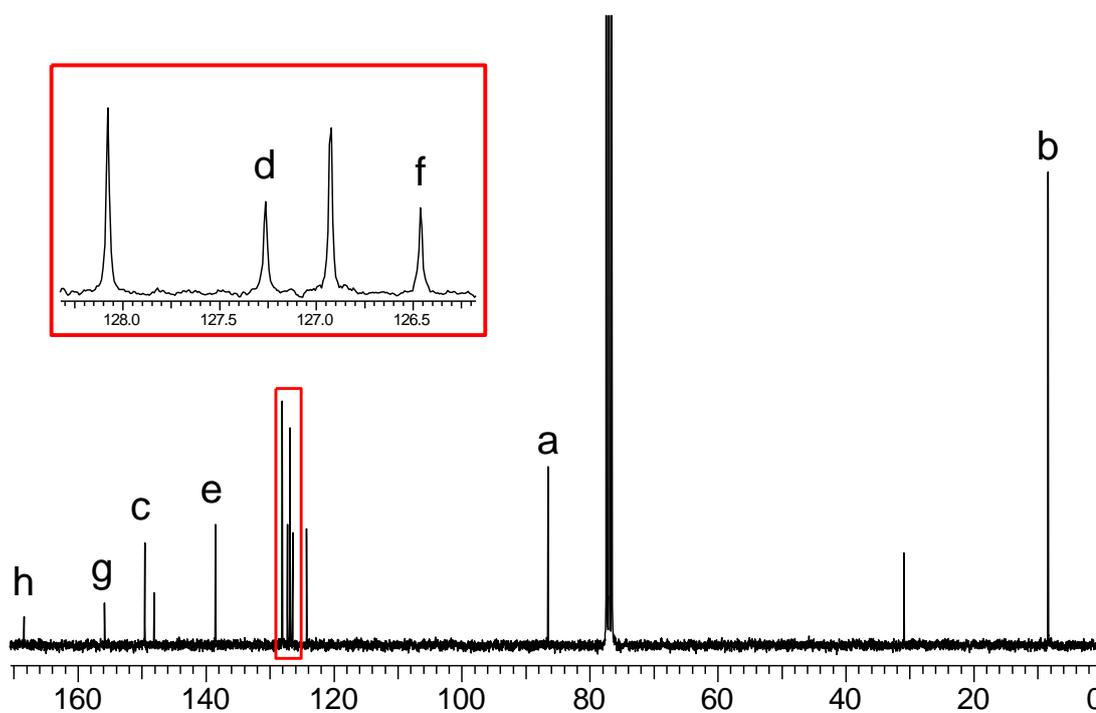
Figure 1.4 ^{13}C{^{1}H} NMR of pyridyl protons in **4.1** (unassigned peaks correspond to carbons in the aniline ring or solvents)

4.2.2 X-ray Crystallography Data

All of the crystallised complexes have a piano stool configuration, with a pseudo octahedral geometry around the metal centre, whereby the chloride occupies one site, the picolinamide occupies two sites and the Cp* or hydroxyl tethered Cp* based ligand occupies three coordination sites. Due to the rigidity of the picolinamide ligand, the angle between the two nitrogens is smaller than 90°, between 76.3 and 77.1°. The angle between the pyridyl nitrogen and the terminal halide is between 81.5 and 88.5°, and between the amide nitrogen and the terminal halide is between 85.5 and 89.7°. As the functionalised Cp* lies in the middle of 3 coordination sites, the angle between the functionalised Cp* centroid and either of the picolinamide's nitrogens or the halide is between 123 and 135°. The picolinamide ligands adopt non-planar configurations, presumably to avoid a steric clash between the ring defined as C(37)-C(42) and the functionalised Cp* ring. The torsion angle between the picolinamide rings ranges from 37 to 70° with no distinct trend for the varied picolinamide substituents. The two tethered complexes **4.15** and **4.19** have the smallest torsion angles with 46.27(15) and 37.3(3)° respectively. Most of the compounds crystallised in a monoclinic cell.

a)   b)   c)
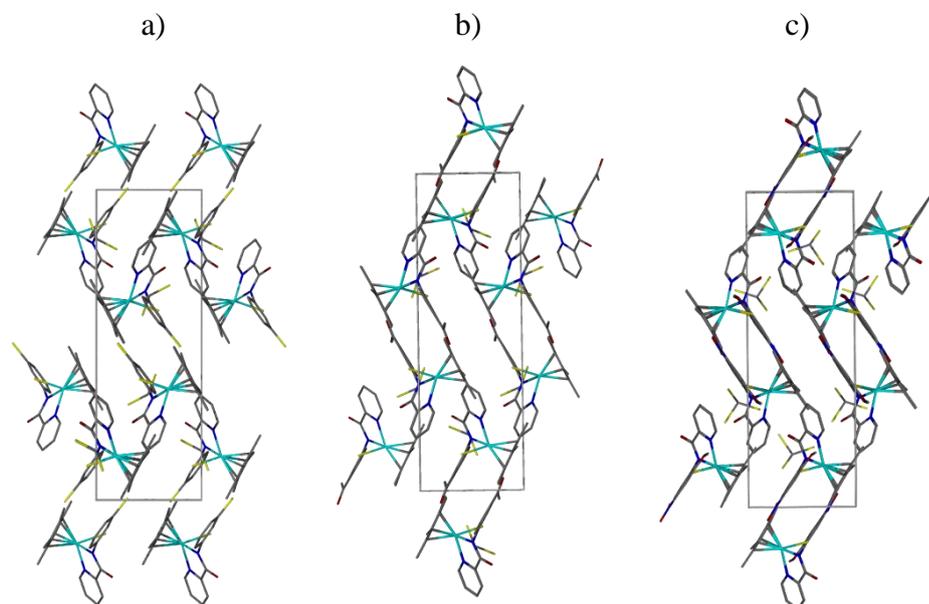
Figure 1.5 Packing diagrams of **a) 4.6**, **b) 4.9**, and **c) 4.12**, viewed down the c axis. Hydrogen atoms are omitted for clarity

There are similarities in the way that some of the compounds pack, for instance compounds **4.6**, **4.9** and **4.12** (which all crystallised with either a dichloromethane or

chloroform solvent molecule), when viewed from the c axis, all display a herringbone arrangement (**Figure 1.5**). Compounds **4.7** and **4.13** (which both crystallised with a molecule of water) have similar packing diagrams, most noticeably when viewed down the a axis, as shown in **Figure 1.6**, where the molecules pack top to tail in both directions.

a)   b)
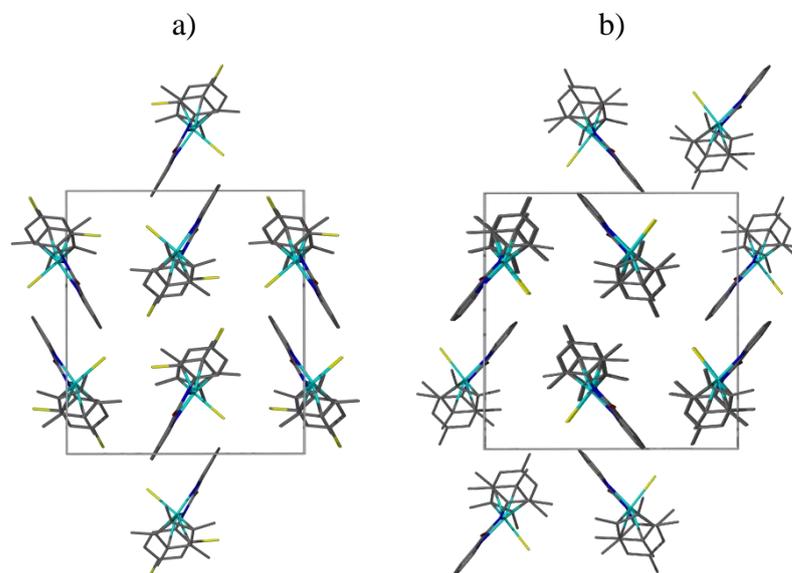
Figure 1.6 Packing diagrams of compounds **a) 4.7** and **b) 4.13** when viewed down the a axis. Hydrogen atoms are omitted for clarity

a)   b)   c)
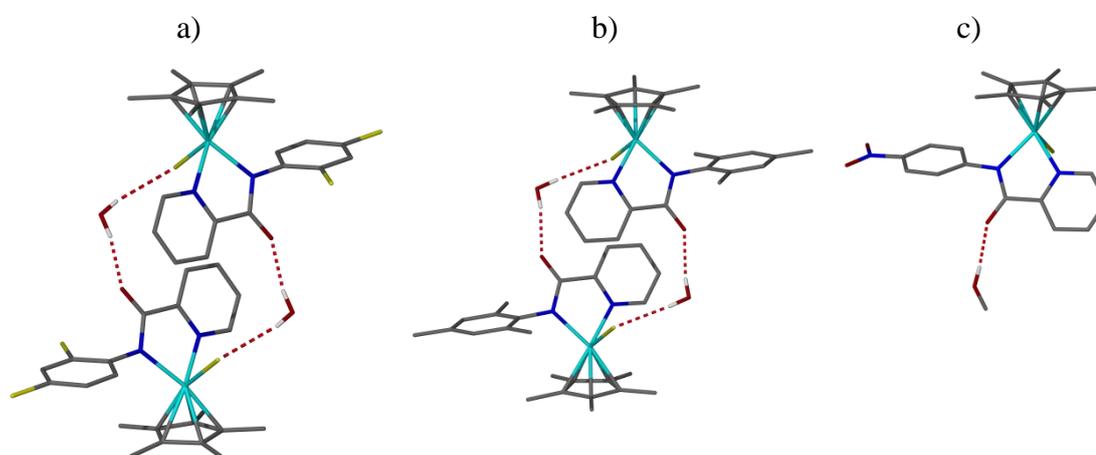
Figure 1.7 Intermolecular hydrogen bonds in compounds **a) 4.7**, **b) 4.13**, and **c) 4.10**

A water molecule hydrogen bonds with the chloride of one molecule and the carbonyl of an adjacent molecule forming an intermolecular dimer, as demonstrated in **Figure 1.7**. Compound **4.10** crystallises with a molecule of methanol, which forms a hydrogen bond with the carbonyl of the picolinamide. In the cases of the tethered complexes **4.15** and **4.19**, hydrogen bonds are seen between the hydroxyl group of the tether and carbonyl group of the amide, demonstrated in **Figure 1.8**.

a)

b)
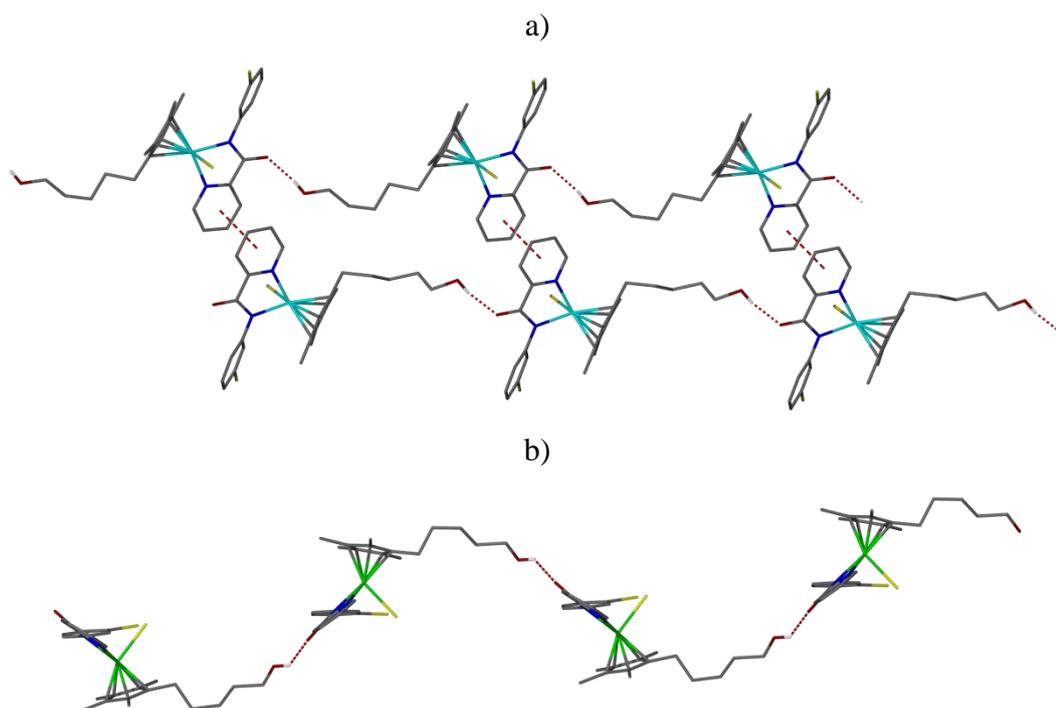
Figure 1.8 Packing diagrams of compounds **a) 4.15**, and **b) 4.19** showing intermolecular hydrogen bonds and π-π stacking. Hydrogen atoms (apart from the hydroxyl) are omitted for clarity

4.3 Synthesis of Iridium Cp* Halide Picolinamide Complexes

A range of iridium Cp* halide picolinamide complexes were synthesised using two different methods. For compounds **4.1**, **4.3**, **4.4**, **4.10**-**4.13**, [IrCp*Cl$_2$]$_2$ was refluxed in ethanol overnight with two equivalents of the picolinamide and an excess of ammonium hexafluorophosphate (method a shown in **Scheme 1.1**).
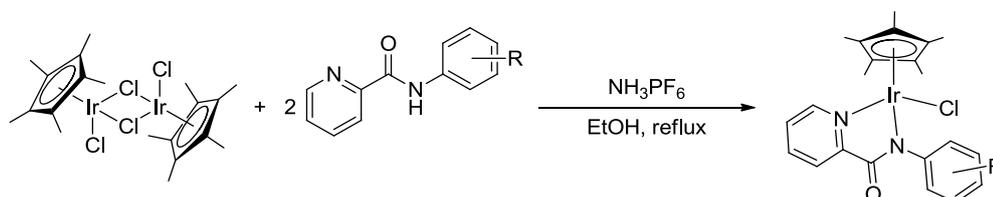
Scheme 1.1 Synthesis of iridium Cp* halide picolinamide complexes *via* method a

For compounds **4.2**, **4.5**-**4.9** and **4.14**, [IrCp*X$_2$]$_2$ was microwaved in methanol at 150 °C for 10 minutes with two equivalents of both the picolinamide and sodium bicarbonate (method b shown in **Scheme 1.2**). The purification procedures varied, depending on the complex.
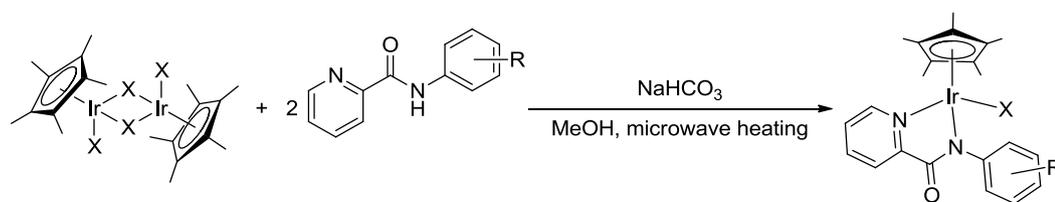
Scheme 1.2 Synthesis of iridium Cp* halide picolinamide complexes *via* method b

4.3.1 NMR Characterisation of Iridium Cp* Halide Picolinamide Complexes

Upon complexation, in the ^{1}H NMR spectrum, the methyl protons shift from 1.59 ppm (for [IrCp*Cl$_2$]$_2$ to 1.41-1.48 ppm for the iridium chloride complexes **4.1**-**4.13**, and from 1.83 ppm (for [IrCp*I$_2$]$_2$ to 1.52 ppm for the iodide analogue **4.14**.

Figure 1.9 shows a ^{1}H NMR spectrum of compound **4.4** with its labelled diagram in **Figure 1.10**. The proton defined as k splits into what appears a triplet of doublets, but is actually a ddd splitting where the proton has equal $^3J(^1\text{H-}^1\text{H})$ and $^3J(^1\text{H-}^{19}\text{F})$ coupling values and a smaller $^4J(^1\text{H-}^{19}\text{F})$ coupling value.
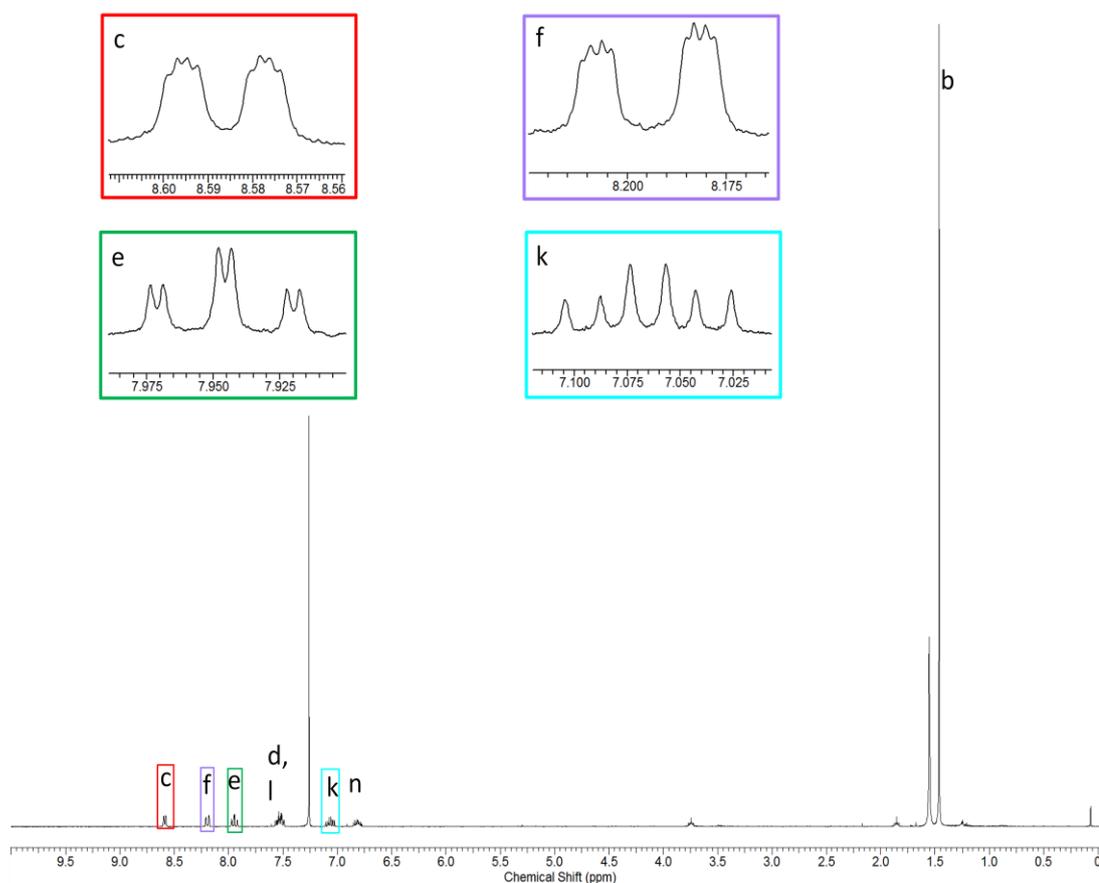
Figure 1.9 ^{1}H NMR spectrum of compound **4.4** (CDCl$_3$, 300 K, 300 MHz)
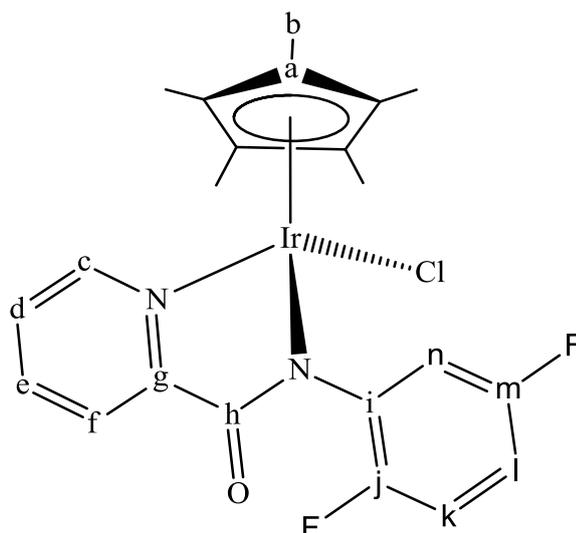
Figure 1.10 Labelled diagram of compound **4.4**

4.3.2 X-ray Crystallography Data for Iridium Cp* Halide Picolinamide Complexes

The iridium Cp* halide picolinamide complexes were either crystallised by slow diffusion from a methanolic solution, vapour diffusion of pentane into a chloroform/ dichloromethane solution or layer diffusion from a dichloromethane/hexane solvent system. In all cases, the product crystallised with a solvent molecule.

4.3.2.1 X-ray Crystallography Data for Compound 4.6

Orange crystals of compound **4.6** suitable for single X-ray crystallography were obtained *via* layer diffusion from a dichloromethane/hexane solvent system. Compound **4.6** was solved in a monoclinic cell and structural solution was performed in the space group *P2₁/n*. The asymmetric unit contains a complex molecule with a molecule of dichloromethane. The molecular structure is shown in **Figure 1.11** and selected bond lengths and angles in **Table 1.1**. The torsion angle between the picolinamide rings N(1)-C(35) and C(37)-C(42) is 70.03(11) °.
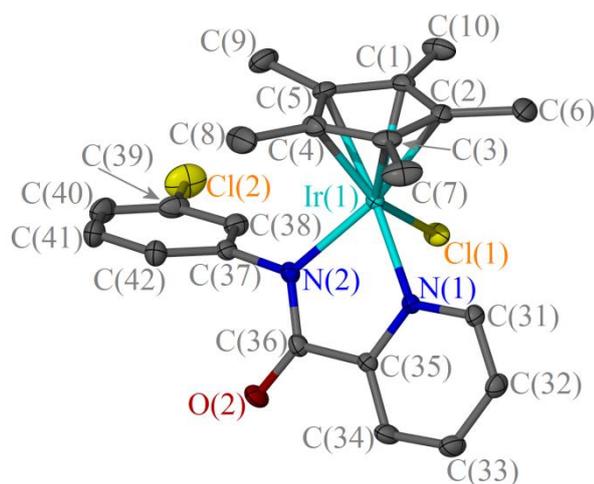
Figure 1.11 A crystal structure of compound **4.6,** displacement ellipsoids are at the 50% probability level. Dichloromethane and hydrogen atoms are omitted for clarity

Bond	Distance (Å)	Bond	Angle (°)
Ir(1)-Cl(1)	2.4305(6)	N(1)-Ir(1)-Cl(1)	84.63(5)
Ir(1)-N(1)	2.1061(16)	N(1)-Ir(1)-N(2)	76.27(6)
Ir(1)-N(2)	2.1151(16)	N(2)-Ir(1)-Cl(1)	86.25(5)
Ir(1)-C$_g$		N(1)-Ir(1)-C$_g$	132.09(5)
		N(2)-Ir(1)-C$_g$	132.75(5)
		Cl(1)-Ir(1)-C$_g$	126.74(3)

Table 1.1 Selected interatomic distances and angles for compound **4.6** with s.u.s shown in parenthesis

4.3.2.2 X-ray Crystallography Data for Compound 4.7

Yellow plates of compound **4.7** suitable for X-ray crystallography were obtained *via* layer diffusion from a dichloromethane/hexane solvent system. Compound **4.7** was solved in a monoclinic cell and structural solution was performed in the space group *P2₁/n*. The asymmetric unit contains a complex molecule with a molecule of water. The molecular structure is shown in **Figure 1.12** and selected bond lengths and angles in **Table 1.2**. The torsion angle between the picolinamide rings N(1)-C(35) and C(37)-C(42) is 67.43(13) °.
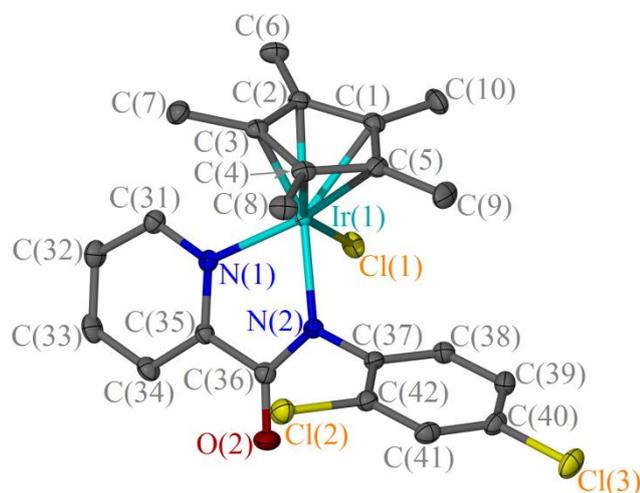
Figure 1.12 A crystal structure of compound **4.7**, displacement ellipsoids are at the 50% probability level. Water and hydrogen atoms are omitted for clarity

Bond	Distance (Å)	Bond	Angle (°)
Ir(1)-Cl(1)	2.4475(7)	N(1)-Ir(1)-Cl(1)	83.26(6)
Ir(1)-N(1)	2.115(2)	N(1)-Ir(1)-N(2)	76.28(8)
Ir(1)-N(2)	2.124(2)	N(2)-Ir(1)-Cl(1)	85.75(7)
Ir(1)-C$_g$	1.8110(12)	N(1)-Ir(1)-C$_g$	132.99(7)
		N(2)-Ir(1)-C$_g$	133.95(7)

Table 1.2 Selected interatomic distances and angles for compound **4.7** with s.u.s shown in parenthesis

4.3.2.3 X-ray Crystallography Data for Compound 4.9

Yellow plates of compound **4.9** suitable for X-ray crystallography were obtained *via* layer diffusion from a dichloromethane/hexane solvent system. Compound **4.9** was solved in a monoclinic cell and structural solution was performed in the space group *P2$_1$/n*. The asymmetric unit contains a complex molecule with a molecule of dichloromethane. The molecular structure is shown in **Figure 1.13** and selected bond lengths and angles in **Table 1.3**. The torsion angle between the picolinamide rings N(31)-C(35) and C(37)-C(42) is 61.32(19)°.
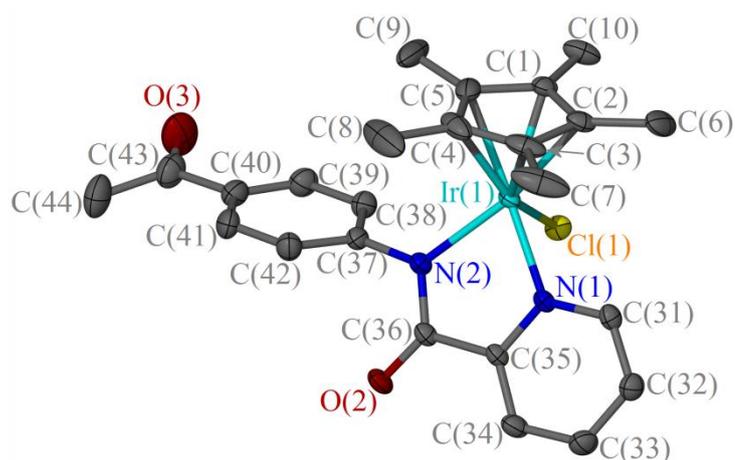
Figure 1.13 A crystal structure of compound **4.9,** displacement ellipsoids are at the 50% probability level. Dichloromethane and hydrogen atoms are omitted for clarity

Bond	Distance (Å)	Bond	Angle (°)
Ir(1)-Cl(1)	2.4392(9)	N(1)-Ir(1)-Cl(1)	84.54(8)
Ir(1)-N(1)	2.112(3)	N(1)-Ir(1)-N(2)	76.72(11)
Ir(1)-N(2)	2.131(3)	N(2)-Ir(1)-Cl(1)	87.24(9)
Ir(1)-C$_g$	1.8104(19)	N(1)-Ir(1)-C$_g$	132.06(10)
		N(2)-Ir(1)-C$_g$	131.63(10)
		Cl(1)-Ir(1)-C$_g$	126.93(7)

Table 1.3 Selected interatomic distances and angles for compound **4.9** with s.u.s shown in parenthesis

4.3.2.4 X-ray Crystallography Data for Compound 4.10

Orange crystals of compound **4.10** suitable for X-ray crystallography were obtained *via* slow diffusion from a methanolic solution. Compound **4.10** was solved in a triclinic cell and structural solution was performed in the space group $P\,\bar{1}$. The asymmetric unit contains one complex molecule with a molecule of methanol. The molecular structure is shown in **Figure 1.14** and selected bond lengths and angles in **Table 1.4**. The torsion angle between the picolinamide rings N(1)-C(35) and C(37)-C(42) is 47.48(11)°.
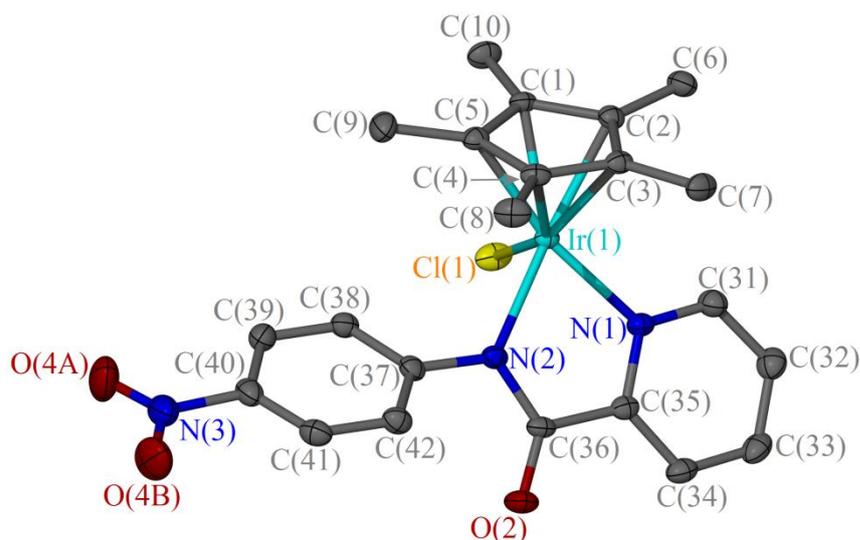
Figure 1.14 A crystal structure of compound **4.10**, displacement ellipsoids are at the 50% probability level. Methanol and hydrogen atoms are omitted for clarity

Bond	Distance (Å)	Bond	Angle (°)
Ir(1)-Cl(1)	2.4131(5)	N(1)-Ir(1)-Cl(1)	85.02(4)
Ir(1)-N(1)	2.1059(16)	N(1)-Ir(1)-N(2)	76.27(7)
Ir(1)-N(2)	2.1146(17)	N(2)-Ir(1)-Cl(1)	88.17(5)
Ir(1)-C_g	1.7988(9)	N(1)-Ir(1)-C_g	131.61(6)
		N(2)-Ir(1)-C_g	133.13(6)
		Cl(1)-Ir(1)-C_g	125.27(3)

Table 1.4 Selected interatomic distances and angles for compound **4.10** with s.u.s shown in parenthesis

4.3.2.5 X-ray Crystallography Data for Compound 4.12

Yellow crystals of compound **4.12** suitable for X-ray crystallography were obtained *via* vapour diffusion of pentane into a chloroform solution. Compound **4.12** was solved in a monoclinic cell and structural solution was performed in the space group *P2₁/n*. The asymmetric unit contains a complex molecule with a molecule of chloroform. The molecular structure is shown in **Figure 1.15** and selected bond lengths and angles in **Table 1.5**. The torsion angle between the picolinamide rings N(1)-C(35) and C(37)-C(42) is 63.6(4) °.
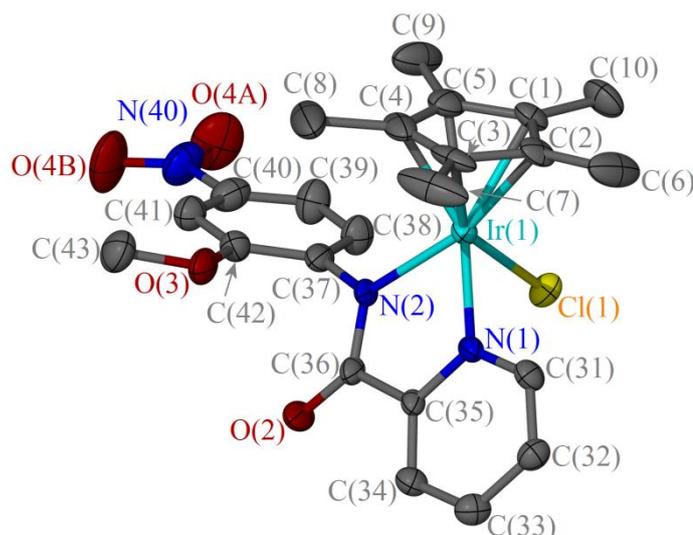
Figure 1.15 A crystal structure of compound **4.12**, displacement ellipsoids are at the 50% probability level. Chloroform and hydrogen atoms are omitted for clarity

Bond	Distance (Å)	Bond	Angle (°)
Ir(1)-Cl(1)	2.4283(19)	N(1)-Ir(1)-Cl(1)	84.43(17)
Ir(1)-N(1)	2.112(6)	N(1)-Ir(1)-N(2)	77.1(2)
Ir(1)-N(2)	2.107(6)	N(2)-Ir(1)-Cl(1)	85.49(19)
Ir(1)-C_g	1.790(4)	N(1)-Ir(1)-C_g	132.9(2)
		N(2)-Ir(1)-C_g	132.1(2)
		Cl(1)-Ir(1)-C_g	126.72(14)

Table 1.5 Selected interatomic distances and angles for compound **4.12** with s.u.s shown in parenthesis

4.3.2.6 X-ray Crystallography Data for Compound 4.13

Orange crystals of compound **4.13** suitable for X-ray crystallography were obtained *via* slow diffusion from a methanolic solution. Compound **4.13** was solved in a monoclinic cell and structural solution was performed in the space group *P2$_1$/c*. The asymmetric unit contains one complex molecule with a molecule of water. The molecular structure is shown in **Figure 1.16** and selected bond lengths and angles in **Table 1.6**. The torsion angle between the picolinamide rings N(1)-C(35) and C(37)-C(42) is 69.85(9)°.
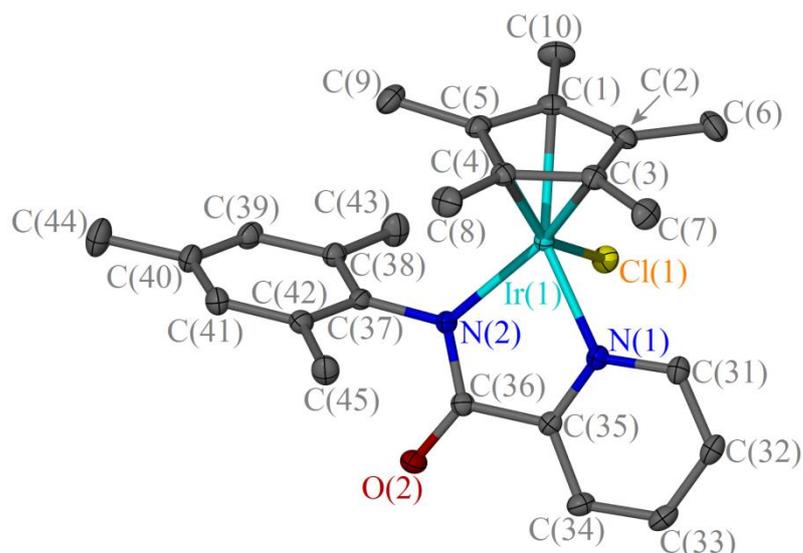
Figure 1.16 A crystal structure of compound **4.13**, displacement ellipsoids are at the 50% probability level. Water and hydrogen atoms are omitted for clarity

Bond	Distance (Å)	Bond	Angle (°)
Ir(1)-Cl(1)	2.4733(5)	N(1)-Ir(1)-Cl(1)	81.51(4)
Ir(1)-N(1)	2.1059(15)	N(1)-Ir(1)-N(2)	76.97(6)
Ir(1)-N(2)	2.1284(16)	N(2)-Ir(1)-Cl(1)	89.74(4)
Ir(1)-C$_g$	1.8067(9)	N(1)-Ir(1)-C$_g$	133.23(5)
		N(2)-Ir(1)-C$_g$	134.58(5)
		Cl(1)-Ir(1)-C$_g$	122.89(3)

Table 1.6 Selected interatomic distances and angles for compound **4.13** with s.u.s shown in parenthesis

4.3.2.7 X-ray Crystallography Data for Compound 4.14

Orange crystals of compound **4.14** suitable for X-ray crystallography were obtained *via* layer diffusion using a dichloromethane/hexane solvent system. Compound **4.14** was solved in a triclinic cell and structural solution was performed in the space group $P\bar{1}$. The asymmetric unit contains a complex molecule with an equivalent of sodium iodide, methanol, dichloromethane and water. The molecular structure is shown in **Figure 1.17** and selected bond lengths and angles in **Table 1.7**. The torsion angle between the picolinamide rings N(1)-C(35) and C(37)-C(42) is 69.85(9)°.
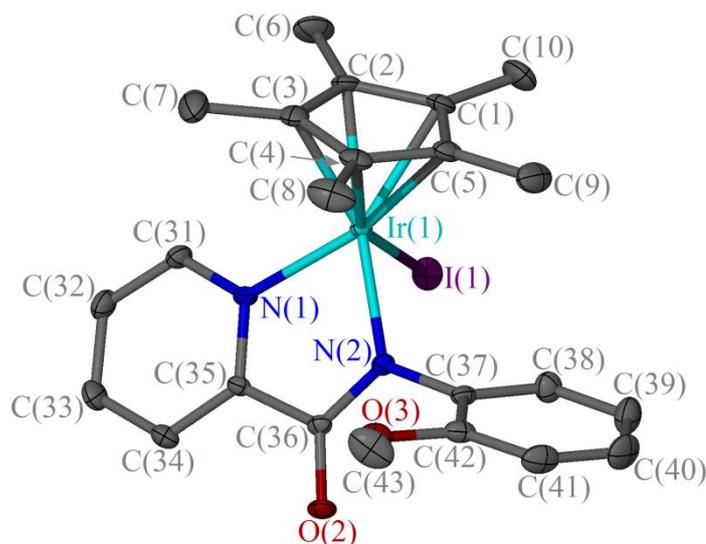
Figure 1.17 A crystal structure of compound **4.14**, displacement ellipsoids are at the 50% probability level. Sodium iodide, methanol, dichloromethane, water and hydrogen atoms are omitted for clarity

Bond	Distance (Å)	Bond	Angle (°)
Ir(1)-I(1)	2.7263(3)	N(1)-Ir(1)-I(1)	83.67(7)
Ir(1)-N(1)	2.091(2)	N(1)-Ir(1)-N(2)	76.80(9)
Ir(1)-N(2)	2.114(2)	N(2)-Ir(1)-I(1)	88.60(7)
Ir(1)-C$_g$		N(1)-Ir(1)-C$_g$	
		N(2)-Ir(1)-C$_g$	
		I(1)-Ir(1)-C$_g$	

Table 1.7 Selected interatomic distances and angles for compound **4.14** with s.u.s shown in parenthesis

4.4 Synthesis of Iridium Hydroxyl Tethered Cp* based Chloride Picolinamide Complex

The iridium hydroxyl tethered Cp* based chloride picolinamide complex **4.15** was synthesised by stirring $[Ir\{\eta^5\text{-}C_5(CH_3)_4C_5H_{10}OH\}Cl_2]_2$ with 2 equivalents of the picolinamide and triethylamine in dichloromethane overnight, shown in **Scheme 1.3**. The resulting solution was evaporated to dryness and the residue recrystallised using vapour diffusion with a dichloromethane/pentane solvent system, to give the product as orange crystals.
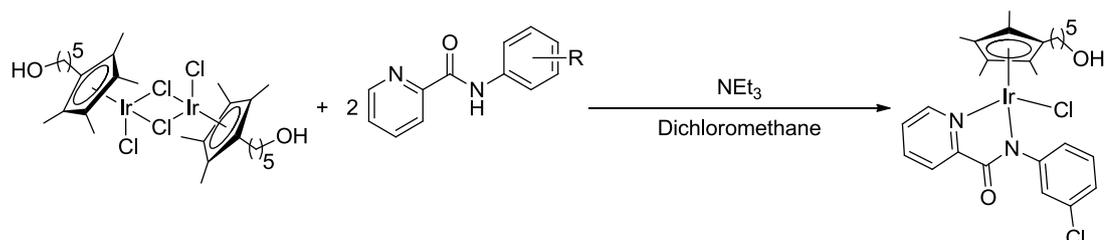
Scheme 1.3 Synthesis of iridium hydroxyl tethered Cp* based chloride picolinamide complex **4.15**

4.4.1.1 X-ray Crystallography Data for 4.15

Orange single crystals of compound **4.15** suitable for X-ray crystallography were obtained *via* layer diffusion using a dichloromethane/hexane solvent system. Compound **4.15** was solved in a monoclinic cell and structural solution was performed in the space group *P2₁/c*. The asymmetric unit contains two complex molecules with two molecules of dichloromethane. The molecular structure is shown in **Figure 1.18** and selected bond lengths and angles in **Table 1.8**. The torsion angle between the picolinamide rings N(1)-C(35) and C(37)-C(42) is 46.27(15) °. There is intermolecular hydrogen bonding between O(1)-H and O(2) with an O…O distance of 2.747(4) Å, shown in **Figure 1.8 a)**.
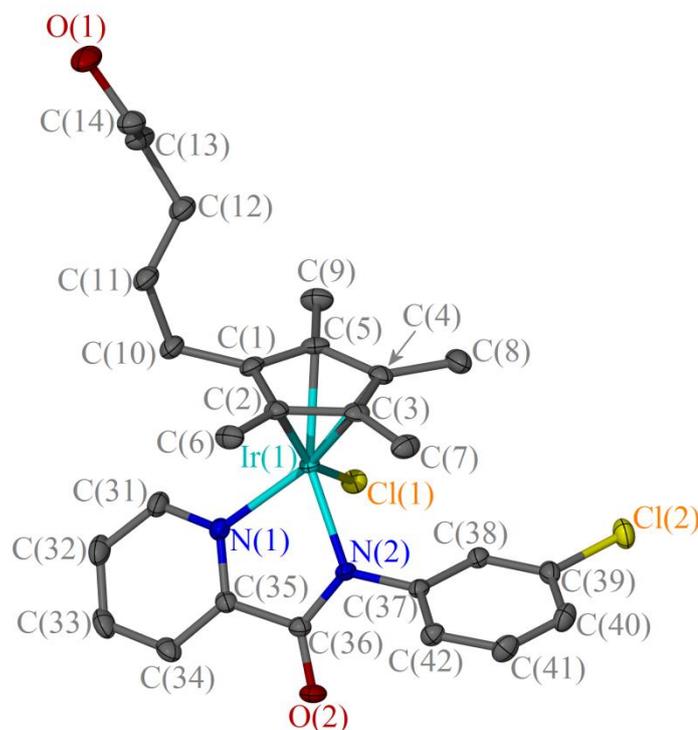
Figure 1.18 A crystal structure of compound **4.15**, displacement ellipsoids are at the 50% probability level. Dichloromethane and hydrogen atoms are omitted for clarity

Bond	Distance (Å)	Bond	Angle (°)
Ir(1)-Cl(1)	2.4417(8)	N(1)-Ir(1)-Cl(1)	84.56(8)
Ir(1)-N(1)	2.121(3)	N(1)-Ir(1)-N(2)	76.63(10)
Ir(1)-N(2)	2.114(3)	N(2)-Ir(1)-Cl(1)	86.49(8)
Ir(1)-C_g	1.8094(14)	N(1)-Ir(1)-C_g	133.22(9)
		N(2)-Ir(1)-C_g	132.14(9)
		Cl(1)-Ir(1)-C_g	125.94(5)

Table 1.8 Selected interatomic distances and angles for compound **4.15** with s.u.s shown in parenthesis

4.5 Synthesis of a Rhodium Cp* Chloride Picolinamide Complex

The rhodium Cp* halide picolinamide complex **4.16** was synthesised by refluxing [RhCp*Cl$_2$]$_2$ with 2 equivalents of the picolinamide and sodium bicarbonate in methanol overnight, shown in **Scheme 1.4**. Compound **4.17** was prepared according to method a in **Scheme 1.1**.
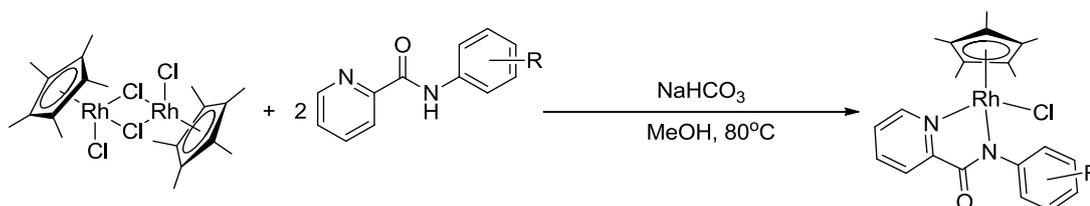
Scheme 1.4 Synthesis of rhodium Cp* chloride picolinamide complexes **4.16** and **4.17**

4.6 Synthesis of Rhodium Hydroxyl Tethered Cp* based Picolinamide Complexes

The rhodium hydroxyl tethered Cp* based halide picolinamide complexes **4.18** and **4.19** were synthesised by stirring [Rh η^5-{C$_5$(CH$_3$)$_4$C$_5$H$_{10}$OH}Cl$_2$]$_2$ with 2 equivalents of the picolinamide and sodium bicarbonate in water at 80 °C overnight. The resulting orange suspensions were filtered, washed with diethyl ether and dried to give analytically pure orange solids.
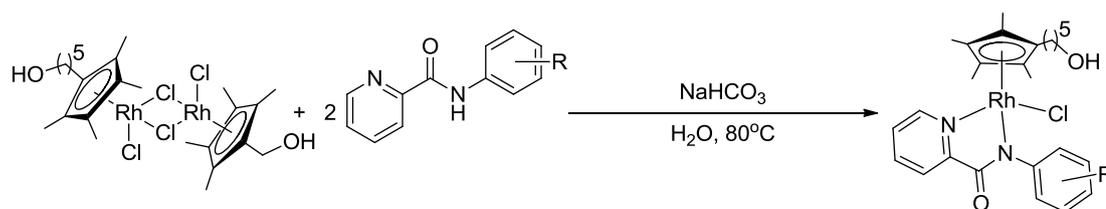
Scheme 1.5 Synthesis of rhodium hydroxyl tethered Cp* based chloride picolinamide complexes **4.18** and **4.19**

4.6.1.1 X-ray Crystallography Data for 4.19

Red crystals of compound **4.19** suitable for X-ray crystallography were obtained *via* slow diffusion from a methanolic solution. Compound **4.19** was solved in an orthorhombic cell and structural solution was performed in the space group *Pca2₁*. The asymmetric unit contains one molecule. The molecular structure is shown in **Figure 1.19** and selected bond lengths and angles in **Table 1.9**. The torsion angle between the picolinamide rings N(1)-C(35) and C(37)-C(42) is 37.3(3)°. As with its iridium analogue (**4.15**), compound **4.19** exhibits intermolecular hydrogen bonding between O(1)-H and O(2) with an O…O distance of 2.789(7) Å, as shown in **Figure 1.8 b)**.
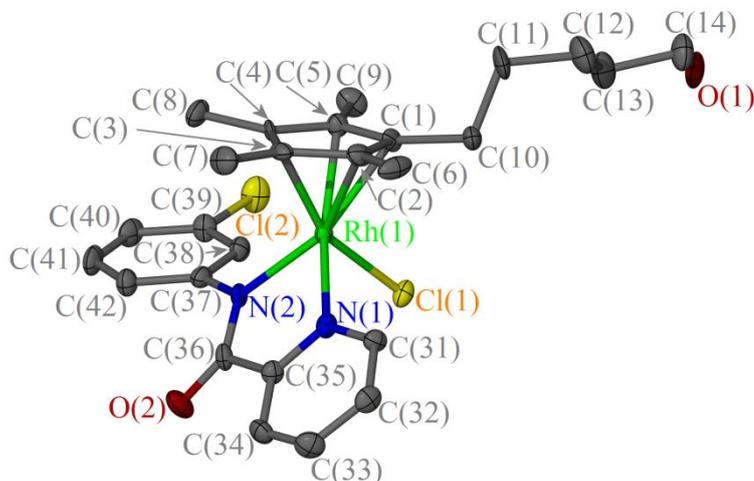
**Figure 1.19** A crystal structure of compound **4.19**, displacement ellipsoids are at the 50% probability level. Hydrogen atoms are omitted for clarity

Bond	Distance (Å)	Bond	Angle (°)
Rh(1)-Cl(1)	2.4506(16)	N(1)-Rh(1)-Cl(1)	88.54(14)
Rh(1)-N(1)	2.136(5)	N(1)-Rh(1)-N(2)	77.05(19)
Rh(1)-N(2)	2.125(5)	N(2)-Rh(1)-Cl(1)	88.50(14)
Rh(1)-C$_g$	1.824(3)	N(1)-Rh(1)-C$_g$	130.75(19)
		N(2)-Rh(1)-C$_g$	130.89(15)
		Cl(1)-Rh(1)-C$_g$	125.22(11)

Table 1.9 Selected interatomic distances and angles for compound **4.19** with s.u.s shown in parenthesis

4.7 Conclusions

A series of nine group 9 Cp* and hydroxyl tethered Cp* based halide picolinamide complexes have been synthesised from their corresponding metal halide Cp* or Cp* based dimers and picolinamides. They were synthesised using various methods depending on the metal and the ligands. These complexes have been prepared for use as transfer hydrogenation catalysts, discussed in Chapter 6. Some of these complexes have also been tested as anti-cancer agents, with the results discussed in Chapter 8.

4.8 References

(1)   K. D. Camm; A. El-Sokkary; A. L. Gott; P. G. Stockley; T. Belyaeva; P. C. McGowan *Dalton Trans.* **2009**, 10914-10925.
(2)   S. H. van Rijt; A. J. Hebden; T. Amaresekera; R. J. Deeth; G. J. Clarkson; S. Parsons; P. C. McGowan; P. J. Sadler *J. Med. Chem.* **2009**, *52*, 7753-7764.
(3)   H. Brunner; B. Nuber; M. Prommesberger *J. Organomet. Chem.* **1996**, *523*, 179-185.
(4)   V. Chandrasekhar; B. Mahanti; P. Bandipalli; K. Bhanuprakash; N. N. Nair *J. Organomet. Chem.* **2011**, *696*, 2711-2719.
(5)   D. Cuervo; J. Díez; M. P. Gamasa; J. Gimeno *Organometallics* **2005**, *24*, 2224-2232.
(6)   M. Dasgupta; H. Tadesse; A. J. Blake; S. Bhattacharya *J. Organomet. Chem.* **2008**, *693*, 3281-3288.
(7)   G. Gupta; S. Gloria; S. L. Nongbri; B. Therrien; K. M. Rao *J. Organomet. Chem.* **2011**, *696*, 2014-2022.
(8)   W. Lai; M.-K. Lau; V. Chong; W.-T. Wong; W.-H. Leung; N.-T. Yu *J. Organomet. Chem.* **2001**, *634*, 61-68.
(9)   S.-T. Mak; V. W.-W. Yam; C.-M. Che; T. C. W. Mak *J. Chem. Soc., Dalton Trans.* **1990**, 2555-2564.
(10)   P. Paul; B. Tyagi; A. K. Bilakhiya; M. M. Bhadbhade; E. Suresh; G.

Ramachandraiah *Inorg. Chem.* **1998**, *37*, 5733-5742.

(11) P. Paul; B. Tyagi; A. K. Bilakhiya; M. M. Bhadbhade; E. Suresh *J. Chem. Soc., Dalton Trans.* **1999**, 2009-2014.

(12) C. Tejel; M. A. Ciriano; M. P. del Río; F. J. van den Bruele; D. G. H. Hetterscheid; N. Tsichlis i Spithas; B. de Bruin *J. Am. Chem. Soc.* **2008**, *130*, 5844-5845.

(13) C. Tejel; M. P. del Río; L. Asensio; F. J. van den Bruele; M. A. Ciriano; N. Tsichlis i Spithas; D. G. H. Hetterscheid; B. de Bruin *Inorg. Chem.* **2011**, *50*, 7524-7534.

(14) C. Tejel; M. P. del Río; M. A. Ciriano; E. J. Reijerse; F. Hartl; S. Záliš; D. G. H. Hetterscheid; N. Tsichlis i Spithas; B. de Bruin *Chem. Eur. J.* **2009**, *15*, 11878-11889.

(15) M. Wei; B. B. Wayland *Organometallics* **1996**, *15*, 4681-4683.

(16) J. J. Tae; J. S. Ouk; Y. S. Mi, patent number KR20100032874 20100409, **2011**

(17) Y. You; S. Y. Park *J. Am. Chem. Soc.* **2005**, *127*, 12438-12439.

(18) Y.-J. Su; C.-W. Ko, patent number US 2006/0051614 A1, **2006**

(19) W. Masami; O. Fumio, patent number US2007141397, **2007**

(20) S. Yingru; K. Chongwen, patent number CN20041075237, **2005**

(21) I. Toshihiro; I. Tatsuya, patent number JP2004021123620040720, **2006**

(22) J. Margalef; M. Lega; F. Ruffo; O. Pàmies; M. Diéguez *Tetrahedron: Asymmetry* **2012**, *23*, 945-951.

(23) M. Watanbe; J. Hori; K. Murata, patent number US 2010/0234596 A1, **2010**

Chapter 5   Synthesis of Iridium Cp* Chloride Bidentate Complexes

5.1 Introduction

This Chapter is concerned with the synthesis and characterisation of iridium Cp* chloride complexes with bidentate ligands prepared previously within the McGowan group.[1-5] These complexes have been prepared for either their use as homogeneous catalysts for transfer hydrogenation reactions (discussed in Chapter 6) or their use as anti-cancer agents (discussed in Chapter 8). Various aliphatic iridium Cp* diketonate complexes have been previously reported by Maitlis *et al.*[6] Ruthenium-arene analogues of compound **5.1** have been previously prepared within the group and their anti-cancer activity has been evaluated.[2]

A list of compounds discussed in this Chapter is shown in **Figure 5.1**, with full experimental details described in Chapter 9. Compound **5.3** has been previously prepared,[7-10] so its synthesis and characterisation will not be discussed here.
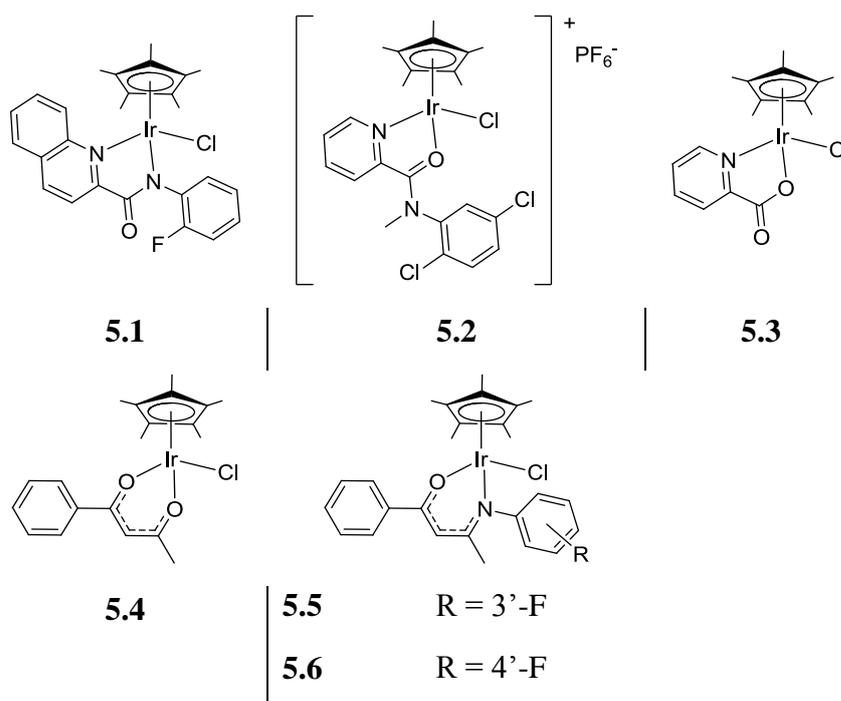
Figure 5.1 List of compounds discussed in Chapter 5

All complexes were characterised by ^{1}H and ^{13}C{^{1}H} NMR, mass spectrometry, elemental analysis and in the cases of compounds **5.1**, **5.2**, **5.4**, **5.5**, and **5.6**, single crystal X-ray crystallography. There is a characteristic peak in the mass spectrum of the molecular ion minus the chloride ligand. Compound **5.1** contains an (*N,N*)-bound bidentate ligand, where the pyridyl nitrogen is a two electron donor and the amide nitrogen is a one electron donor. Compound **5.2** contains an (*N,O*)-bound bidentate

ligand, where both the nitrogen and oxygen are two electron donors. In order for the iridium to maintain its +3 oxidation state, the resulting complex is charged. Compound **5.3** contains an (*N,O*)-bound bidentate ligand, where the nitrogen is a two electron donor and the oxygen a one electron donor. In compounds **5.5** and **5.6**, the ketoiminate ligand is aromatic, so the types of donors of each atom are less clear cut, but overall the ligand is a three electron donor. **5.4** has an (*O,O*)-bound diketonate ligand, which, similarly to the ketoiminate ligand, behaves as a three electron donor.

5.2 X-ray Crystallography Data for Iridium Cp* Chloride Bidentate Complexes

All of the crystallised complexes have a piano stool configuration, with a pseudo octahedral geometry around the metal centre, whereby the chloride occupies one site, the bidentate ligand occupies two sites, and the Cp* ligand occupies three coordination sites. In all of the compounds, the asymmetric unit contained one molecule and in the case of compound **5.5** a dichloromethane molecule. Compound **5.6** crystallised in a triclinic cell, compound **5.1** crystallised in a monoclinic cell and compounds **5.2**, **5.4**, and **5.5** crystallised in an orthorhombic unit cell.

5.3 Synthesis and Characterisation of Compound 5.1

The quinaldamide complex, **5.1**, is similar to the picolinamide complexes discussed in Chapter 4, but with a fused pyridine and benzene ring. It was prepared by reaction of [IrCp*Cl$_2$]$_2$ with 2 equivalents of the quinaldamide ligand and triethylamine in dichloromethane. The amide of the quinaldimide becomes deprotonated and binds to the iridium in an LX bidentate fashion (**Scheme 5.1**).
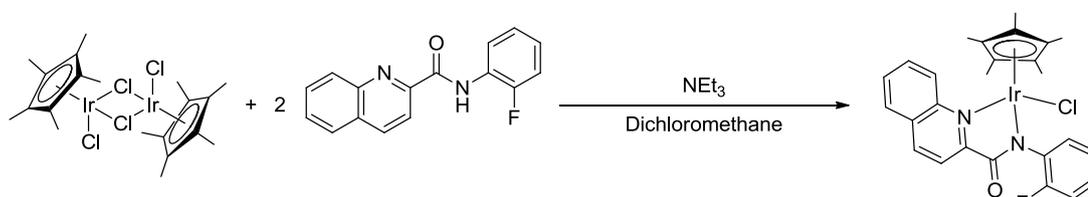
Scheme 5.1 Synthesis of the iridium Cp* chloride quinaldamide complex, **5.1**

Removal of the amide proton at 10.6 ppm in the ^{1}H NMR is diagnostic for complexation, demonstrated in **Figure 5.2**. There is also an upfield shift of the methyl groups from 1.6 to 1.4 ppm.
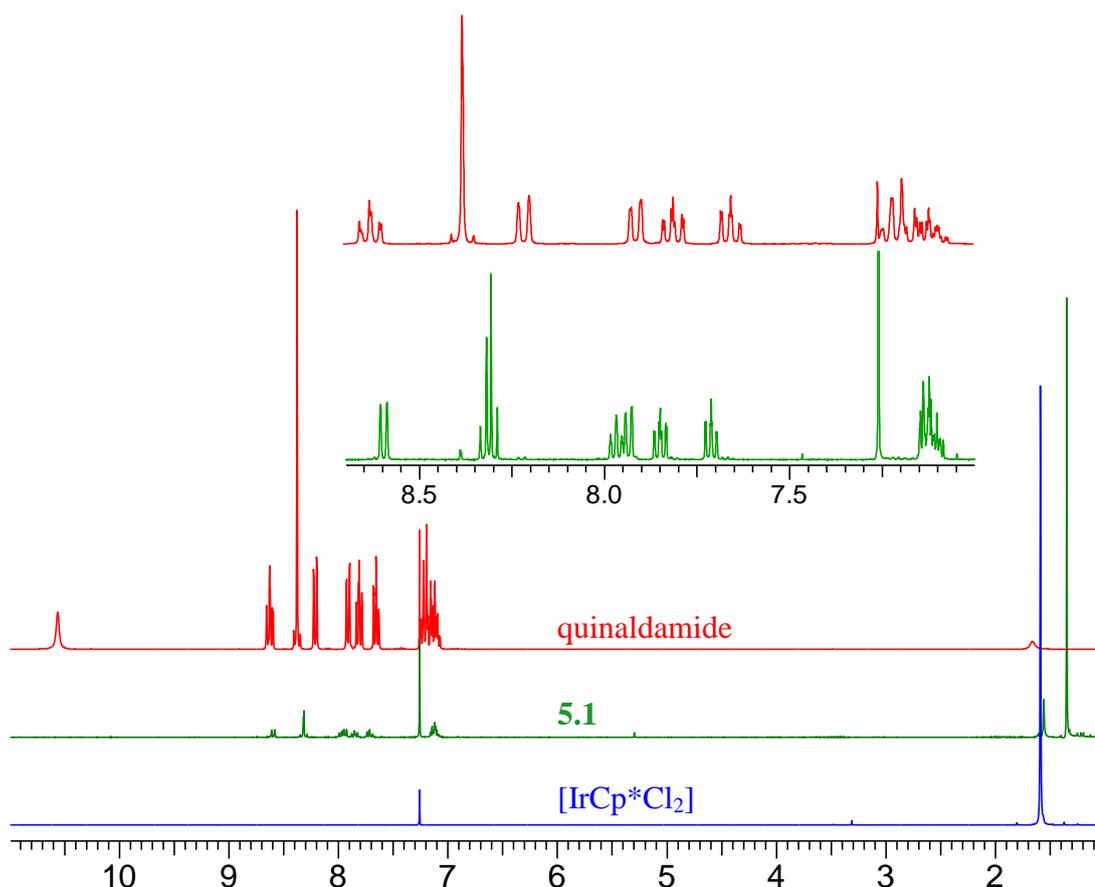
Figure 5.2 [^1]H NMR spectrum of compound **5.1** compared to its constituent starting materials

5.3.1 X-ray Crystallography Data for Compound 5.1

Red crystals of compound **5.1** were grown using vapour diffusion with a dichloromethane/diethylether solvent system.
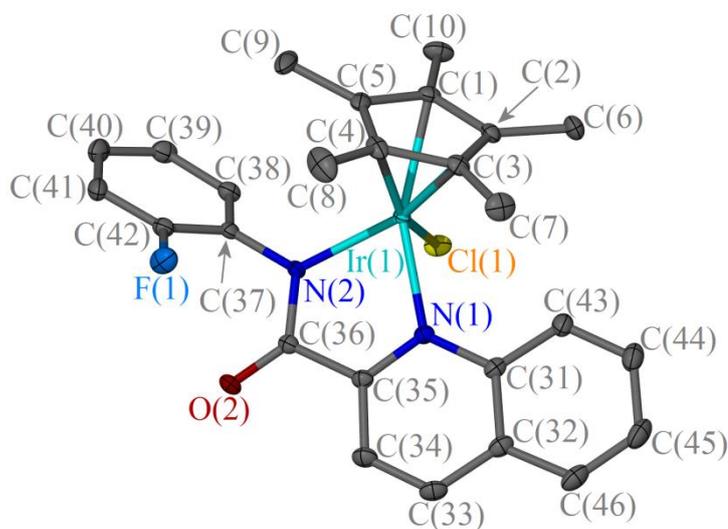
**Figure 5.3** A crystal structure of **5.1**, displacement ellipsoids are at the 50% probability level. Hydrogen atoms are omitted for clarity

Compound **5.1** was solved in an orthorhombic cell and structural solution was performed in the space group *Pca2₁*. The molecular structure is shown in **Figure 5.3** and selected bond lengths and angles in **Table 5.1**. The torsion angle between the quinaldamide rings N(1)-C(35) and C(37)-C(42) is 52.26(9)°.

Bond	Distance (Å)	Bond	Angle (°)
Ir(1)-Cl(1)	2.4502(5)	N(1)-Ir(1)-Cl(1)	85.43(4)
Ir(1)-N(1)	2.1452(16)	N(1)-Ir(1)-N(2)	76.14(6)
Ir(1)-N(2)	2.1058(15)	N(2)-Ir(1)-Cl(1)	89.09(4)
Ir(1)-C$_g$	1.8122(9)	N(1)-Ir(1)-C$_g$	133.78(5)
		N(2)-Ir(1)-C$_g$	129.44(5)
		Cl(1)-Ir(1)-C$_g$	126.01(3)

Table 5.1 Selected interatomic distances and angles for compound **5.1** with s.u.s shown in parenthesis

5.4 Synthesis and Characterisation of Compound 5.2

The N-methylpicolinamide complex, **5.2**, is prepared using the same method as the picolinamide complexes discussed in Chapter 4 (**Scheme 5.2**). As the amide is tertiary, the picolinamide is forced to bind through the amide oxygen along with the pyridyl nitrogen. As it behaves as an L$_2$ ligand, the complex is cationic, in order for the iridium to retain its +3 oxidation state. The initial chloride counterion is replaced with the PF$_6^-$ group.
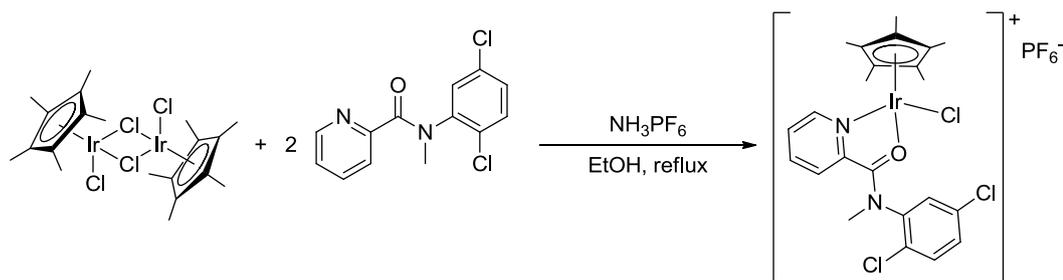
Scheme 5.2 Synthesis of the iridium Cp* chloride N-methylpicolinamide complex, **5.2**

The ^{1}H NMR of compound **5.2**, along with its substituent starting materials [IrCp*Cl$_2$]$_2$ and N-methylpicolinamide ligand, is shown in **Figure 5.4**. There is a downfield shift of the Cp* and picolinamide methyl groups, and a separation of the aromatic peaks.
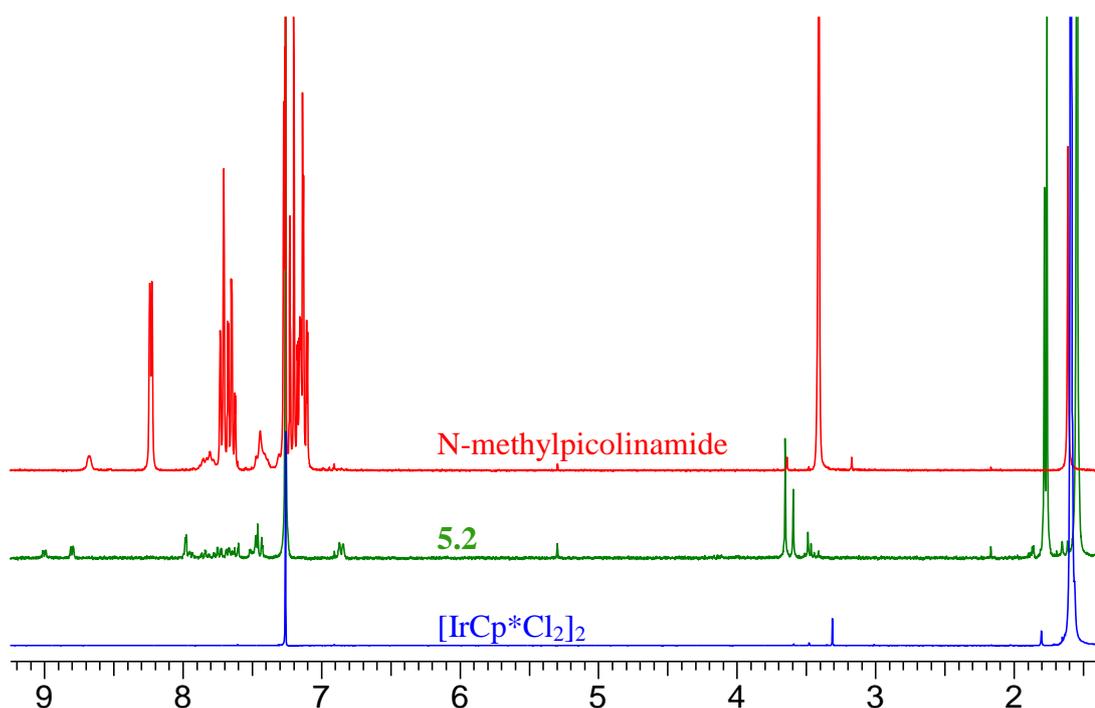
Figure 5.4 ^{1}H NMR spectrum of compound **5.2** compared to its constituent starting materials

In comparison to the ^{1}H NMR of the unsubstitued picolinamide complex **4.8**, discussed in Chapter 4, the aromatic region of compound **5.2** is less well defined, shown in **Figure 5.5**.
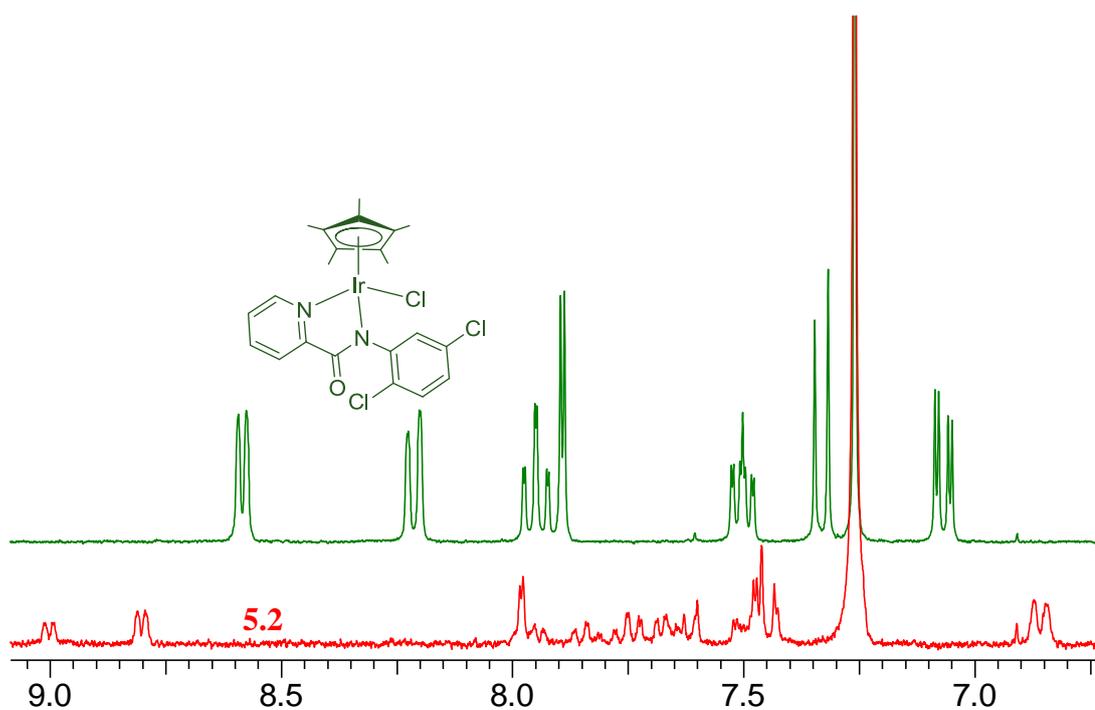
Figure 5.5 ^{1}H NMR spectrum of **5.2** compared to the analogous unsubstituted picolinamide complex **4.8**

There are two peaks at 8.6 and 9.0 ppm for the proton attached to the carbon adjacent to the pyridyl nitrogen, implying two isomers of compound **5.2.**

5.4.1 X-ray Crystallography Data for Compound 5.2

Yellow crystals of compound **5.2** were grown using vapour diffusion with a dichloromethane/pentane solvent system. Compound **5.2** was solved in an orthorhombic cell and structural solution was performed in the space group *Pbca*. The molecular structure is shown in **Figure 5.6** and selected bond lengths and angles in **Table 5.2**.
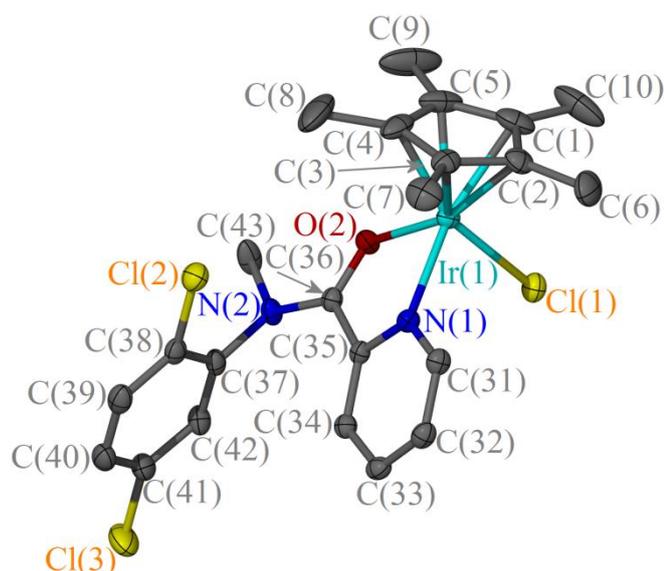

Figure 5.6 A crystal structure of compound **5.2**, displacement ellipsoids are at the 50% probability level. Hydrogen atoms are omitted for clarity

Bond	Distance (Å)	Bond	Angle (°)
Ir(1)-Cl(1)	2.4174(6)	N(1)-Ir(1)-Cl(1)	82.55(5)
Ir(1)-N(1)	2.1265(18)	N(1)-Ir(1)-O(2)	75.73(6)
Ir(1)-O(2)	2.1667(15)	O(2)-Ir(1)-Cl(1)	87.54(4)
Ir(1)-C_g	1.784	N(1)-Ir(1)-C_g	136.42
		O(2)-Ir(1)-C_g	128.06
		Cl(1)-Ir(1)-C_g	127.98

Table 5.2 Selected interatomic distances and angles for **5.2** with s.u.s shown in parenthesis

5.5 Synthesis and Characterisation of Compound 5.4

The diketonate complex, **5.4**, was prepared by reaction of [IrCp*Cl$_2$]$_2$ with 2

equivalents of the diketonate ligand and triethylamine in dichloromethane. The diketonate becomes deprotonated and binds to the iridium in an LX bidentate fashion, resulting in a neutral piano stool complex where the diketonate ligand is aromatic (**Scheme 5.3**). Upon complexation, the OH peak at 16.2 ppm disappears, the diketonate CH peak and CH$_3$ peaks shift upfield and the Cp* CH$_3$ peak shifts downfield.
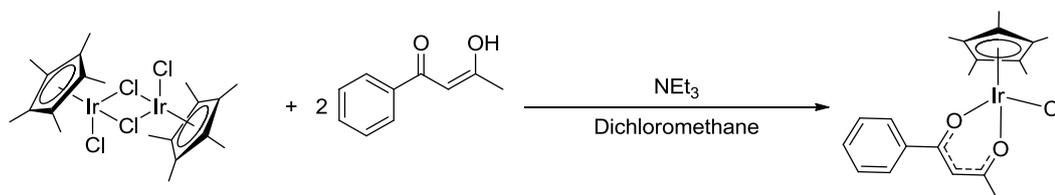
Scheme 5.3 Synthesis of the iridium Cp* chloride diketonate complex, **5.4**
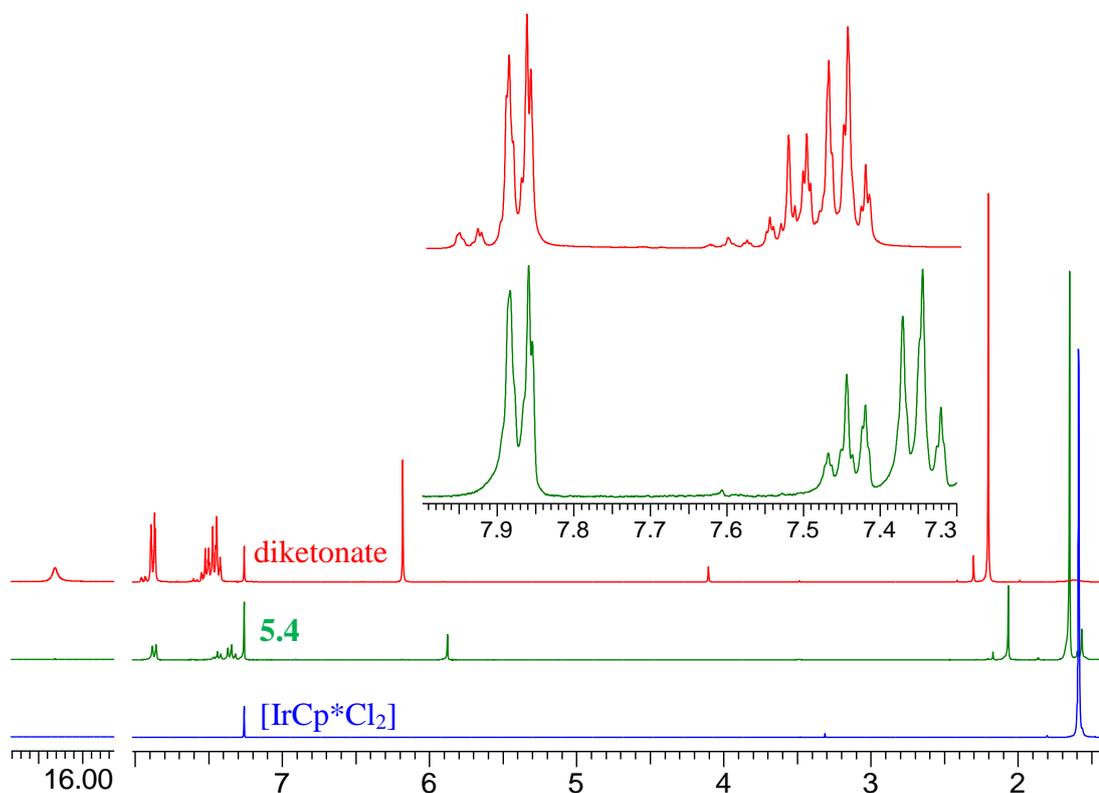
Figure 5.7 ^{1}H NMR spectrum of compound **5.4** compared to its constituent starting materials

5.5.1 X-ray Crystallography Data for Compound 5.4

Yellow crystals of compound **5.4** were grown using vapour diffusion with a chloroform/pentane solvent system. Compound **5.4** was solved in an orthorhombic cell and structural solution was performed in the space group *P2$_1$2$_1$2$_1$*. The molecular structure is shown in **Figure 5.8** and selected bond lengths and angles in **Table 5.3**.
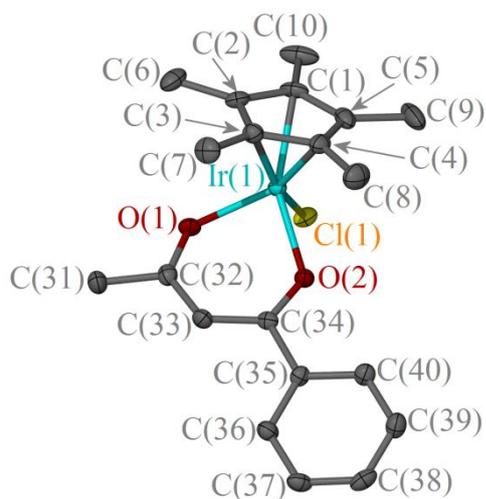
Figure 5.8 A crystal structure of compound **5.4**, displacement ellipsoids are at the 50% probability level. Hydrogen atoms are omitted for clarity

Bond	Distance (Å)	Bond	Angle (°)
Ir(1)-Cl(1)	2.4324(8)	O(1)-Ir(1)-Cl(1)	86.53(6)
Ir(1)-O(1)	2.111(2)	O(1)-Ir(1)-O(2)	85.80(9)
Ir(1)-O(2)	2.1215(18)	O(2)-Ir(1)-Cl(1)	86.64(7)
Ir(1)-C_g	1.7680(14)	O(1)-Ir(1)-C_g	125.42(7)
		O(2)-Ir(1)-C_g	128.70(10)
		Cl(1)-Ir(1)-C_g	129.27(5)

Table 5.3 Selected interatomic distances and angles for compound **5.4** with s.u.s shown in parenthesis

5.6 Synthesis and Characterisation of Compounds 5.5 and 5.6

The ketoiminate complexes, **5.5** and **5.6**, were prepared by reaction of [IrCp*Cl$_2$]$_2$ with 2 equivalents of the ketoiminate ligand and triethylamine in dichloromethane. The ketoiminate becomes deprotonated and binds to the iridium in an LX bidentate fashion, resulting in a neutral piano stool complex where the ketoiminate ligand is aromatic (**Scheme 5.4**).
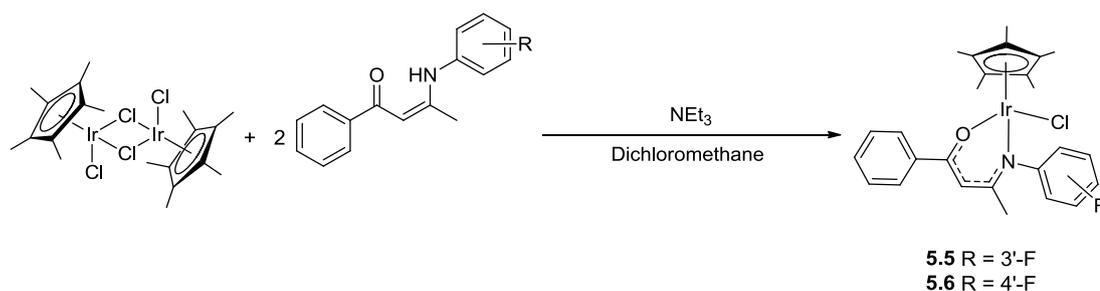
Scheme 5.4 Synthesis of the iridium Cp* chloride ketoiminate complexes **5.5** and

5.6

Removal of the amine proton, at 13.1 ppm in the ^{1}H NMR spectrum for compound **5.5**, is diagnostic for complexation (demonstrated in **Figure 5.9)**. There is also an upfield shift of the methyl groups (from 1.6 to 1.3 ppm for compound **5.5**), and the ketoiminate CH proton (from 5.9 to 5.5 ppm for compound **5.5**).
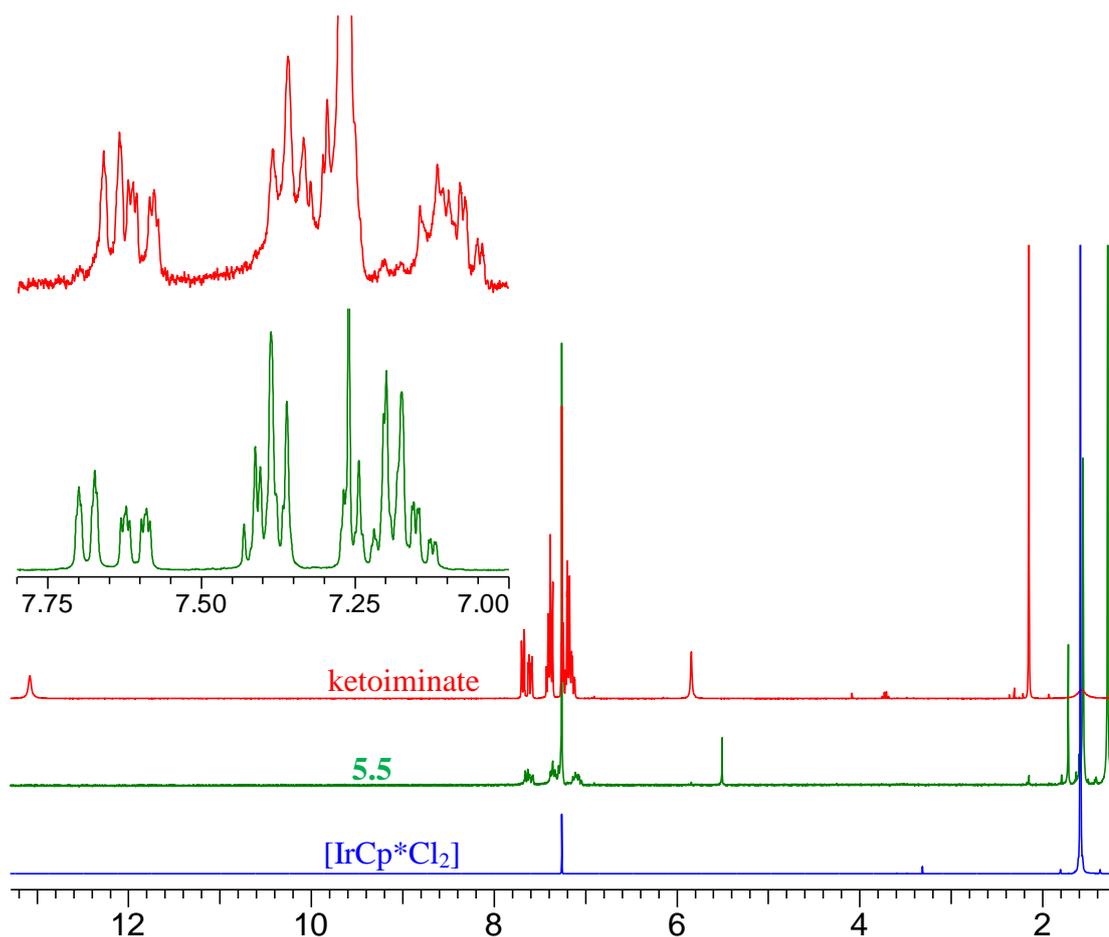
Figure 5.9 ^{1}H NMR spectrum of compound **5.5** compared to its constituent starting materials

5.6.1 X-ray Crystallography Data for Compound 5.5

Red crystals of compound **5.5** were grown *via* layer diffusion using a dichloromethane/hexane solvent system. Compound **5.5** was solved in an orthorhombic cell and structural solution was performed in the space group $P2_12_12_1$. The molecular structure is shown in **Figure 5.10** and selected bond lengths and angles in **Table 5.4**. The torsion angle between the ketoiminate rings C(35)-C(40) and C(41)-C(46) is 88.8(2)°.
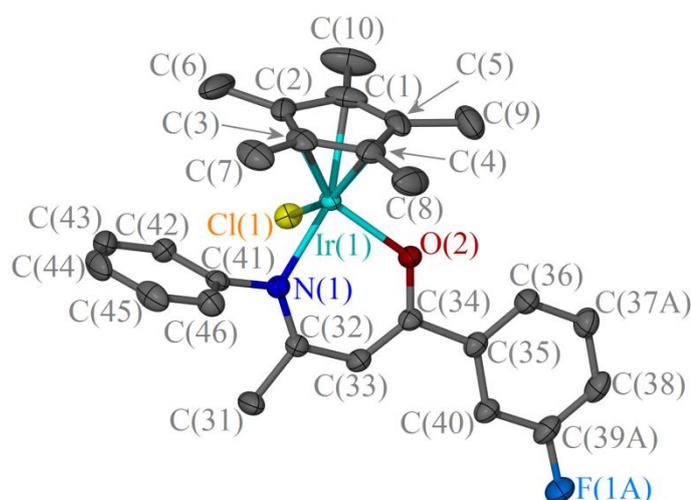
Figure 5.10 A crystal structure of compound **5.5**, displacement ellipsoids are at the 50% probability level. Dichloromethane and hydrogen atoms are omitted for clarity

Bond	Distance (Å)	Bond	Angle (°)
Ir(1)-Cl(1)	2.4832(9)	N(1)-Ir(1)-Cl(1)	83.55(7)
Ir(1)-N(1)	2.123(2)	N(1)-Ir(1)-O(2)	88.51(9)
Ir(1)-O(2)	2.101(2)	O(2)-Ir(1)-Cl(1)	86.07(7)
Ir(1)-C_g	1.8049(18)	N(1)-Ir(1)-C_g	134.99(9)
		O(2)-Ir(1)-C_g	122.56(9)
		Cl(1)-Ir(1)-C_g	126.08(6)

Table 5.4 Selected interatomic distances and angles for **5.5** with s.u.s shown in parenthesis

5.6.2 X-ray Crystallography Data for Compound 5.6

Red crystals of compound **5.6** were grown using slow diffusion from a methanolic solution. Compound **5.6** was solved in a triclinic cell and structural solution was performed in the space group $P\bar{1}$. The molecular structure is shown in **Figure 5.11**

and selected bond lengths and angles in **Table 5.5**. The torsion angle between the ketoiminate rings C(35)-C(40) and C(41)-C(46) is 71.34(10)°.
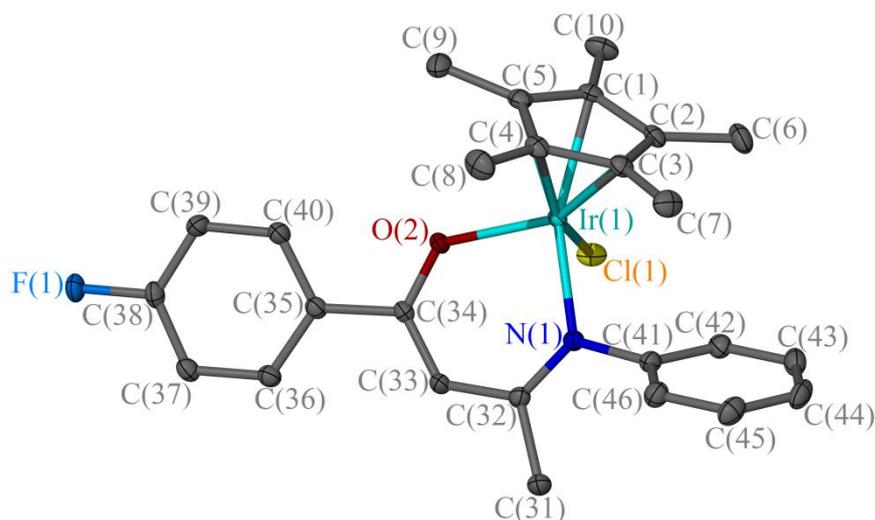
Figure 5.11 A crystal structure of compound **5.6**, displacement ellipsoids are at the 50% probability level. Hydrogen atoms are omitted for clarity

Bond	Distance (Å)	Bond	Angle (°)
Ir(1)-Cl(1)	2.4697(6)	N(1)-Ir(1)-Cl(1)	85.07(5)
Ir(1)-N(1)	2.1208(17)	N(1)-Ir(1)-O(2)	88.82(6)
Ir(1)-O(2)	2.0930(15)	O(2)-Ir(1)-Cl(1)	85.57(5)
Ir(1)-C_g	1.8018(9)	N(1)-Ir(1)-C_g	133.86(6)
		O(2)-Ir(1)-C_g	122.29(5)
		Cl(1)-Ir(1)-C_g	126.52(3)

Table 5.5 Selected interatomic distances and angles for compound **5.6** with s.u.s shown in parenthesis

5.7 Conclusion

A series of group 9 Cp* chloride complexes incorporating either (*N,N*), (*N,O*) or (*O,O*) bidentate ligands have been synthesised from [IrCp*Cl$_2$]$_2$ and their corresponding ligands. They were synthesised using various methods depending on the ligands. These complexes have been prepared either for their use as transfer hydrogenation catalysts, discussed in Chapter 6 or as anti-cancer agents, with the results discussed in Chapter 8.

5.8 References

(1) Z. Almodares, PhD Thesis, University of Leeds, **2010**.

(2) K. D. Camm; A. El-Sokkary; A. L. Gott; P. G. Stockley; T. Belyaeva; P. C. McGowan *Dalton Trans.* **2009**, 10914-10925.

(3) R. M. Lord, unpublished work, **2011**

(4) S. J. Lucas; R. M. Lord; R. L. Wilson; R. M. Phillips; V. Sridharan; P. C. McGowan *Dalton Trans.* **2012**, *41*, 13800-13802.

(5) J. J. Mannion, PhD Thesis, University of Leeds, **2008**.

(6) W. Rigby; H.-B. Lee; P. M. Bailey; J. A. McCleverty; P. M. Maitlis *Journal of the Chemical Society, Dalton Transactions* **1979**, 387-394.

(7) P. J. Sadler; A. M. Pizarro; J. J. Soldevilla; Z. Liu; A. Habtemariam, patent number WO 2011/148124 A1, **2011**

(8) M. Gorol; H. W. Roesky; M. Noltemeyer; H.-G. Schmidt *Eur. J. Inorg. Chem.* **2005**, *2005*, 4840-4844.

(9) A. M. Royer; T. B. Rauchfuss; S. R. Wilson *Inorg. Chem.* **2007**, *47*, 395-397.

(10) Z. Liu; A. Habtemariam; A. M. Pizarro; S. A. Fletcher; A. Kisova; O. Vrana; L. Salassa; P. C. A. Bruijnincx; G. J. Clarkson; V. Brabec; P. J. Sadler *J. Med. Chem.* **2011**, *54*, 3011-3026.

Chapter 6　Catalytic Transfer Hydrogenation of Benzaldehyde/Acetophenone Using Group 9 Complexes

6.1 Introduction

The catalytic activities of the compounds prepared in Chapters 2-5 were tested using the procedure shown in **Scheme 6.1** (known as the IPA system which is described in Chapter 1). These conditions were optimised for $[IrCp^*Cl_2]_2$ by Pfizer.[1] This transfer hydrogenation system is common for catalytic reductions, whereby the solvent, propan-2-ol, also behaves as the hydrogen donor, itself becoming oxidised to acetone in the process. Propan-2-ol is used in excess to prevent the reverse reaction. Chapter 1 describes transfer hydrogenation and previous successful catalysts.
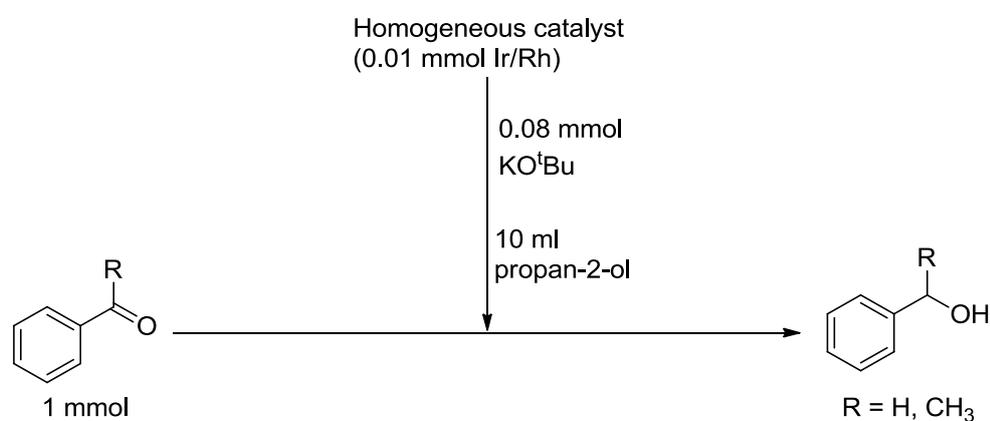
Scheme 6.1 General scheme for catalytic reduction of benzaldehyde with homogeneous complexes

6.2 Reduction of Benzaldehyde/Acetophenone Using Hydroxyl Tethered Cp* based Group 9 Halide Dimers

The functionalised dimers, prepared in Chapter 2 and shown in **Figure 6.1**, were tested as transfer hydrogenation catalysts using the reaction shown in **Scheme 6.1** along with their unfunctionalised Cp* analogues for comparison. This was to ensure that the addition of an alcohol chain to the functionalised Cp* ring did not compromise the complex's catalytic activity, as the functionalised complexes were tethered onto a solid support for use as immobilised catalysts (Chapter 7).

M = Rh, X = Cl		M = Ir, X = Cl		M = Ir, X = I	
2.6	n = 5	**2.10**	n = 5	**2.13**	n = 5
2.7	n = 9	**2.12**	n = 14		
2.8	n = 14				
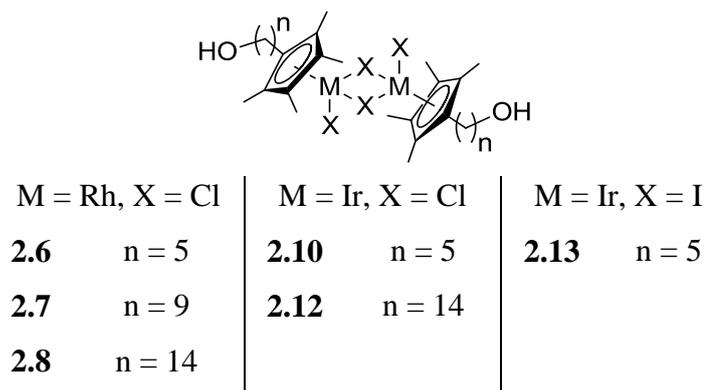
Figure 6.1 List of hydroxyl tethered Cp* based group 9 halide dimers used as homogeneous catalysts in this Chapter

6.2.1 Reduction of Benzaldehyde Using Hydroxyl Tethered Cp* Based Group 9 Halide Dimers

Chart 6.1 highlights the comparison between the activity of the hydroxyl tethered Cp* based iridium chloride dimers **2.10** and **2.12** and their unfunctionalised analogue [IrCp*Cl$_2$]$_2$ as catalysts for the reduction of benzaldehyde.
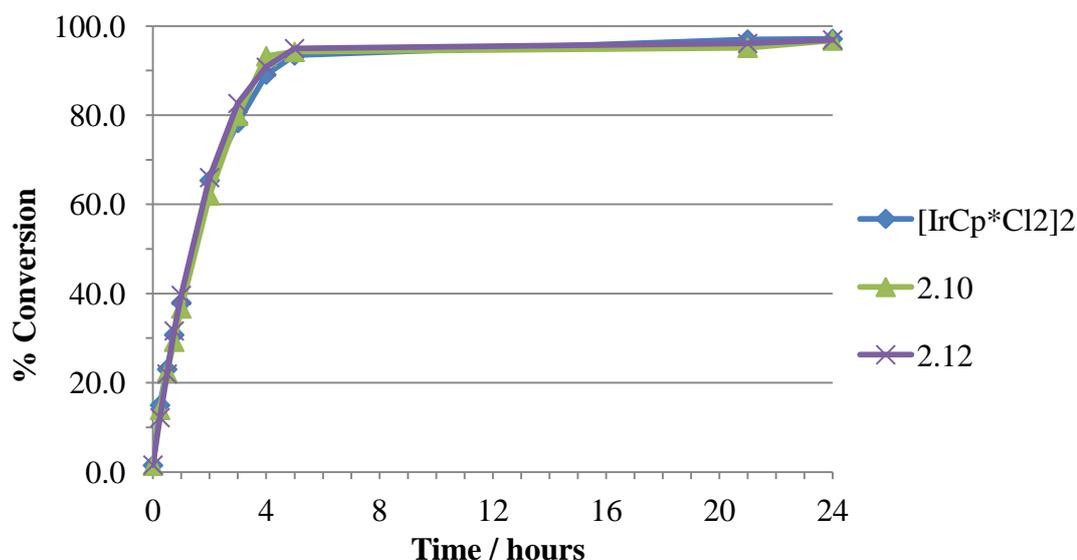
Chart 6.1 Catalytic reduction of benzaldehyde using hydroxyl tethered Cp* based iridium chloride dimers

The activity of the functionalised complexes is comparable to [IrCp*Cl$_2$]$_2$, all with a conversion of *ca* 90% after four hours, implying that the hydroxyl tether is innocent in the catalytic reaction, and consequently that the functionalised complexes are appropriate starting catalysts to immobilise onto a solid support.

Chart 6.2 highlights the comparison between the activity of the hydroxyl tethered Cp* based rhodium chloride dimers **2.6**, **2.7** and **2.8** and their unfunctionalised

analogue $[RhCp*Cl_2]_2$ as catalysts for the reduction same reaction. The activity of the functionalised complexes is comparable with $[RhCp*Cl_2]_2$, all with a conversion of 78-86% after four hours, again implying that the hydroxyl tether is innocent in the catalytic reaction, and consequently that the functionalised complexes are appropriate starting catalysts to immobilise onto a solid support. Compared to the iridium analogues discussed above, the rhodium dimers show slightly slower activity for the reduction of benzaldehyde, most noticeably seen after 1 hour with conversions in the range of 25-30% compared to 37-40% seen for the iridium analogues.
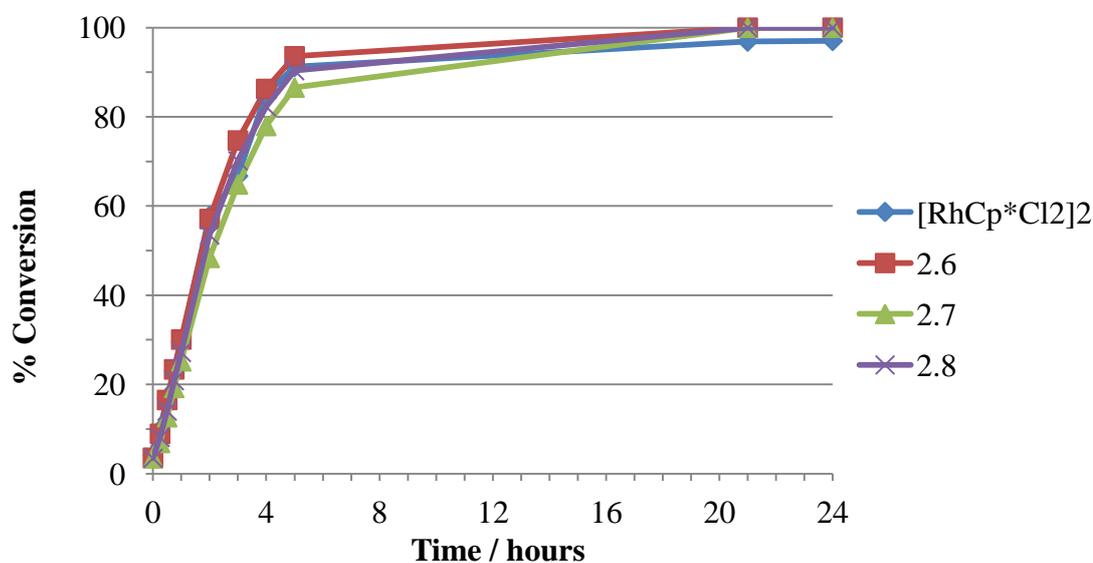
Chart 6.2 Catalytic reduction of benzaldehyde using hydroxyl tethered Cp* based rhodium chloride dimers

6.2.2 Reduction of Acetophenone Using Hydroxyl Tethered Cp* Based Group 9 Halide Dimers

The hydroxyl tethered Cp* based iridium chloride dimers were tested as catalysts for acetophenone reduction. The hydroxyl tethered Cp* based iridium complexes are comparable to their unfunctionalised analogue $[IrCp*Cl_2]_2$, although with longer reaction times than seen for the benzaldehyde reduction (**Chart 6.1**), with conversions after four hours of 68-79%, as demonstrated in **Chart 6.3**.
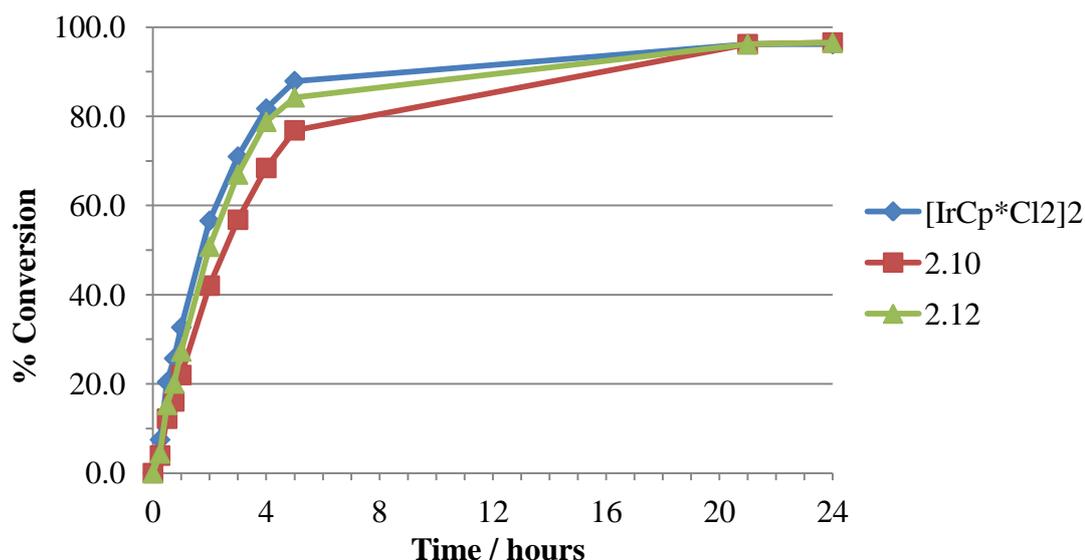
Chart 6.3 Catalytic reduction of acetophenone using hydroxyl tethered Cp* based iridium chloride dimers

For acetophenone reduction, the rhodium dimers are much more active catalysts than their iridium analogues. After 3 hours, the conversion of acetophenone to 1-phenylethanol, using the hydroxyl tethered Cp* based rhodium dimers **2.6**-**2.8**, is 79-89% (**Chart 6.4**), compared to 57-71% when using the iridium analogues.
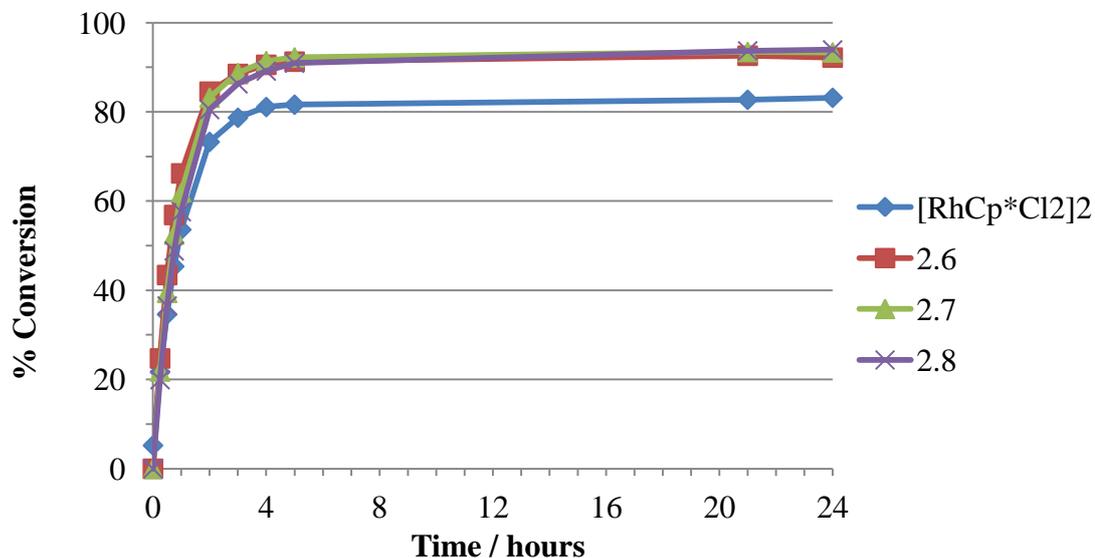
Chart 6.4 Catalytic reduction of acetophenone using hydroxyl tethered Cp* based rhodium chloride dimers

Interestingly, the alcohol tether on the catalyst, seems to improve the stability of the catalyst, compared to [RhCp*Cl$_2$]$_2$, as the initial rate is maintained for longer resulting in a higher final conversion.

6.3 Reduction of Benzaldehyde/Acetophenone Using Group 9 Pyridine Complexes

The dimers [IrCp*Cl$_2$]$_2$ and [RhCp*Cl$_2$]$_2$ are thought to behave as pre-catalysts in transfer hydrogenation reactions, where the active catalyst is a monomeric species. In order to remove this initial monomer forming step, pyridine complexes with the structures shown in **Figure 6.2** were prepared, then used in both benzaldehyde and acetophenone reductions (**Scheme 6.1**). The metal, halide, and substituent on the pyridine ring was varied in order to gain structure and catalytic activity relationships.

3.1   R = H   **3.8**   **3.14**

3.2   R = 3'-F

3.3   R = 3'-Cl

3.4   R = 3'-Br

3.5   R = 3'-I

3.15
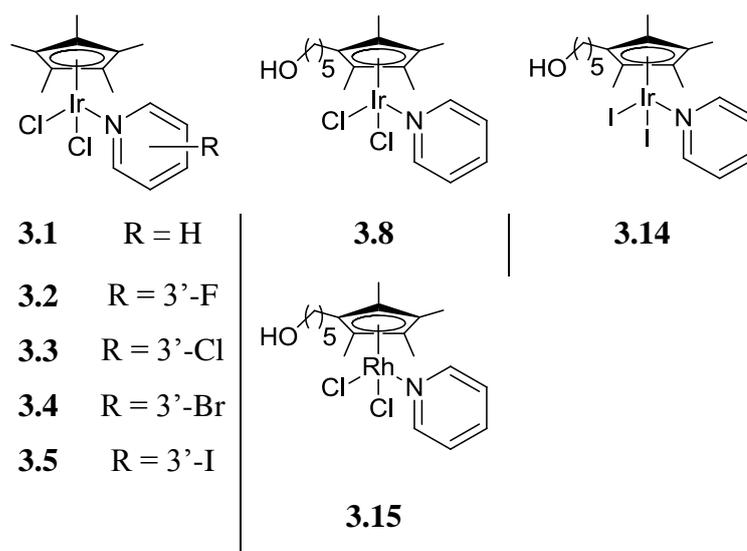
Figure 6.2 List of hydroxyl tethered Cp* based group 9 halide pyridine complexes used as homogeneous catalysts in this Chapter

6.3.1 Reduction of Benzaldehyde Using Group 9 Pyridine Complexes

The iridium Cp* dichloride pyridine complexes **3.1**-**3.5** were tested as catalysts for the reduction of benzaldehyde using the conditions shown in **Scheme 6.1**, with the results shown in **Chart 6.5**. All of the catalysts showed much lower activity than [IrCp*Cl$_2$]$_2$ giving 57-77% compared to 93% conversion after 5 hours. Addition of a halide on the *meta* position of the pyridine ligand can improve activity *cf.* the unsubstituted pyridine complex **3.1**. The 3'-F substituted pyridine complex **3.2**, which was not fully soluble in the reaction mixture, has similar activity to the unsubstituted complex **3.1**, with a conversion of 60% after 5 hours. There is no trend between the other halides and catalytic activity, as the 3'-Cl, 3'-Br and 3'-I substituted pyridine complexes all show comparable activity with a conversion of

73-77% after 5 hours.
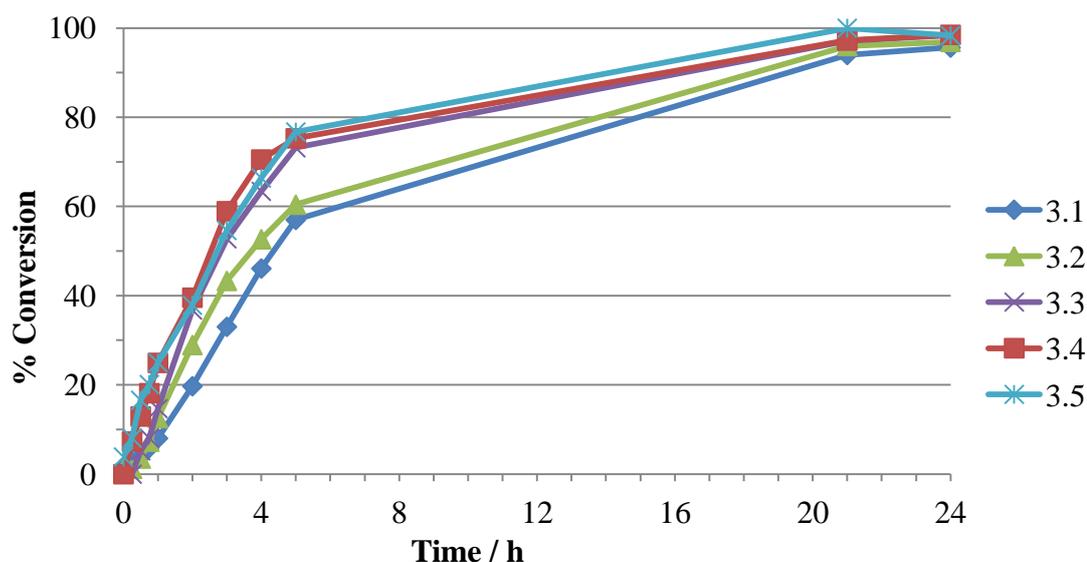
Chart 6.5 Catalytic reduction of benzaldehyde using iridium Cp* dichloride pyridine complexes
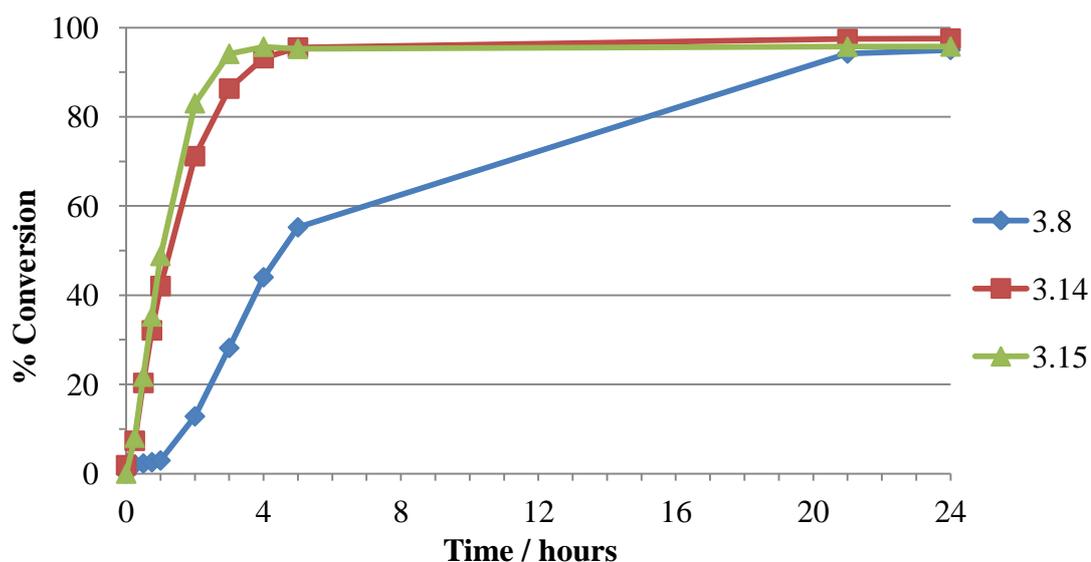
Chart 6.6 Catalytic reduction of benzaldehyde using hydroxyl tethered Cp* based pyridine complexes **3.8**, **3.14** and **3.15**

The choice of metal and halide ligand is crucial for an active catalyst for the reduction of benzaldehyde, as demonstrated in **Chart 6.6.** The iridium chloride complex, **3.8**, shows moderate activity with a conversion after 2 hours of 13%, whereas the iridium iodide and rhodium chloride analogues, **3.14** and **3.15**, show a 71 and 83% conversion respectively.

6.3.2 Reduction of Acetophenone Using Group 9 Pyridine Complexes

The iridium Cp* dichloride pyridine complexes **3.1**-**3.5** were tested as catalysts for the reduction of acetophenone using the conditions shown in **Scheme 6.1**, with the results shown in **Chart 6.7**. All of the catalysts show low activity, with final conversions, after 24 hours, in the range of 6-22% (compared to 94% for [IrCp*Cl$_2$]$_2$). As for benzaldehyde reduction, addition of a halide on the *meta* position of the pyridine ligand slightly improved activity *cf.* the unsubstituted pyridine complex **3.1**, with final conversions of 20% for compound **3.2**, 22% for compound **3.3**, 21% for compound **3.4** and 16% for compound **3.5**, compared to 7% for the unsubstituted complex **3.1**.
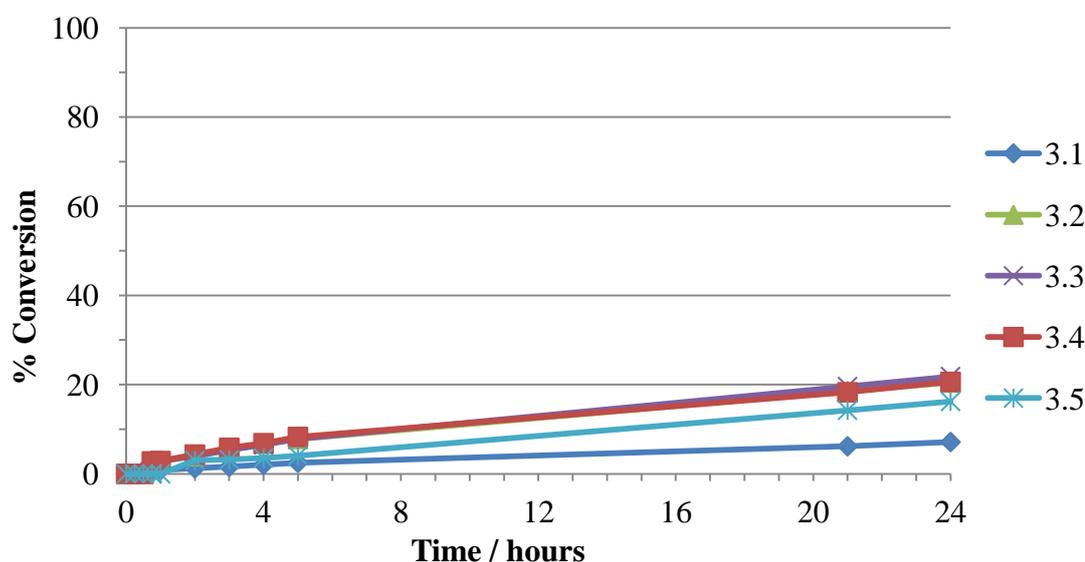
Chart 6.7 Catalytic reduction of acetophenone using iridium Cp* dichloride pyridine complexes

As for benzaldehyde reduction, the choice of metal and halide ligand in the hydroxyl tethered Cp* based pyridine complexes has a large effect on the catalytic activity, as demonstrated in **Chart 6.8**. The iridium chloride and iodide complexes, **3.8** and **3.14**, show poor activity with final conversions of 13% and 6% respectively. The rhodium chloride analogue **3.15**, however, is a much more active catalyst with a final conversion of 87%.
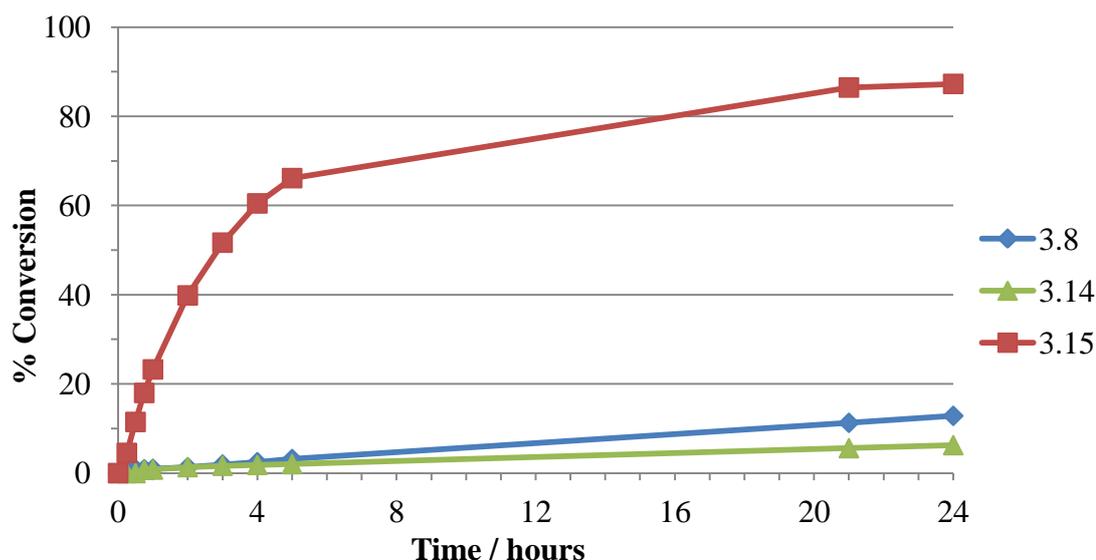
Chart 6.8 Catalytic reduction of acetophenone using hydroxyl tethered Cp* based pyridine complexes **3.8**, **3.14** and **3.15**

6.4 Reduction of Benzaldehyde/Acetophenone Using Iridium Cp* Chloride Picolinamide Complexes

The neutral picolinamide complexes prepared in Chapter 4, along with the picolinate complex and charged N-methyl picolinamide complex prepared in Chapter 5 (shown in **Figure 6.3**) were tested as catalysts for the reduction of benzaldehyde and acetophenone using the conditions shown in **Scheme 1.1**. Picolinamides were chosen as ligands as they are similar to previous ligands used for transfer hydrogenation systems. Similar picolinamide complexes have also been reported as active catalysts for reductive aminations using transfer hydrogenation conditions (discussed in Chapter 1).[2] As the picolinamide can bind through the amide N or O, there is a potential for the complex to switch during the catalytic cycle to accommodate a hydrogen. The N-methylpicolinamide complex **5.2** was tested to compare the activity of a charged, (*N,O*) binding, to a neutral, (*N,N*) binding, picolinamide complex.

4.1	R = H
4.3	R = 2', 4'- diF
4.4	R = 2', 5'- diF
4.8	R = 2', 5'- diCl
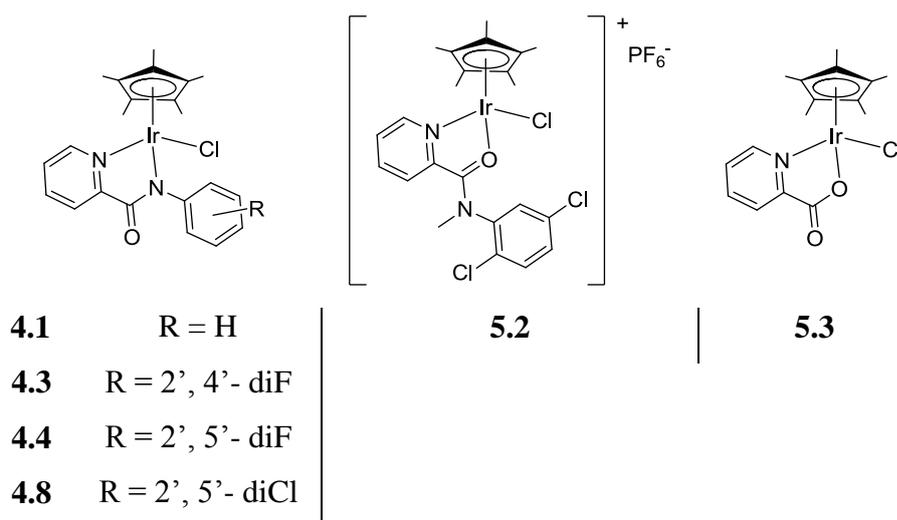
Figure 6.3 List of hydroxyl tethered Cp* based group 9 halide picolinamide complexes used as homogeneous catalysts in this Chapter

The neutral (*N,N*) binding, iridium picolinamide complexes tested against both benzaldehyde and acetophenone reduction were shown to have low activity, especially for acetophenone reduction, as demonstrated in **Table 6.1**.

Compound	% Conversion after 24 hours	
	Benzaldehyde Reduction	Acetophenone Reduction
4.1	-	6.3
4.3	-	5.9
4.4	-	5.6
4.8	25.5	5.8
5.2	97.2	40.6
5.3	27.0	15.8

Table 6.1 Catalytic activity of picolinamide and picolinate complexes for benzaldehyde and acetophenone reduction

By replacing the hydrogen on the amide of the picolinamide ligand with a methyl it is forced to bind as an L_2 ligand, through the pyridyl nitrogen and amide oxygen, forming a cationic complex. This has a significant effect on the resulting complex's catalytic activity, as demonstrated in **Chart 6.9** and **Table 6.1**.
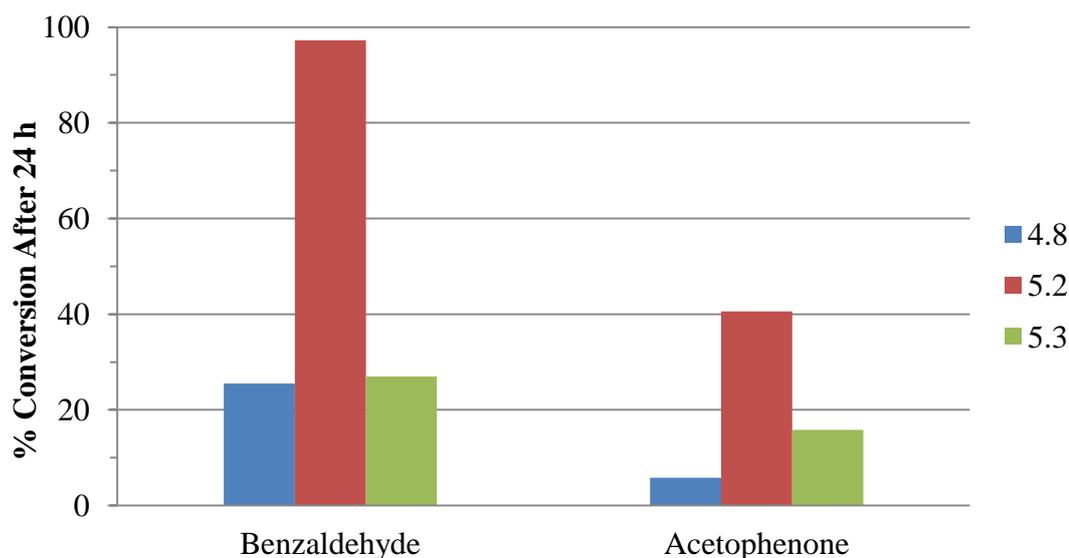
Chart 6.9 Comparison of the neutral N,N bound picolinamide complex **4.8** compared to the charged (*N,O*)-bound picolinamide complex **5.2**, with the picolinate complex **5.3** for comparison

The charged N-methylpicolinamide complex **5.2** is significantly more active than its neutral analogue **4.8**, for both benzaldehyde and acetophenone reduction. This is the most significant for the acetophenone reduction, whereby compound **5.2** converts 41% of acetophenone to its alcohol, compared to the neglible conversion of 6% when using compound **4.8** as the catalyst. In benzaldehyde reduction the final conversions are 97% and 26% using the catalyst **5.2** and **4.8** respectively. The picolinate complex **5.3** was also tested for both reactions as it has an intermediate structure between the neutral and charged picolinamide complexes, being bound through the nitrogen and oxygen (similarly to the N-methyl picolinamide), where the oxygen is an X ligand resulting in a neutral complex. It showed an intermediate conversion of 16% for acetophenone reduction and similar activity to compound **4.8** for benzaldehyde reduction of 27%.

6.5 Conclusion

Several of the complexes prepared in Chapter 2-5 were tested as catalysts for the reduction of benzaldehyde and acetophenone using a transfer hydrogenation system with *iso*-propanol as the hydrogen donor. In most cases, the catalyst is more active for the reduction of benzaldeyde than acetophenone. The hydroxyl tethered Cp* based dimers prepared in Chapter 2 show comparable activity to their Cp* analogues which is an encouraging result as they have been tethered onto a solid support for

use as immobilised catalysts (discussed in Chapter 7).

The pyridine complexes have less catalytic activity than their respective Cp* dimers, however addition of a halide on the 3' position of the pyridine ring slightly improves activity. The choice of metal and halide ligand has a dramatic effect on catalytic activity, especially for acetophenone reduction where the rhodium chloride complex **3.15** converts 87% of acetophenone after 24 hours, compared to the iridium chloride and iodide analogues, **3.8** and **3.14**, which both convert less than 15% of acetophenone after 24 hours.

The neutral picolinamide complexes show trace activity towards acetophenone reduction with a final conversion after 24 hours of less than 10%. The charged N-methylpicolinamide complex, however, has much more activity with a conversion of 41% after 24 hours.

6.6 Future Work

The complexes discussed could be tested as catalysts for alternative transfer hydrogenation systems, particularly the neutral picolinamide complexes which have been reported to be active reductive amination catalysts. Due to the initial success of the N methyl picolinamide complex as an active catalyst for the reduction of acetophenone, a library of similar compounds could be tested to gain a structure activity relationship between the groups on the arene ring and the catalytic activity.

6.7 References

(1)   A. Pettman, unpublished work, **2009**
(2)   M. Watanbe; J. Hori; K. Murata, patent number US 2010/0234596 A1, **2010**

Chapter 7   Immobilisation of Functionalised Cp* Group 9 Chloride Complexes for Use as Transfer Hydrogenation Catalysts

7.1 Introduction

Since the discovery of the Noyori catalyst,[1-3] hydrogen transfer reactions using ruthenium-arene and iridium/rhodium Cp* catalysts have become a much explored topic.[4-14] Whilst these catalysts offer excellent activity and selectivity across a wide range of reactions, they employ precious metals, making large scale processes expensive. Moreover, their separation from the product, to acceptable ppm levels, is often difficult and tiresome. By immobilising the catalyst onto a solid support, it should be easily removed from the reaction mass *via* decantation /filtration and ideally recycled making the reaction commercially viable. Furthermore, a solid phase catalyst can be used in continuous flow processes. The main problems associated with current immobilised catalysts are metal leaching, loss of activity and selectivity and catalyst degradation. Previous immobilisation strategies for these catalysts have focused on tethering through a diamine ligand with varied success and most report metal leaching (discussed in further detail in Chapter 1).[15-22] The most promising system was reported by Li *et al* whose poly(ethylene glycol)-supported ruthenium complex is active against the reduction of acetophenone over 14 runs, however with reduced conversions and increased reaction times.[19] Tethering through the bidentate ligand restricts the catalysts to these reactions, limiting the scope.

The iridium Cp* iodide dimer, **2.13** (**Figure 7.1**), was immobilised onto polyethylene glycol and used as a racemisation catalyst in the asymmetric transformation of racemic into optically active sertraline, though the catalyst showed a loss in activity over two reuses possibly due to inactive substrate-catalyst insertion complexes formed at higher temperatures (discussed further in Chapter 1).[23]
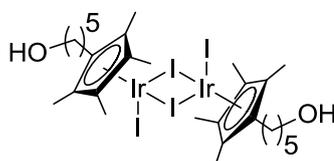
Figure 7.1 The iridium iodide dimer **2.13**, synthesised in Chapter 2

This immobilisation strategy focuses on covalent attachment of Group 9 Cp* catalysts, with the general structure shown in **Figure 7.2**, via the hydroxyl tethered Cp* based ligand. Both the strong η^5 coordination between the functionalised Cp* ring and the metal, and the covalent attachment of the tether to the support should prevent any metal leaching throughout the catalytic reaction. Another advantage of

immobilising through the functionalised Cp* ligand is the ability to add different ancillary ligands to the metal enabling flexible use of the system in a variety of different reactions. By including a linker between the ring and the support, this should provide enough flexibility that the active centre still behaves homogeneously, and therefore retains the selectivity of the analogous homogeneous catalyst. The choice of metal, length of the linker, and their effect on catalytic activity was investigated.
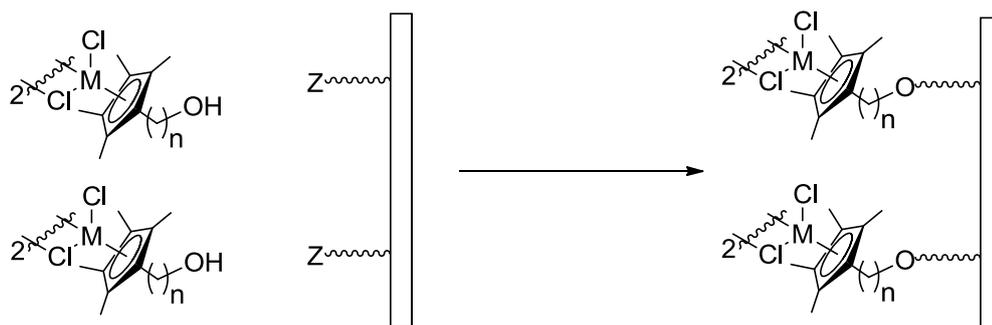
Figure 7.2 Immobilisation strategy of hydroxyl tethered Cp* based Group 9 Complexes onto a solid support

The solid used as a support here is a polystyrene supported Wang resin (with particle sizes of 100-200 mesh, 1% cross linking of divinylbenzene and a 1.51 mmol/g loading). As the resin is cross-linked, it is insoluble in all common solvents. The resin swells in aprotic solvents, with the swelling data for common solvents listed in **Table 7.1**.[23] The degree of swelling in the reaction solvent will affect the catalytic activity of the immobilised catalyst.

Solvent	Swelling factor (ml/g of resin)	Solvent	Swelling factor (ml/g of resin)
Tetrahydrofuran	5.5	Acetonitrile	4.7
Toluene	5.3	Dimethylformamide	3.5
Dichloromethane	5.2	Diethyl ether	3.2
Ethanol	3.2	Methanol	1.8
Dioxane	4.9	Water	1.0 (no swelling)

Table 7.1 Swelling data for 1% crosslinked polystyrene in common solvents

7.2 Synthesis and Optimisation of Immobilisation Method

The immobilisation method was adapted from a method originally devised by Pfizer.[24] The hydroxyl tethered Cp* based metal halide dimers **2.6** and **2.8**-**2.12**,

prepared in Chapter 2 were immobilised onto a polystyrene supported Wang resin *via* a triflate intermediate, prepared *in situ* under inert conditions (**Scheme 7.1**).

2.6	M = Rh	n = 5	**2.10**	M = Ir	n = 5
2.8	M = Rh	n = 14	**2.11**	M = Ir	n = 9
2.9	M = Ir	n = 3	**2.12**	M = Ir	n = 14

7.1	M = Rh	n = 5	**7.4**	M = Ir	n = 5
7.2	M = Rh	n = 14	**7.5**	M = Ir	n = 9
7.3	M = Ir	n = 3	**7.6**	M = Ir	n = 14

7.7	M = Rh	n = 5	**7.10**	M = Ir	n = 5
7.8	M = Rh	n = 14	**7.11**	M = Ir	n = 9
7.9	M = Ir	n = 3	**7.12**	M = Ir	n = 14
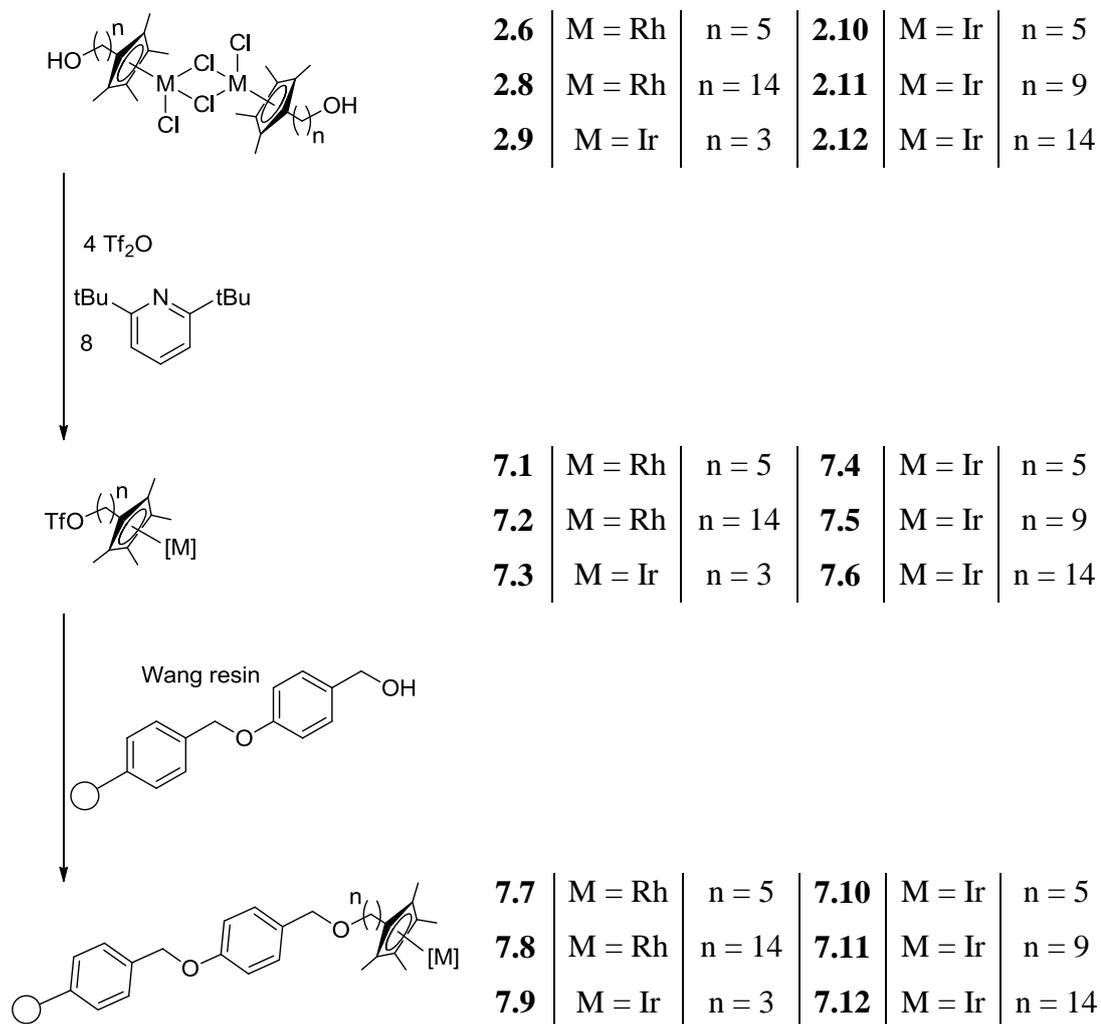
Scheme 7.1 Immobilisation of hydroxyl tethered Cp* based metal halide complexes onto polystyrene supported Wang resin

2,6-Di-*tert*-butylpyridine was added to triflic anhydride at -10°C. The hydroxyl tethered Cp* based metal halide dimer was added slowly to the mixture at -10°C (over 30 minutes for a small scale 200 mg synthesis, or an hour for a 5 g synthesis). The solution was then left to stir at room temperature for an hour, where for the iridium analogues **2.9**, **2.10**, **2.11** and **2.12**, a dark green/brown solution was obtained and for the rhodium analogues **2.6** and **2.8**, a red solution was obtained. When 2,6-di-*tert*-butylpyridine was replaced with 2,6-lutidine, there were multiple peaks in the 3-4 ppm region for the ^{1}H NMR of **7.4**, along with extra peaks between 5 and 6 ppm. As demonstrated in Chapter 3, a less substituted pyridine couldn't be used as a base as it behaves as a ligand and binds to the metal centre and results in a poorer catalyst.

An excess of triflic anhydride, along with slow addition of the metal dimer was necessary to avoid the formation of secondary products, which are presumably ethers formed by reaction of the starting dimer with a triflate intermediate. Under these conditions, the triflate always formed in over 90% conversion. The conversion was monitored by ^{1}H NMR, by the shift of the CH_2 peak adjacent to the oxygen in the alkyl chain, as demonstrated in **Figure 7.3** for compound **7.4**, where the peak at 4.5 ppm represents the C$\underline{H}_2$OTf protons and the peaks at 3.5 and 3.4 ppm presumably represent C$\underline{H}_2$OR protons. The peak for the C$\underline{H}_2$OH for **2.10** has disappeared, indicating that the reaction is complete.
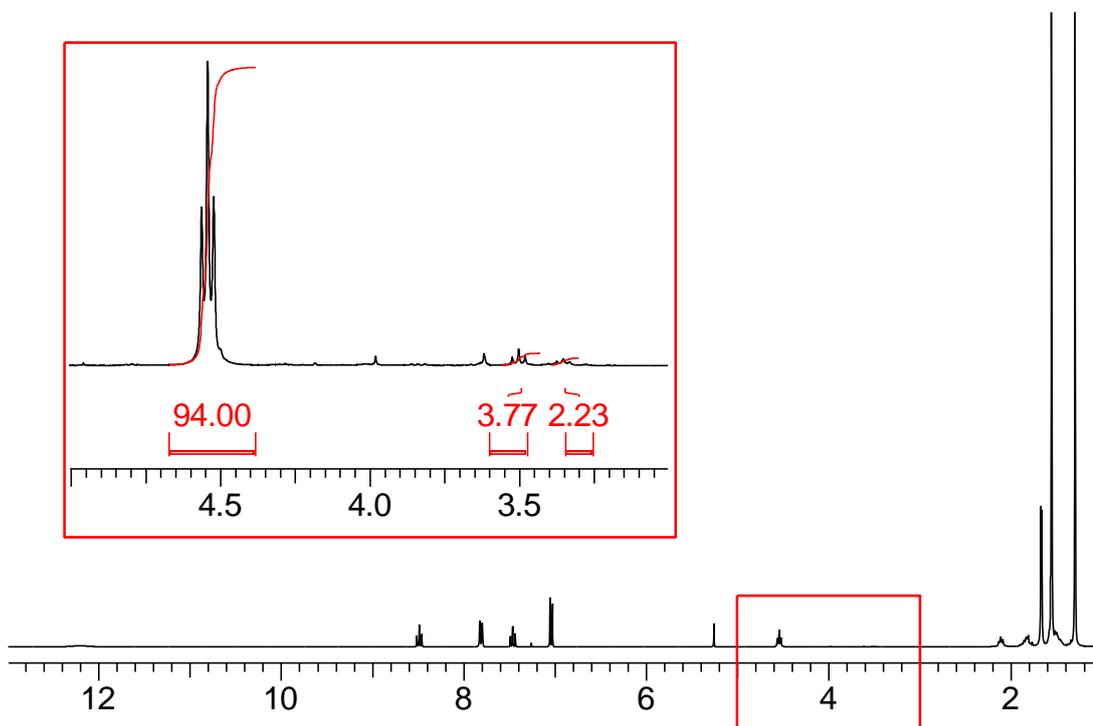
Figure 7.3 ^{1}H NMR spectrum of the *in situ* triflate intermediate **7.4**, showing 94% conversion to the triflate *cf.* secondary products

After removal of the excess triflic anhydride by vacuum distillation, the triflate intermediate was added to the Wang resin and the mixture was agitated overnight. The resulting red resin was washed with dichloromethane until the filtrate was colourless, and this was followed sequentially by a wash with water, 1M HCl, water and methanol.

7.3 Control Homogeneous Reactions

In order to determine the true nature of the immobilised complex, a control reaction was performed, whereby [IrCp*Cl$_2$] was reacted with triflic anhydride and

2,6-di-*tert*-butylpyridine in dichloromethane. The initial orange solution instantly turned yellow upon addition of the triflic anhydride. After evaporation of the dichloromethane, yellow single crystals of the product were obtained by vapour diffusion from a dichloromethane/pentane solvent system. Although the counterion could not be modelled, $[IrCp*Cl_{1.5}]_2^+$ can be seen, as shown in **Figure 7.4**.
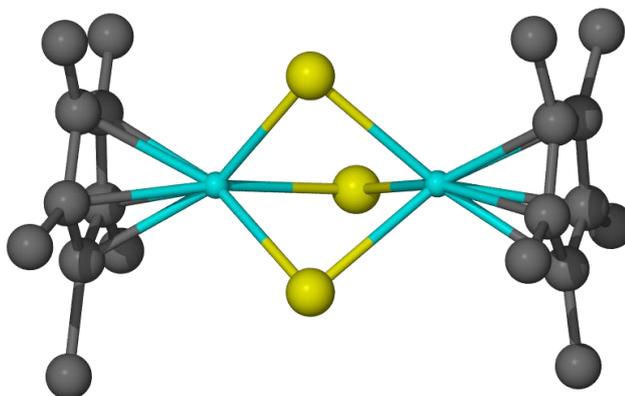
Figure 7.4 Partially solved crystal structure of the product formed from the reaction of $[IrCp*Cl_2]_2$ with triflic anhydride and 2,6-di-*tert*-butylpyridine

As purification of the material was difficult, the reaction was repeated but adding the reagents stepwise. $[IrCp*Cl_2]$ was reacted with triflic anhydride in dichloromethane (shown in **Scheme 7.2**) which, as previously, resulted in a yellow solution.
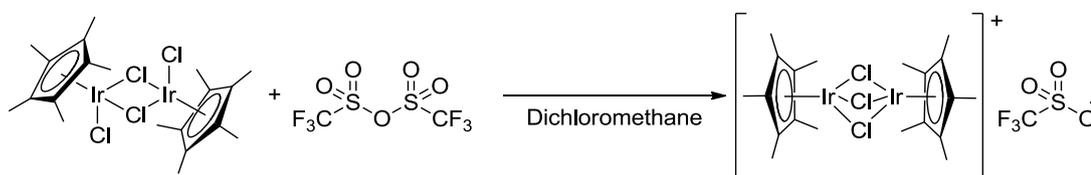
Scheme 7.2 Synthesis of compound **7.13**

After purification, CHN analysis matched the formation of $C_{21}H_{30}Cl_3F_3Ir_2O_3S$, corresponding to the tri-chloro bridged dimer with a triflate counterion, $[IrCp*Cl_{1.5}]_2^+$ TfO$^-$ **7.13**. There is a noticeable shift of the methyl protons in the ^1H NMR from 1.6 to 1.7 ppm, along with a single peak for the fluorides of the triflate counterion in the ^{19}F NMR, and a quarternary peak at 120.9 ppm for the carbon of the triflate counterion. Compound **7.13** does not react with 2,6-di-*tert*-butylpyridine. Although compound **7.13** is novel there are similar analogues with the same cation but different anions.[25] The diagnostic methyl peak shift is also observed for the triflate intermediates in the immobilisation procedure (from 1.59-1.62 ppm, for the

iridium di-chloro bridged dimers **2.9**-**2.12**, to 1.67-1.73 ppm for the triflate intermediates **7.3**-**7.6**) implying that the functionalised dimers form analogous tri-chloro bridged species as well as their hydroxyl group becoming triflated. The same trend is also seen for the rhodium analogues, where the methyl peaks shift from 1.61-1.65 ppm for the dichloride bridged dimers **2.6** and **2.8**, to 1.69-1.71 ppm for the triflate intermediates **7.1** and **7.2**.

Compound **7.13** was tested as a catalyst for the reduction of benzaldehyde according to **Figure 7.3** (the same procedure as for the homogeneous catalysts in Chapter 6).
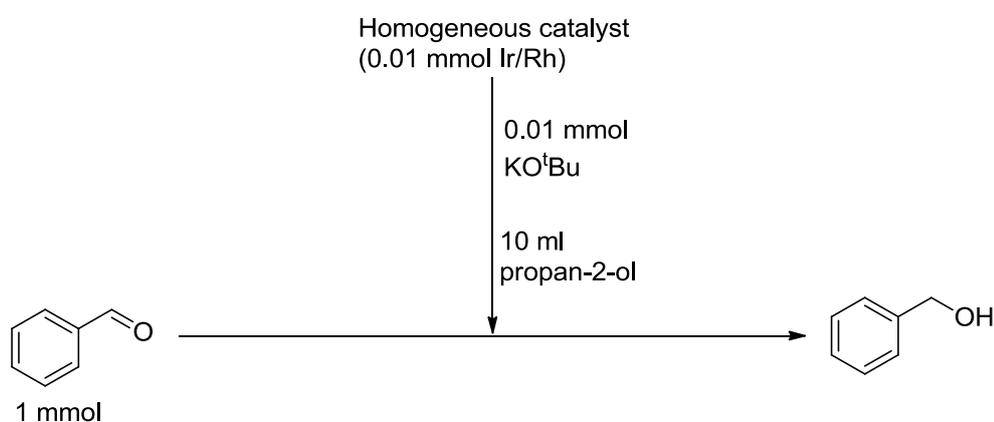
Scheme 7.3 General scheme for catalytic reduction of benzaldehyde with homogeneous complexes

The tri-chloro bridged dimer **7.13** has almost identical activity to $[IrCp*Cl_2]_2$ for the reduction of benzaldehyde, reaching almost quantitative conversion after 5 hours (**Chart 7.1**). The activity of a similar species with a perchlorate counterion was shown in 1988.[25]
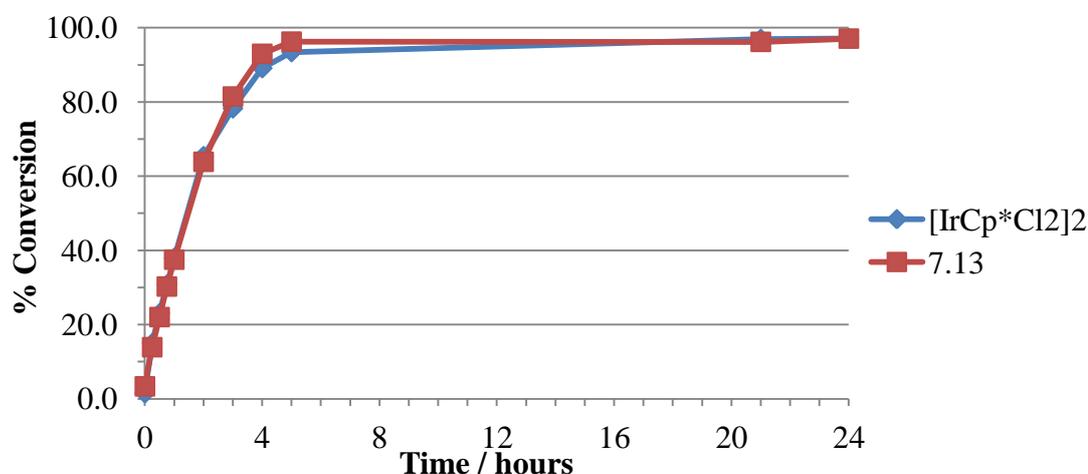
Chart 7.1 Catalytic activity of the tri chloro bridged dimer **7.13** for the reduction of benzaldehyde *cf.* $[IrCp*Cl_2]_2$

In the immobilisation procedure, the immobilised complex is washed with 10 ml of 1M HCl. When the tri-chloro bridged dimer **7.13** was reacted with 1M HCl, the yellow mixture instantly turned orange, and after filtering, the ^{1}H NMR of the resulting orange powder, along with the disappearance of a fluoride peak in the ^{19}F NMR, and $\underline{C}F_3$ in the $^{13}C\{^1H\}$ NMR, showed the compound to be $[IrCp*Cl_2]_2$. This has also been shown with the similar compound $[IrCp*Cl_{1.5}]_2{}^+BF_4{}^-$.[26]
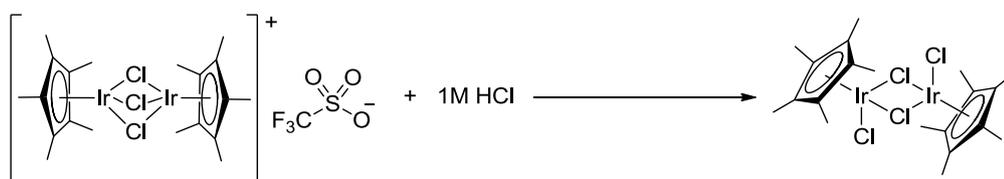
Scheme 7.4 The reaction of compound **7.13** with 1M HCl to form $[IrCp*Cl_2]_2$

This suggests that the HCl wash in the immobilisation procedure, may convert the immobilised tri-chloro bridged species back to the di-chloro bridged species.

7.4 Characterisation of Immobilised Complexes

The loading of metal on the immobilised complexes has been determined using Inductively Coupled Plasma (ICP) analysis. Although this gives a determination of the amount of metal attached to the resin, it does not give any information about what form the metal species is in, *i.e.* the oxidation state, geometry, whether it is in the form of an active catalyst or not. Due to this uncertaintly, the mol% of catalyst stated in the heterogeneous catalytic reactions is assuming that each metal centre is part of an active catalyst, so in effect states the maximum catalyst loading possible.

Immobilised Complex	Washing procedure	% of Metal (Ir/Rh)	Metal (Ir/Rh) loading (mmol/g)
7.7	60°C 1:1 *iso*-propanol:dichlorometane, room temperature acetone	7.9	0.77
7.8	60°C 1:1 *iso*-propanol:dichlorometane, room temperature acetone	6.6	0.64
7.10	60°C iso-propanol	12.4	0.65
7.10	60°C 1:1 *iso*-propanol:dichlorometane, room temperature acetone	11.7	0.61
7.12	60°C 1:1 *iso*-propanol:dichlorometane, room temperature acetone	9.0	0.47

Table 7.2 ICP Analysis of immobilised complexes **7.7**, **7.8**, **7.10** and **7.12**

The metal loading of immobilised complexes **7.7**, **7.8**, **7.10** and **7.12**, determined

by ICP analysis, are shown in **Table 7.2**. The solid state NMR of immobilised complex **7.10** is shown in **Figure 7.5** with peak values, and in **Figure 7.7** with comparison to the initial dimer **2.10** and the Wang resin. The quarternary functionalised Cp* peaks (labelled **a** in **Figure 7.6**) cannot be seen (between 60 and 100 ppm for compound **2.10**), due to their low intensity. The peaks at 10.1, 10.5 and 11.7 ppm correspond to the carbons b, the methyl groups attached to the functionalised Cp* ring. The peaks at 25.0, 27.2, 28.2, and 30.3 ppm correspond to the CH$_2$ groups on the alkyl chain c, d, e and f respectively. The CH$_2$ group g appears at 73.4 ppm compared to 62.5 ppm for the functionalised dimer **2.10**.

There was one peak at -76.8 ppm in the solid state ^{19}F NMR of the immobilised complex **7.10**, in the same region as the triflate peak for **7.13** in its solution state ^{19}F NMR. This implies that at least some of the immobilised complex could be in the form of the cationic tri-chloro bridged complex analogous to **7.13**.
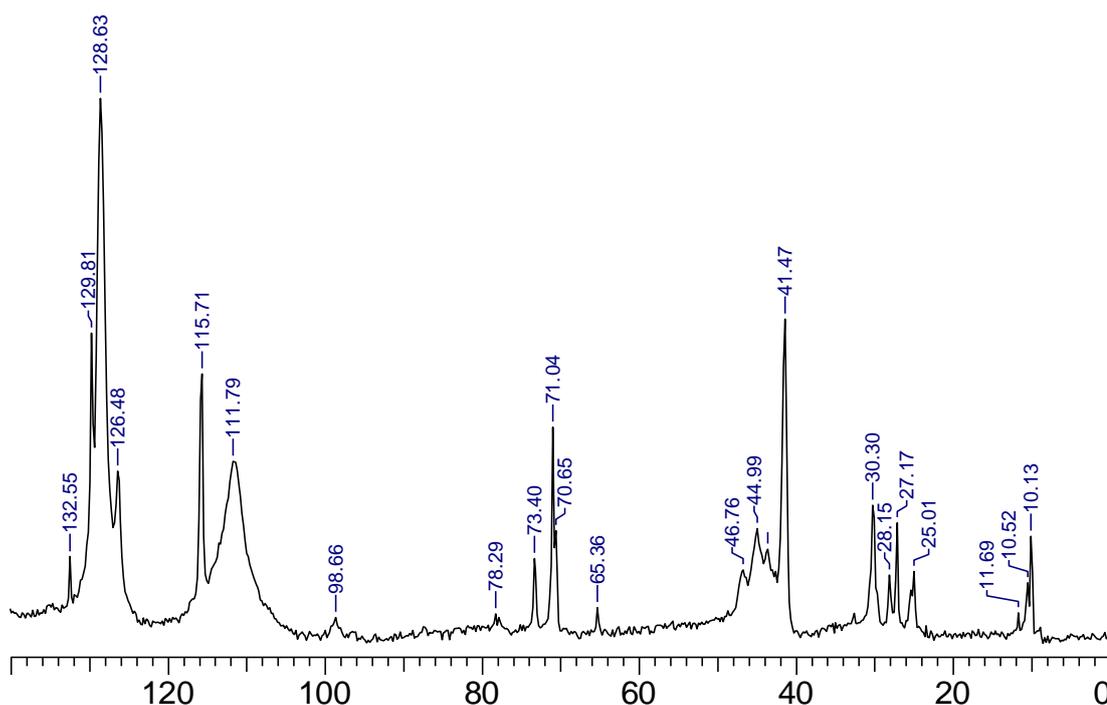
Figure 7.5 Solid state ^{13}C{^{1}H}NMR of the immobilised complex **7.10**
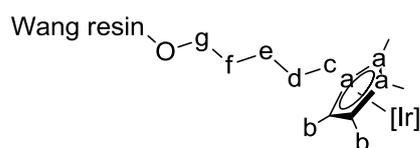
Figure 7.6 Labelled diagram of compound **7.10**
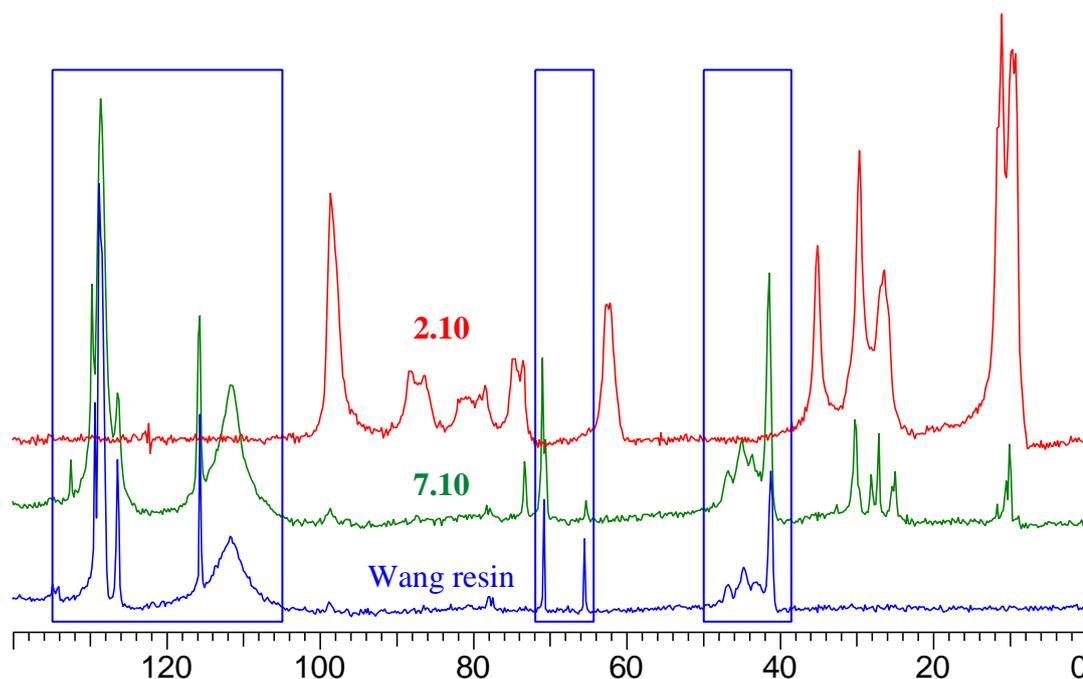
Figure 7.7 Solid state ^{13}C{^{1}H}NMR of the immobilised complex **7.10**, along with the functionalised dimer **2.10** and polystyrene supported Wang resin for reference. The blue boxes highlight the peaks due to the resin

7.5 Activity of Immobilised Catalysts for Benzaldehyde Reduction

7.5.1 Catalytic Activity and Recyclability of Immobilised Complex 7.10

The immobilised iridium complex **7.10** was originally prepared by reacting the triflate intermediate **7.4** with 1 equivalent of the Wang resin (Ir:Wang ratio of 2:1) in an attempt to saturate the resin with catalyst. Further washing and catalytic testing of the catalysts in batch reactions, including homogeneous comparisons, was conducted by Ben Crossley at Yorkshire Process Technology Ltd. Compound **7.10** was repeatedly heated in 10 ml of *iso*-propanol at 60°C, until the filtrate was colourless. 57 mg of compound **7.10** was used to catalyse the reduction of 0.5 mmol of benzaldehyde to benzyl alcohol, equating to a catalyst loading of 7.4 mol% iridium (by ICP). The general catalytic procedure is shown in **Scheme 7.5**.
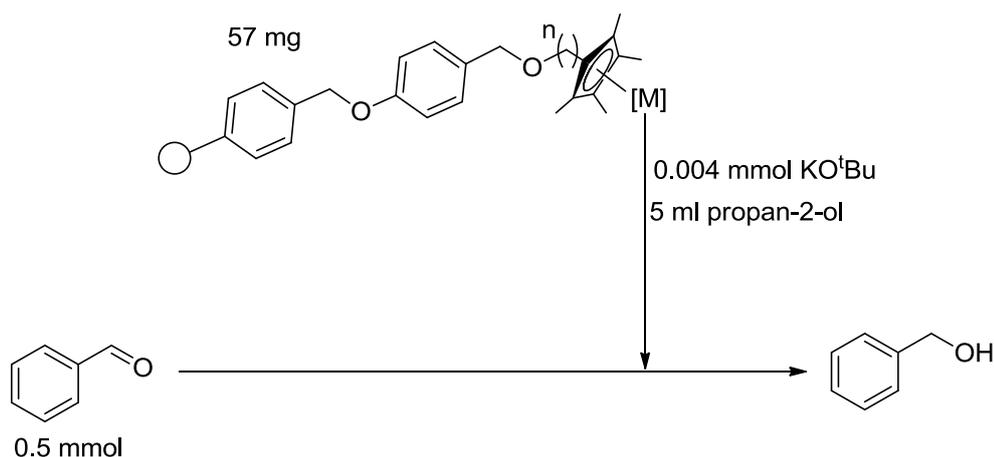
Scheme 7.5 General scheme for catalytic reduction of benzaldehyde with immobilised complexes

The immobilised complex **7.10** is an active catalyst for the reduction of benzaldehyde, reaching quantitative conversion after 24 hours. This is moderate activity compared to its homogeneous analogue **2.10** (demonstrated in **Chart 7.2**) with conversion after four hours being 37% compared to 98%.
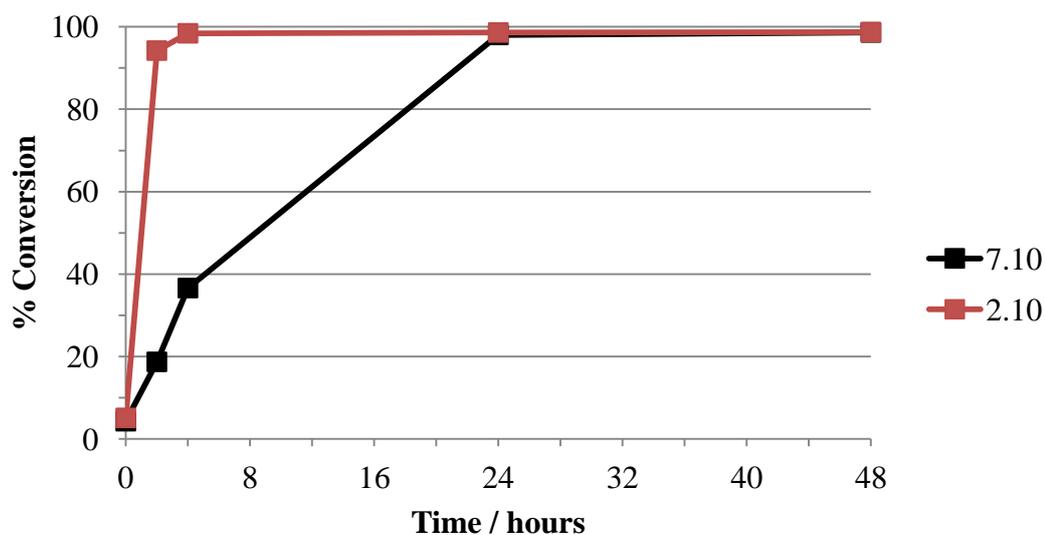
Chart 7.2 Catalytic activity of the immobilised complex **7.10** compared to the homogeneous analogue **2.10** (1 mol% homogeneous catalyst)

After 48 hours, the immobilised complex **7.10** was recycled by decanting the liquor and immediately adding new solvent/base/substrate. The catalyst was used for 35 runs for benzaldehyde reduction, with the results shown in **Table 7.3** and **Chart 7.3**. Run three shows the highest initial rate, reaching 49% conversion after four hours. The first 15 runs each give high conversion after 48 hours, and at least 87% after 24 hours. From run 15 through to run 26, **7.10** becomes progressively less

active, presumably due to catalyst decomposition/a loss of resin in the decantation steps (*vide infra*). By the 26th run the conversion after 48 hours had tailed-off to 80%. Between runs 26 and 27 the solution was decanted from the catalyst, *iso*-propanol was added and the mixture was left to stand for 96 hours, compared to the standard decantation followed by addition of new reagents/solvent. This had a detrimental effect on the catalytic activity, where the initial rate almost halved on run 27 *cf.* run 26. This shows that the catalyst is unstable when removed from the reaction solution. This could be an indication for the slightly reduced activity after the decantation steps.
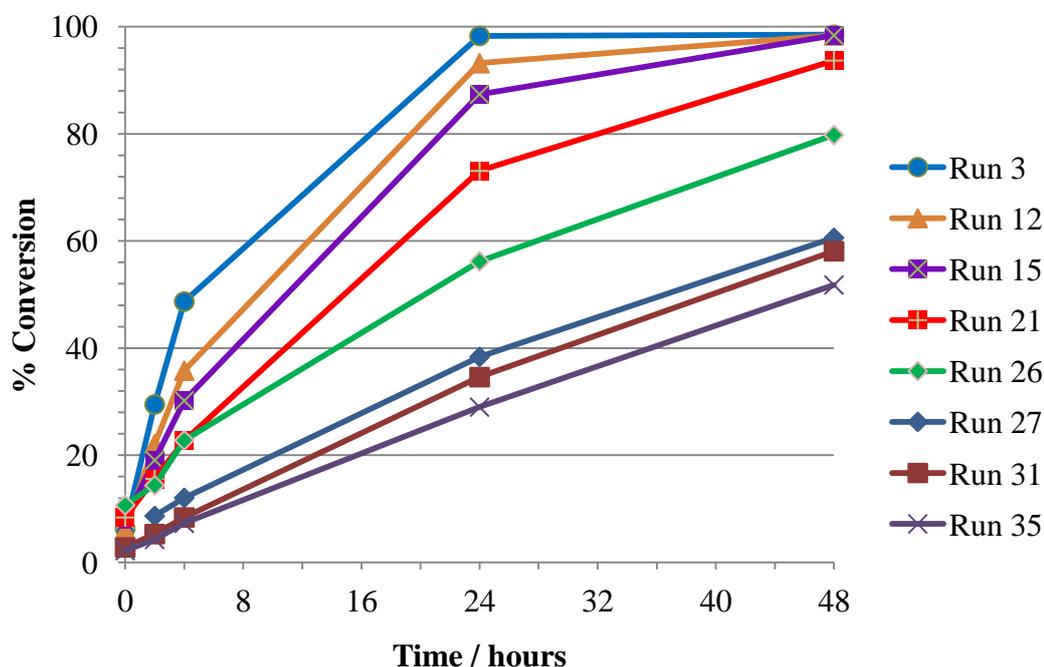
Chart 7.3 Reuse data for reduction of benzaldehyde by catalyst **7.10**

35 mg of the resin **7.10** was recovered post reaction, *cf.* the original 57 mg, and was washed with *iso*-propanol and dichloromethane to remove any residues, then dried in a vacuum oven overnight. ICP analysis of the recovered resin **7.10** showed the iridium content to be 11.5% weight equating to 0.60 mmol Ir/g (*cf.* the original 0.65 mmol Ir/g). This 0.05 mmol Ir/g loss can mostly be attributed to the loss of unbound material as more intensive washes with hot 1:1 dichloromethane/*iso*-propanol, followed by a room temperature acetone wash leave the resin with a 0.61 mmol Ir/g loading. This shows that, once any unbound material has been removed, there is minimal catalyst leaching, making this system a promising candidate for industrial reactions.

Compound	% Conversion/h				
	0	2	4	24	48
2.10	5.1	94.2	98.4	98.6	98.7
7.10 (run 1)	4.3	18.7	36.6	98.0	98.6
7.10 (run 2)	6.4	22.0	38.7	98.0	98.1
7.10 (run 3)	6.3	29.5	48.7	98.3	98.5
7.10 (run 12)	6.1	22.1	35.8	93.2	98.4
7.10 (run 15)	8.0	19.1	30.2	87.4	98.4
7.10 (run 16)	5.1	16.5	26.2	83.1	98.2
7.10 (run 17)	5.7	17.0	25.9	80.0	96.1
7.10 (run 18)	7.0	16.6	25.2	75.9	95.0
7.10 (run 19)	8.8	16.8	25.6	74.6	94.7
7.10 (run 20)	8.6	15.8	27.0	75.1	94.2
7.10 (run 21)	8.4	15.6	22.7	73.1	93.7
7.10 (run 22)	7.1	15.4	22.6	67.1	89.8
7.10 (run 23)	9.9	15.2	20.3	61.7	86.3
7.10 (run 24)	7.6	11.9	17.4	56.4	82.7
7.10 (run 25)	10.9	18.1	21.3	58.4	81.9
7.10 (run 26)	10.7	14.4	22.8	56.2	79.8
7.10 (run 27)	-	8.7	12.1	38.4	60.6
7.10 (run 28)	0.6	4.2	7.5	36.5	63.1
7.10 (run 29)	2.3	5.6	9.0	38.3	64.0
7.10 (run 30)	2.1	5.4	8.8	37.6	61.3
7.10 (run 31)	2.8	5.3	8.4	34.6	58.1
7.10 (run 32)	2.0	4.3	6.7	32.4	53.2
7.10 (run 33)	2.8	5.2	7.9	33.2	56.4
7.10 (run 34)	2.9	5.2	7.8	31.2	52.3
7.10 (run 35)	2.2	4.3	7.3	29.0	51.8

Table 7.3 Reuse data for reduction of benzaldehyde by catalyst **7.10**

A new catalytic run was initiated where 35 mg of Catalyst **7.10** was tested for the reduction of benzaldehyde (**Scheme 7.5**), in order to determine whether the activity loss is due to a loss of resin over the decantation steps (**Chart 7.4**). The activity of 35 mg of catalyst **7.10**, is higher than the 35th run for 57 mg of catalyst **7.10** (**Chart**

7.3), confirming that the activity loss is mostly due to catalyst deactivation. Its activity, however, is similar to that of runs 12-21 for 57 mg of catalyst **7.10**, indicating that the loss of resin over decantation steps has an effect on the catalyst's performance and can partly be attributed to the activity loss over 35 runs. In a large scale reactor, the resin loss would be less significant. In flow systems, the separation step of the catalyst from the solution is avoided, eliminating a resin loss over time.
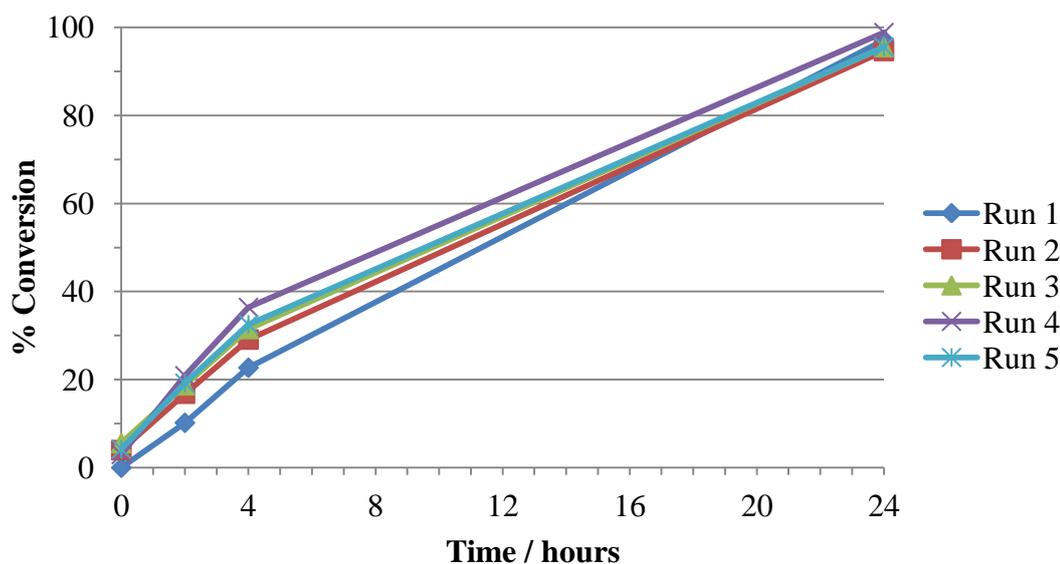
Chart 7.4 35 mg of catalyst **7.10** for the reduction of benzaldehyde *via* **Scheme 7.5**

7.5.2 Catalytic Activity of the Immobilised Complexes After a Washing Regime

It was found, that by repeatedly washing the immobilised complexes firstly in a 1:1 dichloromethane:*iso*-propanol solution at 60°C, followed by a room temperature acetone wash, firstly leaching of metal is seen, and secondly that the catalyst has a higher performance. It is thought that this leaching occurs because the resin is more swelled than in the original neat *iso*-propanol wash, so non-bound material leaches into solution. **Chart 7.5** highlights the increased activity observed due to this new washing regime. The run chosen for each system is the most active run (run three for the original hot propan-2-ol wash, and run two for the hot dichloromethane:*iso*-propanol followed by a room temperature acetone wash).
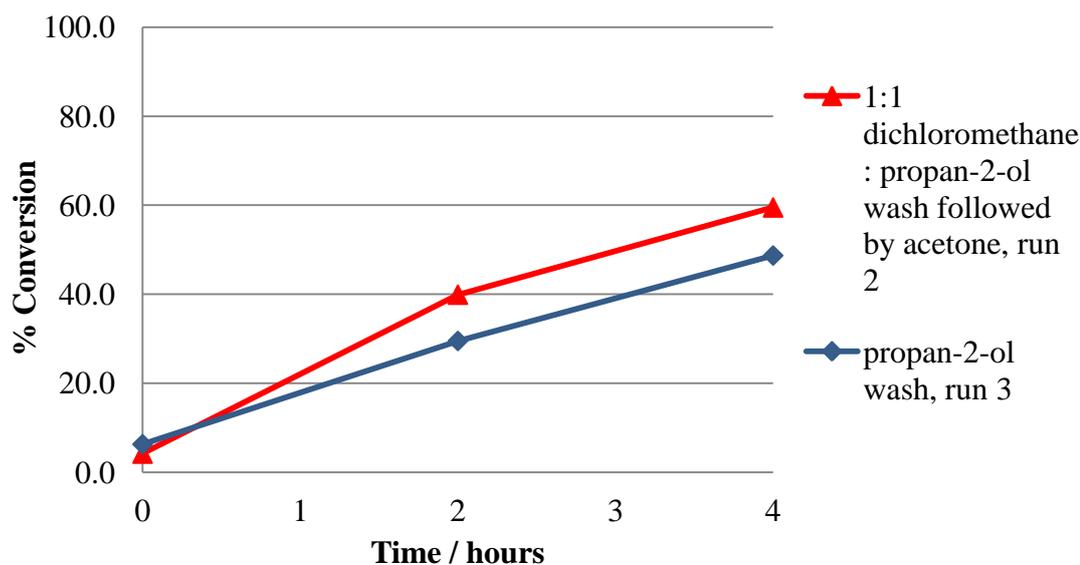
Chart 7.5 A graph to highlight the improved catalytic activity of catalyst **7.10** for the reduction of benzaldehyde *via* **Scheme 7.5**, with a new washing regime

7.5.2.1 The Effect of Metal and Tether Length on Catalytic Activity

The rhodium and iridium hydroxyl tethered Cp* based dimers were prepared with variable tether lengths between the functionalised Cp* ring and the hydroxyl, in order to investigate the effect of metal and tether length on catalytic activity of the immobilised complexes, for the reduction of benzaldehyde, using the method shown in **Scheme 7.5**. As discussed in Chapter 6, the tethered dimers show similar activity to their Cp* analogues under homogeneous conditions, so any variation in activity is due to the effect of a variable tether length between the catalyst and support. As stated previously, the immobilised iridium complex **7.10** with a 5 carbon linker between the functionalised Cp* ring and the hydroxyl group has slightly higher activity when pre-washed with hot dichloromethane:*iso*-propanol, followed by acetone. The catalyst shows similar activity for the first ten runs, followed by a small loss for each consecutive run up to run 16 (**Chart 7.6**).
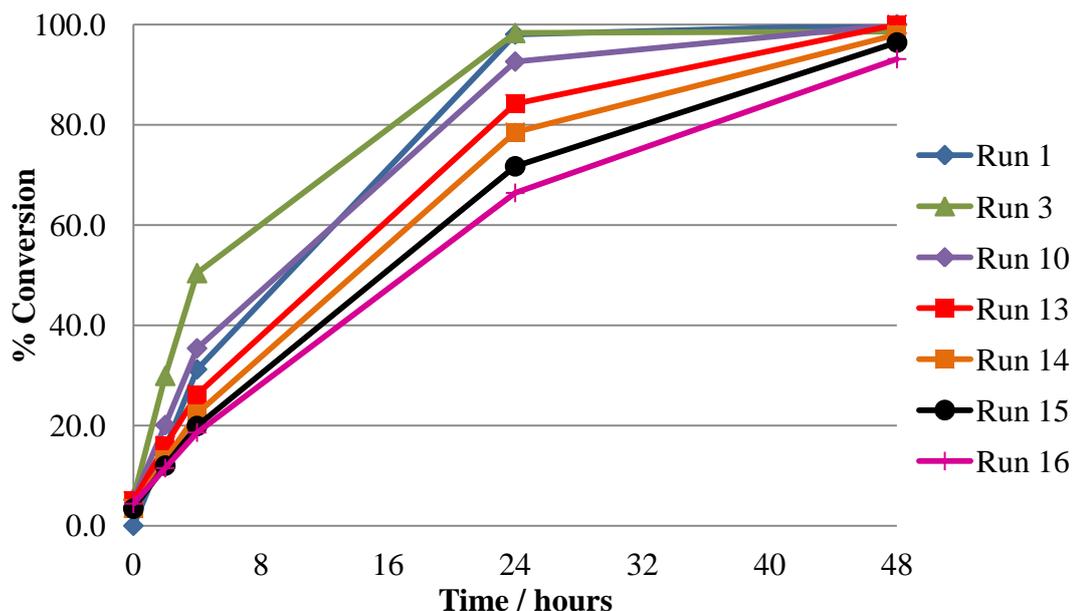
Chart 7.6 Reuse data for the reduction of benzaldehyde by catalyst **7.10** *via* **Scheme 7.5**

The immobilised iridium complex **7.9**, with the smaller, 3 carbon, linker between the functionalised Cp* ring and hydroxyl group, has a higher initial catalytic activity compared to compound **7.10**, demonstrated in **Chart 7.7**. The first two runs are consistent, however the third run shows a drop in activity, from quantitative conversion to 74% after 24 hours, showing similar activity to run 15 for the longer tethered catalyst **7.10**. In run four, catalyst **7.9** only converts 24% of benzaldehyde to benzyl alcohol after 48 hours. The fifth, sixth and seventh runs show trace activity, with conversions of 8, 4 and 4% after 48 hours respectively.
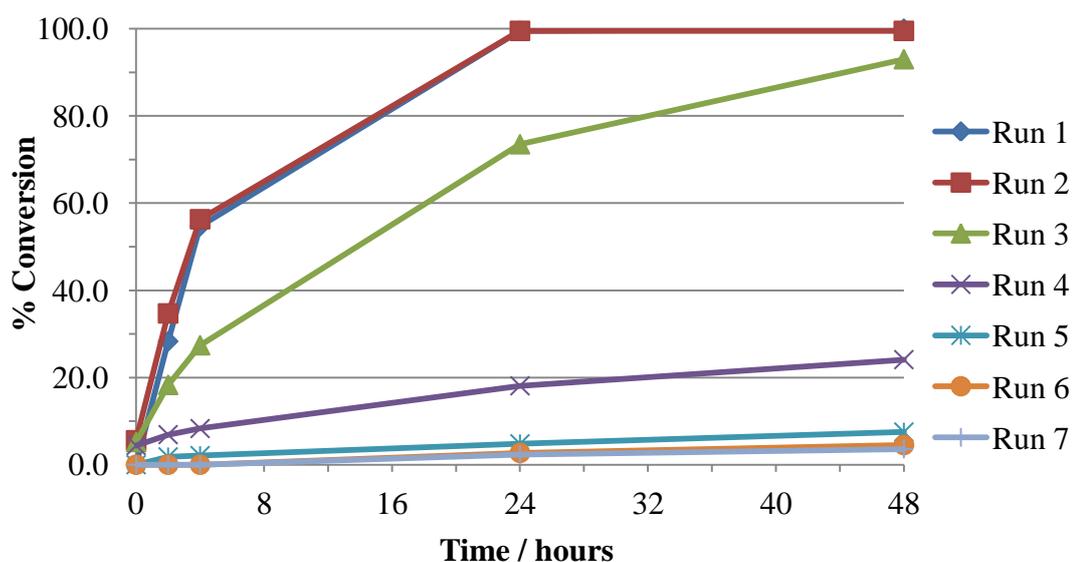
Chart 7.7 Reuse data for the reduction of benzaldehyde by **7.9** *via* **Scheme 7.5**

The immobilised iridium complex **7.11**, with the long, 9 carbon linker between the functionalised Cp* ring and hydroxyl group, has initial catalytic activity similar to the homogeneous catalyst [IrCp*Cl$_2$]$_2$, demonstrated in **Chart 7.8**.
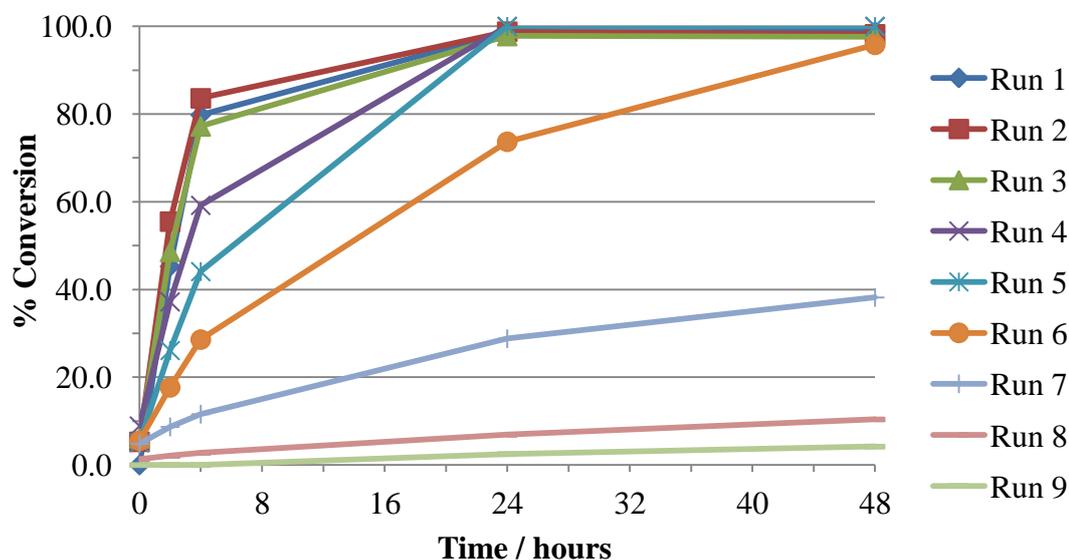
Chart 7.8 Reuse data for the reduction of benzaldehyde by catalyst **7.11** *via* **Scheme 7.5**

The first three runs are consistent, with conversions of 80, 84, and 77% after four hours. The fourth and fifth runs show a slower initial rate, but with quantitative conversion after 24 hours. Run six shows a drop in activity, from quantitative conversion to 74% after 24 hours, showing similar activity to run three for catalyst **7.9** and run 15 for catalyst **7.10**. In run seven, catalyst **7.11** only converts 38% of benzaldehyde to benzyl alcohol after 48 hours. The eighth and ninth runs show trace activity, with conversions of 10 and 4% after 48 hours.

The immobilised iridium complex **7.12**, with the long, 14 carbon linker between the functionalised Cp* ring and hydroxyl group, has initial catalytic activity similar to the homogeneous catalyst [IrCp*Cl$_2$]$_2$, demonstrated in **Chart 7.9**. Runs one and three are consistent, with run two being slightly more active and all reaching over 80% conversion after four hours. As with the 9 carbon tethered catalyst **7.11**, the fourth and fifth runs show a slower initial rate, but with quantitative conversion after 24 hours. Run six shows a drop in activity, from quantitative conversion to 91% after 24 hours. In run seven, catalyst **7.12** converts 81% of benzaldehyde to benzyl alcohol after 48 hours. The eighth run show much lower activity, with a 31% conversion after 48 hours.
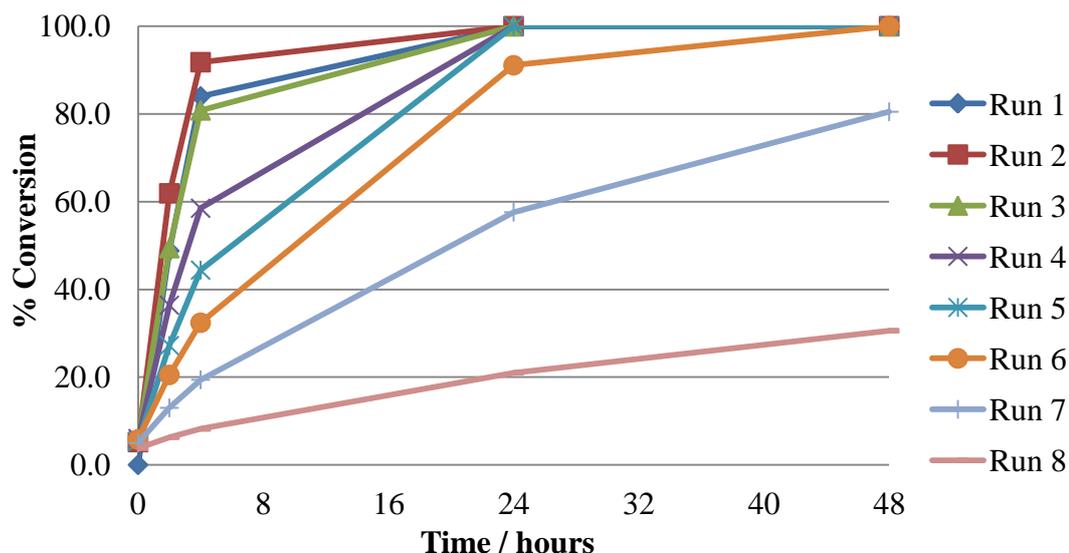
Chart 7.9 Reuse data for the reduction of benzaldehyde by catalyst **7.12** *via* **Scheme 7.5**

The immobilised rhodium complex **7.7**, with a 5 carbon linker between the functionalised Cp* ring and hydroxyl group, is a poorer catalyst than its iridium analogue **7.10** in terms of both the initial rate and its recyclability, **Chart 7.10**. The most active run (run two) only converts 60% of benzaldehyde to benzyl alcohol after 24 hours, and 89% after 48 hours. The third run is less active, with a 71% conversion after 48 hours. The catalyst's activity declines regularly from run three to ten, where the conversion after 48 hours is 43%.
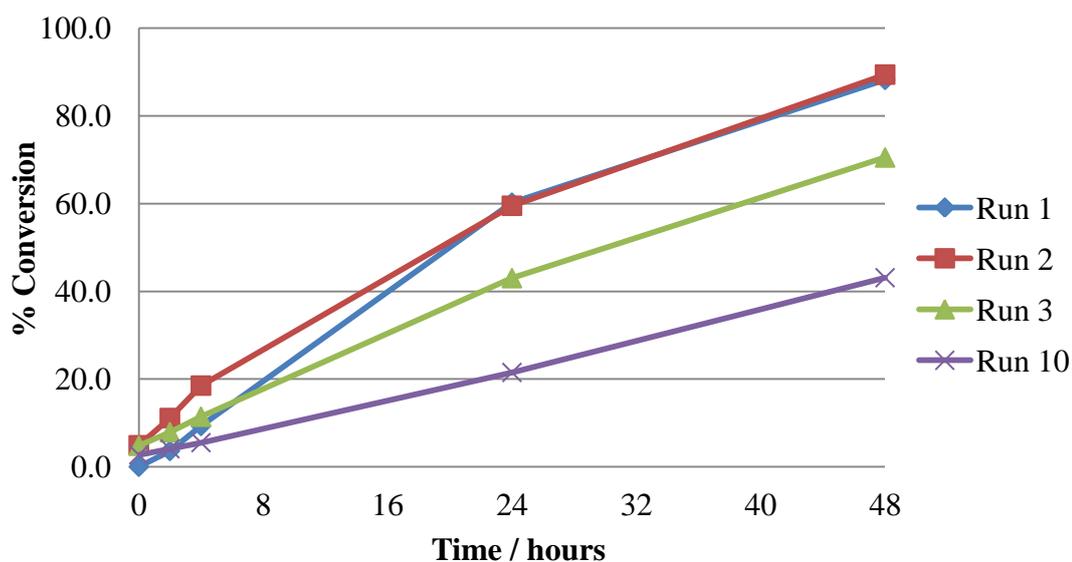
Chart 7.10 Reuse data for the reduction of benzaldehyde by catalyst **7.7** *via* **Scheme 7.5**

The immobilised rhodium complex **7.8**, with a 14 carbon linker between the

functionalised Cp* ring and hydroxyl group, is a poorer catalyst than its iridium analogue **7.12** in terms of its initial rate, as demonstrated in **Chart 7.11**.
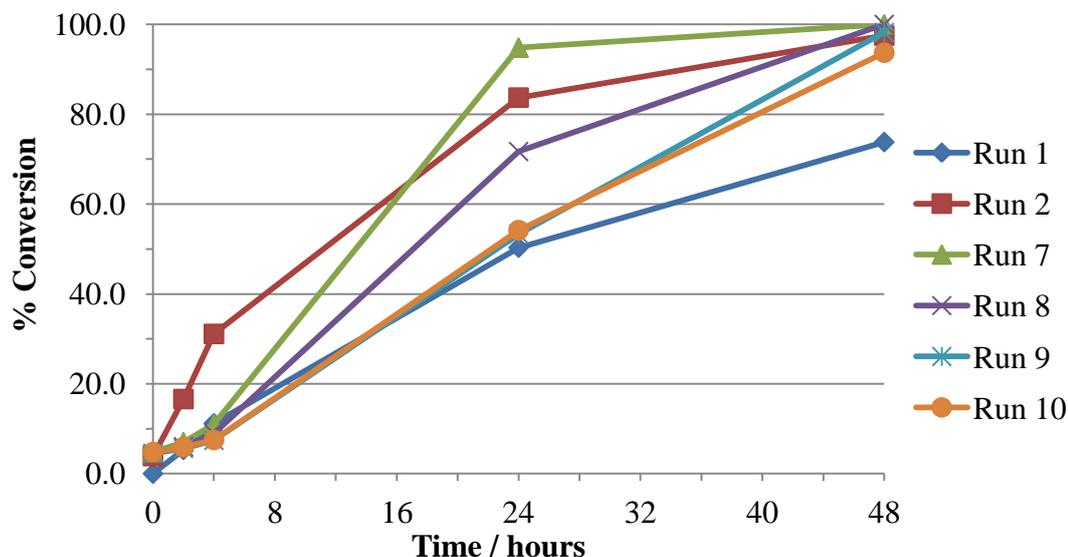
Chart 7.11 Reuse data for the reduction of benzaldehyde by catalyst **7.8** *via* **Scheme 7.5**

The initial run has low activity, with a conversion of benzaldehyde to benzyl alcohol of 74% after 48 hours. The catalyst deteriorates after the second run, from a conversion of 31% after four hours, to 8% on the tenth run. All runs, except the first, give a conversion of over 90% after 48 hours. As with the iridium analogues, the most active run for the rhodium catalyst **7.8**, with the longer 14 carbon chain between the catalyst and the support, has a higher initial rate than the smaller 5 carbon chain linker for the rhodium catalyst **7.7**. As the rhodium catalysts show poorer activity than their iridium analogues no further derivatives were tested.

7.5.2.2 Comparison of Immobilised Catalysts

The conversion at four hours into the catalytic reaction gives a good indication as to the activity of the catalyst. As demonstrated in **Chart 7.12**, the conversion for all of the immobilised iridium catalysts at four hours, after a slight increase at the beginning, drops over the runs. This is presumably due to catalyst deactivation as well as slight losses of resin in the decantation step. The decay, after the most active second or third run appears to be linear in all cases. More interestingly, the rhodium and iridium catalysts **7.7** and **7.10** respectively, with the 5 carbon linker between the functionalised Cp* ring and hydroxyl group, have distinctly different patterns compared to catalysts **7.9**, **7.11** and **7.8**/**7.12** with a 3, 9 and 14 carbon linker

respectively. The more initially active catalysts lose activity rapidly, whereas the loss of activities for **7.10** and **7.7** are much more gradual.
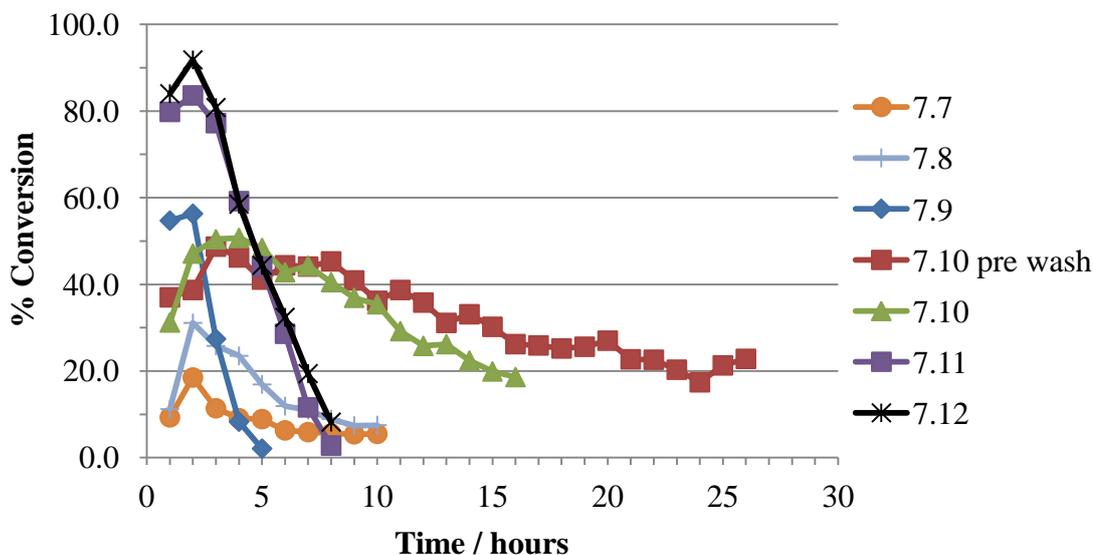
Chart 7.12 Comparison of the recyclability of the immobilised complexes from the conversion of benzaldehyde to benzyl alcohol at four hours

The activity of the rhodium catalyst **7.8**, with the 14 carbon linker, has a shallower decline in activity compared to its iridium analogue **7.12**, presumably due to the lower initial activity. The longer tethered catalysts show a higher initial activity compared to the smaller 5 carbon tethered catalysts. This is presumably because the more flexible tether allows the catalyst to behave more homogeneously and hence have the activity associated with the homogeneous analogue. The different washing regimes and immobilisation procedures for **7.10** appear to have little effect on its catalytic activity after four hours until run 11 where the fully washed resin's activity decreases more quickly. This could be due to an experimental error, such as a slightly longer decantation step for the resin (for **7.10** which has had the washing regime) or a bigger loss of resin than usual during this decantation step.

A summary of the activities of the tested immobilised systems is shown in **Table 7.4**. Unfortunately, as ICP analysis of compounds **7.9** and **7.11** was not obtained, their TON, TOF or catalytic loading cannot be determined. In terms of the most active run, the iridium compound **7.12**, with a 14 carbon tether, is the most active with a TOF of 4.3 h^{-1}, however the most recyclable catalyst is compound **7.10**, with an overall TON of 403 and a catalytic loading over all runs of 0.2 mol%.

Compound	Metal	Halide	Chain length (of carbons)	Number of runs	Consistency in activity	Most Active Run			All runs	
						No.	TOF/h-1	TON	TON	Catalytic loading/mol%
7.7	rhodium	chloride	5	10	gradual decline from run 3-10	2	0.5	10.2	69.2	0.9
7.8	rhodium	chloride	14	10	moderate decline from run 2-10	2	1.1	13.6	131.8	0.7
7.9	iridium	chloride	3	5	large decline from run 2-5	2	-	-	-	-
7.10 (initial wash regime)	iridium	chloride	5	35	gradual decline from run 3-10	3	1.6	13.3	403.4	0.2
7.10 (wash regime including acetone)	iridium	chloride	5	16	gradual decline from run 3-10	3	1.8	14.2	228.9	0.4
7.11	iridium	chloride	9	8	large decline from run 2-8	2	-	-	-	-
7.12	iridium	chloride	14	8	large decline from run 2-8	2	4.3	18.9	134.2	0.7

Table 7.4 Comparison of immobilised catalysts for the reduction of benzaldehyde. As the catalytic loading of compounds **7.9** and **7.11** were unknown, their TON, TOF and catalytic loading could not be determined

7.5.2.3 Reactivation of Immobilised Catalysts

As demonstrated in section **7.5.2.1**, the immobilised catalyst **7.12**, although showing high initial activity, quickly becomes deactivated over eight runs. It was thought that a HCl wash may reactivate the catalyst, as the deactivated catalyst may have lost a chloride/chlorides and resemble a species similar to **7.13**. After the eighth run, the immobilised complex **7.12** was stirred in 1M HCl in ethanol overnight. The resin was filtered and washed with ethanol, followed by water to remove any residual HCl. **Chart 7.13** shows that there is an increase in activity after the HCl wash compared to the last run prior to washing (run eight). The regained activity (run nine) is lower than the most active run for the catalyst but is substantially higher than the previous run (run eight). The catalyst's activity increases further for run ten with a conversion of 52% after 24 hours, compared to runs nine and ten with a conversion of 20 and 37% respectively.
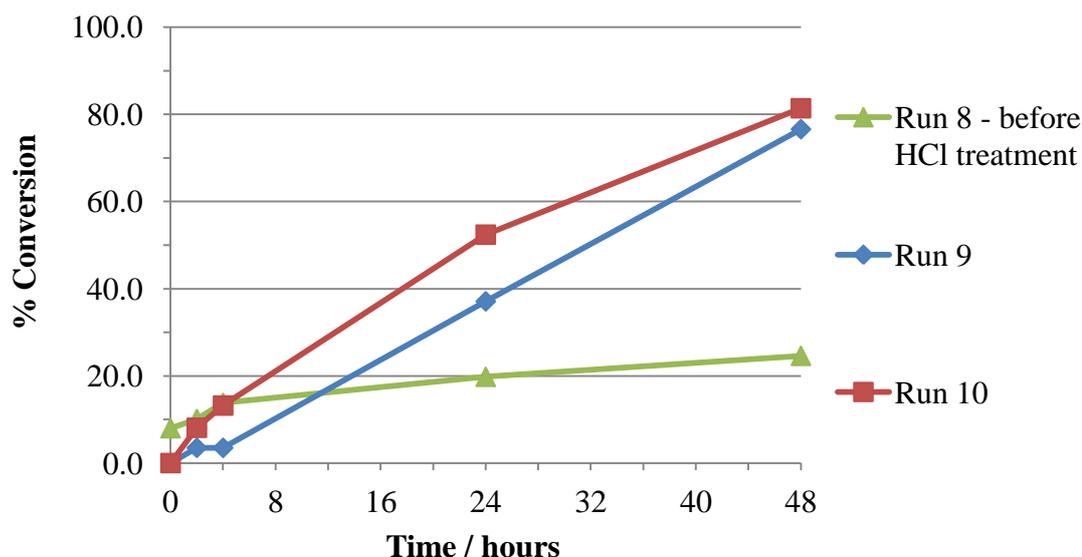
Chart 7.13 Catalytic activity of **7.12** after a HCl incubation

7.5.2.4 Reduction of Benzaldehyde by Catalyst 7.12 in Flow

The immobilised catalyst **7.12** was used in a flow system for the reduction of benzaldehyde. Although **7.12** is less consistent as a recyclable catalyst than catalyst **7.10**, it has a higher initial rate in the first few runs making it more applicable for flow systems where a high initial rate is essential. The flow apparatus used is shown in **Figure 7.8**. A 10 cm HPLC column with a diameter of 0.64 cm was packed with 0.93 g of pre washed catalyst **7.12**. The column was encased inside a metal block

which was heated by a stirrer hot plate. This was connected to a pump *via* PTFE tubing.
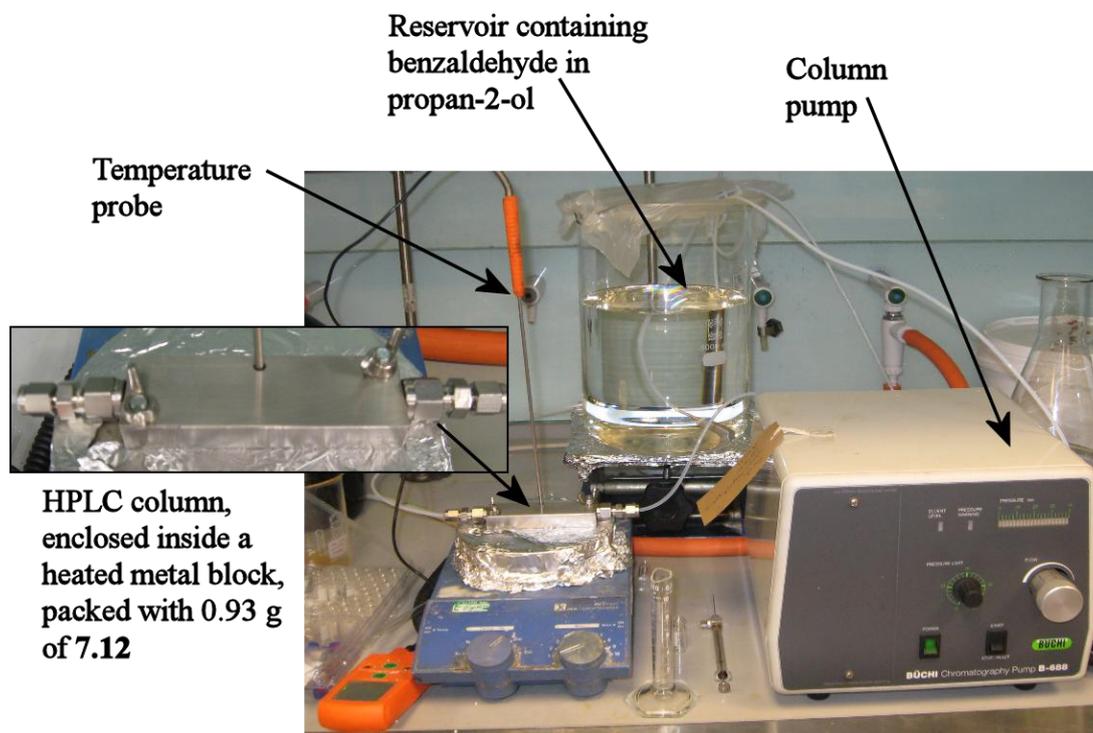
Figure 7.8 Flow apparatus used for the reduction of benzaldehyde by catalyst **7.12**

To compliment the most active batch conditions, the resin was first washed with 400 ml of a 1:1 mixture of dichloromethane/*iso*-propanol at 60°C, where the eluted solution was initially yellow, and became less coloured and eventually colourless. This was followed by a 150 ml acetone wash at room temperature.

In the first catalytic run, the substrate amount and concentration was kept similar to the batch conditions. A solution of 39 mg of potassium *tert*-butoxide and 0.89 ml of benzaldehyde was dissolved in 100 ml of *iso*-propanol and pumped through the column at 60°C at a flow rate of 1.45 ml/min for 60 minutes. The eluted solution had a 19% conversion of benzaldehyde to benzyl alcohol. The eluted solution was poured back into the starting material solution and recycled through the column for 24 hours. This was to allow the resin to be fully activated by the potassium *tert*-butoxide. The reaction was complete after 24 hours as indicated in **Chart 7.14**. The resulting solution was yellow implying metal leaching.
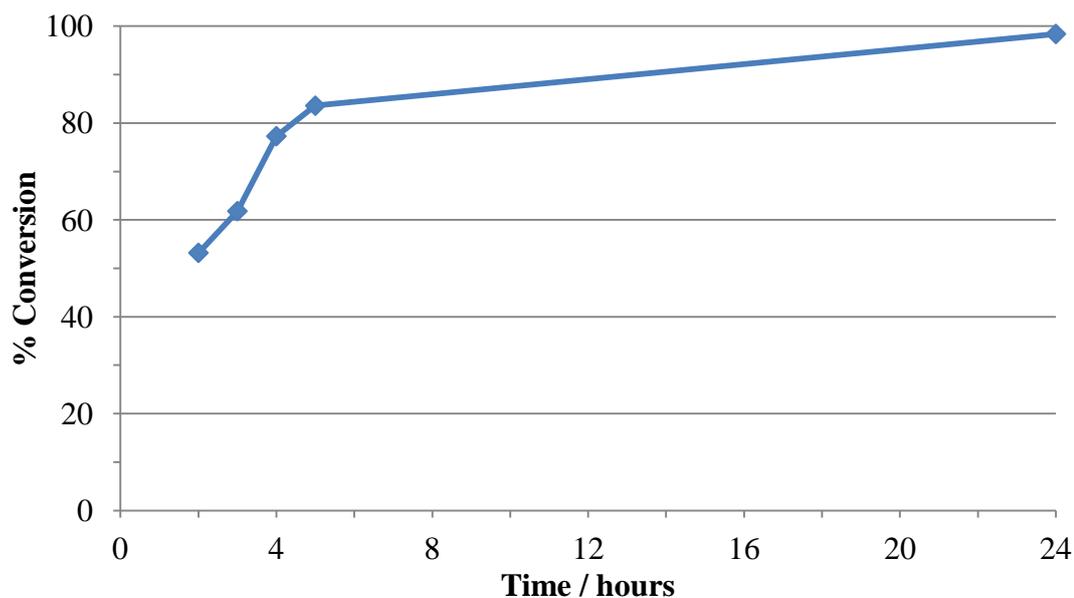
Chart 7.14 Run one-reduction of benzaldehyde by catalyst **7.12** using recycled flow conditions

In the second catalytic run, there was no base present in the starting solution and the concentration of benzaldehyde was decreased by a factor of 5 in an attempt to increase the conversion of benzaldehyde eluting through the column. The flow rate was initially modified to find an optimum flow rate that gives a high conversion to product. After 6 hours the flow rate was left at 0.54 ml/min which gave a 76.6% conversion of benzaldehyde to benzyl alcohol. After 24 hours, the flow rate had significantly reduced so was increased to 1.30 ml/min. The same was observed after 48 hours and the flow rate was increased to 1.49 ml/min. After 72 hours the flow rate had increased to the extent that all of the reservoir had been pumped through the column, leaving the resin exposed to air. The reservoir was refilled, but the eluted solution contained no benzyl alcohol. At 79 hours the total eluted solution was poured into the reservoir and the solution was recycled through the resin for a week, however the catalyst remained inactive. The resulting solution was colourless, implying no or little iridium leaching into the solution which is promising as an industrial application. Due to the inconsistent flow rates, it is difficult to determine whether the catalytic activity of the immobilised complex **7.12** was consistent over the first 75 hours (prior to the catalyst being exposed to air). **Chart 7.15** shows the % conversion with respect to flow rate. The blue markers indicate the data taken before 6 hours (when the flow rate was being modified to find an optimum) and the red markers indicate the data taken between 24 and 75 hours (before the resin was

exposed to air). As expected, there is a clear trend, with a negative correlation, indicating that the conversion decreases upon increasing the flow rate of the system. At the faster flow rates, between 1.2-1.6 ml/min, it appears that the activity of the immobilised catalyst **7.12** has remained consistent. At the slower flow rates, however, it appears that after 24 hours, the catalyst is less active, for example, at 48 hours, a flow rate of 0.30 ml/min gives 85% conversion whereas at 0 hours, a faster flow rate of 0.49 ml/min gives quantitative conversion, implying that the catalyst is becoming less active over time.
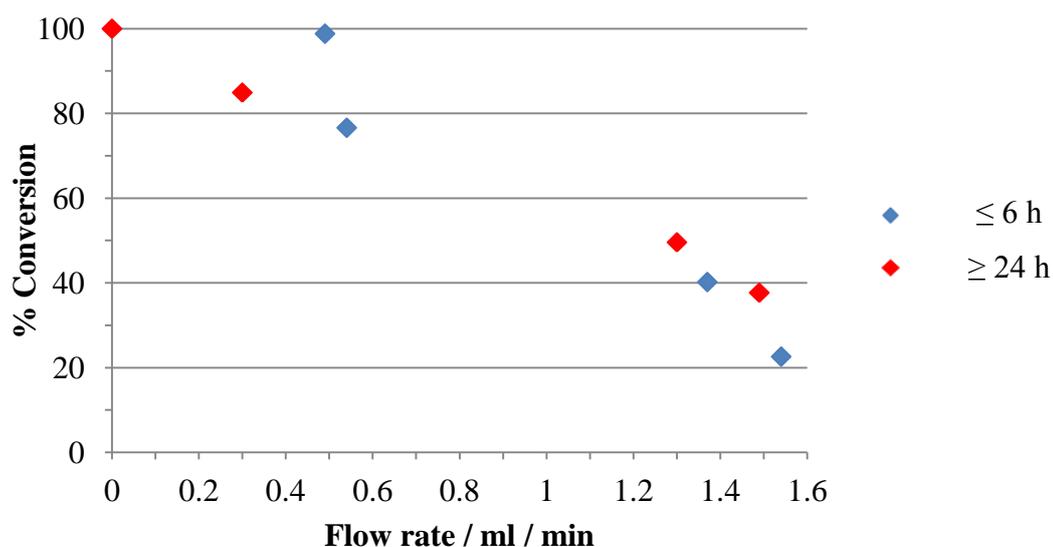
Chart 7.15 Run two-Conversion of benzaldehyde to benzyl alcohol against the flow rate

It is encouraging that the immobilised catalyst **7.12** is active in flow systems and that it remains active over a period of days. In order to optimise the flow rate and conversion, an increased residence time would be required, made possible by using a longer resin packed column. The activity of the second run showed that once the catalyst has been activated by the base, that extra base is not necessary. Including both run one and run two, 0.44 mmol of iridium converted 45.9 mmol benzaldehyde into benzyl alcohol resulting in an effective catalytic loading of 0.95 mol%. The flow rate was inconsistent throughout run two which may be due to the error of the pump, or intrinsically due to the reaction, from either solid formation during the reaction, blocking the filters or using a swellable solid catalyst.

Time/h Time/h	Flow rate/ml/min	Local Conversion/%	Estimated total eluted solution/ml	Estimated total benzaldehyde eluted/mmol	Conversion of total eluted solution/%
0	0.49	98.8	-	-	-
1	1.54	22.6	-	-	-
5	1.37	40.2	-	-	-
6	0.54	76.6	480	8.4	33.9
24	-	100.0	750	13.1	69.4
24*	1.30	49.6	-	-	-
48	0.30	84.9	1800	31.4	54.5
50	1.49	37.7	-	-	-
75	0.67	0.0	3750	65.4	28.8
79	-	-	4000	69.8	58.4
262	-	-	4000	69.8	53.5

Table 7.5 Run two-reduction of benzaldehyde by catalyst **7.12** using continuous flow conditions

7.6 Activity of Immobilised Catalysts For Acetophenone Reduction

As stated in Chapter 6, [IrCp*Cl$_2$]$_2$ and the functionalised iridium dimers **2.10** and **2.12**, with a 5 carbon and 14 carbon chain linker respectively, are less active catalysts for the reduction of acetophenone than benzaldehyde with a conversion of 82% compared to 91% after four hours. As seen for the reduction of benzaldehyde, discussed in section **7.5.2.1**, the longer 14 carbon alkyl tethered immobilised catalyst **7.12** shows higher initial activity but a lower consistency than the shorter 5 carbon alkyl tethered analogue **7.10** for the reduction of acetophenone (using the conditions stated in **Scheme 7.5**).
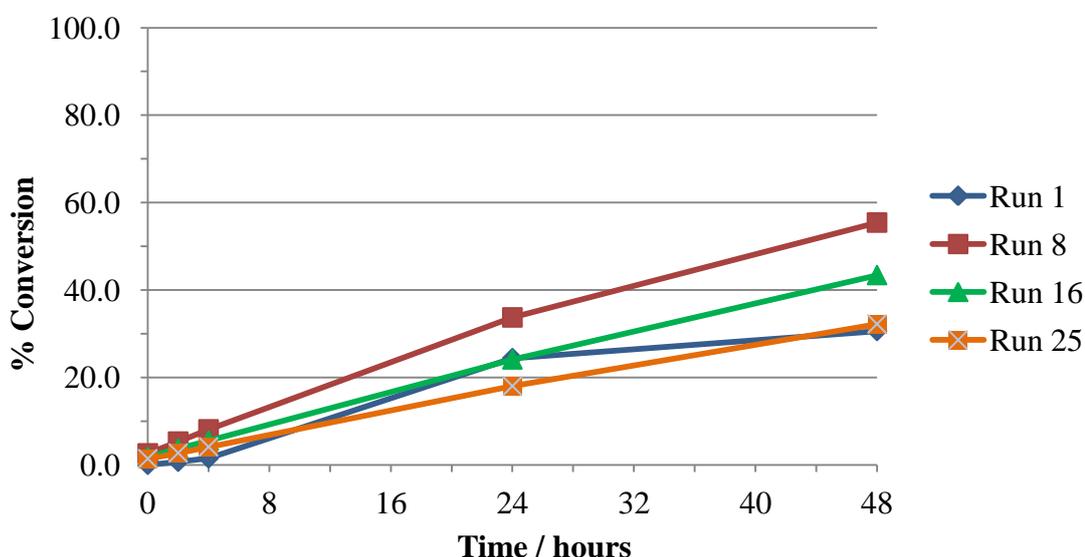
Chart 7.16 Reuse data for the reduction of acetophenone by catalyst **7.10** *via* **Scheme 7.5**

Chart 7.16 shows the reduction of acetophenone by the 5 carbon alkyl tethered iridium catalyst **7.10**, whose most active run (run eight) shows a low conversion of 55% after 48 hours. The activity, although being slow, is consistent over 25 runs, where on the 25th run, the conversion is 32%.

Chart 7.17 shows the reduction of acetophenone by the 14 carbon alkyl tethered iridium catalyst **7.12**, where the most active run (run two) shows modest activity with a 74% conversion after 24 hours and 93% conversion after 48 hours. The activity over consecutive runs declines faster than the smaller tethered analogue **7.10** where the conversion after 48 hours for run ten is 48%.
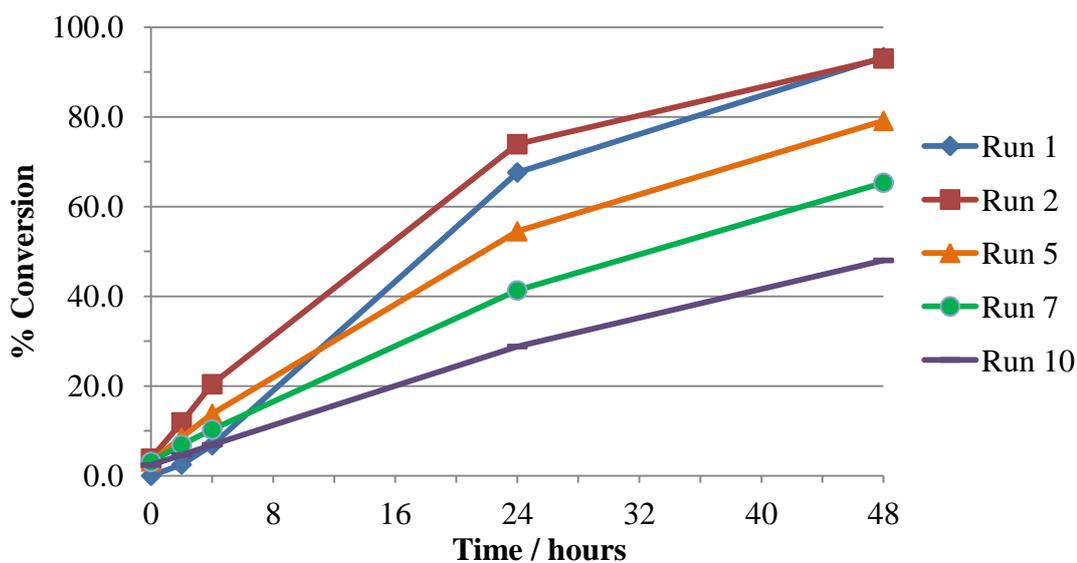
Chart 7.17 Reuse data for the reduction of acetophenone by catalyst **7.12** *via* **Scheme 7.5Scheme 6.1**

7.7 Control Heterogeneous Reactions

Three control immobilisation reactions were performed to demonstrate whether the catalyst on the immobilised resins is covalently bound or attached through weaker non covalent interactions. The resulting resins from all three control reactions give trace activity compared to the immobilised resin **7.10**, confirming firstly that the catalyst is covalently bound to the Wang resin and secondly that the majority of activity is due to the covalently bound species.

7.7.1 Control Reaction One

The first control reaction was to replace the hydroxyl tethered Cp* based iridium chloride dimer with [IrCp*Cl$_2$]$_2$ in the immobilisation method (**Scheme 7.6**). As there is no hydroxyl group on the iridium dimer, it cannot covalently attach to the Wang resin, so any activity observed will be due to non-covalently bound material. This control resin was tested as a catalyst for benzaldehyde reduction using the procedure in **Scheme 7.5**, with the results shown in **Chart 7.18**. It shows trace activity, converting 4.6% of the benzaldehyde to benzyl alcohol after 48 hours.
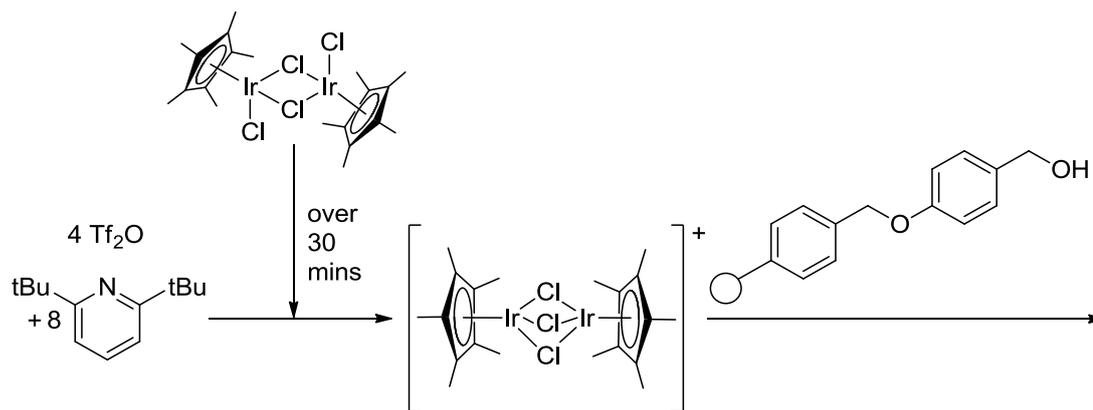
Scheme 7.6 Control one-replacing a hydroxyl tethered Cp* based iridium chloride dimer with [IrCp*Cl$_2$]$_2$
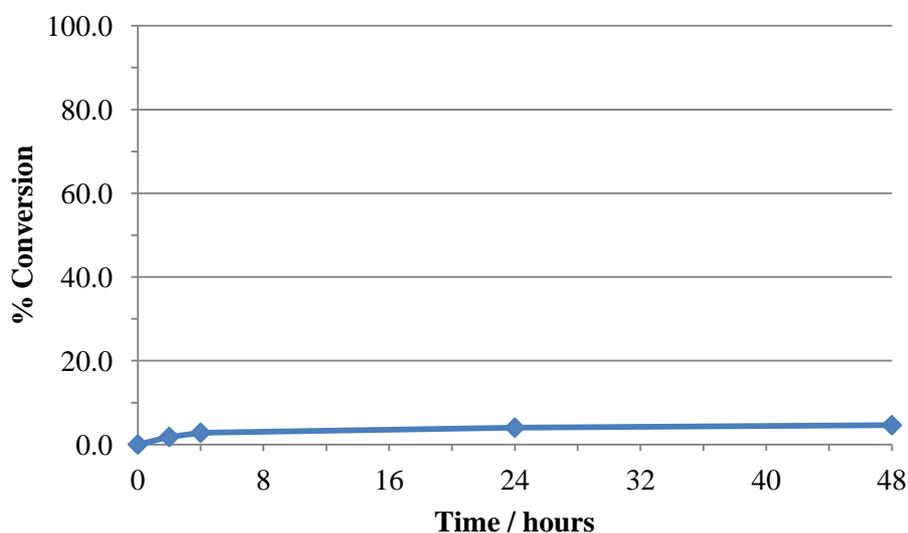
Chart 7.18 Resin formed from control reaction one as a catalyst for the reduction of benzaldehyde *via* **Scheme 7.5**

7.7.2 Control Reaction Two

The second control reaction was to remove the triflic anhydride from the immobilisation procedure (**Scheme 7.7**). As the hydroxyl group cannot become triflated, it cannot covalently bind to the Wang resin. This control resin was tested as a catalyst for benzaldehyde reduction using the procedure in **Scheme 7.5**, with the results shown in **Chart 7.19**. As with control reaction one, the resulting resin shows trace activity converting 1.1% of benzaldehyde to benzyl alcohol over 48 hours.
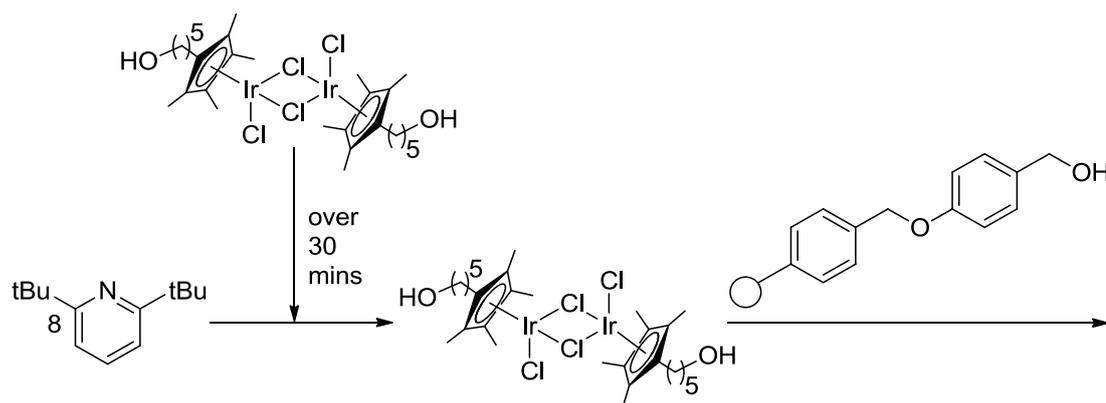
Scheme 7.7 Control two – removing triflic anhydride from the immobilisation procedure
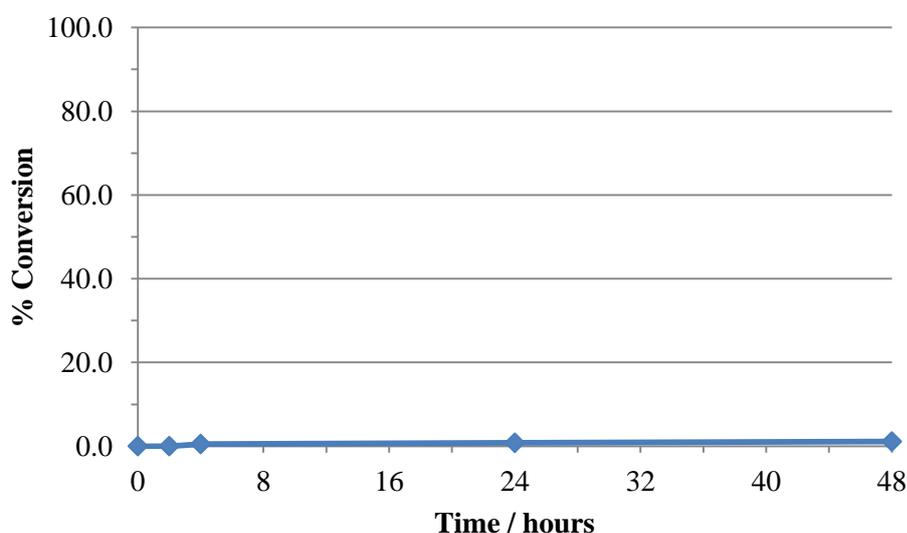
Chart 7.19 Resin formed from control reaction two as a catalyst for the reduction of benzaldehyde *via* **Scheme 7.5**

7.7.3 Control Reaction Three

The third control reaction was to react the by-product of the triflation step with the Wang resin. The by-product was prepared by adding 2 equivalents of triflic anhydride slowly onto a mixture of the starting dimer **2.10** and 2,6-di-*tert*-butylpyridine over 30 minutes. The product was a brown oil and, using the same analysis described in section **7.2**, ^{1}H NMR showed that the by-product had formed in a 74% yield, along with the formation of some of compound **7.4**. After recrystallising the oil from dichloromethane/hexane layer diffusion, a brown solid was obtained which was quantitatively the by-product. 0.91 g of this product was agitated with the Wang resin overnight. This control resin was tested as a catalyst for benzaldehyde reduction using the procedure in **Scheme 7.5**, with the results shown

in **Chart 7.20**. In comparison to control reactions one and two, the resulting resin from control reaction three shows higher activity, converting 11.5% of benzaldehyde to benzyl alcohol over 48 hours in run one and 5.2% in run two. In the immobilisation method, however, there is always <10% of this by-product formed, whereas 0.91 g of material was used here, so any activity given by a non-covalently bound by-product will be small.
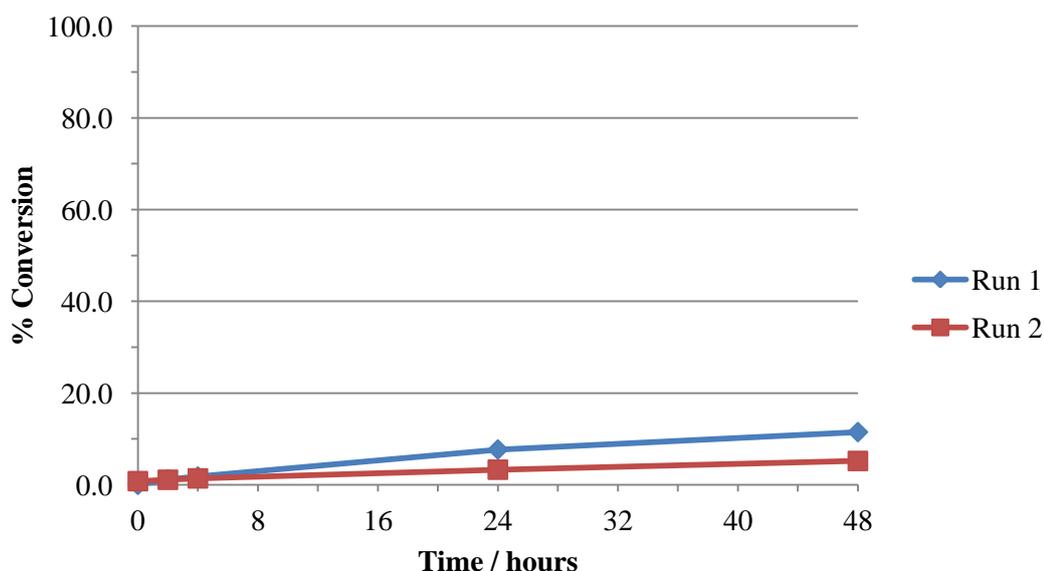
Chart 7.20 Resin formed from control reaction three as a catalyst for the reduction of benzaldehyde *via* **Scheme 7.5**

7.8   Conclusion

A viable method has been found for immobilising hydroxyl tethered Cp* based iridium/rhodium dimers onto a Wang resin using a triflate intermediate. This methodology represents a powerful way of attaching organometallic catalysts to supports with subsequent reuses of the catalyst. Control immobilisation reactions confirm that the majority of activity from the immobilised complexes is due to covalently bound material.

Although the exact structure of the immobilised catalyst is unknown, control homogeneous reactions suggest that the original immobilised complex is a tri chloride bridged species, which is reactive towards many of the solvents used in the washes prior to catalytic testing. Solid state NMR confirms the presence of the functionalised Cp* ligand.

A resulting immobilised Ir Cp* complex **7.10**, with a 5 carbon linker between the

functionalised Cp* ring and the oxygen, has been shown to be both effective and recyclable in the transfer hydrogenation of benzaldehyde over 35 runs, making the effective catalyst concentration 0.2 mol% /reaction.

A rigorous washing regime involving a hot 1:1 dichloromethane:*iso*-propanol wash followed by a room temperature acetone wash was shown to slightly increase the activity of the immobilised complexes, as well as removing non-covalently bound material from the Wang resin.

The immobilised complexes are less active for the reduction of acetophenone compared to benzaldehyde, as expected due to the activity of homogeneous catalysts. The rhodium catalysts are slower than the iridium analogues, and the longer tethered immobilised complexes with 9 and 14 carbon linkers show a higher initial rate than the 5 carbon linker catalysts, however are less consistent over consecutive runs with the activity declining rapidly.

An immobilised complex was used in a flow system for the reduction of benzaldehyde and was active over 5 days, showing promise for future scale up reactions.

7.9 Future Work

There is an industrial intention to optimise the discussed immobilised system, with respect to its synthesis and activity. The synthesis is an air sensitive procedure due to the triflate intermediate so alternative leaving groups could be investigated along with other bases as 2,6-di-*tert*-butylpyridine is expensive. There is also wasted iridium/rhodium in this preparation which remains unattached to the support, so attempts to modify the procedure to limit this or to recover and reuse the metal would be worthwhile. Altering the support may improve the activity and stability of the resulting catalyst. Further characterisation of the species would be useful to identify the exact species bound to the Wang resin, for example using XPS (X-ray photoelectron spectroscopy).

Optimisation of the tether length is crucial to obtain a compromise between catalytic activity and recyclability, and the use of more rigid tethers would be worth investigating to limit any interaction between both adjacent catalytic centres and the catalyst and the support. As ICP analysis has shown for the catalyst **7.10** that, after 35 runs for benzaldehyde reduction the majority of the iridium is still attached to the

support, the catalyst may be able to be reactivated, which requires a knowledge of the mechanism of deactivation. Addition of known ligands to the system in attempts to improve the activity and/or induce chirality into the catalyst would be desirable, for example in the case of acetophenone where the catalyst, although consistent over multiple runs, has a poor activity and presumably gives a racemic mixture of the resulting alcohol. The catalysts could also be tested on a library of aldehydes/ketones along with being used in other transfer hydrogenation systems. Initial attempts at benzaldehyde reduction in flow were successful so further study into this would determine how long the catalyst is active and allow the option for scale up.

7.10 References

(1)   S. Hashiguchi; A. Fujii; J. Takehara; T. Ikariya; R. Noyori *J. Am. Chem. Soc.* **1995**, *117*, 7562-7563.
(2)   J. Takehara; S. Hashiguchi; A. Fujii; S. Inoue; T. Ikariya; R. Noyori *Chem. Commun.* **1996**, 233-234.
(3)   A. Fujii; S. Hashiguchi; N. Uematsu; T. Ikariya; R. Noyori *J. Am. Chem. Soc.* **1996**, *118*, 2521-2522.
(4)   K. Fujita; Y. Enoki; R. Yamaguchi *Tetrahedron* **2008**, *64*, 1943-1954.
(5)   X. Wu; J. Xiao *Chem. Commun.* **2007**, 2449-2466.
(6)   M. Ito; Y. Endo; N. Tejima; T. Ikariya *Organometallics*, *29*, 2397-2399.
(7)   K.-i. Fujita; N. Tanino; R. Yamaguchi *Org. Lett.* **2006**, *9*, 109-111.
(8)   A. M. Hayes; D. J. Morris; G. J. Clarkson; M. Wills *J. Am. Chem. Soc.* **2005**, *127*, 7318-7319.
(9)   O. Saidi; A. J. Blacker; M. M. Farah; S. P. Marsden; J. M. J. Williams *Chem. Commun.* **2010**, *46*, 1541-1543.
(10)   A. J. Blacker; M. M. Farah; M. I. Hall; S. P. Marsden; O. Saidi; J. M. J. Williams *Org. Lett.* **2009**, *11*, 2039-2042.
(11)   U. Karlsson; G. Z. Wang; J. E. Backvall *J. Org. Chem.* **1994**, *59*, 1196-1198.
(12)   G.-Z. Wang; U. Andreasson; J.-E. Backvall *J. Chem. Soc., Chem. Commun.* **1994**, 1037-1038.
(13)   T. Ikariya; A. J. Blacker *Acc. Chem. Res.* **2007**, *40*, 1300-1308.
(14)   S. Bähn; S. Imm; L. Neubert; M. Zhang; H. Neumann; M. Beller *ChemCatChem* **2011**, *3*, 1853-1864.
(15)   Y. Arakawa; N. Haraguchi; S. Itsuno *Tetrahedron Lett.* **2006**, *47*, 3239-3243.
(16)   D. J. Bayston; C. B. Travers; M. E. C. Polywka *Tetrahedron: Asymmetry* **1998**, *9*, 2015-2018.
(17)   Y.-C. Chen; T.-F. Wu; J.-G. Deng; H. Liu; X. Cui; J. Zhu; Y.-Z. Jiang; M. C. K. Choi; A. S. C. Chan *J. Org. Chem.* **2002**, *67*, 5301-5306.
(18)   L. Jiang; T.-F. Wu; Y.-C. Chen; J. Zhu; J.-G. Deng *Org. Biomol. Chem.* **2006**, *4*, 3319-3324.
(19)   X. Li; X. Wu; W. Chen; F. E. Hancock; F. King; J. Xiao *Org. Lett.* **2004**, *6*, 3321-3324.
(20)   G. Liu; J. Wang; T. Huang; X. Liang; Y. Zhang; H. Li *J. Mater. Chem.* **2010**, *20*, 1970-1975.

(21) P. N. Liu; J. G. Deng; Y. Q. Tu; S. H. Wang *Chem. Commun.* **2004**, 2070-2071.
(22) P.-N. Liu; P.-M. Gu; J.-G. Deng; Y.-Q. Tu; Y.-P. Ma *Eur. J. Org. Chem.* **2005**, *2005*, 3221-3227.
(23) aapptec, "Resins General Information", company website: www.aapptec.com
(24) A. Pettman; A. D. Vassileiou, unpublished work, **2011**
(25) M. Valderramma; M. Scotti; P. Campos; R. Sariego; K. Peters; H. G. v. Schnering; H. Werner *New J. Chem.* **1988**, *12*, 633-639.
(26) M. I. Rybinskaya; A. R. Kudinov; V. S. Kaganovich *J. Organomet. Chem.* **1983**, *246*, 279-285.

Chapter 8   Group 9 Complexes as Anti-Cancer Agents

8.1 Introduction

Since the discovery of cisplatin's ability as an anti-cancer agent,[1] much focus has been dedicated to the design of coordination/organometallic complexes for this application. Although there have been many examples of the isoelectronic ruthenium/osmium arene complexes as active drugs, there are relatively few examples of the rhodium/iridium Cp* analogues,[2-4] with the majority reported by Sheldrick,[5-9] Dyson[10-12] and Sadler.[13-16]

Sadler *et al.* have recently shown that increasing the phenyl substitution on cyclopentadienyl ligands of iridium complexes (**Figure 8.1**) increases their cytotoxicity towards A2780 human ovarian cancer cells, with IC_{50} values of >100, 6.70 ± 0.62 and 0.72 ± 0.01 μM for A,B and C respectively where the IC_{50} value for cisplatin is 1.22 ± 0.12 μM.[13]
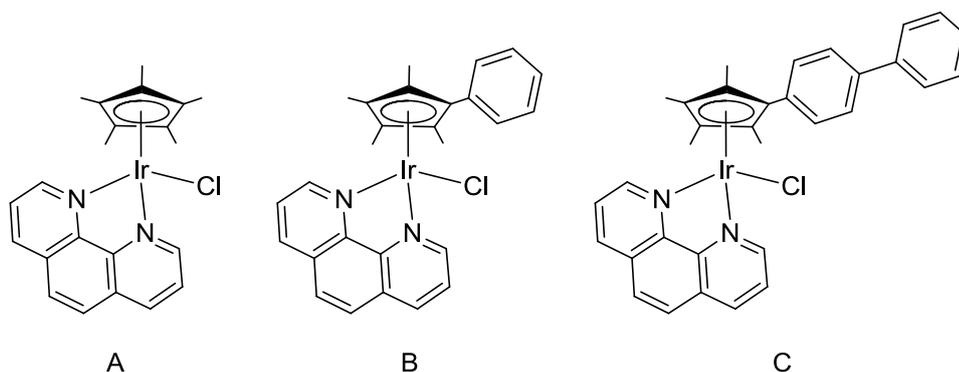
Figure 8.1 Monomeric iridium complexes with a increasing phenyl substitution on the cyclopentadienyl ligands.

This trend of increased cytotoxicity with increased phenyl substitution positively correlates with increased hydrophobicity, hydrolysis of Ir-Cl bond, cellular accumulation, viscosity of Ir-DNA adducts (equating to DNA intercalation) and negatively correlates with the rate of hydrolysis of the Ir-Cl bond.

The aims of this work were to firstly test the hydroxyl tethered Cp* based dimers, whose preparation and characterisation were discussed in Chapter 2, as anti-cancer agents against a variety of cancer cell lines. Secondly, selected iridium and rhodium Cp* and hydroxyl tethered Cp* based monomeric complexes, synthesised in Chapter 3, Chapter 4 and Chapter 5 were also tested. The IC_{50} values were obtained by either Rianne Lord or Aida Basri at the University of Bradford. The selection of compounds and interpretation of the results were made by the author.

8.2 Anti-Cancer Activity of Hydroxyl Tethered Cp* Based Iridium /Rhodium Halide Dimers

As mentioned in section **8.1**, the functionalisation of Cp* ligands for iridium complexes can have a positive effect on the complex's cytotoxicity. With this is mind, the cytotoxicities of the hydroxyl tethered Cp* based iridium/rhodium halide dimers (prepared in Chapter 2, and shown in **Figure 8.2**) were tested on the A2780 (human ovarian carcinoma) and HT-29 (human colon carcinoma) cell lines.
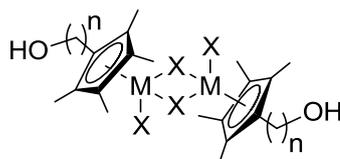
M = Rh, X = Cl		M = Ir, X = Cl		M = Ir, X = I	
2.6	n = 5	**2.9**	n = 3	**2.13**	n = 5
2.7	n = 9	**2.10**	n = 5		
2.8	n = 14	**2.12**	n = 14		

Figure 8.2 List of hydroxyl tethered Cp* based iridium/rhodium halide complexes tested against cancer cell lines in this Chapter

Apart from the anomalous iridium compound **2.9**, there is a clear trend for both the iridium and rhodium chloride dimers that increased functionalisation of the functionalised Cp* ligand, *i.e.* a longer alcohol chain increases the complex's cytotoxicity. The iridium iodide dimers show the same trend but with higher IC_{50} values for the for HT-29 cells, however the opposite trend for A2780 cells, where the tethered complex **2.13** is inactive but the unfunctionalised analogue $[IrCp*I_2]_2$ has an IC_{50} value of 6.7 μM, comparable with compound **2.12**.

Compound	HT-29		A2780	
	$IC_{50}/\mu mol$	Error/μmol	$IC_{50}/\mu mol$	Error/μmol
cisplatin	2.4[a]/2.52[b]	0.1[a]/0.09[b]	0.93	0.04
$[RhCp*Cl_2]_2$[b]	141	2	95	2
2.6[b]	123	2	85	7
2.7[b]	13.0	0.2	6.2	0.3
2.8[b]	12.7	0.4	3.9	0.1
$[IrCp*Cl_2]_2$[a]	91.9	3.5	30.9	0.4
2.9[b]	118	5	8.87	0.07
2.10[a]	29.7	1.4	23.2	0.8
2.12[a]	10.6	0.8	5.2	0.2
$[IrCp*I_2]_2$[b]	159	2	6.7	0.1
2.13[b]	110	3	137	5

where a and b refer to different cell cultures

Table 8.1 IC_{50} values for hydroxyl tethered Cp* based iridium/rhodium dimers for HT-29 and A2780 cancer cell lines, with their respective unfunctionalised Cp* analogues and cisplatin for reference

8.3 Anti-Cancer Activity of Hydroxyl Tethered Cp* Based Iridium/Rhodium (III) Pyridine Complexes

Due to the promising activity seen by the hydroxyl tethered Cp* based dimers, the pyridine monomeric analogues, **3.8** and **3.15** (whose synthesis and characterisation is described in Chapter 3) were tested against HT-29 cells with their IC_{50} values shown in **Table 8.2**.
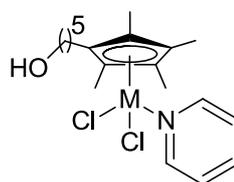
3.8   M = Ir

3.15   M = Rh

Figure 8.3 List of hydroxyl tethered Cp* based iridium/rhodium halide pyridine complexes tested against cancer cell lines in this Chapter

Compound	HT-29	
	IC$_{50}$/µmol	Error/µmol
cisplatin	2.4[a]/2.52[b]	0.1[a]/0.09[b]
3.8[a]	92	1
3.15[a]	132	2
2.10[a]	29.7	1.4
2.6[b]	123	2

where a and b refer to different cell cultures

Table 8.2 IC$_{50}$ values for hydroxyl tethered Cp* based iridium/rhodium halide pyridine complexes against the HT-29 cell line, with their respective hydroxyl tethered Cp* based starting dimers and cisplatin for reference

Both the iridium and rhodium pyridine complexes show low activity with IC$_{50}$ values of 92 and 132 µM respectively. In comparison to its starting dimer **2.10**, the iridium pyridine complex **3.8** is 3 times less active, and the rhodium pyridine complex **3.15**, has slightly lower activity than its starting dimer **2.6**, both with IC$_{50}$ values of over 100 µM for HT-29 cells. This shows that replacing a bridging chloride with pyridine is unfavourable for anti-cancer activity.

8.4 Anti-Cancer Activity of Cp* and Hydroxyl Tethered Cp* based Iridium/Rhodium Bidentate Complexes

Due to the promising anti-cancer activity of both ruthenium-arene picolinamide[17,18] and ketoiminate complexes,[19] some of their iridium rhodium Cp* analogues, prepared in Chapter 4 and Chapter 5 respectively and shown in **Figure 8.4**, were tested against HT-29 and MCF-7 cell lines with the IC$_{50}$ values shown in **Table 8.3**.[4]

4.3	R = 2', 4'- diF	**5.5**	R = 3'-F
4.4	R = 2', 5'- diF		
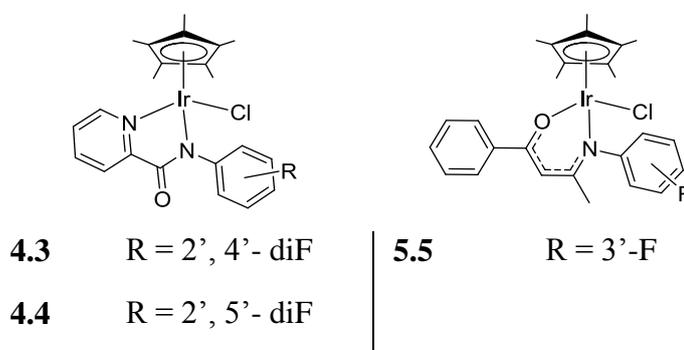
Figure 8.4 List of Cp* iridium halide complexes, with picolinamide and ketoiminate ligands, tested against cancer lines in this Chapter

Compound	HT-29		MCF-7 IC$_{50}$/µmol	
	IC$_{50}$/µmol	Error/µmol	IC$_{50}$/µmol	Error/µmol
cisplatin	2.4	± 0.1	0.528^a/1.09^b	± 0.003^a/0.08^b
[IrCp*Cl$_2$]$_2$^{a}	92	± 4	100	± 2
4.3^a	34.1	± 0.7	39	± 2
4.4^a	81	± 1	149	± 1
5.5^b	5.1	± 0.3	3.4	0.2

where a and b refer to different cell cultures

Table 8.3 IC$_{50}$ values for Cp* iridium halide complexes, with picolinamide and ketoiminate ligands, against HT-29 and MCF-7 cell lines, with [IrCp*Cl$_2$]$_2$ and cisplatin for reference

Due to an infection of the MCF-7 cells, the ketoiminate compound, **5.5**, was tested on a second culture of cells along with its ruthenium analogue for comparison. A new value for cisplatin was obtained for the second culture for comparison purposes. The picolinamide complexes **4.3** and **4.4** show moderate and low activity respectively with IC$_{50}$ values of 34 and 81 µM against HT-29 cells and 39 and 149 µM against MCF-7 cells. This indicates that the position of the fluorides on the aryl ring is crucial for activity. Interestingly, compound **4.4** is less active than the [IrCp*Cl$_2$]$_2$ starting dimer against the MCF-7 cell line, but more active against the HT-29 cell line. The ketoiminate complex, **5.5**, is highly active against both HT-29 and MCF-7 cell lines with respective IC$_{50}$ values of 5.1 and 3.4 µM, comparable with the cisplatin values of 2.4 and 1.1 µM. Compound **5.5** is slightly less active than its ruthenium *p*-cymene analogue.[1]

A series of iridium and rhodium Cp* picolinamide complexes with varying chloride substituents (shown in **Figure 8.5**) were also tested on A2780 cells. Due to the promising activity seen by the hydroxyl tethered Cp* based dimers **2.6** and **2.10**, the picolinamide complexes **4.15** and **4.19** (shown in **Figure 8.5**) which incorporate the hydroxyl tethered Cp* based ligand with the 5 carbon alcohol chain were also tested with the IC$_{50}$ results shown in **Table 8.4**.

4.1   R = H

4.5   R = 2'-Cl

4.6   R = 3'-Cl

4.7   R = 2', 4'- diCl

4.8   R = 2', 5'- diCl
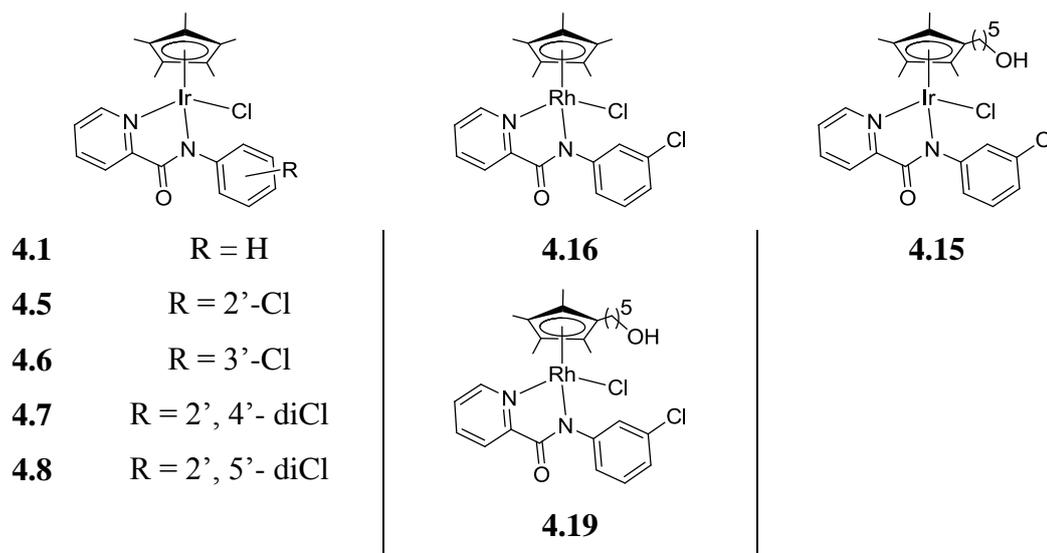
Figure 8.5 List of Cp* and hydroxyl tethered Cp* based iridium/rhodium chloride complexes, with picolinamide ligands, tested against cancer lines in this Chapter

Compound	A2780	
	IC_{50}/µmol	Error/µmol
cisplatin	0.93^a/0.97^b/1.42^c	0.04^a/0.07^b/0.34^c
2.10[a]	23.2	0.8
2.6[a]	85	7
4.1[c]	66	2
4.5[c]	25	3
4.6[c]	33	1
4.7[c]	18.6	0.4
4.8[c]	23	1
4.15[b]	52.5	0.8
4.16[c]	28.8	0.5
4.19[b]	85	4

where a, b and c refer to different cell cultures

Table 8.4 IC_{50} values for Cp* iridium/rhodium halide complexes, with picolinamide ligands, against A2780 cell lines, with their functionalised starting materials and cisplatin for reference

The presence and position of the chloride substituents on the picolinamide ligand has a significant effect on the complex's anti-cancer activity for A2780 cells. The unsubstituted IrCp* complex **4.1** shows poor activity with an IC_{50} value of 66 µM,

whereas the addition of a chloride group on the *ortho* and *meta* position of the arene ring of the picolinamide decreases the IC_{50} value to 25 and 33 μM respectively. The dichloro substituted picolinamide complexes show even higher activity with IC_{50} values of 19 and 23 μM for **4.7** and **4.8** respectively. As shown in both the mono and di chloro substituted picolinamide complexes, a chloride on the *ortho* position of the arene ring gives a more active complex than one on the *meta* position. The rhodium complex **4.16** is slightly more active than its iridium analogue **4.6**, with an IC_{50} value of 28 μM compared to 33 μM. Unfortunately, there appears to be no benefit to adding a picolinamide ligand to the hydroxyl tethered Cp* based dimers, as the iridium picolinamide complex **4.15** is half as active as its starting dimer **2.10**, and the rhodium picolinamide complex **4.19** has the same activity as its starting dimer **2.6**. The tethered complexes are also less active than their Cp* analogues.

8.5 Conclusion

Iridium and rhodium Cp* complexes have recently attracted interest as anti-cancer agents. The Cp* functionalised iridium and rhodium dimers prepared in Chapter 2 showed promising activity with a clear trend between longer carbon chains between the functionalised Cp* ring and hydroxyl, and anti-cancer activity on HT-29 and A2780 cell lines. The two pyridine complexes **3.8** and **3.15** were practically inactive against HT-29 cells. The iridium Cp* picolinamide complexes have potential as anti-cancer agents with the complexes **4.3** and **4.4** showing modest cytotoxic activity. In relation to A2780 cells, group 9 Cp* picolinamide complexes also show moderate activity, with the addition of electron withdrawing chloride groups to the arene increasing the anti-cancer activity of the complex significantly. The Cp* functionalised picolinamide complexes **4.15** and **4.19**, however, show the same or lower activity than their respective dimers and unfunctionalised Cp* analogues indicating that incorporating a picolinamide and functionalising the Cp* ring with a hydroxyl tether, doesn't lead to an additive effect on anti-cancer activity. The most promising iridium Cp* monomer was the ketoiminate complex **5.5** with comparable activity to cisplatin on both HT-29 and MCF-7 cell lines.

8.6 Future Work

As the hydroxyl tethered Cp* based dimers with the longest 14 carbon chain show the most promise in their series as anti-cancer agents, complexes with longer chains could be prepared in attempts to increase the anti-cancer activity. The iridium Cp* ketoiminate complex shows activity in the same magnitude as cisplatin, so modifications of this structure in attempts to increase the anti-cancer activity would be worthwhile. Further picolinamide complexes could be tested on various cell lines, particularly any with electron withdrawing groups on the arene ring as the chloride substituents show higher activity than the unsubstituted analogue. In order to optimise the potency of these drugs, an understanding of the mechanism of action is crucial.

8.7 References

(1)   B. Rosenberg; L. V. Camp; T. Krigas *Nature* **1965**, *205*, 698.
(2)   A. R. de Souza; R. Najjar; S. Glikmanas; S. Ber Zyngier *J. Inorg. Biochem.* **1996**, *64*, 1-5.
(3)   J. Ruiz; V. Rodriguez; N. Cutillas; K. G. Samper; M. Capdevila; O. Palacios; A. Espinosa *Dalton Trans.* **2012**, *41*, 12847-12856.
(4)   S. J. Lucas; R. M. Lord; R. L. Wilson; R. M. Phillips; V. Sridharan; P. C. McGowan *Dalton Trans.* **2012**, *41*, 13800-13802.
(5)   A. Fehn; T. Ederer; S. Mihan; W. Beck *J. Organomet. Chem.* **2001**, *621*, 109-119.
(6)   M. Harlos; I. Ott; R. Gust; H. Alborzinia; S. Wölfl; A. Kromm; W. S. Sheldrick *J. Med. Chem.* **2008**, *51*, 3924-3933.
(7)   M. A. Scharwitz; I. Ott; Y. Geldmacher; R. Gust; W. S. Sheldrick *J. Organomet. Chem.* **2008**, *693*, 2299-2309.
(8)   Y. Geldmacher; R. Rubbiani; P. Wefelmeier; A. Prokop; I. Ott; W. S. Sheldrick *J. Organomet. Chem.* **2011**, *696*, 1023-1031.
(9)   M. A. Nazif; R. Rubbiani; H. Alborzinia; I. Kitanovic; S. Wolfl; I. Ott; W. S. Sheldrick *Dalton Trans.* **2012**, *41*, 5587-5598.
(10)   A. Dorcier; W. H. Ang; S. Bolaño; L. Gonsalvi; L. Juillerat-Jeannerat; G. Laurenczy; M. Peruzzini; A. D. Phillips; F. Zanobini; P. J. Dyson *Organometallics* **2006**, *25*, 4090-4096.
(11)   H. Amouri; J. Moussa; A. K. Renfrew; P. J. Dyson; M. N. Rager; L.-M. Chamoreau *Angew. Chem. Int. Ed.* **2010**, *49*, 7530-7533.
(12)   M. Gras; B. Therrien; G. Suss-Fink; A. Casini; F. Edafe; P. J. Dyson *J. Organomet. Chem.* **2010**, *695*, 1119-1125.
(13)   Z. Liu; A. Habtemariam; A. M. Pizarro; S. A. Fletcher; A. Kisova; O. Vrana; L. Salassa; P. C. A. Bruijnincx; G. J. Clarkson; V. Brabec; P. J. Sadler *J. Med. Chem.* **2011**, *54*, 3011-3026.
(14)   Z. Liu; A. Habtemariam; A. M. Pizarro; G. J. Clarkson; P. J. Sadler

Organometallics **2012**, *30*, 4702-4710.

(15)   Z. Liu; L. Salassa; A. Habtemariam; A. M. Pizarro; G. J. Clarkson; P. J. Sadler *Inorg. Chem.* **2012**, *50*, 5777-5783.

(16)   A. L. Noffke; A. Habtemariam; A. M. Pizarro; P. J. Sadler *Chem. Commun.* **2012**, *48*, 5219-5246.

(17)   K. D. Camm; A. El-Sokkary; A. L. Gott; P. G. Stockley; T. Belyaeva; P. C. McGowan *Dalton Trans.* **2009**, 10914-10925.

(18)   S. H. van Rijt; A. J. Hebden; T. Amaresekera; R. J. Deeth; G. J. Clarkson; S. Parsons; P. C. McGowan; P. J. Sadler *J. Med. Chem.* **2009**, *52*, 7753-7764.

(19)   R. M. Lord, unpublished work, **2012**

Chapter 9   Experimental

9.1 General Experimental Considerations

All experiments requiring dry conditions were conducted using standard Schlenk line techniques under an inert dry nitrogen atmosphere using a dual vacuum/dinitrogen line or in a Braun Labmaster 100 glove box. Dry dinitrogen was obtained by passing gaseous dinitrogen through a double column of self-indicating phosphorous pentoxide and activated 4 Ǻ molecular sieves.

Dichloromethane, methanol, tetrahydrofuran and toluene were dried using a Pure Solvent MD Solvent Purification System, with solvents purified by copper catalysts and activated alumina columns. Acetone was distilled from calcium hydride and hexane from sodium. All solvents were subsequently stored in glass ampoules under dinitrogen.

All glassware, cannulae and filter papers were stored in an oven at 100-150℃ prior to use. The majority of crystallisations took place at room temperature.

Chemicals were purchased from Sigma-Aldrich Chemicals Co, Acros Organics and Alfa Aeser. These were all used as received.

Deuterated NMR solvents were used as purchased from Goss scientific Ltd and Apollo Scientific and dried by reflux with calcium hydride and separated by distillation under nitrogen.

9.1.1 Instrumentation

9.1.1.1 NMR

Solution-state NMR spectra were recorded by the author on a Bruker DPX 300 spectrometer or by Simon Barrett using a Bruker DRX 500 spectrometer. Solid-state NMR spectra were recorded by David Apperley and Fraser Markwell as follows:

A solid-state ^{13}C spectrum of complex **7.4** was recorded at 100.56 MHz using a Varian VNMRS spectrometer and a 6 mm (rotor o.d.) magic-angle spinning probe.

The spectrum was obtained using cross-polarisation with a 5 s recycle delay, 3 ms contact time, at ambient probe temperature (~25 °C) and at a sample spin-rate of 6.8 kHz. 136 repetitions were accumulated. Spectral referencing was with respect to an external sample of neat tetramethylsilane (carried out by setting the high-frequency signal from adamantane to 38.5 ppm). Carbon spectra from **7.10** and Wang resin swollen in $CDCl_3$ were obtained using the same instrument but with direct excitation (using a 90° pulse of duration 4.4 μs), proton decoupling a 0.5 s recycle and at a spin rate of 3 kHz. Spectral referencing is with respect to neat tetramethylsilane in both cases.

A solid-state ^{19}F spectrum of complex **7.4** was recorded at 282.09 MHz using a Varian Unity Inova spectrometer and a 4 mm (rotor o.d.) magic-angle spinning probe. The spectra were obtained using direct excitation (with a 4 μs 90° pulse) with a 1 s recycle delay, at ambient probe temperature (~30 °C) and at a sample spin-rate of 12-14 kHz. 560 to 2416 repetitions were accumulated. Spectral referencing was with respect to an external sample of neat $CFCl_3$.

9.1.1.2 Elemental Analysis

Elemental analysis was obtained by Ian Blakeley and Martin C. Huscroft at the University of Leeds Microanalytical Service.

9.1.1.3 Mass Spectrometry

Mass spectra were recorded by Tanya Marinko-Covell on a Micromass ZMD spectrometer using electrospray ionisation at the University of Leeds Mass Spectrometry Service.

9.1.1.4 Gas Chromatography

Gas chromatography analysis was performed by the author using a Hewlett Packard HP 6890 Series GC System.

9.1.1.5 Inductively Coupled Plasma

ICP analysis was performed by Matthew Stirling at the University of Huddersfield using the following procedure:

Between 15 – 30 mg of each sample was accurately weighed into a microwave

digestion tube. 1.5 ml trace-metal concentrated sulfuric acid was pipetted into each tube and the samples digested. 10 ml trace-metal concentrated nitric acid and 3.0 ml trace-metal concentrated hydrochloric acid were added to each vessel, any effervescence allowed to subside then the samples were digested. The samples were allowed to cool to room temperature then transferred to 100 ml plastic volumetric flasks and made up to volume with ultra-pure water. 2.0 ml of each sample was then pipetted into 100 ml plastic volumetric flasks containing ~10 ml ultra-pure water 2.0 ml trace-metal concentrated nitric acid, 1.0 ml trace-metal concentrated hydrochloric acid and 1.0 ml of the 50 ppm internal standard solution. The samples were made up to volume with ultra-pure water, mixed well and transferred to ICP sample tubes for analysis.

9.1.1.6 X-ray Crystallography

X-ray data was collected by the author. A suitable single crystal was selected and immersed in an inert oil. The crystal was then mounted onto a glass capillary and attached to a goniometer head on a Bruker X8 Apex diffractor using graphite monochromated Mo-Kα radiation (λ= 0.71073 Å) and 1.0° φ-rotation frames

The crystal was then cooled to 150K by an oxford cryostream low temperature device.[1] The full data set was recorded and the images processed using DENZO and SCALEPACK programs.[2] The structures were solved by the author.

Structure solution by direct methods was achieved through the use of SHELXS86[3], SIR92[4] or SIR97[5] programs, and the structural model defined by full matrix least squares on F^2 using SHELX97.[3] Molecular graphics were plotted using POV-Ray[6] *via* the XSeed program. Editing of Crystallographic Information files and construction of tables of bond lengths and angles was achieved using WC [7] and PLATON.[8] Unless otherwise stated, hydrogen atoms were placed using idealised geometric positions (with free rotation for methyl groups), allowed to move in a "riding model" along with the atoms to which they were attached, and refined isotropically.

9.1.1.7 Microwave Reactions

Microwave reactions were performed using a Biotage Initiator Sixty variable power microwave.

9.1.1.8 Flow reaction

The immobilised catalyst **7.12** (0.93 g) was packed into a 10 cm HPLC column with a diameter of 0.64 cm. The column was encased inside a metal block which was fitted with a temperature probe and heated by a stirrer hot plate. The column was connected to a Buchi *B-688 chromatography* pump *via* PTFE tubing, which itself was connected to a reservoir containing the reaction reagents. The other end of the column was connected to a vessel to store the eluted reacted solution.

9.1.2 Cell Line Testing

The *in vitro* tests were performed by Rianne M. Lord at the Institute of Cancer Therapeutics, Bradford, on MCF7 (human breast adenocarcinoma), A2780 (human ovarian carcinoma) and HT-29 (human colon adenocarcinoma) cell lines. Cells were incubated in 96-well plates at a concentration of 2×10^4 cells cells/ml. 200 μL of growth media (RPMI 1640 supplemented with 10% foetal calf serum, sodium pyruvate (1 mM) and L-glutamine (2 mM)) was added to each well and the plates were incubated for 24 hours at 37 °C in an atmosphere of 5% CO_2 prior to drug exposure. The compounds was dissolved in dimethylsulphoxide at a concentration of 25 mM and diluted further with medium to obtain drug solutions ranging from 250 to 0.49 μM. The final dimethylsulphoxide concentration was 0.1% (v/v) which is non-toxic to cells. Drug solutions were applied to cells and incubated for 5 days at 37 °C in an atmosphere of 5% CO_2. 20 μL of MTT (5 mgml^{-1}) was added to each well and incubated for 3 hours at 37 °C in an atmosphere of 5% CO_2. The solutions were then removed and 150 μL of dimethylsulphoxide was added to each well to dissolve the purple formazan crystals. A Thermo Scientific Multiskan EX microplate photometer was used to measure the absorbance at 540 nm. Lanes containing medium only and cells in medium (no drug) were used as blanks for the spectrophotometer and 100% cell survival respectively. Cell survival was determined as the absorbance of treated cells divided by the absorbance of controls and expressed as a percentage. The IC_{50} values were determined from plots of % survival

against drug concentration. Each experiment was repeated 3 times and a mean value obtained.

9.2 Cp* Based Ligands and their Metal Halide Dimers

$C_5(CH_3)_4C_5H_{10}OH$[9] (**2.2**), $[Rh\{\eta^5\text{-}C_5(CH_3)_4C_5H_{10}OH\}Cl_2]_2$[10] (**2.6**), $[Ir\{\eta^5\text{-}C_5(CH_3)_4C_5H_{10}OH\}Cl_2]_2$[9] (**2.10**) and $[Ir\{\eta^5\text{-}C_5(CH_3)_4C_5H_{10}OH\}I_2]_2$[9] (**2.13**) were prepared according to the literature method.

9.2.1 Synthesis of $C_5(CH_3)_4C_3H_6OH$ (2.1)

Under a nitrogen atmosphere, lithium wire (8 g, 1.15 mol, washed with hexane) was added to anhydrous diethyl ether (250 ml) and the lithium suspension was vigorously stirred. 2-bromo-2-butene (40 g, 0.30 mol, mixture of *cis* and *trans* isomers) was added to a dropping funnel and a small portion added to the reaction mixture to initiate the reaction. Diethyl ether (70 ml) was also added to the remaining 2-bromo-2-butene, which was then added at a rate that maintained a gentle reflux. After complete addition of 2-bromo-2-butene the reaction was stirred at r.t. for 2 hours. γ-Butyrolactone (22 g, 0.26 mol) in diethyl ether (50 ml) was then added dropwise and the mixture stirred for 1 hour. The resulting mixture was poured into saturated NH_4Cl (aq) (600 ml) and after separating the ether layer, the aqueous layer was extracted with *tert*-butyl methyl ether (3 x 100 ml). The combined ether layers were washed with brine, dried over magnesium sulfate and concentrated to *ca.* 100 ml. 10% aqueous HCl (300 ml) was added to the resulting concentrate and the biphasic mixture was stirred for 3h at r.t. After separating the ether layer, the aqueous layer was extracted with *tert*-butyl methyl ether (3 x 50 ml). The combined organic layers were washed with water (2 x 100 ml), dried over Na_2SO_4, and the solvent evaporated to leave a brown oil, which was purified through a large plug of silica (hexane/EtOAc 10:1 as eluent) gave a pale yellow oil containing 3 regioisomers of **2.1** (19.4 g, 0.11 mmol, 41.4%). **2.1** was used without further purification. ES-MS (CH_2Cl_2, m/z): 181.2 [M+H].

^{1}H NMR (300 MHz, $CDCl_3$, 300 K) 3.63 (t, $^3J(^1H\text{-}^1H)$ = 7.5 Hz, 7.5 Hz, 2H, CH_2OH), 2.13-2.50 (m, 2H, C$\underline{H}_2CH_2CH_2OH$), 1.57-1.66 (m, 2H, C$\underline{H}_2CH_2OH$), 1.55 (s, 6H, $2 \times CH_3$), 1.51 (s, 3H, CH_3), 0.93 ($2 \times$ d, $^3J(^1H\text{-}^1H)$ = 7.0 Hz, 3H, CH_3).

^{13}C{^{1}H} NMR (75 MHz, $CDCl_3$, 300 K) 144.1, 139.2, 135.4 and 134.7 (alkene C

of functionalised Cp* ring), 68.7, 51.4 and 49.4 (allyl CH of functionalised Cp* ring), 63.1 (CH_2OH), 31.8 ($\underline{C}H_2CH_2OH$), 26.9 ($\underline{C}H_2CH_2CH_2OH$), 17.4, 15.9, 15.1, 13.4 and 11.8 (CH_3 groups of functionalised Cp* ring).

9.2.2 Synthesis of $C_5(CH_3)_4C_9H_{18}OH$ (2.3)

Triethylamine (9.4 g, 0.09 mol) was added to methyl 10-hydroxydecanoate (9.0 g, 0.05 mmol) in dichloromethane (150 ml). Trimethylsilyl chloride (5.3 g, 0.05 mol) was added dropwise. The solution was stirred at ambient temperature overnight. The resulting solution was washed with saturated ammonium chloride solution (50 ml). The water layer was extracted with diethyl ether (2 × 30 ml) and the ether and dichloromethane layers were combined, washed with brine (30 ml), dried over magnesium sulfate, evaporated to dryness and purified by column chromatography (hexane:ethyl acetate 4:1 as eluent) to afford a yellow oil **A** (8.7 g, 0.03 mmol, 63%)

Under a nitrogen atmosphere, lithium wire (0.9 g, 0.13 mol, washed with hexane) was added to anhydrous diethyl ether (100 ml) and the lithium suspension was vigorously stirred. 2-bromo-2-butene (9.4 g, 0.07 mol, mixture of *cis* and *trans* isomers) was added in small portions. The reaction was initiated through gentle heating, then left at ambient temperature for two hours. **A** (8.7 g, 0.03 mol) in diethyl ether (100 ml) was then added dropwise and the mixture stirred for 1 hour. The resulting mixture was poured into sat NH_4Cl (aq) (100 ml) and after separating the ether layer, the aqueous layer was extracted with *tert*-butyl methyl ether (3 x 50 ml). The combined ether layers were washed with brine (50 ml), dried over magnesium sulfate and concentrated to *ca*. 50 ml. 10% aqueous HCl (100 ml) was added to the resulting concentrate and the biphasic mixture was stirred for 3h at r.t. After separating the ether layer, the aqueous layer was extracted with *tert*-butyl methyl ether (3 x 50 ml). The combined organic layers were washed with water (2 x 100 ml), dried over magnesium sulfate, and the solvent evaporated to leave a brown oil, which was purified through a large plug of silica (hexane/ethyl acetate 5:1 as eluent) to give **2.3** as a pale yellow oil with 3 regioisomers (3.5 g, 0.01 mmol, 42%). **2.3** was used without further purification. ES-MS (CH_2Cl_2, m/z): 285.1 [M-2H+Na].

^{1}H NMR (300 MHz, $CDCl_3$, 300 K) 3.64 (t, $^{3}J(^{1}H-^{1}H)$ = 6.6 Hz, 2H, $C\underline{H}_2OH$), 2.23-2.65 (m, 2H, CH_2), 1.81 (br. s, 3H, CH_3), 1.77 (br. s, 6H, 2 × CH_3), 1.65-1.75 (m, 2H, CH_2), 1.49-1.65 (m, 3H, CH_2 and allyl CH), 1.30 (br. s, 10H, 10 × CH_2),

1.00 (2 × d, $^3J(^1H\text{-}^1H)$ = 7.6 Hz, 3H, CH$_3$). ^{13}C{^{1}H} NMR (75 MHz, CDCl$_3$, 300 K) 142.8, 142.8, 138.8, 138.1, 138.0, 135.5, 135.2, 134.2, 134.0, 133.7 and 130.1 (alkene C of functionalised Cp* ring), 64.4, 51.4 and 49.3 (allyl CH of functionalised Cp* ring), 63.0 (CH$_2$OH), 32.7 (CH$_2$), 29.5 (br. s, CH$_2$), 29.3 (CH$_2$), 29.3 (CH$_2$), 29.1 (CH$_2$), 29.1 (CH$_2$), 25.7 (CH$_2$), 25.0 (CH$_2$), 23.5, 22.6, 14.0, 11.6 and 11.0 (CH$_3$ groups of functionalised Cp* ring).

9.2.3 Synthesis of C$_5$(CH$_3$)$_4$C$_{14}$H$_{28}$OH (2.4)

Under a nitrogen atmosphere, lithium wire (2 g, 0.29 mol, washed with hexane) was added to anhydrous diethyl ether (100 ml) and the lithium suspension was vigorously stirred. 2-bromo-2-butene (20 g, 0.15 mol, mixture of *cis* and *trans* isomers) was added to a dropping funnel and a small portion added to the reaction mixture to initiate the reaction. Diethyl ether (70 ml) was also added to the remaining 2-bromo-2-butene, which was then added at a rate that maintained a gentle reflux. After complete addition of 2-bromo-2-butene the reaction was stirred at r.t. for 2 hours. Pentadecanolide (16.8 ml, 0.06 mol) in diethyl ether (50 ml) was then added dropwise and the mixture stirred for 1 hour. The resulting mixture was poured into saturated NH$_4$Cl (aq) (300 ml) and after separating the ether layer, the aqueous layer was extracted with *tert*-butyl methyl ether (3 x 100 ml). The combined ether layers were washed with brine, dried over magnesium sulfate and concentrated to *ca*. 100 ml. 10% aqueous HCl (150 ml) was added to the resulting concentrate and the biphasic mixture was stirred for 3h at r.t. After separating the ether layer, the aqueous layer was extracted with *tert*-butyl methyl ether (3 x 50 ml). The combined organic layers were washed with water (2 x 100 ml), dried over Na$_2$SO$_4$, and the solvent evaporated to leave a brown oil, which was purified through a large plug of silica (hexane/EtOAc 3:1 as eluent) to give **2.4** as a pale yellow oil with 3 regioisomers (15.7 g, 0.05 mol, 83%). **2.4** was used without further purification. ES-MS (CH$_2$Cl$_2$, m/z): 489.4 [M-4H+3Na+2 formates].

^{1}H NMR (300 MHz, CDCl$_3$, 300 K) 3.62 (t, $^3J(^1H\text{-}^1H)$ = 6.6 Hz, 2H, C$\underline{H}_2$OH), 2.13-2.65 (m, 2H, CH$_2$), 1.81 (s, 3H, CH$_3$), 1.77 (s, 6H, 2 × CH$_3$), 1.66-1.72 (m, 2H, CH$_2$), 1.50-1.63 (m, 3H, CH$_2$ and allyl CH), 1.20-1.40 (m, 20H, 10 × CH$_2$), 1.00 (2 × d, $^3J(^1H\text{-}^1H)$ = 7.6 Hz, 3H, CH$_3$) ^{13}C{^{1}H} NMR (75 MHz, CDCl$_3$, 300 K) 142.9, 138.9, 138.1, 138.0, 137.8, 136.7, 135.5, 135.3, 134.2, 134.1, 133.76 and 130.1

(alkene C of functionalised Cp* ring), 67.8, 51.4 and 49.4 (allyl CH of functionalised Cp* ring), 63.1 (CH_2OH), 32.8 (CH_2), 29.7 (CH_2), 29.6 (CH_2), 29.6 (CH_2), 25.7 (CH_2), 23.8, 22.9, 14.1, 11.6 and 11.1 (CH_3 groups of functionalised Cp* ring).

9.2.4 Synthesis of $[Rh\{\eta^5\text{-}C_5(CH_3)_4C_3H_6OH\}Cl_2]_2$ (2.5)

Under a nitrogen atmosphere, rhodium trichloride hydrate (0.10 g, 0.38 mmol) was added to 1-(3-hydroxypropyl)-2,3,4,5-tetramethylcyclopentadiene (0.14 g, 0.78 mmol) in MeOH (30 ml) and the mixture was heated under reflux for 15 h. After evaporation of the solvent, the powder was dissolved in dichloromethane and the product precipitated using hexane, and collected by filtration to yield **2.5** as red crystals suitable for X-ray crystallography (0.03 g, 0.04 mmol, 22%). ES-MS (CH_2Cl_2, m/z): 671.0 [M-Cl].

Anal. Found: C: 39.2, H: 5.2, Cl: 22.2%. **Anal. Calculated** (with 0.35 molecules of dichloromethane)**:** C: 39.7, H: 5.3, Cl: 22.6%

^{1}H NMR (300 MHz, $CDCl_3$, 300 K) 3.66 (br. s, 4H, 2 × C$\underline{H}_2$OH), 2.37 (t, $^1J(^1$H-^{1}H) = 7.9 Hz, 4H, 2 × CH_2Cp), 1.67-1.80 (m, 4H, 2 × C$\underline{H}_2CH_2$OH), 1.65 (s, 12H, 4 × CH_3), 1.63 (s, 12H, 4 × CH_3). ^{13}C$\{^1$H$\}$ NMR (125 MHz, $CDCl_3$, 300 K) 94.5 (d, $^1J(^{13}$C-^{103}Rh) = 7.4 Hz, $\underline{C}CH_3$), 62.2 (CH_2OH), 29.7 ($\underline{C}H_2CH_2OH$), 20.8 ($\underline{C}H_2$Cp), 9.4 (s, 2 × CH_3), 9.4 (s, 2 × CH_3).

9.2.5 Synthesis of $[Rh\{\eta^5\text{-}C_5(CH_3)_4C_9H_{18}OH\}Cl_2]_2$ (2.7)

Under a nitrogen atmosphere, rhodium trichloride hydrate (0.20 g, 0.76 mmol) was added to 1-(9-hydroxynonyl)-2,3,4,5-tetramethylcyclopentadiene (**2.3**) (0.40 g, 1.51 mmol) in MeOH (30 ml) and the mixture was heated under reflux for 15 h. After evaporation of the solvent, the powder was dissolved in a minimum of dichloromethane and the product precipitated using hexane, collected by filtration. The precipitation step was repeated and the powder dried *in vacuo* to give the product as a red powder (0.34 g, 0.39 mmol, 51%). ES-MS (CH_2Cl_2, m/z): 837.2 [M-Cl].

Anal. Found: C: 49.7, H: 7.2, Cl: 15.9%. **Anal. Calculated:** C: 49.4, H: 7.2, Cl: 16.2%

^{1}H NMR (300 MHz, $CDCl_3$, 300 K) 3.63 (t, $^3J(^1$H-^{1}H) = 6.5 Hz, 4H, 2 × C$\underline{H}_2$OH),

2.25 (m, $^1J(^1H\text{-}^1H)$ = 6.7 Hz, 4H, 2 × CH$_2$Cp), 1.75-2.00 (m, 4H, C$\underline{H}_2$CH$_2$OH), 1.63 (s, 12H, 4 × CH$_3$), 1.61 (s, 12H, 4 × CH$_3$), 1.50-1.59 (m, 4H, 2 × CH$_2$), 1.30 (br. s, 20H, 10 × CH$_2$). ^{13}C{^{1}H} NMR (75 MHz, CDCl$_3$, 300 K) 96.2 (d, ^1J (^{13}C-^{103}Rh) = 9.4 Hz, $\underline{C}$CH$_3$), 94.5 (d, ^1J (^{13}C-^{103}Rh) = 9.4 Hz, $\underline{C}$CH$_3$), 94.2 (d, ^1J (^{13}C-^{103}Rh) = 9.3 Hz, $\underline{C}$CH$_3$), 63.0 (s, CH$_2$OH), 32.7 (s, CH$_2$), 29.6 (s, CH$_2$), 29.3 (s, CH$_2$), 29.1 (s, CH$_2$), 27.5 (s, CH$_2$), 25.6 (s, CH$_2$), 24.0 (s, $\underline{C}$H$_2$Cp), 9.4 (s, 2 × CH$_3$), 9.4 (s, 2 × CH$_3$).

9.2.6 Synthesis of [Rh{η^5-C$_5$(CH$_3$)$_4$C$_{14}$H$_{28}$OH}Cl$_2$]$_2$ (2.8)

Under a nitrogen atmosphere, rhodium trichloride hydrate (0.10 g, 0.38 mmol) was added to 1-(14-hydroxytetradecyl)-2,3,4,5-tetramethylcyclopentadiene (**1b**) (0.26 g, 0.78 mmol) in MeOH (30 ml) and the mixture was heated under reflux for 15 h. After evaporation of the solvent, the powder was dissolved in a minimum of dichloromethane and the product precipitated using hexane, collected by filtration and the dried *in vacuo* to give the product as a red powder (0.18 g, 0.18 mmol, 47%). ES-MS (CH$_2$Cl$_2$, m/z): 977.4 [M-Cl].

Anal. Found: C: 54.0, H: 8.1, Cl: 13.8%. **Anal. Calculated:** C: 54.5, H: 8.1, Cl: 14.0%

^{1}H NMR (300 MHz, CDCl$_3$, 300 K) 3.64 (t, $^3J(^1H\text{-}^1H)$ = 6.6 Hz, 4H, 2 × C$\underline{H}_2$OH), 2.25 (m, 4H, 2 × CH$_2$), 1.63 (s, 12H, 4 × CH$_3$), 1.62 (s, 12H, 4 × CH$_3$), 1.55 (m, 4H, 2 × CH$_2$), 1.49 (br. s, 4H, 2 × CH$_2$), 1.20-1.40 (m, 40H, 20 × CH$_2$). ^{13}C{^{1}H} NMR (75 MHz, CDCl$_3$, 300 K) 96.3 (d, ^1J (^{13}C-^{103}Rh) = 9.8 Hz, $\underline{C}$CH$_3$), 94.5 (d, ^1J (^{13}C-^{103}Rh) = 9.3 Hz, $\underline{C}$CH$_3$), 94.1 (d, ^1J (^{13}C-^{103}Rh) = 9.3 Hz, $\underline{C}$CH$_3$), 63.1 (s, CH$_2$OH), 32.8 (s, CH$_2$), 29.7 (s, CH$_2$), 29.6 (s, CH$_2$), 29.5 (s, CH$_2$), 29.4 (s, CH$_2$), 29.4 (s, CH$_2$), 29.4 (s, CH$_2$), 29.3 (s, CH$_2$), 27.5 (s, CH$_2$), 25.7 (s, CH$_2$), 9.4 (s, 2 × CH$_3$), 9.4 (s, 2 × CH$_3$).

9.2.7 Synthesis of [Ir{η^5-C$_5$(CH$_3$)$_4$C$_3$H$_6$OH}Cl$_2$]$_2$ (2.9)

Under a nitrogen atmosphere, iridium trichloride hydrate (0.70 g, 1.99 mmol) and sodium bicarbonate (0.18 g, 2.14 mmol) were added to degassed methanol (10 ml) in a 30 ml capacity microwave tube and the suspension was purged with nitrogen for 10 minutes. After adding 1-(3-hydroxypropyl)-2,3,4,5-tetramethylcyclopentadiene (0.70 g, 3.88 mmol), the suspension was purged for a further 5 minutes. The tube was then

sealed and microwave heating was applied at 150 $^{\circ}$C for 10 minutes. After effervescence from the solution had subsided, the tube was opened and the solution was diluted with dichloromethane (50 ml), washed with water (20 ml), brine (20 ml), dried over Na_2SO_4 and the solvent evaporated. The resulting oily red residue was recrystallised from methanol, filtered and washed with diethyl ether to yield an orange powder (0.46 g, 0.52 mmol, 26%).

Anal. Found: C: 33.5, H: 4.5, Cl: 14.7%. **Anal. Calculated** (with 2 molecules of methanol)**:** C: 32.9, H: 4.9, Cl: 15.0%

^{1}H NMR (300 MHz, CDCl$_3$, 300 K) 3.66 (t, ^3J(^{1}H-^{1}H) = 6.3 Hz, 4H, 2 × C$\underline{H}_2$OH), 2.20-2.27 (m, 4H, 2 × C$\underline{H}_2$Cp), 1.64-1.75 (m, 4H, 2 × CH$_2$), 1.62 (s, 12H, 4 × CH$_3$), 1.59 (s, 12H, 4 × CH$_3$). ^{13}C{^{1}H} NMR (75 MHz, CDCl$_3$, 300 K) 87.3 ($\underline{C}$CH$_3$), 86.8 ($\underline{C}$CH$_3$), 86.4 ($\underline{C}$CH$_3$), 62.3 ($\underline{C}$H$_2$OH), 30.5 (CH$_2$), 20.9 (C$\underline{H}_2$Cp), 9.4 (s, CH$_3$), 9.3 (s, CH$_3$).

9.2.8 Synthesis of [Ir{η^5-C$_5$(CH$_3$)$_4$C$_9$H$_{18}$OH}Cl$_2$]$_2$ (2.11)

Under a nitrogen atmosphere, iridium trichloride hydrate (0.70 g, 1.99 mmol) and sodium bicarbonate (0.18 g, 2.14 mmol) were added to degassed methanol (10 ml) in a 30 ml capacity microwave tube and the suspension was purged with nitrogen for 10 minutes. After adding 1-(9-hydroxynonyl)-2,3,4,5-tetramethylcyclopentadiene (1.05 g, 3.97 mmol), the suspension was purged for a further 5 minutes. The tube was then sealed and microwave heating was applied at 150 $^{\circ}$C for 10 minutes. After effervescence from the solution had subsided, the tube was opened and the solution was diluted with dichloromethane (50 ml), washed with water (20 ml), brine (20 ml), dried over Na_2SO_4 and the solvent evaporated. The resulting oily red residue was dissolved in dichloromethane, precipitated with hexane, and the process repeated to yield an orange powder (0.30 g, 0.28 mmol, 14%). ES-MS (CH$_2$Cl$_2$, m/z): 1017.3 [M-Cl].

Anal. Found: C: 42.2, H: 6.1%. **Anal. Calculated:** C: 41.1, H: 5.9%

^{1}H NMR (300 MHz, CDCl$_3$, 300 K) 3.64 (t, ^3J(^{1}H-^{1}H) = 6.6 Hz, 4H, 2 × C$\underline{H}_2$OH), 2.09-2.16 (m, 4H, 2 × C$\underline{H}_2$Cp), 1.61 (s, 12H, 4 × CH$_3$), 1.59 (s, 12H, 4 × CH$_3$), 1.50-1.58 (m, 4H, 2 × CH$_2$), 1.25-1.45 (br. s, 20H, 10 × CH$_2$). ^{13}C{^{1}H} NMR (75 MHz, CDCl$_3$, 300 K) 88.2 ($\underline{C}$CH$_3$), 86.5 ($\underline{C}$CH$_3$), 86.4 ($\underline{C}$CH$_3$), 63.0 (CH$_2$OH), 32.7 (CH$_2$), 29.6 (CH$_2$), 29.3 (CH$_2$), 29.3 (CH$_2$), 29.1 (CH$_2$), 27.6 (CH$_2$), 25.7 (CH$_2$), 24.1

(CH$_2$Cp), 9.4 (CH$_3$), 9.4 (CH$_3$).

9.2.9 Synthesis of [Ir{η^5-C$_5$(CH$_3$)$_4$C$_{14}$H$_{28}$OH}Cl$_2$]$_2$ (2.12)

Under a nitrogen atmosphere, iridium trichloride hydrate (0.10 g, 0.28 mmol) and sodium bicarbonate (0.02 g, 0.24 mmol) were added to degassed methanol (3 ml) in a 10 ml capacity microwave tube and the suspension was purged with nitrogen for 10 minutes. After adding 1-(14-hydroxytetradecyl)-2,3,4,5-tetramethylcyclopentadiene (0.19 g, 0.57 mmol), the suspension was purged for a further 5 minutes. The tube was then sealed and microwave heating was applied at 150 $^\circ$C for 10 minutes. After effervescence from the solution had subsided, the tube was opened and the solution was diluted with dichloromethane (20 ml), washed with water (10 ml), brine (10 ml), dried over Na$_2$SO$_4$ and the solvent evaporated. The resulting oily red residue was dissolved in dichloromethane, precipitated with hexane and left overnight to yield an orange powder (0.14 g, 0.12 mmol, 42%). ES-MS (CH$_2$Cl$_2$, m/z): 1158.5 [M-Cl].

Anal. Found: C: 46.7, H: 7.0, Cl: 10.9%. **Anal. Calculated**: C: 46.3, H: 6.9, Cl: 11.9%

^{1}H NMR (300 MHz, CDCl$_3$, 300 K) 3.64 (t, $^3J(^1$H-^{1}H) = 6.6 Hz, 4H, 2 × C<u>H</u>$_2$OH), 2.12 (t, $^3J(^1$H-^{1}H) = 7.6 Hz, 4H, 2 × CH$_2$), 1.80-2.04 (m, 4H, 2 × CH$_2$), 1.61 (s, 12H, 4 × CH$_3$), 1.59 (s, 12H, 4 × CH$_3$), 1.50-1.58 (m, 4H, 2 × CH$_2$), 1.20-1.45 (m, 40H, 10 × CH$_2$). ^{13}C{^{1}H} NMR (75 MHz, CDCl$_3$, 300 K) 88.2 (<u>C</u>CH$_3$), 86.5 (<u>C</u>CH$_3$), 86.4 (<u>C</u>CH$_3$), 63.1 (CH$_2$OH), 32.8 (CH$_2$), 29.7 (CH$_2$), 29.6 (CH$_2$), 29.5 (CH$_2$), 29.4 (CH$_2$), 29.3 (CH$_2$), 27.7 (CH$_2$), 25.7 (CH$_2$), 24.1 (CH$_2$) 9.4 (CH$_3$), 9.4 (CH$_3$).

9.3 Pyridine Complexes

9.3.1 Synthesis of Ir(η^5-C$_5$(CH$_3$)$_5$){C$_5$H$_5$N}Cl$_2$ (3.1)

[IrCp*Cl$_2$]$_2$ (0.50 g, 0.63 mmol) was dissolved in pyridine (25 ml) and the solution was stirred for 25 hours. The resulting yellow solution was evaporated to dryness and the crude product recrystallised using layer diffusion from a dichloromethane/hexane solvent system to give **3.1** as a yellow powder (0.54 g, 1.13 mmol, 90%)

Anal. Found: C:37.5, H: 4.1, N: 2.9, Cl 14.3%. **Anal. Calculated**: C: 37.7, H:

4.2, N: 2.9, Cl: 14.9%

^{1}H NMR (300 MHz, CDCl$_3$, 300 K) 8.99 (br. d, $^{3}J(^{1}$H-^{1}H) = 6.1 Hz, 2H, 2 × CH *ortho* to N of pyridine), 7.74 (br. t, $^{3}J(^{1}$H-^{1}H) = 7.6 Hz, 1H, CH *para* to N of pyridine), 7.35 (vt (dd), $^{3}J(^{1}$H-^{1}H) = 6.8 Hz, $^{3}J(^{1}$H-^{1}H) = 6.8 Hz, 2H, 2 × CH *meta* to N of pyridine), 1.54 (s, 15H, 5 × CH$_3$). ^{13}C{^{1}H} NMR (75 MHz, CDCl$_3$, 300 K) 153.5 (2 × C *ortho* to N on pyridine ring), 137.7 (C *para* to N on pyridine ring), 125.4 (2 × C *meta* to N on pyridine ring), 85.7 (5 × CCH$_3$), 8.5 (5 × CCH$_3$).

9.3.2 Synthesis of Ir(η^5-C$_5$(CH$_3$)$_5$){C$_5$H$_4$NF}Cl$_2$ (3.2)

3-Fluoropyridine (0.04 ml, 0.49 mmol) was added to [IrCp*Cl$_2$]$_2$ (0.10 g, 0.13 mmol) in tetrahydrofuran (10 ml). The mixture was stirred overnight, then filtered. The resulting yellow powder was recrystallised using vapour diffusion (dichloromethane/pentane solvent system) to give the **3.2** as orange crystals (0.10 g, 0.20 mmol, 78%)

Anal. Found: C: 36.4, H: 3.9, N: 2.8, Cl: 14.2%. **Anal. Calculated**: C: 36.4, H: 3.9, N: 2.8, Cl: 14.3%

^{1}H NMR (300 MHz, CDCl$_3$, 300 K) 8.96 (br. s, 1H, CH on pyridyl ring *ortho* to F and N), 8.84 (br. d, $^{3}J(^{1}$H-^{1}H) = 5.4 Hz, 1H, CH on pyridyl ring *para* to F), 7.51 (dddd, $^{3}J(^{1}$H-^{19}F) = 7.9 Hz, $^{3}J(^{1}$H-^{1}H) = 7.9 Hz, $^{4}J(^{1}$H-^{1}H) = 2.7 Hz, $^{4}J(^{1}$H-^{1}H) = 1.2 Hz, 1H, CH on pyridyl ring *para* to N), 7.36 (vdt (ddd), $^{3}J(^{1}$H-^{1}H) = 8.6 Hz, $^{3}J(^{1}$H-^{1}H) = 5.5 Hz, $^{4}J(^{1}$H-^{19}F) = 5.5 Hz, 1H, CH on pyridyl ring *meta* to N), 1.55 (s, 15H, 5 × CH$_3$). ^{13}C{^{1}H} NMR (75 MHz, CDCl$_3$, 300 K) 159.6 (d, $^{1}J(^{13}$C-^{19}F) = 255.0 Hz, CF), 149.8 (br. s, CH on pyridyl ring *para* to F), 142.4 (d, $^{2}J(^{13}$C-^{19}F) = 32.4 Hz, CH on pyridyl ring *ortho* to F and N), 125.9 (d, $^{3}J(^{13}$C-^{19}F) =5.6 Hz, CH on pyridyl ring *meta* to N), 125.1 (d, $^{2}J(^{13}$C-^{19}F) = 17.4 Hz, CH on pyridyl ring *para* to N), 85.9 (CCH$_3$), 8.5 (CCH$_3$)

9.3.3 Synthesis of Ir(η^5-C$_5$(CH$_3$)$_5$){C$_5$H$_4$NCl}Cl$_2$ (3.3)

3-Chloropyridine (0.10 ml, 1.05 mmol) was added to [IrCp*Cl$_2$]$_2$ (0.10 g, 0.13 mmol) in tetrahydrofuran (10 ml). The mixture was stirred overnight, then filtered. The resulting yellow powder was recrystallised using vapour diffusion (dichloromethane/pentane solvent system) to give **3.3** as orange crystals (0.09 g, 0.18 mmol, 71%)

Anal. Found: C: 35.6, H: 3.8, N: 2.6, Cl: 20.2%. **Anal. Calculated**: C: 35.2, H: 3.7, N: 2.7, Cl: 20.8%

^{1}H NMR (300 MHz, CDCl$_3$, 300 K) 9.00 (br. d, $^4J(^1$H-^{1}H) = 2.2 Hz, 1H, CH on pyridyl ring *ortho* to Cl and N), 8.90 (br. dd, $^3J(^1$H-^{1}H) = 5.6, $^4J(^1$H-^{1}H) = 1.0 Hz, 1H, CH on pyridyl ring *para* to Cl), 7.75 (ddd, $^3J(^1$H-^{1}H) = 8.3 Hz, $^4J(^1$H-^{1}H) = 2.0 Hz, $^4J(^1$H-^{1}H) = 1.2 Hz, 1H, CH on pyridyl ring *para* to N), 7.32 (dd, $^3J(^1$H-^{1}H) = 8.2 Hz, $^3J(^1$H-^{1}H) = 5.6 Hz 1H, CH on pyridyl ring *meta* to N), 1.54 (s, 15H, 5 × CH$_3$). ^{13}C{^{1}H} NMR (75 MHz, CDCl$_3$, 300 K) 152.6 (CH on pyridyl ring *ortho* to N and Cl), 151.5 (CH on pyridyl ring *para* to Cl), 137.9 (CH on pyridyl ring *para* to N), 133.4 (CCl), 125.7 (CH on pyridyl ring *meta* to N), 86.0 (C̲CH$_3$), 8.6 (CC̲H$_3$).

9.3.4 Synthesis of Ir(η^5-C$_5$(CH$_3$)$_5$){C$_5$H$_4$NBr}Cl$_2$ (3.4)

3-Bromopyridine (0.04 ml, 0.42 mmol) was added to [IrCp*Cl$_2$]$_2$ (0.10 g, 0.13 mmol) in tetrahydrofuran (10 ml). The mixture was stirred overnight, then filtered. The resulting yellow powder was recrystallised using vapour diffusion (dichloromethane/pentane solvent system) to give **3.4** as orange crystals (0.10 g, 0.18 mmol, 72%)

Anal. Found: C: 32.5, H: 3.5, N: 2.4%. **Anal. Calculated**: C: 32.4, H: 3.4, N: 2.5%

^{1}H NMR (300 MHz, CDCl$_3$, 300 K) 9.08 (br. d, $^4J(^1$H-^{1}H) = 2.0 Hz, 1H, CH on pyridyl ring *ortho* to Br and N), 8.93 (dd, $^3J(^1$H-^{1}H) = 5.5 Hz, $^4J(^1$H-^{1}H) = 1.0 Hz, 1H, CH on pyridyl ring *para* to Br), 7.89 (ddd, $^3J(^1$H-^{1}H) = 8.2 Hz, $^3J(^1$H-^{1}H) = 2.1 Hz, $^4J(^1$H-^{1}H) = 1.3 Hz, 1H , CH on pyridyl ring *para* to Br), 7.26 (masked vt (dd), $^3J(^1$H-^{1}H) = 6.0 Hz, 1H , CH on pyridyl ring *meta* to N), 1.54 (s, 15H, 5 × CH$_3$). ^{13}C{^{1}H} NMR (75 MHz, CDCl$_3$, 300 K) 154.2 (CH on pyridyl ring *ortho* to N and Br), 151.9 (CH on pyridyl ring *para* to Br), 140.7 (CH on pyridyl ring *para* to N), 126.1 (CCl), 121.3 (CH on pyridyl ring *meta* to N), 86.0 (C̲CH$_3$), 8.6 (CC̲H$_3$).

9.3.5 Synthesis of Ir(η^5-C$_5$(CH$_3$)$_5$){C$_5$H$_4$IN}Cl$_2$ (3.5)

3-Iodopyridine (0.10 g, 0.82 mmol) was added to [IrCp*Cl$_2$]$_2$ (0.10 g, 0.13 mmol) in tetrahydrofuran (10 ml). The mixture was stirred overnight, then filtered. The resulting yellow powder was recrystallised using vapour diffusion (dichloromethane/pentane solvent system) to give **3.5** as an orange/yellow powder

(0.07 g, 0.12 mmol, 46%).

Anal. Found: C: 29.9, H: 3.2, N: 2.2% **Anal. Calculated**: C: 29.9, H: 3.2, N: 2.3%

^{1}H NMR (300 MHz, CDCl$_3$, 300 K) 9.20 (br. d, $^4J(^1$H-^{1}H) = 1.6 Hz, 1H, CH on pyridyl ring *ortho* to I and N), 8.96 (br. d, $^3J(^1$H-^{1}H) = 5.5 Hz, 1H, CH on pyridyl ring *para* to I), 8.05 (vtd, $^3J(^1$H-^{1}H) = 8.0 Hz, $^3J(^1$H-^{1}H) = 1.6 Hz, $^4J(^1$H-^{1}H) = 1.6 Hz, 1H , CH on pyridyl ring *para* N), 7.13 (dd, $^3J(^1$H-^{1}H) = 8.0 Hz, $^3J(^1$H-^{1}H) = 5.6 Hz, 1H , CH on pyridyl ring *meta* to N), 1.54 (s, 15H, 5 × CH$_3$). ^{13}C{^{1}H} NMR (75 MHz, CDCl$_3$, 300 K) 159.0 (CH on pyridyl ring *ortho* to N and I), 152.2 (CH on pyridyl ring *para* to I), 146.2 (CH on pyridyl ring *para* to N), 126.3 (CH on pyridyl ring *meta* to N), 92.8 (C-I), 85.9 (CCH$_3$), 8.6 (CCH$_3$).

9.3.6 Synthesis of Ir(η^5-C$_5$(CH$_3$)$_5$){C$_7$H$_{12}$N$_2$}Cl$_2$ (3.6)

4-Dimethylaminopyridine (0.03 g, 0.26 mmol) was added to [IrCp*Cl$_2$]$_2$ (0.1g, 0.13 mmol) in tetrahydrofuran (10 ml) and the solution was stirred for 25 hours. The suspension was filtered and the crude product washed with ether, then recrystallised using vapour diffusion (dichloromethane/pentane solvent system) to give **3.6** as orange crystals (0.09 g, 0.18 mmol, 70%)

Anal. Found: C: 39.4, H: 4.8, N: 5.2% **Anal. Calculated**: C: 39.2, H: 4.8, N: 5.4%

^{1}H NMR (300 MHz, CDCl$_3$, 300 K) 8.39 (br. dd, $^3J(^1$H-^{1}H) = 5.7 Hz, $^4J(^1$H-^{1}H) = 1.4 Hz, 1H, CH on pyridyl ring *meta* to NMe$_2$), 6.43 (br. dd, $^3J(^1$H-^{1}H) = 5.6 Hz, $^4J(^1$H-^{1}H) = 1.4 Hz, 1H, CH on pyridyl ring *ortho* to NMe$_2$), 3.05 (s, 6H, N(CH$_3$)$_2$, 1.54 (s, 15H, 5 × CH$_3$). ^{13}C{^{1}H} NMR (75 MHz, CDCl$_3$, 300 K) 154.2 (CNMe$_2$), 151.7 (CH on pyridyl ring *meta* to NMe$_2$), 107.9 (CH on pyridyl ring *ortho* to NMe$_2$), 85.1 (CCH$_3$ on Cp*), 39.2 (N(CH$_3$)$_2$) 8.6 (CCH$_3$ on Cp*).

9.3.7 Synthesis of Ir(η^5-C$_5$(CH$_3$)$_4$C$_3$H$_6$OH){C$_5$H$_5$N}Cl$_2$ (3.7)

[Ir{η^5-C$_5$(CH$_3$)$_4$C$_3$H$_6$OH}Cl$_2$]$_2$ (0.05 g, 0.06 mmol) was dissolved in an excess of pyridine (25 ml) and the solution was stirred for 16 hours. After evaporation of the solvent, the residue was dissolved in a minimum of dichloromethane and the product precipitated using hexane, then collected by filtration and dried *in vacuo* to give **3.7** as a yellow powder (0.04 g, 0.07 mmol, 68%).

Anal. Found: C: 39.3, H: 4.6, N 2.5% **Anal. Calculated:** C 39.2, H 4.6, N 2.7%

^{1}H NMR (300 MHz, CDCl$_3$, 300 K) 8.98 (br. d, $^3J(^1$H-^{1}H) = 5.2 Hz, 2H, 2 × CH *ortho* to N of pyridine), 7.74 (tt, $^3J(^1$H-^{1}H) = 7.8 Hz, $^4J(^1$H-^{1}H) = 1.4 Hz, 1H, CH *para* to N of pyridine), 7.35 (vt (dd), $^3J(^1$H-^{1}H) = 6.9 Hz, $^3J(^1$H-^{1}H) = 6.9 Hz, 2H, 2 × CH *meta* to N of pyridine), 3.67 (t, $^3J(^1$H-^{1}H) = 6.3 Hz, 2H, CH$_2$OH), 2.12 (t, $^3J(^1$H-^{1}H) = 7.9 Hz, 2H, CH$_2$(CH$_2$)$_2$OH), 1.66-1.78 (m, 2H, CH$_2$CH$_2$OH), 1.56 (s, 6H, 2 × CH$_3$ *meta* to alkyl chain on aryl ring), 1.55 (s, 6H, 2 × CH$_3$ *ortho* to alkyl chain on aryl ring). ^{13}C{^{1}H} NMR (75 MHz, CDCl$_3$, 300 K) 153.5 (2 × C *ortho* to N on pyridine ring), 137.8 (C *para* to N on pyridine ring), 125.4 (2 × C *meta* to N on pyridine ring), 87.2 (quaternary C of functionalised Cp* ring), 86.6 (quaternary C of functionalised Cp* ring), 85.8 (quarternary C of functionalised Cp* ring), 62.0 (CH$_2$OH), 30.7 (CH$_2$CH$_2$OH), 20.1 (CH$_2$CH$_2$CH$_2$OH), 8.6 (2 × CH$_3$), 8.5 (2 × CH$_3$).

9.3.8 Synthesis of Ir(η^5-C$_5$(CH$_3$)$_4$C$_5$H$_{10}$OH){C$_5$H$_5$N}Cl$_2$ (3.8)

[Ir{η^5-C$_5$(CH$_3$)$_4$C$_5$H$_{10}$OH}Cl$_2$]$_2$ (0.50 g, 0.66 mmol) was dissolved in an excess of pyridine (25 ml) and the solution was stirred for 20 hours. After evaporation of the solvent, the residue was dissolved in a minimum of dichloromethane and the product precipitated using hexane, then collected by filtration and dried *in vacuo* to give **3.8** as a yellow powder (0.57 g, 1.13 mmol, 86%). Yellow crystals suitable for single crystal X-ray diffraction were obtained via vapour diffusion (chloroform/diisopropylether).

Anal. Found: C: 41.8, H: 5.2, N: 2.4, Cl: 12.5% **Anal. Calculated:** C: 41.5, H: 5.1, N: 2.6, Cl: 12.9%

^{1}H NMR (300 MHz, CDCl$_3$, 300 K) 8.97 (br. dd, $^3J(^1$H-^{1}H) = 6.9 Hz, $^4J(^1$H-^{1}H) = 1.4 Hz, 2H, 2 × CH *ortho* to N of pyridine), 7.74 (tt, $^3J(^1$H-^{1}H) = 7.6 Hz, $^4J(^1$H-^{1}H) = 1.4 Hz, 1H, CH *para* to N of pyridine), 7.35 (ddd, $^3J(^1$H-^{1}H) = 7.6 Hz, $^3J(^1$H-^{1}H) = 6.7 Hz, $^4J(^1$H-^{1}H) = 1.4 Hz, 2H, 2 × CH *meta* to N of pyridine), 3.64 (m, 2H, CH$_2$OH), 2.03 (m, 2H, CH$_2$(CH$_2$)$_4$OH), 1.58 (m, 2H, CH$_2$CH$_2$OH), 1.56 (s, 6H, 2 × CH$_3$ *meta* to alkyl chain on aryl ring), 1.55 (s, 6H, 2 × CH$_3$ *ortho* to alkyl chain on aryl ring), 1.34-1.50 (m, 4H, CH$_2$CH$_2$CH$_2$OH). ^{13}C{^{1}H} NMR (75 MHz, CDCl$_3$, 300 K) 153.5 (2 × C *ortho* to N on pyridine ring), 137.7 (C *para* to N on pyridine ring), 125.4 (2 × C *meta* to N on pyridine ring), 87.2 (quaternary C of functionalised Cp* ring), 86.2 (quaternary C of functionalised Cp* ring), 85.9 (quarternary C of

functionalised Cp* ring), 62.6 (CH_2OH), 32.4 ($\underline{C}H_2CH_2OH$), 27.8 ($\underline{C}H_2CH_2CH_2OH$), 26.0 ($\underline{C}H_2CH_2CH_2CH_2OH$), 23.6 ($\underline{C}H_2CH_2CH_2CH_2CH_2OH$), 8.6 ($2 \times CH_3$), 8.5 ($2 \times CH_3$).

9.3.9 Synthesis of $Ir(\eta^5\text{-}C_5(CH_3)_4C_{14}H_{28}OH)\{C_5H_5N\}Cl_2$ (3.9)

$[Ir\{\eta^5\text{-}C_5(CH_3)_4C_{14}H_{28}OH\}Cl_2]_2$ (0.10 g, 0.84 mmol) was dissolved in an excess of pyridine (25 ml) and the solution was stirred for 20 hours. After evaporation of the solvent, the residue was dissolved in a minimum of dichloromethane and the product precipitated using hexane, then collected by filtration and dried *in vacuo* to give **3.9** as a yellow powder (0.91 g, 1.35 mmol, 80%).

Anal. Found: C: 50.0, H: 6.9, N: 1.8, Cl: 10.1% **Anal. Calculated:** C: 49.8, H 6.9, N: 2.1, Cl: 10.5%

^{1}H NMR (300 MHz, CDCl$_3$, 300 K) 8.98 (br. d, $^3J(^1H\text{-}^1H) = 5.2$ Hz, 2H, $2 \times CH$ *ortho* to N of pyridine), 7.73 (t, $^3J(^1H\text{-}^1H) = 7.7$ Hz, 1H, CH *para* to N of pyridine), 7.34 (vbr. t (dd), $^3J(^1H\text{-}^1H) = 6.9$ Hz, $^3J(^1H\text{-}^1H) = 6.9$ Hz, 2H, $2 \times CH$ *meta* to N of pyridine), 3.64 (t, $^3J(^1H\text{-}^1H) = 6.6$ Hz, 2H, C$\underline{H}_2$OH), 1.94-2.01 (m, 2H, C$\underline{H}_2$(CH$_2$)$_{13}$OH), 1.58-1.70 (m, 2H, C$\underline{H}_2$CH$_2$OH), 1.56 (s, 6H, $2 \times CH_3$ *meta* to alkyl chain on aryl ring), 1.54 (s, 6H, $2 \times CH_3$ *ortho* to alkyl chain on aryl ring), 1.20-1.45 (m, 22H, $11 \times CH_2$). ^{13}C{^{1}H} NMR (75 MHz, CDCl$_3$, 300 K) 153.5 ($2 \times C$ *ortho* to N on pyridine ring), 137.7 (C *para* to N on pyridine ring), 125.4 ($2 \times C$ *meta* to N on pyridine ring), 87.7 (quaternary C of functionalised Cp* ring), 86.0 (quaternary C of functionalised Cp* ring), 85.9 (quarternary C of functionalised Cp* ring), 63.1 (CH_2OH), 32.8 ($\underline{C}H_2CH_2OH$), 29.7 (s, CH_2), 29.6 (s, CH_2), 29.6 (s, CH_2), 29.5 (s, CH_2), 29.5 (s, CH_2), 29.4 (s, CH_2), 29.4 (s, CH_2), 28.0 (s, CH_2), 25.7 (s, CH_2), 23.5 (s, CH_2) 8.6 (s, CH_3), 8.6 (s, CH_3).

9.3.10 Synthesis of $Ir(\eta^5\text{-}C_5(CH_3)_4C_5H_{10}OH)(C_5H_4NCl)Cl_2$ (3.10)

3-Chloropyridine (0.02 ml, 0.22 mmol) was added to $[Ir\{\eta^5\text{-}C_5(CH_3)_4C_5H_{10}OH\}Cl_2]_2$ (0.10 g, 0.11 mmol) in dichloromethane (25 ml) and left to stir for 30 minutes. After evaporation of the solvent, the residue was dissolved in a minimum of dichloromethane and the product precipitated using hexane, then collected by filtration and recrystallised using vapour diffusion (dichloromethane/pentane solvent system) to give **3.10** as yellow crystals (0.07 g,

0.12 mmol, 56%).

Anal. Found: C: 39.3, H: 4.7, N: 2.2% **Anal. Calculated:** C: 39.1, H 4.7, N 2.4%

^{1}H NMR (300 MHz, CDCl$_3$, 300 K) 9.00 (br. d, $^4J(^1$H-^{1}H) = 2.2 Hz, 1H, CH of pyridyl *ortho* to N and Cl), 8.90 (br. d, $^3J(^1$H-^{1}H) = 5.6 Hz, 1H, CH of pyridyl *para* to Cl), 7.76 (br. d, $^3J(^1$H-^{1}H) = 7.9 Hz, 1H, CH of pyridyl *para* to N), 7.32 (br. t, $^3J(^1$H-^{1}H) = 6.6 Hz, 1H, CH *meta* to N), 3.64 (t, $^3J(^1$H-^{1}H) = 6.3 Hz, 2H, CH$_2$OH), 2.02 (t, $^3J(^1$H-^{1}H) = 7.7 Hz, 2H, CH$_2$(CH$_2$)$_4$OH), 1.59-1.75 (m, 2H, CH$_2$CH$_2$OH), 1.57 (s, 6H, 2 × CH$_3$ *meta* to alkyl chain on aryl ring), 1.56 (s, 6H, 2 × CH$_3$ *ortho* to alkyl chain on aryl ring), 1.40-1.52 (m, 4H, CH$_2$CH$_2$CH$_2$CH$_2$OH). ^{13}C{^{1}H} NMR (125 MHz, CDCl$_3$, 300 K) 152.3 (CH on pyridyl ring *ortho* to N and Cl), 151.7 (CH on pyridyl ring *para* to Cl), 137.9 (CH on pyridyl ring *para* to N), 133.4 (CCl), 125.7 (CH on pyridyl ring *meta* to N), 87.5 (quarternary C of functionalised Cp* ring), 86.4 (quarternary C of functionalised Cp* ring), 86.1 (quarternary of functionalised Cp* ring), 62.6 (CH$_2$OH), 32.4 (CH$_2$CH$_2$OH), 27.8 (CH$_2$CH$_2$CH$_2$OH), 26.0 (CH$_2$CH$_2$CH$_2$CH$_2$OH), 23.6 (CH$_2$CH$_2$CH$_2$CH$_2$CH$_2$OH), 8.7 (CH$_3$), 8.6 (CH$_3$).

9.3.11 Synthesis of Ir(η^5-C$_5$(CH$_3$)$_4$C$_5$H$_{10}$OH)(C$_5$H$_4$NBr)Cl$_2$ (3.11)

3-Bromopyridine (0.02 ml, 0.22 mmol) was added to [Ir{η^5-C$_5$(CH$_3$)$_4$C$_5$H$_{10}$OH}Cl$_2$]$_2$ (0.10 g, 0.11 mmol) in dichloromethane (25 ml) and left to stir for 40 minutes. After evaporation of the solvent, the residue was dissolved in a minimum of dichloromethane and the product precipitated using hexane, to give yellow crystals suitable for single crystal X-ray diffraction. The crude product was recrystallised using vapour diffusion (dichloromethane/pentane solvent system) to give **3.11** as yellow crystals (0.09 g, 0.14 mmol, 64%).

Anal. Found: C: 36.4, H: 4.3, N: 2.1% **Anal. Calculated:** C: 36.3, H: 4.3, N: 2.2%

^{1}H NMR (300 MHz, CDCl$_3$, 300 K) 9.09 (br. d, $^4J(^1$H-^{1}H) = 1.9 Hz, 1H, CH of pyridyl ring *ortho* to N and Br), 8.94 (br. dd, $^3J(^1$H-^{1}H) = 5.7 Hz, $^4J(^1$H-^{1}H) = 1.2 Hz, 1H, CH of pyridyl ring *para* to Br), 7.90 (vdq (ddd), $^3J(^1$H-^{1}H) = 8.1 Hz, $^4J(^1$H-^{1}H) = 2.4 Hz, $^4J(^1$H-^{1}H) = 1.4 Hz 1H, CH of pyridyl ring *para* to N), 7.26 (masked dd, $^3J(^1$H-^{1}H) = 8.3 Hz, $^3J(^1$H-^{1}H) = 5.7 Hz, 1H, CH of pyridyl ring *meta* to N), 3.65 (t, $^3J(^1$H-^{1}H) = 6.2 Hz, 2H, CH$_2$OH), 2.02 (m, 2H, CH$_2$(CH$_2$)$_4$OH), 1.89

(m, 2H, CH$_2$CH$_2$OH), 1.56 (s, 6H, 2 × CH$_3$ *meta* to alkyl chain on aryl ring) , 1.56 (s, 6H, 2 × CH$_3$ *ortho* to alkyl chain on aryl ring), 1.40-1.45 (m, 4H, CH$_2$CH$_2$CH$_2$CH$_2$OH). ^{13}C{^{1}H} NMR (75 MHz, CDCl$_3$, 300 K) 154.3 (CH on pyridyl ring *ortho* to N and Br), 151.9 (CH on pyridyl ring *para* to Br), 138.8 (CH on pyridyl ring *para* to N), 126.0 (CH on pyridyl ring *meta* to N), 121.3 (CBr), 87.5 (quarternary C of functionalised Cp* ring), 86.4 (quarternary C of functionalised Cp* ring), 86.1 (quarternary of functionalised Cp* ring), 62.5 (CH$_2$OH), 32.4 (CH$_2$CH$_2$OH), 27.8 (CH$_2$CH$_2$CH$_2$OH), 26.0 (CH$_2$CH$_2$CH$_2$CH$_2$OH), 23.6 (CH$_2$CH$_2$CH$_2$CH$_2$CH$_2$OH), 8.7 (CH$_3$), 8.6 (CH$_3$).

9.3.12 Synthesis of Ir(η^5-C$_5$(CH$_3$)$_4$C$_5$H$_{10}$OH)(C$_5$H$_4$NI)Cl$_2$ (3.12)

3-Iodopyridine (0.13 g, 1.11 mmol) was added to [Ir{η^5-C$_5$(CH$_3$)$_4$C$_5$H$_{10}$OH}Cl$_2$]$_2$ (0.10 g, 0.11 mmol) in dichloromethane (25 ml) and left to stir for 20 hours. After evaporation of the solvent, the residue was dissolved in a minimum of dichloromethane and the product precipitated using hexane, then collected by filtration and dried *in vacuo* to give **3.12** as a yellow powder (0.12 g, 0.18 mmol, 81%)

Anal. Found: C: 38.1, H: 4.6, N: 1.9% **Anal. Calculated:** C: 35.8, H: 4.0, N: 2.1%

^{1}H NMR (300 MHz, CDCl$_3$, 300 K) 9.19 (br. d, ^4J(^{1}H-^{1}H) = 1.8 Hz, 1H, CH of pyridyl *ortho* to N and I), 8.95 (br. d, ^3J (^{1}H-^{1}H) = 5.7 Hz, 1H, CH of pyridyl ring *para* to I), 8.07 (br. d, ^3J (^{1}H-^{1}H) = 6.7 Hz, 1H, CH of pyridyl ring *para* to N), 7.14 (vt (dd), ^3J (^{1}H-^{1}H) = 7.9 Hz, ^3J (^{1}H-^{1}H) = 7.9 Hz, 1H, CH pyridyl ring *meta* to N), 3.64 (t, ^3J (^{1}H-^{1}H) = 6.3 Hz, 2H, CH$_2$OH), 2.01 (t, 2H, ^3J(^{1}H-^{1}H) = 7.6 Hz, CH$_2$(CH$_2$)$_4$OH), 1.56-1.62 (m, 2H, CH$_2$CH$_2$OH), 1.56 (s, 12H, 4 × CH$_3$) 1.40-1.51 (m, 4H, CH$_2$CH$_2$CH$_2$OH). ^{13}C{^{1}H} NMR (75 MHz, CDCl$_3$, 300 K) 159.0 (CH *ortho* to N and I), 152.4 (CH *para* to I), 146.3 (CH *para* to N), 126.4 (CH *meta* to N), 92.7 (CI), 87.5 (quarternary C of functionalised Cp* ring), 86.4 (quarternary C of functionalised Cp* ring), 86.1 (quarternary C of functionalised Cp* ring), 62.5 (CH$_2$OH), 32.4 (CH$_2$CH$_2$OH), 27.8 (CH$_2$CH$_2$CH$_2$OH), 26.0 (CH$_2$CH$_2$CH$_2$CH$_2$OH), 23.6 (CH$_2$CH$_2$CH$_2$CH$_2$CH$_2$OH), 8.7 (2 × CH$_3$), 8.6 (2 × CH$_3$).

9.3.13 Synthesis of Ir(η^5-C$_5$(CH$_3$)$_4$C$_5$H$_{10}$OH)(C$_6$H$_9$N)Cl$_2$ (3.13)

4-Methylpyridine (0.02 ml, 0.22 mmol) was added to [Ir{η^5-C$_5$(CH$_3$)$_4$C$_5$H$_{10}$OH}Cl$_2$]$_2$ (0.10 g, 0.11 mmol) in dichloromethane (25 ml) and left to stir for 20 hours. After evaporation of the solvent, the residue was dissolved in a minimum of dichloromethane and the product precipitated using hexane, to obtain a mixture of a yellow oil and yellow needles suitable for X-ray crystallography. The product was recrystallised using vapour diffusion (dichloromethane/pentane solvent system) to give **3.13** as a yellow solid (0.09 g, 1.6 mmol, 75%)

Anal. Found: C: 44.2, H: 5.6, N: 2.6, Cl: 11.2% **Anal. Calculated:** C: 42.6, H: 5.4, N: 2.5, Cl: 12.6%

^{1}H NMR (300 MHz, CDCl$_3$, 300 K) 8.74 (br. d, ^3J(^{1}H-^{1}H) = 6.4 Hz, 2H, 2 × CH *ortho* to N of pyridine), 7.13 (br. d, ^3J(^{1}H-^{1}H) = 6.0 Hz, 2H, 2 × CH *meta* to N of pyridine), 3.60 (t, ^3J(^{1}H-^{1}H) = 6.4 Hz, 2H, C$\underline{H}_2$OH), 2.42 (br. s, 3H, CH$_3$ on pyridyl ring), 1.94-2.01 (m, 2H, C$\underline{H}_2$(CH$_2$)$_4$OH), 1.50-1.60 (masked m, 2H, C$\underline{H}_2$CH$_2$OH), 1.53 (s, 6H, 2 × CH$_3$ *meta* to alkyl chain on aryl ring), 1.51 (s, 6H, 2 × CH$_3$ *ortho* to alkyl chain on aryl ring), 1.34-1.50 (m, 4H, C$\underline{H}_2$C$\underline{H}_2$CH$_2$OH). ^{13}C{^{1}H} NMR (75 MHz, CDCl$_3$, 300 K) 152.6 (2 × C *ortho* to N on pyridyl ring), 149.8 (C *para* to N on pyridyl ring), 126.3 (2 × C *meta* to N on pyridyl ring), 87.1 (quaternary C of functionalised Cp* ring), 86.0 (quaternary C of functionalised Cp* ring), 85.7 (quarternary C of functionalised Cp* ring), 62.4 (CH$_2$OH), 32.4 ($\underline{C}$H$_2$CH$_2$OH), 27.8 ($\underline{C}$H$_2$CH$_2$CH$_2$OH), 26.0 ($\underline{C}$H$_2$CH$_2$CH$_2$CH$_2$OH), 23.5 ($\underline{C}$H$_2$CH$_2$CH$_2$CH$_2$CH$_2$OH), 20.8 (CH$_3$ on pyridyl ring), 8.6 (CH$_3$ on functionalised Cp* ring), 8.5 (CH$_3$ on functionalised Cp* ring).

9.3.14 Synthesis of Ir(η^5-C$_5$(CH$_3$)$_4$C$_5$H$_{10}$OH){C$_5$H$_4$N}I$_2$ (3.14)

[Ir{η^5-C$_5$(CH$_3$)$_4$C$_5$H$_{10}$OH}I$_2$]$_2$ (0.30 g, 0.23 mmol) was dissolved in an excess of pyridine (25 ml) and the solution was stirred for 20 hours. After evaporation of the solvent, the resulting powder was dissolved in a minimum of dichloromethane and the product precipitated using hexane, then collected by filtration. The precipitation process was repeated to give orange crystals of **3.14** suitable for single crystal X-ray diffusion (0.28 g, 0.38 mmol, 83%).

Anal. Found: C: 29.9, H: 3.7, N: 1.7% **Anal. Calculated** (with 0.5 molecules of dichloromethane): C: 30.2, H: 3.8, N: 1.8%

^{1}H NMR (300 MHz, CDCl$_3$, 300 K) 9.38 (br. s, 2H, 2 × CH *ortho* to N of pyridine), 7.72 (br. t, 1H, CH *para* to N of pyridine), 7.23 (m, 2H, 2 × CH *meta* to N of pyridine), 3.64 (t, ^3J (^{1}H-^{1}H) = 6.4 Hz, 2H, C$\underline{H}_2$OH), 2.12 (br. t, ^3J (^{1}H-^{1}H) = 7.15 Hz, 2H, C$\underline{H}_2$(CH$_2$)$_4$OH), 1.90 (m, 2H, C$\underline{H}_2$CH$_2$OH), 1.70 (s, 12H, 4 × CH$_3$ of aryl ring), 1.41-1.64 (m, 4H, C$\underline{H}_2$C$\underline{H}_2$CH$_2$OH). ^{13}C{^{1}H} NMR (75 MHz, CDCl$_3$, 300 K) 158.6 (2 × C *ortho* to N on pyridine ring), 137.5 (C *para* to N on pyridine ring), 125.5 (2 × C *meta* to N on pyridine ring), 89.5 (quaternary C of functionalised Cp* ring), 8.7 (quaternary C of functionalised Cp* ring), 87.6 (quarternary C of functionalised Cp* ring), 62.6 (CH$_2$OH), 32.4 ($\underline{C}$H$_2$CH$_2$OH), 28.1 ($\underline{C}$H$_2$CH$_2$CH$_2$OH), 26.0 ($\underline{C}$H$_2$CH$_2$CH$_2$CH$_2$OH), 25.0 ($\underline{C}$H$_2$CH$_2$CH$_2$CH$_2$CH$_2$OH), 10.2 (2 × CH$_3$), 10.1 (2 × CH$_3$).

9.3.15 Synthesis of Rh(η^5-C$_5$(CH$_3$)$_4$C$_5$H$_{10}$OH){C$_5$H$_4$N}Cl$_2$ (3.15)

[Rh{η^5-C$_5$(CH$_3$)$_4$C$_5$H$_{10}$OH}Cl$_2$]$_2$ (0.30 g, 0.39 mmol) was dissolved in an excess of pyridine (25 ml) and the solution was stirred for 20 hours. After evaporation of the solvent, the red powder was dissolved in a minimum of dichloromethane and the product precipitated using hexane, then collected by filtration. The precipitation process was repeated and the product was dried *in vacuo* to give **3.15** as a red powder (0.32 g, 0.70 mmol, 88%). Red crystals suitable for single crystal X-ray diffraction were obtained using vapour diffusion (chloroform/pentane).

Anal. Found: C: 49.9, H: 6.4, N: 2.8, Cl: 15.8% **Anal. Calculated:** C 49.6, H 6.1, N: 3.0, Cl: 15.4%

^{1}H NMR (300 MHz, CDCl$_3$, 300 K) 8.99 (br. s, 2H, 2 × CH *ortho* to N of pyridine), 7.78 (br. s, 1H, CH *para* to N of pyridine), 7.38 (br. s, 2H, 2 × CH *meta* to N of pyridine), 3.64 (br. s, 2H, C$\underline{H}_2$OH), 2.14 (br. s, 2H, C$\underline{H}_2$(CH$_2$)$_4$OH), 1.67 (br. s, 2H, C$\underline{H}_2$CH$_2$OH), 1.61 (s, 6H, 2 × CH$_3$ *meta* to alkyl chain on aryl ring), 1.60 (s, 6H, 2 × CH$_3$ *ortho* to alkyl chain on aryl ring), 1.44 (br. s, 4H, C$\underline{H}_2$C$\underline{H}_2$CH$_2$OH). ^{13}C{^{1}H} NMR (75 MHz, CDCl$_3$, 300 K) 153.6 (2 × C *ortho* to N on pyridine ring), 137.8 (C *para* to N on pyridine ring), 125.3 (2 × C *meta* to N on pyridine ring), 96.0 (d, ^1J(^{13}C-^{103}Rh) = 9.0 Hz, quaternary C of functionalised Cp* ring), 94.4 (d, ^1J (^{13}C-^{103}Rh) = 8.3 Hz, 2C, quaternary C of functionalised Cp* ring), 94.1 (d, ^1J (^{13}C-^{103}Rh) = 8.7 Hz, 4 C, quaternary C of functionalised Cp* ring), 62.4 (CH$_2$OH), 32.3 ($\underline{C}$H$_2$CH$_2$OH), 27.9 ($\underline{C}$H$_2$CH$_2$CH$_2$OH), 26.0 ($\underline{C}$H$_2$CH$_2$CH$_2$CH$_2$OH), 23.7

($\underline{C}H_2CH_2CH_2CH_2CH_2OH$), 9.0 ($2 \times CH_3$), 8.9 ($2 \times CH_3$).

9.3.16 Synthesis of Rh(η^5-$C_5(CH_3)_4C_5H_{10}OH$)(C_5H_4NCl)Cl_2 (3.16)

3-Chloropyridine (0.03 ml, 0.26 mmol) was added to [Rh{η^5-$C_5(CH_3)_4C_5H_{10}OH$}Cl_2]$_2$ (0.10 g, 0.13 mmol) in dichloromethane (25 ml) and left to stir for 25 hours. After evaporation of the solvent, the residue was dissolved in a minimum of dichloromethane and the product precipitated using hexane, then collected by filtration and recrystallised using vapour diffusion (dichloromethane/pentane solvent system) to give **3.16** as red crystals (0.07 g, 0.14 mmol, 54%).

Anal. Found: C: 46.3, H: 5.7, N: 2.4, Cl: 21.5% **Anal. Calculated:** C: 46.1, H: 5.5, N: 2.8, Cl: 21.5%

^{1}H NMR (300 MHz, CDCl$_3$, 300 K) 8.96 (br. s, 1H, CH of pyridyl *ortho* to N and Cl), 8.88 (br.s, 1H, CH of pyridyl *ortho* to N), 7.78 (br. d, ^3J (^{1}H-^{1}H) = 8.1 Hz, 1H, CH of pyridyl *para* to N), 7.35 (br. dd, ^3J (^{1}H-^{1}H) = 7.7 Hz, ^3J(^{1}H-^{1}H) = 5.6 Hz, 1H, CH *meta* to N), 3.63 (t, ^3J (^{1}H-^{1}H) = 6.1 Hz, 2H, C$\underline{H}_2$OH), 2.14 (t, ^3J (^{1}H-^{1}H) = 6.8 Hz, 2H, C$\underline{H}_2$(CH$_2$)$_4$OH), 1.61 (s, 12H, 4 × CH$_3$) , 1.51-1.57 (m, 2H, C$\underline{H}_2$CH$_2$OH), 1.35-1.50 (m, 4H, C$\underline{H}_2$C$\underline{H}_2$CH$_2$CH$_2$OH). ^{13}C{^{1}H} NMR (75 MHz, CDCl$_3$, 300 K) 151.7 (CH on pyridyl ring *ortho* to N and Cl), 151.1 (CH on pyridyl *para* to Cl), 137.6 (CH on pyridyl ring *para* to N), 133.0 (CCl), 125.3 (CH on pyridyl ring *meta* to N), 96.2 (d, ^1J(^{13}C-^{103}Rh) = 9.3 Hz, quarternary C of functionalised Cp* ring), 94.6 (d, ^1J(^{13}C-^{103}Rh) = 8.1 Hz, quarternary C of functionalised Cp* ring), 94.3 (d, ^1J(^{13}C-^{103}Rh) = 8.7 Hz, quarternary of functionalised Cp* ring), 62.4 (CH$_2$OH), 32.3 ($\underline{C}H_2$CH$_2$OH), 27.7 ($\underline{C}H_2$CH$_2$CH$_2$OH), 25.9 ($\underline{C}H_2$CH$_2$CH$_2$CH$_2$OH), 23.7 ($\underline{C}H_2$CH$_2$CH$_2$CH$_2$CH$_2$OH), 8.9 (CH$_3$ on Cp), 8.9 (CH$_3$ on Cp).

9.3.17 Synthesis of Rh(η^5-$C_5(CH_3)_4C_5H_{10}OH$)(C_5H_4NBr)Cl_2 (3.17)

3-Bromopyridine (0.21 ml, 0.26 mmol) was added to [Rh{η^5-$C_5(CH_3)_4C_5H_{10}OH$}Cl_2]$_2$ (0.10 g, 0.13 mmol) in dichloromethane (25 ml) and left to stir for 19 hours. After evaporation of the solvent, the residue was recrystallised using vapour diffusion (dichloromethane/pentane solvent system) to give **3.17** as a red powder (0.09 g, 0.17 mmol, 64%).

Anal. Found: C: 42.7, H: 5.1, N 2.4% **Anal. Calculated:** C 42.3, H 5.1, N 2.6%

^{1}H NMR (300 MHz, CDCl$_3$, 300 K) 9.06 (br. s, 1H, CH of pyridyl *ortho* to N and Br), 8.93 (br.s, 1H, CH *para* to Br), 7.95 (br.s, 1H, CH of pyridyl *para* to N), 7.32 (br. s, CH of pyridyl *meta* to N), 3.65 (br. s, 2H, CH$_2$OH), 2.15 (br. s, 2H, CH$_2$(CH$_2$)$_4$OH), 1.62 (s, 12H, 4 × CH$_3$) , 1.52-1.66 (br. s, 2H, CH$_2$CH$_2$OH), 1.44 (br. s, 4H, CH$_2$CH$_2$CH$_2$CH$_2$OH). ^{13}C{^{1}H} NMR (75 MHz, CDCl$_3$, 300 K) 153.8 (br. s, CH on pyridyl ring *ortho* to N and Br), 151.5 (br. s, CH on pyridyl ring *para* to Br), 140.4 (CH on pyridyl ring *para* to N), 125.6 (CH on pyridyl ring *meta* to N), 121.2 (CBr), 96.0 (br. d, ^1J(^{13}C-^{103}Rh) = 24.6 Hz, CCH$_2$), 94.4 (br. d, ^1J(^{13}C-^{103}Rh) = 18.6 Hz, 4 × CCH$_3$), 62.5 (CH$_2$OH), 32.3 (CH$_2$CH$_2$OH), 27.7 (CH$_2$CH$_2$CH$_2$OH), 26.0 (CH$_2$CH$_2$CH$_2$CH$_2$OH), 23.8 (CH$_2$CH$_2$CH$_2$CH$_2$CH$_2$OH), 8.9 (4 × CH$_3$).

9.4 Picolinamide Complexes

9.4.1 Synthesis of Ir(η^5-C$_5$(CH$_3$)$_5$)Cl(C$_{12}$H$_{11}$N$_2$O) (4.1)

Pyridine-2-carboxylic acid phenylamide (0.05 g, 0.26 mmol) was added to a stirred suspension of [Ir{η^5-C$_5$(CH$_3$)$_5$}Cl$_2$]$_2$ (0.10 g, 0.13 mmol) in ethanol (30 ml) at 80 °C. After 15 minutes Ammonium hexafluorophosphate (0.10 g, 0.61 mmol) was added and the mixture was stirred at 80 °C for 20 hours. The solvent was evaporated and the residue dissolved in dichloromethane (50 ml), washed with water (2 × 20 ml), brine (20 ml), dried over sodium sulfate and evaporated to form an orange solid. The crude product was recrystallised using vapour diffusion (dichloromethane/pentane solvent system) to give **4.1** as orange crystals (0.06 g, 0.11 mmol, 46 %). ES-MS (CH$_2$Cl$_2$, m/z): 525.2 [M-Cl].

Anal. Found: C: 46.5, H: 4.5, N: 4.8, Cl: 6.7% **Anal. Calculated** (with 0.05 molecules of dichloromethane): C: 46.9, H: 4.3, N: 5.0, Cl: 6.9%

^{1}H NMR (300 MHz, CDCl$_3$, 300 K) 8.57 (br. d, ^3J (^{1}H-^{1}H) = 5.4 Hz, 1H, pyridyl CH *ortho* to N), 8.17 (br. d, ^3J (^{1}H-^{1}H) = 8.0 Hz, 1H, pyridyl CH *meta* to N, *ortho* to amide), 7.92 (vtd (ddd), ^3J (^{1}H-^{1}H) = 7.7 Hz, ^3J (^{1}H-^{1}H) = 7.7 Hz, ^4J (^{1}H-^{1}H) = 1.4 Hz, 1H, pyridyl CH *para* to N), 7.65 (br. dd, ^3J (^{1}H-^{1}H) = 8.3 Hz, ^4J (^{1}H-^{1}H) = 1.1 Hz, 2H, 2 × phenyl CH *ortho* to amide), 7.49 (ddd, ^3J (^{1}H-^{1}H) = 7.5 Hz, ^3J (^{1}H-^{1}H) = 5.6 Hz, ^4J (^{1}H-^{1}H) = 1.7 Hz, 1H, pyridyl CH *para* to amide), 7.32 (m, 2H, 2 × phenyl CH *meta* to amide), 7.09 (t, ^3J (^{1}H-^{1}H) = 7.3 Hz,) 1H, phenyl CH *para* to amide),

1.41 (s, 15H, 5 × CH$_3$). ^{13}C{^{1}H} NMR (75 MHz, CD$_2$Cl$_3$, 300 K) 168.4 (NCO), 155.8 (CCON) 149.5 (CH *ortho* to N on pyridyl ring), 148.1 (CNCO), 138.5 (CH *para* to N on pyridyl ring), 128.1 (CH *meta* to NCOR), 127.3 (CH *para* to CO on pyridyl ring) 126.9 (CH *ortho* to NCOR), 126.5 (CH *ortho* to CON on pyridyl ring), 124.3 (CH *para* to NCO), 86.5 (CCH$_3$), 8.4 (CCH$_3$).

9.4.2 Synthesis of Ir(η^5-C$_5$(CH$_3$)$_5$)Cl(C$_{12}$H$_{10}$FN$_2$O) (4.2)

Pyridine-2-carboxylic acid (4-fluoro-phenyl) amide (0.05 g, 0.26 mmol) was added to a stirred suspension of [Ir{η^5-C$_5$(CH$_3$)$_5$}Cl$_2$]$_2$ (0.10 g, 0.13 mmol) and sodium bicarbonate (0.02 g, 0.26 mmol) in methanol (3 ml) in a 10 ml capacity microwave tube. The tube was then sealed and microwave heating was applied at 150 °C for 10 minutes. After effervescence from the solution had subsided, the tube was opened and left to cool. The resulting suspension was filtered, washed with diethylether and dried *in vacuo* to yield orange crystals of **4.2** (0.10 g, 0.17 mmol, 69 %). ES-MS (CH$_2$Cl$_2$, m/z): 543.1 [M-Cl].

Anal. Found: C: 41.4, H: 3.6, N: 4.3, Cl: 11.2% **Anal. Calculated** (with 1 molecule of NaCl): C: 41.5, H: 3.6, N: 4.4, Cl: 11.1%

^{1}H NMR (300 MHz, CDCl$_3$, 300 K) 8.64 (br. d, ^3J (^{1}H-^{1}H) = 5.2 Hz, 1H, pyridyl CH *ortho* to N), 8.10 (br. d, ^3J (^{1}H-^{1}H) = 8.0 Hz, 1H, pyridyl CH *meta* to N, *ortho* to amide), 8.01 (vtd (ddd), ^3J (^{1}H-^{1}H) = 7.7 Hz, ^3J (^{1}H-^{1}H) = 7.7 Hz, ^4J (^{1}H-^{1}H) = 1.3 Hz, 1H, pyridyl CH *para* to N), 7.63 (ddd, ^3J (^{1}H-^{1}H) = 7.4 Hz, ^3J (^{1}H-^{1}H) = 5.7 Hz, ^4J (^{1}H-^{1}H) = 1.6 Hz, 1H, pyridyl CH *para* to amide) 7.44 (dd, ^3J (^{1}H-^{1}H) = 8.9 Hz, ^4J (^{1}H-^{19}F) = 5.1 Hz, 2H, phenyl CH *meta* to amide), 6.97 (vt (dd), ^3J (^{1}H-^{1}H) = 8.6 Hz, ^3J (^{1}H-^{19}F) = 8.6 Hz, 2H, phenyl CH *meta* to amide), 1.41 (s, 15H, 5 × CH$_3$). ^{13}C{^{1}H} NMR (125 MHz, CD$_2$Cl$_2$, 300K) 168.4 (NCO), 160.2 (d, ^1J(^{13}C-^{19}F) = 243.8 Hz, CF), 153.3 (CCON), 150.0 (CH *ortho* to N on pyridyl ring), 139.1 (CH *para* to N on pyridyl ring), 128.2 (d, ^4J(^{13}C-^{19}F) = 3.4 Hz, CNCO), 127.6 (d, ^3J(^{13}C-^{19}F) = 7.9 Hz, 2 × CH *ortho* to NCO) 127.0 (CH *ortho* to CO and *meta* to N on pyridyl ring), 126.6 (CH *ortho* to CON on pyridyl ring), 115.1 (d, ^2J(^{13}C-^{19}F) = 22.5 Hz, 2 × CH *meta* to NCO) 87.2 (CCH$_3$), 8.4 (CCH$_3$).

9.4.3 Synthesis of Ir(η^5-C$_5$(CH$_3$)$_5$)Cl(C$_{12}$H$_9$F$_2$N$_2$O) (4.3)

Pyridine-2-carboxylic acid (2,4-difluoro-phenyl) amide (0.07 g, 0.30 mmol) and

[IrCp*Cl$_2$]$_2$ (0.10 g, 0.13 mmol) were dissolved in ethanol (30 ml) and the solution was refluxed for 30 minutes. Ammonium hexafluorophosphate (0.10g, 0.61 mmol) was added and the mixture was refluxed overnight. The resulting yellow solution was evaporated to dryness, redissolved in dichloromethane (50 ml) and washed with water (2 × 10 ml) & brine (10 ml), dried using sodium sulfate and filtered. **4.3** was recrystallised by dichloromethane/hexane layer diffusion (0.06 g, 0.10 mmol, 40%). ES-MS (CH$_2$Cl$_2$, m/z): 561.1 [M-Cl].

Anal. Found: C: 43.8, H: 3.8, N: 4.4% **Anal. Calculated:** C: 44.3, H: 3.7, N: 4.7%

^{1}H NMR (300 MHz, CDCl$_3$, 300 K) 8.58 (br. d, ^3J (^{1}H-^{1}H) = 5.6 Hz, 1H, pyridyl CH *ortho* to N), 8.18 (br. d, ^3J (^{1}H-^{1}H) = 7.5 Hz, 1H, pyridyl CH *meta* to N, *ortho* to amide), 7.94 (vdt (ddd), ^3J (^{1}H-^{1}H) = 7.8 Hz, ^3J (^{1}H-^{1}H) = 7.5 Hz, ^4J (^{1}H-^{1}H) = 1.4 Hz, 1H, pyridyl CH *para* to N), 7.75 (vbr. q (ddd), ^3J (^{1}H-^{1}H) = 8.6 Hz, ^3J (^{1}H-^{1}H) = 8.6 Hz, ^4J (^{1}H-^{19}F) = 8.6 Hz, 1H, phenyl CH *ortho* to NCO and F), 7.51 (ddd, ^3J (^{1}H-^{1}H) = 7.3 Hz, ^3J (^{1}H-^{1}H) = 5.8 Hz, ^4J (^{1}H-^{1}H) = 1.7 Hz, 1H, pyridyl CH *para* to amide), 6.86 (m, 2H, CH *ortho* to F groups and CH *ortho* and *para* to F), 1.45 (s, 15H, 5 × CH$_3$). ^{13}C{^{1}H} NMR (125 MHz, CDCl$_3$, 300 K) 168.4 (NCO), 159.9 (dd, ^1J (^{13}C-^{19}F) = 245.1 Hz , ^4J (^{13}C-^{19}F) = 11.1 Hz, CF), 157.6 (dd, ^1J (^{13}C-^{19}F) = 294.4 Hz , ^4J (^{13}C-^{19}F) = 11.8 Hz, CF), 154.4 (<u>C</u>CON), 149.6 (CH *ortho* to N on pyridyl ring), 138.6 (CH *para* to N on pyridyl ring), 132.2 (dd, ^2J (^{13}C-^{19}F) =13.2 Hz , ^4J (^{13}C-^{19}F) = 3.9 Hz, <u>C</u>NCO), 128.8 (dd, ^3J (^{13}C-^{19}F) = 9.3 Hz , ^3J (^{13}C-^{19}F) = 4.1 Hz, CH *ortho* to NCO), 127.5 (CH *para* to CONR), 126.7 (CH *ortho* to CO and *meta* to N on pyridyl ring), 111.0 (dd, ^2J (^{13}C-^{19}F) =21.5 Hz , ^4J (^{13}C-^{19}F) = 3.5 Hz, CH *meta* to NCO and *para* to F), 103.4 (vt (dd), ^2J (^{13}C-^{19}F) =25.5 Hz , ^2J (^{13}C-^{19}F) =25.5 Hz, CH *ortho* to F groups), 86.6 (5 × <u>C</u>CH$_3$), 8.4 (5 × C<u>C</u>H$_3$).

9.4.4 Synthesis of Ir(η^5-C$_5$(CH$_3$)$_5$)Cl(C$_{12}$H$_9$F$_2$N$_2$O) (4.4)

Pyridine-2-carboxylic acid (2,5-difluoro-phenyl) amide (0.07 g, 0.30 mmol) and [IrCp*Cl$_2$]$_2$ (0.10 g, 0.13 mmol) were dissolved in ethanol (30 ml) and the solution was refluxed for 30 mins. Ammonium hexafluorophosphate (0.10 g, 0.61 mmol) was added and the mixture was refluxed overnight. The resulting yellow solution was evaporated to dryness, redissolved in dichloromethane (50 ml) and washed with water (2 × 10 ml) & brine (10 ml), dried using sodium sulfate and filtered. **4.4** was

recrystallised by dichloromethane/hexane layer diffusion (0.07 g, 0.12 mmol, 47%). ES-MS (CH$_2$Cl$_2$, m/z): 561.1 [M-Cl].

Anal. Found: C: 44.5, H: 3.7, N: 4.6% **Anal. Calculated:** C: 44.3, H: 3.7, N: 4.7%

^{1}H NMR (300 MHz, CDCl$_3$, 300 K) 8.59 (ddd, ^3J (^{1}H-^{1}H) = 5.5 Hz, ^3J (^{1}H-^{1}H) = 1.4 Hz, ^3J (^{1}H-^{1}H) = 0.7 Hz, 1H, pyridyl CH *ortho* to N), 8.19 (ddd, ^3J (^{1}H-^{1}H) = 7.8 Hz, ^4J (^{1}H-^{1}H) = 1.6 Hz, ^5J (^{1}H-^{1}H) = 0.7 Hz, 1H, pyridyl CH *meta* to N, *ortho* to amide), 7.95 (vdt (ddd), ^3J (^{1}H-^{1}H) = 7.7 Hz, ^3J (^{1}H-^{1}H) = 7.7 Hz, ^4J (^{1}H-^{1}H) = 1.4 Hz, 1H, pyridyl CH *para* to N), 7.48-7.58 (m, 2H, pyridyl CH *para* to amide and phenyl CH *ortho* to NCO and F), 7.07 (vtd (ddd), ^3J (^{1}H-^{1}H) = 5.1 Hz, ^3J (^{1}H-^{1}H) = 9.2 Hz, ^4J (^{1}H-^{1}H) = 9.2 Hz, 1H, phenyl CH *meta* to amide), 6.77 − 6.85 (m, 1H, phenyl CH *para* to NCO) 1.46 (s, 15H, 5 × CH$_3$). ^{13}C{^{1}H} NMR (125 MHz, CDCl$_3$, 300 K) 168.2 (NCO), 159.8 (dd, ^1J(^{13}C-^{19}F) = 242.5 Hz, ^4J(^{13}C-^{19}F) = 2.3 Hz, CF *meta* to NCO), 153.4 (dd, ^1J(^{13}C-^{19}F) = 242.4 Hz, ^4J(^{13}C-^{19}F) = 2.9 Hz, CF *ortho* to NCO), 154.4 (<u>C</u>CON), 149.6 (CH *ortho* to N on pyridyl ring), 138.7 (CH *para* to N on pyridyl ring), 137.1 (dd, ^2J(^{13}C-^{19}F) = 15.7 Hz, ^3J(^{13}C-^{19}F) = 11.3 Hz, <u>C</u>NCO), 127.6 (CH *para* to CONR), 126.8 (CH *ortho* to CO and *meta* to N on pyridyl ring), 115.7 (dd, ^2J (^{19}F-^{13}C) = 23.9 Hz, ^3J (^{19}F-^{13}C) = 9.7 Hz, CH *meta* to NCO), 114.9 (dd, ^2J (^{19}F-^{13}C) = 24.7 Hz, ^3J (^{19}F-^{13}C) = 2.9 Hz, CH *ortho* to NCO) 112.1(dd, ^2J (^{19}F-^{13}C) = 24.3 Hz, ^3J (^{19}F-^{13}C) = 7.9 Hz, CH *para* to NCO), 86.7 (5 × <u>C</u>CH$_3$), 8.4 (5 × C<u>C</u>H$_3$).

9.4.5 Synthesis of Ir(η^5-C$_5$(CH$_3$)$_5$)Cl(C$_{12}$H$_8$ClN$_2$O) (4.5)

Pyridine-2-carboxylic acid (2-chloro-phenyl) amide (0.06 g, 0.26 mmol) was added to a stirred suspension of [Ir{η^5-C$_5$(CH$_3$)$_5$}Cl$_2$]$_2$ (0.10 g, 0.13 mmol) and sodium bicarbonate (0.02 g, 0.26 mmol) in methanol (3 ml) in a 10 ml capacity microwave tube. The tube was then sealed and microwave heating was applied at 150 °C for 10 minutes. After effervescence from the solution had subsided, the tube was opened and left to cool. The resulting suspension was filtered, washed with diethyl ether and dried *in vacuo* to yield orange crystals of **4.5** (0.10 g, 0.17 mmol, 65 %). ES-MS (CH$_2$Cl$_2$, m/z): 559.1 [M-Cl].

Anal. Found: C: 44.2, H: 4.1, N: 4.6, Cl: 11.5% **Anal. Calculated:** C: 44.4, H:

3.9, N: 4.7, Cl 11.9%.

^{1}H NMR (300 MHz, CDCl$_3$, 300 K) 8.58 (ddd, ^3J (^{1}H-^{1}H) = 5.5 Hz, ^4J (^{1}H-^{1}H) = 1.4 Hz, ^5J (^{1}H-^{1}H) = 0.7 Hz, 1H, pyridyl CH *ortho* to N), 8.21 (ddd, ^3J (^{1}H-^{1}H) = 7.9 Hz, ^4J (^{1}H-^{1}H) = 1.7 Hz, ^5J (^{1}H-^{1}H) = 0.7 Hz, 1H, pyridyl CH *meta* to N, *ortho* to amide), 7.93 (vtd (ddd), ^3J (^{1}H-^{1}H) = 8.1 Hz, ^3J (^{1}H-^{1}H) = 7.8 Hz, ^4J (^{1}H-^{1}H) = 1.4 Hz, 1H, pyridyl CH *para* to N), 7.84 (dd, ^3J (^{1}H-^{1}H) = 7.9 Hz, ^4J (^{1}H-^{1}H) = 1.7 Hz, 1H, phenyl CH *ortho* to amide), 7.49 (vt (dd), ^3J (^{1}H-^{1}H) = 6.6 Hz, ^3J (^{1}H-^{1}H) = 5.6 Hz, ^4J (^{1}H-^{1}H) = 1.4 Hz, 1H, pyridyl CH *para* to amide), 7.40 (dd, ^3J (^{1}H-^{1}H) = 7.9 Hz, ^4J (^{1}H-^{1}H) = 1.6 Hz, 1H, phenyl CH *ortho* to Cl), 7.23 (masked vtd (ddd), ^3J (^{1}H-^{1}H) = 8.1 Hz, ^3J (^{1}H-^{1}H) = 7.6 Hz, ^4J (^{1}H-^{1}H) = 1.4 Hz, 1H, phenyl CH *para* to Cl), 7.09 (ddd, ^3J (^{1}H-^{1}H) = 8.1 Hz, ^3J (^{1}H-^{1}H) = 7.8 Hz, ^4J (^{1}H-^{1}H) = 1.7 Hz,, 1H, phenyl CH *para* to amide), 1.47 (s, 15H, 5 × CH$_3$). ^{13}C{^{1}H} NMR (125 MHz, CD$_2$Cl$_2$, 300 K) 168.5 (NCO), 155.2 (CCON), 150.4 (CH *ortho* to N on pyridyl ring), 147.2 (CNCO), 139.2 (C *para* to N on pyridyl ring), 132.8 (CCl), 129.5 (CH *ortho* to Cl and *meta* to NCO), 128.7 (CH *ortho* to NCO and *meta* to Cl), 128.0 (CH *para* to CO and *meta* to N on pyridyl ring), 127.9 (CH *para* to Cl), 126.9 (CH *ortho* to CO and *meta* to N on pyridyl ring), 126.3 (CH *para* to NCO), 87.5 (CCH$_3$), 9.0 (CCH$_3$).

9.4.6 Synthesis of Ir(η^5-C$_5$(CH$_3$)$_5$)Cl(C$_{12}$H$_8$ClN$_2$O) (4.6)

Pyridine-2-carboxylic acid (3-chloro-phenyl) amide (0.06 g, 0.26 mmol) was added to a stirred suspension of [Ir{η^5-C$_5$(CH$_3$)$_5$}Cl$_2$]$_2$ (0.10 g, 0.13 mmol) and sodium bicarbonate (0.02 g, 0.26 mmol) in methanol (3 ml) in a 10 ml capacity microwave tube. The tube was then sealed and microwave heating was applied at 150 $^\circ$C for 10 minutes. After effervescence from the solution had subsided, the tube was opened and left to cool. The resulting suspension was filtered, washed with hexane and dried *in vacuo* to yield orange crystals of **4.6** (0.11 g, 0.19 mmol, 71 %). ES-MS (CH$_2$Cl$_2$, m/z): 559.1 [M-Cl].

Anal. Found: C: 44.1, H: 4.3, N: 4.3, Cl: 11.5% **Anal. Calculated:** C: 44.4, H: 3.9, N: 4.7, Cl: 11.9%

^{1}H NMR (300 MHz, CDCl$_3$, 300 K) 8.58 (ddd, J = Hz, 1H, CH of pyridyl *ortho* to N), 8.16 (ddd, 1H, CH of pyridyl *meta* to N, *ortho* to CON), 7.94 (vtd (ddd), 1H, CH of pyridyl *para* to N), 7.73 (vt (dd), 1H, CH *ortho* to NCO and Cl), 7.61 (ddd,

1H, CH of phenyl *para* to NCO), 7.50 (ddd, 1H, CH of pyridyl *meta* to N, *para* to CON), 7.24 (vt (dd), 1H, CH of phenyl *meta* to NCO and Cl), 7.08 (ddd, 1H, CH *para* to Cl), 1.43 (s, 15H, 5 × CH$_3$). ^{13}C{^{1}H} NMR (75 MHz, CDCl$_2$, 300 K) 168.4 (NCO), 155.4 (CCON), 149.6 (CH *ortho* to N on pyridyl ring), 149.4 (CNCO), 138.7 (C *para* to N on pyridyl ring), 133.5 (CCl), 129.0 (CH *meta* to Cl and NCO), 127.5 (CH *para* to CO and *meta* to N on pyridyl ring), 127.3 (CH *ortho* to NCO and Cl), 126.6 (CH *ortho* to CO and *meta* to N on pyridyl ring), 125.3 (CH *ortho* to Cl and *meta* to NCO), 124.3 (CH *para* to Cl), 86.7 (CCH$_3$), 8.5 (CCH$_3$).

9.4.7 Synthesis of Ir(η^5-C$_5$(CH$_3$)$_5$)Cl(C$_{12}$H$_7$Cl$_2$N$_2$O) (4.7)

Pyridine-2-carboxylic acid (2,4-dichloro-phenyl) amide (0.07 g, 0.26 mmol) was added to a stirred suspension of [Ir{η^5-C$_5$(CH$_3$)$_5$}Cl$_2$]$_2$ (0.10 g, 0.13 mmol) and sodium bicarbonate (0.02 g, 0.26 mmol) in methanol (3 ml) in a 10 ml capacity microwave tube. The tube was then sealed and microwave heating was applied at 150 °C for 10 minutes. After effervescence from the solution had subsided, the tube was opened and left to cool. The resulting suspension was filtered, washed with ether and dried *in vacuo* to yield orange crystals of **4.7** (0.11 g, 0.17 mmol, 67 %). ES-MS (CH$_2$Cl$_2$, m/z): 593.1 [M-Cl].

Anal. Found: C: 41.6, H 3.9, N: 4.1, Cl: 16.0% **Anal. Calculated** (with 0.8 molecules of water): C: 41.1, H: 3.7, N: 4.4, Cl: 16.5%.

^{1}H NMR (300 MHz, CDCl$_3$, 300 K) 8.61 (br. d, ^3J (^{1}H-^{1}H) = 5.7 Hz, 1H, pyridyl CH *ortho* to N), 8.24 (br. d, ^3J (^{1}H-^{1}H) = 8.1 Hz, pyridyl CH *meta* to N, *ortho* to amide), 7.98 (vtd, ^3J (^{1}H-^{1}H) = 7.6 Hz, ^4J (^{1}H-^{1}H) = 1.4 Hz, 1H, pyridyl CH *para* to N), 7.86 (br. d, ^3J (^{1}H-^{1}H) = 8.6 Hz, 1H, phenyl CH *ortho* to amide, *meta* to both Cl), 7.54 (ddd, ^3J (^{1}H-^{1}H) = 7.5 Hz, ^3J (^{1}H-^{1}H) = 5.7 Hz, ^4J (^{1}H-^{1}H) = 1.4 Hz,, 1H, pyridyl CH *para* to amide), 7.47 (d, ^4J (^{1}H-^{1}H) = 2.4 Hz, 1H, phenyl CH *ortho* to both Cl), 7.25 (dd, ^3J (^{1}H-^{1}H) = 8.6 Hz, ^4J (^{1}H-^{1}H) = 2.4 Hz, 1H, phenyl CH *meta* to amide, *ortho* and *para* to Cl), 1.49 (s, 15H, 5 × CH$_3$). ^{13}C{^{1}H} NMR (125 MHz, CD$_2$Cl$_2$, 300 K) 168.6 (NCO), 154.9 (CCON), 150.5 (CH *ortho* to N on pyridyl ring), 146.1 (CNCO), 139.3 (C *para* to N on pyridyl ring), 133.6 (CCl *ortho* to NCO), 130.7 (CCl *para* to NCO) 129.7 (CH *ortho* to NCO and *meta* to both Cl), 129.2 (CH *meta* to NCO and *ortho* to both Cls), 128.2 (CH *para* to CO and *meta* to N on pyridyl ring), 127.0 (CH *ortho* to CO and *meta* to N on pyridyl ring), 87.6 (5 ×

C̲CH$_3$), 9.1 (5 × CC̲H$_3$).

9.4.8 Synthesis of Ir(η^5-C$_5$(CH$_3$)$_5$)Cl(C$_{12}$H$_7$Cl$_2$N$_2$O) (4.8)

Pyridine-2-carboxylic acid (2,5-dichloro-phenyl) amide (0.07 g, 0.26 mmol) was added to a stirred suspension of [Ir{η^5-C$_5$(CH$_3$)$_5$}Cl$_2$]$_2$ (0.10 g, 0.13 mmol) and sodium bicarbonate (0.02 g, 0.26 mmol) in methanol (3 ml) in a 10 ml capacity microwave tube. The tube was then sealed and microwave heating was applied at 150 °C for 10 minutes. After effervescence from the solution had subsided, the tube was opened and left to cool. The resulting suspension was filtered, washed with ether and dried *in vacuo* to yield **4.8** as a yellow powder (0.13 g, 0.21 mmol, 82 %). ES-MS (CH$_2$Cl$_2$, m/z): 593.1 [M-Cl].

Anal. Found: C: 41.5, H: 3.4, N: 4.2, Cl: 16.6% **Anal. Calculated:** C: 42.0, H: 3.5, N, 4.5, Cl: 16.9%.

^{1}H NMR (300 MHz, CDCl$_3$, 300 K) 8.58 (ddd, ^3J (^{1}H-^{1}H) = 5.6 Hz, ^4J (^{1}H-^{1}H) = 1.4 Hz, ^5J (^{1}H-^{1}H) = 0.6 Hz, 1H, pyridyl CH *ortho* to N), 8.22 (ddd, ^3J (^{1}H-^{1}H) = 7.8 Hz, ^4J (^{1}H-^{1}H) = 1.6 Hz, ^5J (^{1}H-^{1}H) = 0.6 Hz, 1H, pyridyl CH *meta* to N, *ortho* to amide), 7.95 (vtd, ^3J (^{1}H-^{1}H) = 7.7 Hz, ^3J (^{1}H-^{1}H) = 7.7 Hz, ^4J (^{1}H-^{1}H) = 1.4 Hz, 1H, pyridyl CH *para* to N), 7.89 (br. d, ^4J(^{1}H-^{1}H) = 2.6 Hz, 1H, CH *ortho* to Cl and NCOR), 7.50 (ddd, ^3J (^{1}H-^{1}H) = 6.5 Hz, ^3J (^{1}H-^{1}H) = 5.6 Hz, ^4J (^{1}H-^{1}H) = 1.7 Hz, 1H, pyridyl CH *para* to amide), 7.33 (br. d, ^3J (^{1}H-^{1}H) = 8.5 Hz, 1H, CH *meta* to NCOR) 7.07 (dd, ^3J (^{1}H-^{1}H) = 8.6 Hz, ^4J (^{1}H-^{1}H) = 2.6 Hz, 1H, CH *para* to NCOR), 1.49 (s, 15H, CC̲H$_3$). ^{13}C{^{1}H} NMR (75 MHz, CDCl$_3$, 300 K) 167.8 (NCO), 154.5 (C̲CON), 149.5 (CH *ortho* to N on pyridyl ring), 147.3 (C̲NCO), 138.7 (C *para* to N on pyridyl ring), 132.6 (CCl *meta* to NCO), 130.8 (CCl *ortho* to NCO) 129.8 (CH *meta* to NCOR), 128.5 (CH *ortho* to NCOR), 127.5 (CH *para* to CO and *meta* to N on pyridyl ring), 127.0 (CH *ortho* to CONR), 125.8 (CH *para* to NCOR), 87.0 (5 × C̲CH$_3$), 8.7 (5 × CC̲H$_3$)

9.4.9 Synthesis of Ir(η^5-C$_5$(CH$_3$)$_5$)Cl(C$_{14}$H$_{11}$ClN$_2$O$_2$) (4.9)

Pyridine-2-carboxylic acid (4-acetyl-phenyl) amide (0.06 g, 0.26 mmol) was added to a stirred suspension of [Ir{η^5-C$_5$(CH$_3$)$_5$}Cl$_2$]$_2$ (0.10 g, 0.13 mmol) and sodium bicarbonate (0.02 g, 0.26 mmol) in methanol (3 ml) in a 10 ml capacity microwave tube. The tube was then sealed and microwave heating was applied at

150 °C for 10 minutes. After effervescence from the solution had subsided, the tube was opened and left to cool. The resulting suspension was filtered, washed with hexane and dried *in vacuo* to yield orange crystals of **4.9** (0.11 g, 0.18 mmol, 70 %). ES-MS (CH$_2$Cl$_2$, m/z): 567.2 [M-Cl].

Anal. Found: C: 47.5, H: 4.4, N: 4.4, Cl: 5.9% **Anal. Calculated:** C: 47.9, H: 4.4, N: 4.7, Cl: 5.9%

^{1}H NMR (300 MHz, CDCl$_3$, 300 K) 8.59 (ddd, ^3J (^{1}H-^{1}H) = 5.5 Hz, ^4J (^{1}H-^{1}H) = 1.5 Hz, ^5J (^{1}H-^{1}H) = 0.7 Hz, 1H, pyridyl CH *ortho* to N), 8.17 (ddd, ^3J (^{1}H-^{1}H) = 7.9 Hz, ^4J (^{1}H-^{1}H) = 1.7 Hz, ^5J (^{1}H-^{1}H) = 0.7 Hz, 1H, pyridyl CH *meta* to N, *ortho* to amide), 7.95 (m, 3H, pyridyl CH *ortho* to N and 2 × phenyl CH *meta* to amide), 7.81 (br. d (ddd, ^3J (^{1}H-^{1}H) = 8.6 Hz, 2H, 2 × phenyl CH *ortho* to amide), 7.52 (ddd, ^3J (^{1}H-^{1}H) = 7.4 Hz, ^3J (^{1}H-^{1}H) = 5.5 Hz, ^4J (^{1}H-^{1}H) = 1.2 Hz, 1H, pyridyl CH *para* to amide), 2.61 (s, 3H, C$\underline{H}_3$CO), 1.42 (s, 15H, 5 × CH$_3$). ^{13}C{^{1}H} NMR (75 MHz, CDCl$_3$, 300 K) 197.6 ($\underline{C}$OCH$_3$), 168.4 (NCO), 155.0 ($\underline{C}$CON), 153.2 ($\underline{C}$NCO), 149.7 (CH *ortho* to N on pyridyl ring), 138.7 (C *para* to N on pyridyl ring), 132.9 ($\underline{C}$COCH$_3$), 128.5 (2 × CH *ortho* to COCH$_3$) 127.6 (CH *para* to CO and *meta* to N on pyridyl ring), 127.0 (2 × CH *meta* to COCH$_3$), 126.4 (CH *ortho* to CO and *meta* to N on pyridyl ring), 86.6 (5 × $\underline{C}$CH$_3$), 8.4 (5 × C$\underline{C}$H$_3$).

9.4.10 Synthesis of Ir(η^5-C$_5$(CH$_3$)$_5$)Cl(C$_{12}$H$_{10}$N$_3$O$_3$) (4.10)

Pyridine-2-carboxylic acid (4-nitro-phenyl) amide (0.03g, 0.12 mmol) was added to a stirred suspension of [Ir{η^5-C$_5$(CH$_3$)$_5$}Cl$_2$]$_2$ (0.05 g, 0.06 mmol) in ethanol (30 ml) at 60 °C. After 15 minutes. Ammonium hexafluorophosphate (0.04 g, 0.25 mmol) was added and the mixture was stirred at 80 °C for 15 hours. The resulting mixture was refluxed for 17 hours and filtered. The solvent was removed from the filtrate and the resulting residue recrystallised from hot methanol to give **4.10** as orange crystals suitable for X-ray crystallography (0.05 g, 0.08 mmol, 66 %). ES-MS (CH$_2$Cl$_2$, m/z): 570.1 [M-Cl].

Anal. Found: C: 43.3, H: 4.2, N: 6.5, Cl: 5.1% **Anal. Calculated** (with 1 molecule of methanol)**:** C: 43.4, H: 4.3, N: 6.6, Cl: 5.6%.

^{1}H NMR (300 MHz, CDCl$_3$, 300 K) 8.61 (br. d, ^3J (^{1}H-^{1}H) = 5.3 Hz, 1H, pyridyl CH *ortho* to N), 8.21 (d, ^3J (^{1}H-^{1}H) = 8.9 Hz, 1H, pyridyl CH *meta* to N, *ortho* to amide), 8.16 – 8.24 (m, 2H, 2 × CH *ortho* to NO$_2$), 7.90 – 8.01 (m, 1H, pyridyl CH

para to N), 7.93 (d, ^3J (^{1}H-^{1}H) = 9.0 Hz, 2H, 2 × CH *meta* to NO$_2$), 7.56 (vbr. t (dd) 1H, pyridyl CH *para* to amide), 1.41 (s, 15H, 5 × CH$_3$). ^{13}C{^{1}H} NMR (75 MHz, CDCl$_3$, 300 K) 168.5 (NCO), 155.0 (CCON or CNCO), 154.7 (CCON or CNCO), 149.9 (CH *ortho* to N on pyridyl ring), 143.7 (CNO$_2$), 138.9 (CH *para* to N on pyridyl ring), 127.9 (2 × CH *meta* to NO$_2$), 127.5 (2 × CH *meta* to NO$_2$) 126.7 (2 × CH *ortho* to NO$_2$), 123.9 (CH *ortho* to CON on pyridyl ring), 86.8 (5 × CCH$_3$), 8.5 (5 × CCH$_3$).

9.4.11 Synthesis of Ir(η^5-C$_5$(CH$_3$)$_5$)Cl(C$_{13}$H$_{13}$N$_2$O$_2$) (4.11)

Pyridine-2-carboxylic acid (2-methoxy-phenyl) amide (0.06 g, 0.26 mmol) was added to a stirred suspension of [Ir{η^5-C$_5$(CH$_3$)$_5$}Cl$_2$]$_2$ (0.10 g, 0.13 mmol) in ethanol (30 ml) at 80 °C. After 15 minutes. Ammonium hexafluorophosphate (0.10 g, 0.61 mmol) was added and the mixture was stirred at 80 °C for 20 hours. The suspension was filtered and the powder dissolved in dichloromethane (50 ml), washed with water (2 × 20 ml), brine (20 ml), dried over sodium sulfate and evaporated to form an orange solid. The crude product was recrystallised using vapour diffusion (dichloromethane/pentane solvent system) to give **4.11** as orange crystals (0.71 g, 0.12 mmol, 48 %). ES-MS (CH$_2$Cl$_2$, m/z): 555.2 [M-Cl].

Anal. Found: C: 45.5, H: 4.6, N: 4.4, Cl: 6.1% **Anal. Calculated** (with 1 molecule of H$_2$O)**:** C: 45.4, H: 4.6, N: 4.6, Cl: 5.8%

^{1}H NMR (300 MHz, CDCl$_3$, 300 K) 8.56(ddd, ^3J(^{1}H-^{1}H) = 5.5 Hz, ^4J(^{1}H-^{1}H) = 1.5 Hz, ^5J(^{1}H-^{1}H) = 0.8 Hz, 1H, pyridyl CH *ortho* to N), 8.17 (ddd, ^3J (^{1}H-^{1}H = 7.8 Hz, ^4J (^{1}H-^{1}H) = 1.5 Hz, ^5J (^{1}H-^{1}H) = 0.8 Hz, 1H, pyridyl CH *meta* to N, *ortho* to amide), 7.90 (vtd (ddd), ^3J (^{1}H-^{1}H) = 7.7 Hz, ^4J (^{1}H-^{1}H) = 1.5 Hz, 1H, pyridyl CH *para* to N), 7.66 (dd, ^3J (^{1}H-^{1}H) = 7.6 Hz, ^3J (^{1}H-^{1}H) = 1.7 Hz, 1H, phenyl CH *ortho* to amide), 7.46 (ddd, ^3J (^{1}H-^{1}H) = 7.4 Hz, ^3J (^{1}H-^{1}H) = 5.6 Hz, ^4J (^{1}H-^{1}H) = 1.7 Hz, 1H, pyridyl CH *para* to amide), 7.11 (ddd, ^3J (^{1}H-^{1}H) = 8.1 Hz, ^3J (^{1}H-^{1}H) = 7.4 Hz, ^4J (^{1}H-^{1}H) = 1.8 Hz, 1H, phenyl CH *para* to amide), 6.94 (dd, ^3J (^{1}H-^{1}H) = 8.3 Hz, ^4J (^{1}H-^{1}H) = 1.3 Hz, 1H, phenyl CH *ortho* to OMe and *para* to NCO), 6.92 (vtd (ddd), ^3J (^{1}H-^{1}H) = 7.4 Hz, ^3J (^{1}H-^{1}H) = 7.4 Hz, ^4J (^{1}H-^{1}H) = 1.5 Hz, 1H, phenyl CH *para* to OMe), 3.87 (s, 3H, OCH$_3$), 1.42 (s, 15H, 5 × CH$_3$). ^{13}C{^{1}H} NMR (75 MHz, CD$_2$Cl$_2$, 300 K) 168.0 (NCO), 155.6 (CCON or COMe), 154.9 (CCON or COMe), 149.5 (CH *ortho* to N on pyridyl ring), 138.3 (CH *para* to N on pyridyl ring), 137.6

(<u>C</u>NCO), 127.4 (CH *ortho* to NCO), 127.0 (CH *para* to CO on pyridyl ring), 126.8 (CH *ortho* to CON on pyridyl ring), 125.8 (CH *para* to NCO), 120.9 (CH *para* to OMe), 110.8 (CH *ortho* to OMe), 86.6 (<u>C</u>CH$_3$), 55.5 (O<u>C</u>H$_3$), 8.4 (C<u>C</u>H$_3$).

9.4.12 Synthesis of Ir(η^5-C$_5$(CH$_3$)$_5$)Cl(C$_{12}$H$_{10}$N$_3$O$_3$) (4.12)

Pyridine-2-carboxylic acid (2-methoxy-4-nitro-phenyl) amide (0.07g, 0.26 mmol) was added to a stirred suspension of [Ir{η^5-C$_5$(CH$_3$)$_5$}Cl$_2$]$_2$ (0.10 g, 0.13 mmol) in ethanol (30 ml) at 80 °C. After 15 minutes. Ammonium hexafluorophosphate (0.10 g, 0.61 mmol) was added and the mixture was stirred at 80 °C for 73 hours. The solvent was evaporated and the residue dissolved in dichloromethane (50 ml), washed with water (2 × 20 ml), brine (20 ml), dried over sodium sulfate and evaporated to form an orange solid. The crude product was recrystallised from hot methanol and washed with hexane to give major and minor isomers of **4.12** as yellow crystals (0.09 g, 0.15 mmol, 56 %). ES-MS (CH$_2$Cl$_2$, m/z): 600.1 [M-Cl].

Anal. Found: C: 44.2, H: 4.3, N: 6.7% **Anal. Calculated** (with 1 molecule of methanol and 0.1 molecules of hexane)**:** C: 43.7, H: 4.5, N: 6.2%.

Major ^{1}H NMR (300 MHz, CDCl$_3$, 300 K) 8.58 (br. d, ^3J (^{1}H-^{1}H) = 5.5 Hz, 1H, pyridyl CH *ortho* to N), 8.16 (br. d, ^3J (^{1}H-^{1}H) = 7.9 Hz, 1H, pyridyl CH *meta* to N, *ortho* to amide), 7.94 (vtd (ddd), ^3J (^{1}H-^{1}H) = 7.7 Hz, ^3J (^{1}H-^{1}H) = 7.6 Hz, ^4J (^{1}H-^{1}H) = 1.4 Hz, 1H, pyridyl CH *para* to N), 7.83-7.89 (m, 3H, 3 × CH on phenyl ring), 7.51 (ddd, ^3J (^{1}H-^{1}H = 7.3 Hz, ^3J (^{1}H-^{1}H) = 5.7 Hz, ^4J (^{1}H-^{1}H) = 1.6 Hz, 1H pyridyl CH *para* to amide), 3.96 (s, 3H, OCH$_3$), 1.43 (s, 15H, 5 × CH$_3$). ^{13}C{^{1}H} NMR (75 MHz, CDCl$_3$) 168.0 (NCO), 155.6 (<u>C</u>CON or <u>C</u>OMe), 154.9 (<u>C</u>CON or <u>C</u>OMe), 149.7 (CH *ortho* to N on pyridyl ring), 138.7 (CH *para* to N on pyridyl ring), 137.6 (<u>C</u>NCO), 127.4 (CH *ortho* to NCO), 127.0 (CH *para* to CO on pyridyl ring) , 126.8 (CH *ortho* to CON on pyridyl ring), 125.8 (CNO$_2$), 120.9 (CH *para* to OMe), 116.8 (CH *ortho* to OMe and NO$_2$), 86.7 (<u>C</u>CH$_3$), 8.5 (C<u>C</u>H$_3$).

Minor ^{1}H NMR (300 MHz, CDCl$_3$, 300 K) 8.58 (br. d, ^3J (^{1}H-^{1}H) = 5.5 Hz, 1H, pyridyl CH *ortho* to N), 8.20 (br. d, ^3J (^{1}H-^{1}H = 7.9 Hz, 1H, pyridyl CH *meta* to N, *ortho* to amide), 7.94 (vtd (ddd), ^3J (^{1}H-^{1}H) = 7.7 Hz, ^3J (^{1}H-^{1}H) = 7.6 Hz, ^4J (^{1}H-^{1}H) = 1.4 Hz, 1H, pyridyl CH *para* to N), 7.86 (vtd (ddd), ^3J (^{1}H-^{1}H) = 7.7 Hz, ^3J (^{1}H-^{1}H) = 6.4 Hz, ^4J (^{1}H-^{1}H) = 1.5 Hz, 1H, CH on phenyl *para* to OMe and NO$_2$), 7.49 (ddd, ^3J (^{1}H-^{1}H) = 5.8 Hz, ^3J (^{1}H-^{1}H) = 4.3 Hz, ^4J (^{1}H-^{1}H) = 1.5 Hz, 1H, pyridyl CH

para to amide), 7.33 (d, ^3J (^{1}H-^{1}H) = 8.6 Hz, 1H, CH on phenyl *ortho* to NCO), 7.06 (dd, ^3J (^{1}H-^{1}H) = 8.5 Hz, ^4J (^{1}H-^{1}H) = 2.5Hz, 1H, CH on phenyl opposite OMe group), 3.96 (s, 3H, OCH$_3$), 1.48 (s, 15H, 5 × CH$_3$). ^{13}C{^{1}H} NMR (75 MHz, CDCl$_3$) 168.0 (NCO), 155.6 (CCON or COMe), 154.9 (CCON or COMe), 149.5 (CH *ortho* to N on pyridyl ring), 138.7 (CH *para* to N on pyridyl ring), 137.6 (CNCO), 129.8 (CH *ortho* to NCO), 127.0 (CH *para* to CO on pyridyl ring) , 127.0 (CH *ortho* to CON on pyridyl ring), 125.8 (CNO$_2$), 120.9 (CH *para* to OMe), 106.3 (CH *ortho* to OMe and NO$_2$), 87.0 (CCH$_3$), 56.1 (OCH$_3$), 8.5 (CCH$_3$).

9.4.13 Synthesis of Ir(η^5-C$_5$(CH$_3$)$_5$)Cl(C$_{12}$H$_{10}$N$_3$O$_3$) (4.13)

Pyridine-2-carboxylic acid (2,4,6-trimethyl-phenyl) amide (0.06 g, 0.26 mmol) was added to a stirred suspension of [Ir{η^5-C$_5$(CH$_3$)$_5$}Cl$_2$]$_2$ (0.10 g, 0.13 mmol) in ethanol (30 ml) at 80 °C. After 15 minutes. Ammonium hexafluorophosphate (0.10 g, 0.61 mmol) was added and the mixture was stirred at 80 °C for 20 hours. The solvent was evaporated and the residue dissolved in dichloromethane (50 ml), washed with water (2 × 20 ml), brine (20 ml), dried over sodium sulfate and evaporated to form an orange solid. The crude product was recrystallised using vapour diffusion (dichloromethane/pentane solvent system) to give **4.13** as orange crystals (0.05 g, 0.83 mmol, 33 %). ES-MS (CH$_2$Cl$_2$, m/z): 567.2 [M-Cl].

Anal. Found: C: 47.4, H: 5.1, N: 4.2, Cl: 6.5% **Anal. Calculated** (with 1 molecule of water and 0.12 molecules of dichloromethane)**:** C: 47.9, H: 5.2, N: 4.5, Cl: 7.0%.

^{1}H NMR (300 MHz, CDCl$_3$, 300 K) 8.53 (br. d, ^3J (^{1}H-^{1}H) = 5.5 Hz, 1H, pyridyl CH *ortho* to N), 8.17 (br. d, ^3J (^{1}H-^{1}H) = 7.8 Hz, 1H, pyridyl CH *meta* to N, *ortho* to amide), 7.91 (vtd (ddd), ^3J (^{1}H-^{1}H) = 7.7 Hz, ^3J (^{1}H-^{1}H) = 7.7 Hz, ^4J (^{1}H-^{1}H) = 1.4 Hz, 1H, pyridyl CH *para* to N), 7.47 (ddd, ^3J (^{1}H-^{1}H) = 7.5 Hz, ^3J (^{1}H-^{1}H) = 5.7 Hz, ^4J (^{1}H-^{1}H) = 1.4 Hz, 1H, pyridyl CH *para* to amide), 6.89 (br. s, 2H, 2 × CH on phenyl ring), 2.30 (s, 3H, CH$_3$ on phenyl ring), 2.28 (s, 3H, CH$_3$ on phenyl ring), 2.05 (s, 3H, CH$_3$ on phenyl ring), 1.42 (s, 15H, 5 × CH$_3$). ^{13}C{^{1}H} NMR (125 MHz, CDCl$_3$) 170.0 (NCO), 155.6 (CCON) 148.8 (CH *ortho* to N on pyridyl ring), 143.0 (CNCO), 138.4 (CH *para* to N on pyridyl ring), 137.5 (CCH$_3$ on phenyl ring), 134.0 (CCH$_3$ on phenyl ring), 133.9 (CCH$_3$ on phenyl ring), 129.3 (CH *meta* to CONR),

128.1 (CH *meta* to CONR), 127.0 (CH *para* to CO on pyridyl ring) 126.7 (CH *ortho* to CON on pyridyl ring), 86.5 (5 × C̲CH$_3$ on Cp* ring), 20.9 (CC̲H$_3$ on phenyl ring), 20.5 (br. s, CC̲H$_3$ on phenyl ring), 19.0 (br. s, CC̲H$_3$ on phenyl ring), 8.4 (CC̲H$_3$ on Cp* ring).

9.4.14 Synthesis of Ir(η^5-C$_5$(CH$_3$)$_5$)I(C$_{13}$H$_{11}$N$_2$O$_2$) (4.14)

Pyridine-2-carboxylic acid (2-methoxy-phenyl) amide (0.06 g, 0.26 mmol) was added to a stirred suspension of [Ir{η^5-C$_5$(CH$_3$)$_5$}I$_2$]$_2$ (0.10 g, 0.09 mmol) and sodium bicarbonate (0.02 g, 0.26 mmol) in methanol (3 ml) in a 10 ml capacity microwave tube. The tube was then sealed and microwave heating was applied at 150 $^{\circ}$C for 10 minutes. After effervescence from the solution had subsided, the tube was opened and left to cool. The resulting suspension was filtered and recrystallised using vapour diffusion (dichloromethane/pentane solvent system) to give **4.14** as orange crystals (0.08 g, 0.12 mmol, 68 %). ES-MS (CH$_2$Cl$_2$, m/z): 683.1 [M-I].

Anal. Found: C: 31.5, H: 3.4, N: 3.0% **Anal. Calculated** (with 1 equivalent of methanol, water, dichloromethane and NaI)**:** C: 31.1, H: 3.6, N: 2.9%.

^{1}H NMR (300 MHz, CDCl$_3$, 300 K) 8.56 (br. d, ^3J (^{1}H-^{1}H) = 5.6 Hz, 1H, pyridyl CH *ortho* to N), 8.10 (br. d, ^3J (^{1}H-^{1}H) = 7.9 Hz, 1H, pyridyl CH *meta* to N and *ortho* to amide), 7.81-7.88 (m, 1H, pyridyl CH *para* to N), 7.84 (d, ^3J (^{1}H-^{1}H) = 7.2 Hz, 1H, phenyl CH *ortho* to amide), 7.41 (ddd, ^3J (^{1}H-^{1}H) = 7.4 Hz, ^3J (^{1}H-^{1}H) = 5.7 Hz, ^4J (^{1}H-^{1}H) = 1.6 Hz, 1H, pyridyl CH *para* to amide), 7.10 (vtd (ddd), ^3J (^{1}H-^{1}H) = 7.7 Hz, ^3J (^{1}H-^{1}H) = 7.7 Hz, ^4J (^{1}H-^{1}H) = 1.7 Hz,1H, phenyl CH *para* to amide), 6.89-6.97 (m, 2H, 2 × phenyl CH *meta* to NCO), 3.85 (s, 3H, OCH$_3$), 1.52 (s, 15H, 5 × CH$_3$). ^{13}C{^{1}H} NMR (75 MHz, CDCl$_3$) 168.7 (NCO), 154.7 (C̲CON or C̲OMe), 154.2 (C̲CON or C̲OMe), 151.3 (CH *ortho* to N on pyridyl ring), 138.3 (CH *para* to N on pyridyl ring or C̲NCO), 138.2 (CH *para* to N on pyridyl ring or C̲NCO), 127.6 (CH *ortho* to NCO), 126.9 (CH *para* to CO on pyridyl ring), 126.7 (CH *ortho* to CON on pyridyl ring), 125.8 (CH *para* to NCO), 120.8 (CH *para* to OMe), 110.9 (CH *ortho* to OMe), 87.5 (5 × C̲CH$_3$), 55.5 (OC̲H$_3$), 9.2 (5 × CC̲H$_3$).

9.4.15 Synthesis of Ir(η^5-C$_5$(CH$_3$)$_4$C$_5$H$_{10}$OH)Cl(C$_{12}$H$_{10}$ClN$_2$O) (4.15)

Triethylamine (0.04 ml, 0.28 mmol) was added.to a solution of [Ir{η^5-C$_5$(CH$_3$)$_4$C$_5$H$_{10}$OH}Cl$_2$]$_2$ (0.10 g, 0.11 mmol) and Pyridine-2-carboxylic acid (3-

chloro-phenyl) amide (0.05 g, 0.22 mmol) in dichloromethane (25 ml). After 19 hours, the resulting yellow solution was washed with water (2×10 ml) and brine (10 ml), dried using sodium sulfate, filtered and the solvent evaporated. **4.15** was recrystallised using vapour diffusion (dichloromethane/pentane solvent system) (0.07 g, 0.10 mmol, 49%). Single crystals suitable for X-ray crystallography were obtained from hot methanol. ES-MS (CH$_2$Cl$_2$, m/z): 631.2 [M-Cl].

Anal. Found: C: 44.4, H: 4.6, N: 3.8% **Anal. Calculated** (with 0.66 molecules of dichloromethane)**:** C: 44.3, H: 4.5, N: 3.9%

^{1}H NMR (300 MHz, CDCl$_3$, 300 K) 8.57 (br. d, ^3J (^{1}H-^{1}H) = 5.5 Hz, 1H, CH of pyridyl *ortho* to N), 8.14 (br. dd, ^3J(^{1}H-^{1}H) = 8.0 Hz, ^4J (^{1}H-^{1}H) = 1.5 Hz, 1H, CH of pyridyl *meta* to N and *ortho* to CON), 7.93 (vtd (ddd), ^3J (^{1}H-^{1}H) = 7.7 Hz, ^4J (^{1}H-^{1}H) = 1.4 Hz, 1H, CH of pyridyl *para* to N), 7.72 (vt (dd), ^4J (^{1}H-^{1}H) = 2.0 Hz, 1H, CH *ortho* to NCO and Cl), 7.61 (ddd, ^3J (^{1}H-^{1}H) = 8.0 Hz, ^4J (^{1}H-^{1}H) = 1.9 Hz, ^4J (^{1}H-^{1}H) = 1.1 Hz, 1H, CH of phenyl *para* to NCO), 7.50 (ddd, ^3J (^{1}H-^{1}H) = 6.6 Hz, ^3J (^{1}H-^{1}H) = 5.6 Hz, ^4J (^{1}H-^{1}H) = 1.7 Hz, 1H, CH of pyridyl *meta* to N and *para* to CON), 7.23 (masked vt (dd), ^3J (^{1}H-^{1}H) = 8.0 Hz, 1H, CH of phenyl *meta* to NCO and Cl), 7.07 (ddd, ^3J (^{1}H-^{1}H) = 8.0 Hz, ^4J (^{1}H-^{1}H) = 2.1 Hz, ^4J (^{1}H-^{1}H) = 1.0 Hz, 1H, CH *para* to Cl), 3.62 (t, ^3J (^{1}H-^{1}H) = 6.3 Hz, 2H, CH$_2$OH), 1.75-1.85 (m, 2H, CH$_2$(CH$_2$)$_4$OH), 1.47-1.62 (m, 2H, CH$_2$CH$_2$OH), 1.47 (s, 3H, CH$_3$), 1.45 (s, 3H, CH$_3$), 1.43 (s, 3H, CH$_3$), 1.40 (s, 3H, CH$_3$), 1.32-1.39 (m, 4H, CH$_2$CH$_2$CH$_2$OH). ^{13}C{^{1}H} NMR (75 MHz, CDCl$_3$, 300 K) 168.4 (NCO), 155.4 (CCON), 149.7 (CH *ortho* to N on pyridyl ring), 149.5 (CNCO), 138.7 (C *para* to N on pyridyl ring), 133.5 (CCl), 129.0 (CH *meta* to Cl and NCO), 127.5 (CH *para* to CO and *meta* to N on pyridyl ring), 127.3 (CH *ortho* to NCO and Cl), 126.6 (CH *ortho* to CO and *meta* to N on pyridyl ring), 125.3 (CH *ortho* to Cl and *meta* to NCO), 124.3 (CH *para* to Cl), 88.1 (quarternary C of functionalised Cp* ring), 87.5 (quarternary C of functionalised Cp* ring), 87.2 (quarternary C of functionalised Cp* ring), 86.8 (quarternary C of functionalised Cp* ring), 86.6 (quarternary C of functionalised Cp* ring), 62.5 (CH$_2$OH), 32.3 (CH$_2$CH$_2$OH), 27.9 (CH$_2$CH$_2$CH$_2$OH), 26.0 (CH$_2$CH$_2$CH$_2$CH$_2$OH), 23.5 (CH$_2$CH$_2$CH$_2$CH$_2$CH$_2$OH), 8.6 (CH$_3$), 8.5 (CH$_3$), 8.5 (CH$_3$), 8.5 (CH$_3$).

9.4.16 Synthesis of Rh(η^5-C$_5$(CH$_3$)$_5$)Cl(C$_{12}$H$_8$ClN$_2$O) (4.16)

Pyridine-2-carboxylic acid (3-chloro-phenyl) amide (0.06 g, 0.26 mmol) and sodium bicarbonate (0.02 g, 0.26 mmol) was added to a stirred suspension of [RhCp*Cl$_2$]$_2$ (0.12 g, 0.13 mmol) in methanol (25 ml). The mixture was heated to reflux for 18 hours. The resulting solution was evaporated to dryness and the crude product recrystallised from hot methanol to give red crystals of **4.16** suitable for X-ray crystallography. The bulk sample was purified using layer diffusion with a dichloromethane/hexane solvent system (0.15 g, 0.30 mmol, 76 %). ES-MS (CH$_2$Cl$_2$, m/z): 469.1 [M-Cl].

Anal. Found: C: 50.8, H: 4.9, N: 4.9% **Anal. Calculated** (with 0.33 molecules of dichloromethane)**:** C: 50.3, H: 4.5, N: 5.3%.

^{1}H NMR (300 MHz, CDCl$_3$, 300 K) 8.63 (br. d, J (^{1}H-^{1}H) = 5.4 Hz, 1H, CH of pyridyl *ortho* to N), 8.16 (br. d, J (^{1}H-^{1}H) = 7.8 Hz, 1H, CH of pyridyl *meta* to N, *ortho* to CON), 7.95 (vtd (ddd), ^3J (^{1}H-^{1}H) = 7.7 Hz, ^3J (^{1}H-^{1}H) = 7.7 Hz, ^4J (^{1}H-^{1}H) = 1.4 Hz, 1H, CH of pyridyl *para* to N), 7.83 (vt (dd), ^4J (^{1}H-^{1}H) = 2.0 Hz, 1H, CH *ortho* to NCO and Cl), 7.72 (ddd, ^3J (^{1}H-^{1}H) = 8.0 Hz, ^4J (^{1}H-^{1}H) = 1.8 Hz, ^4J (^{1}H-^{1}H) = 1.0 Hz, 1H, CH of phenyl *para* to NCO), 7.54 (ddd, ^3J (^{1}H-^{1}H) = 6.5 Hz, ^3J (^{1}H-^{1}H) = 5.6 Hz, ^4J (^{1}H-^{1}H) = 1.6 Hz, 1H, CH of pyridyl *meta* to N, *para* to CON), 7.24 (masked vt (dd), ^3J (^{1}H-^{1}H) = 8.0 Hz, 1H, CH of phenyl *meta* to NCO and Cl), 7.06 (ddd, 1H, ^3J (^{1}H-^{1}H) = 8.0 Hz, ^4J (^{1}H-^{1}H) = 2.1 Hz, ^4J (^{1}H-^{1}H) = 1.1 Hz, CH *para* to Cl), 1.43 (s, 15H, 5 × CH$_3$). ^{13}C{^{1}H} NMR (75 MHz, CDCl$_3$, 300 K) 168.6 (NCO), 156.3 (CCON), 149.7 (CH *ortho* to N on pyridyl ring), 149.6 (CNCO), 138.9 (C *para* to N on pyridyl ring), 133.5 (CCl), 128.9 (CH *meta* to Cl and NCO), 127.4 (CH *para* to CO and *meta* to N on pyridyl ring), 127.1 (CH *ortho* to NCO and Cl), 126.1 (CH *ortho* to CO and *meta* to N on pyridyl ring), 125.5 (CH *ortho* to Cl and *meta* to NCO), 124.0 (CH *para* to Cl), 94.7 (d, ^1J(^{13}C-^{103}Rh) = 8.0 Hz, CCH$_3$), 8.6 (CCH$_3$).

9.4.17 Synthesis of Rh(η^5-C$_5$(CH$_3$)$_5$)Cl(C$_{12}$H$_{10}$N$_3$O$_3$) (4.17)

Pyridine-2-carboxylic acid (4-nitro-phenyl) amide (0.04 g, 0.16 mmol) was added to a stirred suspension of [RhCp*Cl$_2$]$_2$ (0.05 g, 0.08 mmol) in ethanol (25 ml) at 60 °C. After 15 minutes . Ammonium hexafluorophosphate (0.04 g, 0.24 mmol) was added and the mixture was heated to reflux for 15 hours. The solvent was removed

from the filtrate and the resulting residue recrystallised from hot methanol to give **4.17** as red crystals suitable for X-ray crystallography (0.05 g, 0.10 mmol, 60 %). ES-MS (CH$_2$Cl$_2$, m/z): 480.1 [M-Cl].

Anal. Found: C: 47.8, H: 4.3, N: 7.4% **Anal. Calculated**: C: 47.6, H: 4.3, N: 7.4%.

^{1}H NMR (300 MHz, CDCl$_3$, 300 K) 8.61 (d, ^3J (^{1}H-^{1}H) = 5.2 Hz, 1H, pyridyl CH *ortho* to N), 8.22 (d, ^3J (^{1}H-^{1}H) = 9.1 Hz, 1H, pyridyl CH *meta* to N, *ortho* to amide), 8.15-8.34 (m, 1H, 2 × CH *ortho* to NO$_2$), 8.04 (d, ^3J (^{1}H-^{1}H) = 9.0 Hz, 2H, 2 × CH *meta* to NO$_2$), 7.95 – 8.06 (m, 1H, pyridyl CH *para* to N), 7.59 (ddd, , ^3J (^{1}H-^{1}H) = 7.5 Hz, ^3J (^{1}H-^{1}H) = 5.5 Hz, ^4J (^{1}H-^{1}H) = 1.4 Hz, 1H, pyridyl CH *para* to amide), 1.44 (s, 15H, 5 × CH$_3$). ^{13}C{^{1}H} NMR (75 MHz, CDCl$_3$, 300 K) 168.7 (NCO), 155.7 (CCON or CNCO), 155.3 (CCON or CNCO), 149.9 (CH *ortho* to N on pyridyl ring), 143.3 (CNO$_2$), 139.2 (CH *para* to N on pyridyl ring), 127.6 (2 × CH *meta* to NO$_2$), 127.5 (2 × CH *meta* to NO$_2$) 126.3 (2 × CH *ortho* to NO$_2$), 123.8 (CH *ortho* to CON on pyridyl ring), 94.83 (d, ^1J (^{13}C-^{103}Rh) = 8.1 Hz, CCH$_3$), 8.7 (CCH$_3$).

9.4.18 Synthesis of Rh(η^5-C$_5$(CH$_3$)$_4$C$_5$H$_{10}$OH)Cl(C$_{12}$H$_8$ClN$_2$O) (4.18)

Pyridine-2-carboxylic acid (2-chloro-phenyl) amide (0.06g, 0.26 mmol) and sodium bicarbonate (0.02 g, 0.26 mmol) were added to a stirred suspension of [Rh{η^5-C$_5$(CH$_3$)$_4$C$_5$H$_{10}$OH}Cl$_2$]$_2$ (0.10 g, 0.13 mmol) in water (25 ml). The mixture was stirred at 70 °C for 17 hours. The resulting suspension was filtered and the orange powder dried *in vacuo* to give **4.18** (0.13 g, 0.23 mmol, 86 %). ES-MS (CH$_2$Cl$_2$, m/z): 541.1 [M-Cl].

Anal. Found: C: 54.3, H: 5.3, N: 5.0, Cl: 12.4% **Anal. Calculated:** C: 54.1, H: 5.4, N: 4.9, Cl: 12.3%

^{1}H NMR (300 MHz, CDCl$_3$, 300 K) 8.62 (br. d, ^3J (^{1}H-^{1}H) = 5.5 Hz, 1H, pyridyl CH *ortho* to N), 8.19 (br. d, ^3J (^{1}H-^{1}H) = 7.9 Hz, 1H, pyridyl CH *meta* to N, *ortho* to amide), 7.87-7.97 (m, 2H, pyridyl CH *para* to N and phenyl CH *ortho* to amide), 7.52(ddd, ^3J (^{1}H-^{1}H) = 7.3 Hz, ^3J (^{1}H-^{1}H) = 5.6 Hz, ^4J (^{1}H-^{1}H) = 1.6 Hz, 1H, pyridyl CH *para* to amide), 7.41 (dd, ^3J (^{1}H-^{1}H) = 7.9 Hz, ^4J (^{1}H-^{1}H) = 1.4 Hz, 1H, phenyl CH *ortho* to Cl), 7.24 (masked vtd (ddd), ^3J (^{1}H-^{1}H) = 7.8 Hz, ^4J (^{1}H-^{1}H) = 1.4 Hz, 1H, phenyl CH *para* to Cl), 7.08 (vtd (ddd), ^3J (^{1}H-^{1}H) = 7.6 Hz, ^3J (^{1}H-^{1}H) = 7.6

Hz, ^4J (^{1}H-^{1}H) = 1.5 Hz, 1H, phenyl CH *para* to amide), 3.60 (m, 2H, C$\underline{H}_2$OH), 1.85-2.05 (m, 2H, C$\underline{H}_2$(CH$_2$)$_4$OH), 1.45-1.58 (masked m, 2H, C$\underline{H}_2$CH$_2$OH), 1.51 (s, 3H, CH$_3$ *meta* to alkyl chain on aryl ring), 1.49 (s, 3H, CH$_3$ *meta* to alkyl chain on aryl ring), 1.48 (s, 3H, CH$_3$ *ortho* to alkyl chain on aryl ring), 1.45 (s, 3H, CH$_3$ *ortho* to alkyl chain on aryl ring), 1.32-1.39 (m, 4H, C$\underline{H}_2$C$\underline{H}_2$CH$_2$OH). ^{13}C{^{1}H} NMR (75 MHz, CDCl$_3$, 300 K) 165.8 (NCO), 155.6 ($\underline{C}$CON), 149.5 (CH *ortho* to N on pyridyl ring), 146.6 ($\underline{C}$NCO), 138.7 (C *para* to N on pyridyl ring), 132.8 (CCl), 129.2 (CH *ortho* to Cl and *meta* to NCO), 128.3 (CH *ortho* to NCO and *meta* to Cl), 127.4 (CH *para* to Cl), 126.9 (CH *para* to CO and *meta* to N on pyridyl ring), 126.5 (CH *ortho* to CO and *meta* to N on pyridyl ring), 125.6 (CH *para* to NCO), 97.3 (d, ^1J (^{13}C-^{103}Rh) = 8.1 Hz, quaternary C of functionalised Cp* ring), 95.4 (d, ^1J (^{13}C-^{103}Rh) = 8.1 Hz, quaternary C of functionalised Cp* ring), 95.1 (d, ^1J (^{13}C-^{103}Rh) = 8.1 Hz, quaternary C of functionalised Cp* ring), 95.0 (d, ^1J (^{13}C-^{103}Rh) = 8.1 Hz, quaternary C of functionalised Cp* ring), 94.7 (d, ^1J (^{13}C-^{103}Rh) = 8.0 Hz, quaternary C of functionalised Cp* ring), 62.5 (CH$_2$OH), 32.2 (2C, 2 × $\underline{C}$H$_2$CH$_2$OH), 27.9 ($\underline{C}$H$_2$CH$_2$CH$_2$OH), 26.0 ($\underline{C}$H$_2$CH$_2$CH$_2$CH$_2$OH), 23.5 ($\underline{C}$H$_2$CH$_2$CH$_2$CH$_2$CH$_2$OH), 8.9 (CH$_3$), 8.8 (CH$_3$), 8.8 (CH$_3$), 8.7 (CH$_3$).

9.4.19 Synthesis of Rh(η^5-C$_5$(CH$_3$)$_4$C$_5$H$_{10}$OH)Cl(C$_{12}$H$_8$ClN$_2$O) (4.19)

Pyridine-2-carboxylic acid (3-chloro-phenyl) amide (0.06 g, 0.26 mmol) and sodium bicarbonate (0.02 g, 0.26 mmol) were added to a stirred suspension of [Rh{η^5-C$_5$(CH$_3$)$_4$C$_5$H$_{10}$OH}Cl$_2$]$_2$ (0.10 g, 0.13 mmol) in water (25 ml). The mixture was stirred at 80 °C for 18 hours. The resulting suspension was filtered and the orange powder dried *in vacuo* to give **4.19** (0.12 g, 0.21 mmol, 79 %). ES-MS (CH$_2$Cl$_2$, m/z): 541.1 [M-Cl].

Anal. Found: C: 53.3, H: 5.5, N: 4.8, Cl: 12.1% **Anal. Calculated** (with 0.5 molecules of H$_2$O)**:** C: 53.7, H: 5.4, N: 4.6, Cl: 11.8%

^{1}H NMR (300 MHz, CDCl$_3$, 300 K) 8.63 (br. d, ^3J (^{1}H-^{1}H) = 5.7 Hz, 1H, CH of pyridyl *ortho* to N), 8.16 (br. d, ^3J (^{1}H-^{1}H) = 8.0 Hz, 1H, CH of pyridyl *meta* to N and *ortho* to CON), 7.96 (vtd (ddd), ^3J (^{1}H-^{1}H) = 7.7 Hz, ^3J (^{1}H-^{1}H) = 7.7 Hz, ^4J (^{1}H-^{1}H) = 1.4 Hz, 1H, CH of pyridyl *para* to N), 7.84 (vt (dd), ^4J (^{1}H-^{1}H) = 1.9 Hz, ^4J (^{1}H-^{1}H) = 1.9 Hz, 1H, CH *ortho* to NCO and Cl), 7.72 (br. d, ^3J (^{1}H-^{1}H) = 8.1 Hz, 1H, CH of phenyl *para* to NCO), 7.53 (ddd, ^3J (^{1}H-^{1}H) = 9.5 Hz, ^3J (^{1}H-^{1}H) = 5.7

Hz, ^4J (^{1}H-^{1}H) = 1.4 Hz, 1H, CH of pyridyl *meta* to N, *para* to CON), 7.21 (m, 1H, CH of phenyl *meta* to NCO and Cl), 7.07 (br. d, ^3J (^{1}H-^{1}H) = 7.9 Hz, 1H, CH *para* to Cl), 3.62 (br. s, 2H, CH₂OH), 1.88 (t, ^3J (^{1}H-^{1}H) = 7.0 Hz, 1H, C$\underline{H}_2$(CH₂)₄OH), 1.50-1.60 (br. m, 2H, C$\underline{H}_2$CH₂OH), 1.46 (s, 3H, CH₃ *meta* to alkyl chain on aryl ring), 1.46 (s, 3H, CH₃ *meta* to alkyl chain on aryl ring), 1.45 (s, 3H, CH₃ *ortho* to alkyl chain on aryl ring), 1.41 (s, 3H, CH₃ *ortho* to alkyl chain on aryl ring), 1.33-1.39 (m, 4H, C$\underline{H}_2$C$\underline{H}_2$CH₂OH). ^{13}C{^{1}H} NMR (125 MHz, CD₂Cl₂, 300 K) 167.0 (NCO), 156.2 ($\underline{C}$CON), 150.6 ($\underline{C}$NCO), 150.5 (CH *ortho* to N on pyridyl ring), 139.4 (C *para* to N on pyridyl ring), 133.6 (CCl), 129.4 (CH *meta* to Cl and NCO), 127.7 (CH *para* to CO and *meta* to N on pyridyl ring and CH *ortho* to NCO and Cl), 126.2 (CH *ortho* to CO and *meta* to N on pyridyl ring), 126.2 (CH *para* to NCO), 124.1 (CH *para* to Cl), 97.0 (d, ^1J (^{13}C-^{103}Rh) = 8.4 Hz, quaternary C of functionalised Cp* ring), 95.2-95.7 (m, quarternary C of functionalised Cp* ring), 62.8 (CH₂OH), 32.8 (2C, 2 × $\underline{C}$H₂CH₂OH), 28.2 ($\underline{C}$H₂CH₂CH₂OH), 26.3 ($\underline{C}$H₂CH₂CH₂CH₂OH), 23.9 ($\underline{C}$H₂CH₂CH₂CH₂CH₂OH), 9.1 (CH₃), 9.0 (2 × CH₃), 9.0 (CH₃).

9.5 Iridium Cp* Chloride Bidentate Complexes

9.5.1 Synthesis of Ir(η^5-C₅(CH₃)₅)Cl (C₁₆H₁₀FN₂O) (5.1)

Triethylamine (0.04 ml, 0.26 mmol) was added.to a solution of [IrCp*Cl₂]₂ (0.10 g, 0.13 mmol) and quinoline-2-carboxylic acid (2-fluoro-phenyl) amide (0.07 g, 0.26 mmol) in dichloromethane (25 ml). After 74 hours the solution was reduced and layered with hexane. The resulting solid was filtered and recrystallised using vapour diffusion from a dichloromethane/pentane solvent, to give **5.1** as red crystals suitable for X-ray crystallography (0.09 g, 1.4 mmol, 57%) ES-MS (CH₂Cl₂, m/z): 593.2 [M-Cl].

Anal. Found: C: 49.3, H: 4.0, N: 4.3% **Anal. Calculated**: C: 49.7, H: 4.0, N: 4.5%

^{1}H NMR (300 MHz, CDCl₃, 300 K) 8.60 (br. d, ^3J (^{1}H-^{1}H) = 8.6 Hz, 1H, phenyl CH *peri* to N), 8.30-8.41 (m, 2H, 2 × CH of pyridyl ring), 7.93-8.02 (m, 2H, CH *ortho* to NCOR and *meta* to F, and phenyl CH *ortho* to CH *peri* to N), 7.84-7.90 (m,1H, phenyl CH *para* to CH *peri* to N), 7.71 (ddd), ^{3}J (^{1}H-^{1}H) = 7.5 Hz, ^{3}J (^{1}H-^{1}H) = 6.9 Hz, ^4J (^{1}H-^{1}H) = 1.1 Hz, 1H, phenyl CH *meta* to CH *peri* to N), 7.07-7.17 (m,

3H, $2 \times$ CH meta, and $1 \times$ CH para, to NCO), 1.35 (s, 15H, $5 \times CH_3$). $^{13}C\{^1H\}$ NMR (125 MHz, CDCl$_3$, 300 K) 168.5 (NCO), 158.4 (d, $^1J(^{13}C-^{19}F)$ = 247.3 Hz, CF), 156.2 (CN of pyridyl ring) 145.1 ($\underline{C}$CON), 139.4 (CH of pyridyl ring), 135.7 (d, $^2J(^1H-^1H)$ = 12.6 Hz, $\underline{C}$NCO), 130.7 ($\underline{C}$=CN), 130.6 (CH para to CH peri to N), 130.0 (CH peri to N), 128.6 (CH meta to CH peri to N), 128.6 (CH ortho to CH peri to N), 128.2 (d, $^3J(^{13}C-^{19}F)$ = 3.1 Hz (CH ortho to NCOR), 125.9 (d, $^3J(^{13}C-^{19}F)$ = 8.2 Hz, CH meta to F) 124.4 (d, $^4J(^{13}C-^{19}F)$ = 3.4 Hz, CH para to F) 122.8 (CH of pyridyl ring), 115.2 (d, $^2J(^{13}C-^{19}F)$ = 21.1 Hz, CH ortho to F), 87.1 ($5 \times \underline{C}CH_3$), 8.6 ($5 \times C\underline{C}H_3$).

9.5.2 Synthesis of [Ir(η^5-C$_5$(CH$_3$)$_5$){C$_{13}$H$_{12}$Cl$_2$N$_2$O}Cl] PF$_6$ (5.2)

Pyridine-2-carboxylic acid (2,5-dichloro-phenyl)-methyl amide (0.04 g, 0.13 mmol) was added to a solution of [IrCp*Cl$_2$]$_2$ (0.05 g, 0.07 mmol) in ethanol (25ml) and left to reflux for 15 minutes. Ammonium hexafluorophosphate (0.04 g, 0.26 mmol) was added and the suspension was left to reflux overnight. The resulting suspension was filtered, washed with ether and dried *in vacuo* to give **5.2** as a yellow powder (0.06 g, 0.08 mmol, 60%). Yellow crystals suitable for single crystal X-ray diffraction were obtained using vapour diffusion (dichloromethane/pentane). ES-MS (CH$_2$Cl$_2$, m/z): 643.1 [M-PF$_6$].

Anal. Found: C: 34.8, H: 3.2, N: 3.5% **Anal. Calculated:** C: 35.0, H: 3.2, N: 3.6%

Major product: ^1H NMR (500 MHz, CD$_2$Cl$_2$, 300 K) 8.89-8.92 (m, 1H, pyridyl CH ortho to N), 7.84-7.90 (m, 2H, pyridyl CH para to N and pyridyl CH para to CONR), 7.61 (br. d, $^3J(^1H-^1H)$ = 8.7 Hz, 1H, phenyl CH meta to NMeR), 7.53-7.58 (m, 1H, pyridyl CH ortho to CONR), 7.51 (d, $^4J(^1H-^1H)$ = 2.4 Hz, 1H, phenyl CH ortho to NMeR), 6.89-6.94 (m, 1H, phenyl CH para to NMeR), 3.62 (br. s, 3H, NCH$_3$), 1.76 (br. s, 15H, CCH$_3$). $^{13}C\{^1H\}$ NMR (125 MHz, CD$_2$Cl$_2$) 174.8 (NCO), 153.0 (CH ortho to N on pyridyl ring), 148.1 ($\underline{C}$CON), 140.6 (CH para to N on pyridyl ring), 140.5 (CCl), 136.0 ($\underline{C}$NCO on phenyl ring), 133.4 (CH ortho to CONR on pyridyl ring or CH meta to NMeR), 132.9 (CH ortho to CONR on pyridyl ring or CH meta to NMeR), 131.9 (CH meta to N on pyridyl ring), 130.2 (CCl), 129.6 (CH ortho to NMeR), 128.6 (phenyl CH para to NMeR), 88.2 ($5 \times \underline{C}CH_3$), 41.7 (N$\underline{C}H_3$), 9.5 ($5 \times C\underline{C}H_3$).

Minor product: ^{1}H NMR (500 MHz, CD$_2$Cl$_2$, 300 K) 8.85 (br. d, ^3J(^{1}H-^{1}H) = 5.3 Hz, 1H, pyridyl CH *ortho* to N), 7.82 (vtd (ddd), ^3J (^{1}H-^{1}H) = 8.0 Hz, ^3J (^{1}H-^{1}H) = 8.0 Hz, ^4J (^{1}H-^{1}H) = 1.6 Hz, 1H, pyridyl CH *para* to N), 7.77 (ddd, ^3J (^{1}H-^{1}H) = 6.8 Hz, ^3J (^{1}H-^{1}H) = 5.4 Hz, ^4J (^{1}H-^{1}H) = 1.4 Hz, 1H, pyridyl CH *para* to CONR), 7.75 (br. d, ^4J (^{1}H-^{1}H) = 2.0 Hz, 1H, phenyl CH *ortho* to NMeR), 7.53-7.58 (m, 2H, phenyl CH *para* to NMeR, and pyridyl CH *ortho* to CONR), 6.83 (br. d, ^3J (^{1}H-^{1}H) = 8.1 Hz, 1H, phenyl CH *meta* to NMeR), 3.65 (br. s, 3H, NCH$_3$), 1.75 (br. s, 15H, CCH$_3$). ^{13}C{^{1}H} NMR (125 MHz, CD$_2$Cl$_2$) 173.3 (NCO), 152.7 (CH *ortho* to N on pyridyl ring), 147.7 (CCON), 140.5 (CH *para* to N on pyridyl ring), 140.2 (CCl), 135.9 (CNCO), 133.0 (CH *ortho* to CONR on pyridyl ring or CH *meta* to NMeR), 132.8 (CH *ortho* to CONR on pyridyl ring or CH *meta* to NMeR), 131.5 (CH *meta* to N on pyridyl ring), 131.0 (CCl), 129.8 (CH *ortho* to NMeR), 128.7 (phenyl CH *para* to NMeR), 88.1 (5 × CCH$_3$), 42.3 (NCH$_3$), 9.3 (5 × CCH$_3$).

9.5.3 Synthesis of Ir(η^5-C$_5$(CH$_3$)$_5$){C$_6$H$_6$NO$_2$}Cl (5.3)

Potassium pyridine-2-carboxylate (0.04 g, 0.26 mmol) was added to [IrCp*Cl$_2$]$_2$ (0.1 g, 0.13 mmol) in ethanol (30 ml) and the resulting suspension was stirred at 60 °C for 18 hours. The mixture was filtered and the solid washed with diethyl ether to give **5.3** as a yellow powder (0.08 g, 0.16 mmol, 66%). ES-MS (CH$_2$Cl$_2$, m/z): 450.1 [M-Cl].

Anal. Found: C: 39.5, H: 4.0, N: 2.8, Cl: 7.5% **Anal. Calculated**: C: 39.6, H: 4.0, N: 2.9, Cl: 7.3%

^{1}H NMR (300 MHz, CDCl$_3$, 300 K) 8.57 (ddd, ^3J (^{1}H-^{1}H) = 5.5Hz, 1H, ^4J (^{1}H-^{1}H) = 1.4 Hz, 1H, ^5J (^{1}H-^{1}H) = 0.8 Hz, 1H, CH on pyridyl ring *ortho* to N), 8.15 (ddd, ^3J (^{1}H-^{1}H) = 7.8 Hz, ^4J (^{1}H-^{1}H) = 1.5 Hz, ^5J(^{1}H-^{1}H) = 0.7 Hz, 1H, CH on pyridyl ring *ortho* to COO), 7.96 (vtd (ddd), ^3J (^{1}H-^{1}H) = 7.7 Hz, ^3J (^{1}H-^{1}H) = 7.7 Hz, ^4J (^{1}H-^{1}H) = 1.4 Hz, 1H, CH on pyridyl ring *para* to N), 7.56 (ddd, ^3J (^{1}H-^{1}H) = 6.8 Hz, ^3J (^{1}H-^{1}H) = 4.7 Hz, ^4J (^{1}H-^{1}H) = 1.6 Hz,1H, CH on pyridyl ring *para* to COO), 1.72 (s, 15H, 5 × CH$_3$) ^{13}C{^{1}H} NMR (75 MHz, CDCl$_3$, 300 K) 172.7 (NCO), 151.4 (CCON), 149.1 (CH *ortho* to N on pyridyl ring), 139.1 (C *para* to N on pyridyl ring), 128.5 (CH *para* to CO and *meta* to N on pyridyl ring), 127.7 (CH *ortho* to CO and *meta* to N on pyridyl ring), 85.4 (CCH$_3$), 9.0 (CCH$_3$).

9.5.4 Synthesis of Ir(η^5-C$_5$(CH$_3$)$_5$)Cl(C$_{10}$H$_9$O$_2$) (5.4)

Triethylamine (0.04 ml, 0.26 mmol)) was added to a stirred solution of [IrCp*Cl$_2$]$_2$ (0.10 g, 0.13 mmol) and 1-phenyl-butane-1,3-dione (0.04 g, 0.26 mmol) in dichloromethane (25 ml) and left to stir for 17 hours. The resulting solution was washed with water (2 × 10 ml), brine (10 ml) dried over magnesium sulfate and dried *in vacuo* to give **5.4** as a yellow powder (0.10 g, 0.19 mmol, 76%) Yellow crystals suitable for single crystal X-ray diffraction were obtained using vapour diffusion (dichloromethane/pentane). ES-MS (CH$_2$Cl$_2$, m/z): 489.1 [M-Cl].

Anal. Found: C: 45.7, H: 4.6, Cl: 5.8% **Anal. Calculated**: C: 45.9, H: 4.6, Cl: 6.7%

^{1}H NMR (300 MHz, CDCl$_3$, 300 K) 7.87 (br. d, ^3J (^{1}H-^{1}H) = 7.5 Hz, 1H, 2 × phenyl CH *ortho* to CO), 7.44 (br. t, ^3J (^{1}H-^{1}H) =7.3 Hz, 1H, phenyl CH *para* to CO), 7.34 (vbr. t, ^3J (^{1}H-^{1}H) = 7.5 Hz, 2H, 2 × phenyl CH *meta* to CO), 5.89 (s, 1H, C$\underline{H}$COCH$_3$), 2.08 (s, 3H, C$\underline{H}_3$CO), 1.66 (s, 15H, 5 × CH$_3$). ^{13}C{^{1}H} NMR (75 MHz, CDCl$_3$, 300 K) 186.5 (CO), 177.3 (CO), 138.8 ($\underline{C}$CO on phenyl ring), 130.7 ($\underline{C}$H on phenyl ring *para* to CO), 128.1 (CH on phenyl ring *meta* to CO), 127.1 (2 × CH on phenyl ring *ortho* to CO), 97.1 (CO$\underline{C}$HCO), 83.5 ($\underline{C}$CH$_3$ on Cp*), 28.8 ($\underline{C}$H$_3$CO), 8.7 ($\underline{C}$H$_3$ on Cp*).

9.5.5 Synthesis of Ir(η^5-C$_5$(CH$_3$)$_5$)Cl(C$_{16}$H$_{13}$FNO) (5.5)

Triethylamine (0.04 ml, 0.29 mmol) was added to a solution of [IrCp*Cl$_2$]$_2$ (0.10 g, 0.13 mmol) and 1-(3-fluoro-phenyl)-3-phenylamino-but-2-en-1-one (0.07 g, 0.27 mmol) in dichloromethane (25 ml). After 72 hours the solvent was removed and the crude product recrystallised by dichloromethane/hexane layer diffusion to yield large red crystals suitable for X-ray crystallography (0.06 g, 0.10 mmol, 39%). ES-MS (CH$_2$Cl$_2$, m/z): 582.2 [M-Cl].

Anal. Found: C: 47.3, H: 4.4, N: 2.1% **Anal. Calculated** (with 0.75 molecules of dichloromethane): C: 47.2, H: 4.4, N: 2.1%.

^{1}H NMR (300 MHz, CDCl$_3$, 300 K) 7.67 (ddd, ^3J (^{1}H-^{1}H) = 7.8 Hz, 1.5 Hz 1.1 Hz 1H, CH *para* to F), 7.59 (ddd, ^3J (^{1}H-^{19}F) = 10.5 Hz, ^4J (^{1}H-^{1}H) = 2.7 Hz, 1.6 Hz, 1H, CH *ortho* to F and CO), 7.50 (td (ddd), ^3J (^{1}H-^{1}H) = 7.4 Hz, ^4J (^{1}H-^{1}H) = 1.2 Hz, 2H, 2 × CH *meta* to N), 7.32-7.42 (m, 3H, CH *meta* to CO and 2 × C$\underline{H}$ *ortho* to N), 7.09-7.16 (m, 2H, CH *ortho* to CO and CH *para* to N), 5.51 (br. s, 1H, COC$\underline{H}$CN),

1.70 (br. s, 3H, CH$_3$CN), 1.26 (br. s, 15H, 5 × CH$_3$Cp). ^{13}C{^{1}H} NMR (125 MHz, CDCl$_3$, 300 K) 174.3 (CO), 163.6 (CN on phenyl ring), 163.5 (d, ^1J (^{13}C-^{19}F) = 244.6 Hz, CF), 154.5 (CH$_3$CN), 142.8 (d, ^3J (^{13}C-^{19}F) = 7.3 Hz, CCO on phenyl ring), 130.2 (d, ^3J (^{13}C-^{19}F) = 8.1 Hz, CH *meta* to F), 129.8 (2 × CH on phenyl ring *meta* to N), 128.7 (2 ×CH on phenyl ring *ortho* to N), 126.1 (CH on phenyl ring *para* to N), 122.6 (^4J (^{13}C-^{19}F) = 2.8 Hz, CH *para* to F), 116.5 (^2J (^{13}C-^{19}F) = 21.7 Hz, CH *para* to CO), 113.9 (^2J (^{13}C-^{19}F) = 22.7 Hz, CH *ortho* to F and CO), 97.2 (COCHCN), 86.3 (CCH$_3$ on Cp*), 25.5 (CH$_3$CN), 8.7 (CH$_3$ on Cp*)

9.5.6 Synthesis of Ir(η^5-C$_5$(CH$_3$)$_5$)Cl(C$_{16}$H$_{13}$FNO) (5.6)

Triethylamine (0.04 ml, 0.29 mmol) was added.to a solution of [IrCp*Cl$_2$]$_2$ (0.10 g, 0.13 mmol) and 1-(4-Fluoro-phenyl)-3-phenylamino-but-2-en-1-one (0.07 g, 0.27 mmol) in dichloromethane (25 ml). After 72 hours the solvent was removed and the crude product recrystallised using vapour diffusion (dichloromethane/pentane solvent system) to give **5.6** as orange crystals (0.12 g, 0.19 mmol, 77%). ES-MS (CH$_2$Cl$_2$, m/z): 582.2 [M-Cl].

Anal. Found: C: 49.1, H: 4.5, N: 2.0%. **Anal. Calculated** (with 0.33 molecules of dichloromethane): C: 49.0, H: 4.5, N: 2.2%

^{1}H NMR (500 MHz, CDCl$_3$, 213 K) 7.89 (br. dd, ^3J (^{1}H-^{1}H) = 8.7 Hz, ^4J (^{1}H-^{19}F) = 5.6 Hz, 2H, 2 × CH *meta* to F), 7.68 (br. d, ^3J (^{1}H-^{1}H) = 7.0 Hz, 1H, CH *ortho* to N), 7.35-7.41 (m, 1H, CH *meta* to N), 7.31 (br. t, ^3J (^{1}H-^{1}H) = 6.9 Hz, 1H, CH *meta* to N), 7.09-7.16 (m, 1H, CH *para* to N), 7.02 (t, ^3J (^{1}H-^{1}H) = 8.5 Hz, ^3J (^{1}H-^{19}F) = 8.5 Hz, 2H, CH *ortho* to F), 6.86 (br. d, ^3J (^{1}H-^{1}H) = 6.9 Hz, 1H, CH *ortho* to N), 5.52 (br. s, 1H, COCHCN), 1.71 (br. s, 3H, CH$_3$CN), 1.26 (s, 15H, 5 × CH$_3$Cp). ^{13}C{^{1}H} NMR (125 MHz, CDCl$_3$, 213 K) 168.1 (CO), 163.0 (d, ^1J (^{13}C-^{19}F) = 250.8 Hz, CF), 162.0 (CN), 153.4 (CN), 134.9 (d, ^4J (^{13}C-^{19}F) = 2.4 Hz, CCO on phenyl ring), 129.0 (br. s, CH on phenyl ring *meta* to N), 128.6 (d, ^3J (^{13}C-^{19}F) = 8.5 Hz, 2 × CH *meta* to F), 126.8 (CH on phenyl ring *meta* to N), 126.7 (CH on phenyl ring *ortho* to N), 125.3 (CH on phenyl ring *para* to N), 124.1 (br. s, CH on phenyl ring *ortho* to N)114.7 (d, ^2J (^{13}C-^{19}F) = 20.9 Hz, 2 × CH *ortho* to F), 95.6 (COCHCN), 85.4 (CCH$_3$ on Cp*), 25.9 (CH$_3$CN), 8.4 (CH$_3$ on Cp*)

9.6 Homogeneous Catalysis

9.6.1 General Benzaldehyde Reduction

To the selected complex (0.01 mmol Ir/Rh) in a carousel tube was added potassium *tert*-butoxide (1.00 mg, 0.01 mmol) and propan-2-ol (10 ml). The mixture was stirred at 60°C for one hour, and then benzaldehyde (0.10 ml, 1.0 mmol) was added. The mixture was stirred at 60°C and the reaction was monitored by GC at intervals of 0, 2, 4, and 24h.

9.6.2 General Acetophenone Reduction

To the selected complex (0.01 mmol Ir/Rh) in a carousel tube was added potassium *tert*-butoxide (1.00 mg, 0.01 mmol) and propan-2-ol (10 ml). The mixture was stirred at 60°C for one hour, and then acetophenone (0.12 ml, 1.0 mmol) was added. The mixture was stirred at 60°C and the reaction was monitored by GC at intervals of 0, 2, 4, and 24h.

9.7 Immobilisation

9.7.1 Synthesis of 7.7 (Immobilised 2.6)

Under an anhydrous nitrogen atmosphere, a solution of 2,6-di-tert-butylpyridine (0.39 ml, 1.80 mmol) in dichloromethane (0.83 ml) was added to trifluoromethanesulfonic anhydride (0.15 ml, 0.89 mmol) in dichloromethane (0.91 ml) at -10 °C. A solution of **2.6** (0.17 g, 0.22 mmol) in dichloromethane (1 ml) was slowly added over an hour. After stirring for an hour, the solution was evaporated to dryness to remove excess trifluoromethanesulfonic anhydride, leaving a brown residue containing **7.1**. The residue was redissolved in 1.06 ml dichloromethane and 0.06 ml was transferred to an ampoule and evaporated for an NMR sample to confirm triflation.

^{1}H NMR (300 MHz, CDCl$_3$, 300 K) 4.56 (t, ^3J (^{1}H-^{1}H) = 6.1 Hz, 4H, 2 × CH$_2$OTf), 2.25 (t, ^3J (^{1}H-^{1}H) = 7.0 Hz, 4H, 2 × CH$_2$), 1.90-1.75 (m, 4H, 2 × CH$_2$), 1.71 (br. s, 24H, 8 × CH$_3$), 1.40-1.60 (m, 8H, 4 × CH$_2$).

The resulting solution containing **7.1** was transferred to Wang resin (0.28 g, 0.42 mmol) and agitated. After 22 hours the suspension was filtered and washed with

dichloromethane until the filtrate was colourless. The residue was added to water (10 ml) and the slurry filtered. This was repeated with 1M hydrochloric acid, water and methanol respectively. The resulting dark red resin was repeatedly washed with dichloromethane/propan-2-ol (1:1, 10 ml) at 60°C for 1 hour until no colour was seen in solution, followed by acetone (3 × 10 ml) for 1 hour, filtered and dried overnight in a vacuum oven (0.28 g, 0.77 mmol Rh/g, 0.21 mmol Rh)

9.7.2 Synthesis of 7.8 (Immobilised 2.8)

Under an anhydrous nitrogen atmosphere, a solution of 2,6-di-tert-butylpyridine (0.39 ml, 1.80 mmol) in dichloromethane (0.84 ml) was added to trifluoromethanesulfonic anhydride (0.15 ml, 0.89 mmol) in dichloromethane (0.92 ml) at -10 °C. A solution of **2.8** (0.23 g, 0.23 mmol) in dichloromethane (1 ml) was slowly added over an hour. After stirring for an hour, the solution was evaporated to dryness to remove excess trifluoromethanesulfonic anhydride, leaving a brown residue containing **7.2**. The residue was redissolved in 1.07 ml dichloromethane and 0.07 ml was transferred to an ampoule and re-evaporated for an NMR sample to confirm triflation.

^{1}H NMR (300 MHz, CDCl$_3$, 300 K) 4.54 (t, ^3J (^{1}H-^{1}H) = 6.5 Hz, 4H, 2 × CH$_2$OTf), 2.20 (t, ^3J (^{1}H-^{1}H) = 7.6 Hz, 4H, 2 × CH$_2$), 1.89-1.75 (m, 4H, 2 × CH$_2$), 1.71 (br. s, 12H, 4 × CH$_3$), 1.69 (br. s, 12H, 4 × CH$_3$), 1.35-1.60 (m, 8H, 4 × CH$_2$), 1.20-1.40 (m, 36H, 18 × CH$_2$).

The resulting solution containing **7.2** was transferred to Wang resin (0.14 g, 0.21 mmol) and agitated. After 22 hours the suspension was filtered and washed with dichloromethane until the filtrate was colourless. The residue was added to water (10 ml) and the slurry filtered. This was repeated with 1M hydrochloric acid, water and methanol. The resulting dark red resin was repeatedly washed with dichloromethane/propan-2-ol (1:1, 10 ml) at 60 °C for 1 hour until no colour was seen in solution, followed by acetone (3 × 10 ml) for 1 hour, filtered and dried overnight in a vacuum oven (0.19 g, 0.64 mmol Rh/g, 0.12 mmol Rh)

9.7.3 Synthesis of 7.9 (Immobilised 2.9)

Under an anhydrous nitrogen atmosphere, a solution of 2,6-di-tert-butylpyridine (0.14 ml, 0.07 mmol) in dichloromethane (0.30 ml) was added to

trifluoromethanesulfonic anhydride (0.05 ml, 0.34 mmol) in dichloromethane (0.34 ml) at -10 °C. A solution of **2.10** (0.07 g, 0.08 mmol) in dichloromethane (0.39 ml) was slowly added 30 minutes. After stirring for 1 hour, a small portion was transferred to an ampoule and the solvent was removed to leave a brown residue containing **7.3**.

^{1}H NMR (300 MHz, CDCl$_3$, 300 K) 4.64 (t, ^3J (^{1}H-^{1}H) = 5.2 Hz, 4H, 2 × CH_2OTf), 2.29 (t, ^3J (^{1}H-^{1}H) = 7.3 Hz, 4H, 2 × CH$_2$), 1.85-2.24 (m, 4H, 2 × CH$_2$), 1.73 (br. s, 12H, 4 × CH$_3$), 1.69 (br. s, 12H, 4 × CH$_3$).

The resulting solution of **7.3** was evaporated to dryness to remove excess trifluoromethanesulfonic anhydride, The residue was dissolved in dichloromethane (0.39 ml) and transferred to Wang resin, pre-swelled in dichloromethane (0.10 g, 0.15 mmol) and agitated. After 22 hours the suspension was filtered and washed with dichloromethane until the filtrate was colourless. The residue was added to water (10 ml) and the slurry filtered. This was repeated with 1M hydrochloric acid, water methanol, and the resulting dark red resin was repeatedly washed with propan-2-ol (10 ml) at 60°C for 1 hour until no colour was seen in solution, filtered and dried overnight in a vacuum oven (0.08 g).

9.7.4 Synthesis of 7.10 (Immobilised 2.10 – propan-2-ol wash)

Under an anhydrous nitrogen atmosphere, a solution of 2,6-di-tert-butylpyridine (0.37 ml, 0.17 mmol) in dichloromethane (0.78 ml) was added to trifluoromethanesulfonic anhydride (0.14 ml, 0.86 mmol) in dichloromethane (0.86 ml) at -10 °C. A solution of **2.10** (0.20 g, 0.21 mmol) in dichloromethane (1.0 ml) was slowly added over 30 minutes. After stirring for 1 hour, a small portion was transferred to an ampoule and the solvent was removed to leave a brown residue containing **7.4**.

^{1}H NMR (300 MHz, CDCl$_3$, 300 K) 4.57 (t,^3J (^{1}H-^{1}H) = 6.1 Hz, 4H, 2 × CH_2OTf), 2.15 (t, ^3J (^{1}H-^{1}H) = 7.2 Hz, 4H, 2 × CH$_2$), 1.80-1.96 (m, 4H, 2 × CH$_2$), 1.70 (s, 12H, 4 × CH$_3$), 1.70 (s, 12H, 4 × CH$_3$), 1.45-1.48 (m, 8H, 2 × CH$_2$).

The resulting solution of **7.4** was evaporated to dryness to remove excess trifluoromethanesulfonic anhydride, The residue was dissolved in dichloromethane (1.0 ml) and transferred to Wang resin, pre-swelled in dichloromethane (0.14 g, 0.21 mmol) and agitated. After 22 hours the suspension was filtered and washed with

dichloromethane until the filtrate was colourless. The residue was added to water (10 ml) and the slurry filtered. This was repeated with 1M hydrochloric acid, water methanol, and the resulting dark red resin was repeatedly washed with propan-2-ol (10 ml) at 60°C for 1 hour until no colour was seen in solution, filtered and dried overnight in a vacuum oven (0.19 g, 0.65 mmol Ir/g, 0.12 mmol Ir)

9.7.5 Synthesis of 7.10 (Immobilised 2.10 – 1:1 dichloromethane: propan-2-ol and acetone wash)

Under an anhydrous nitrogen atmosphere, a solution of 2,6-di-tert-butylpyridine (5.28 ml, 24.8 mmol) in dichloromethane (11.22 ml) was added to trifluoromethanesulfonic anhydride (2.07 ml, 12.3 mmol) in dichloromethane (12.25 ml) at -10 °C. A solution of **2.10** (2.90 g, 3.08 mmol) in dichloromethane (14.50 ml) was slowly added over an hour. After stirring for 2 hours, 0.69 ml of the solution was transferred to an ampoule and the solvent was removed to leave a brown residue containing **7.4** (see above for NMR)

The resulting solution of **7.4** was evaporated to dryness to remove excess trifluoromethanesulfonic anhydride, The residue was dissolved in dichloromethane (15 ml) and transferred to Wang resin (4.0 g, 6.0 mmol) and agitated. After 22 hours the suspension was filtered and washed with dichloromethane until the filtrate was colourless. The residue was added to water (200 ml) and the slurry filtered. This was repeated with 1M hydrochloric acid, water and methanol. The resulting dark red resin was repeatedly washed with propan-2-ol (200 ml) at 60 °C for 1 hour until no colour was seen in solution, filtered and dried overnight in a vacuum oven (5.9 g). 100 mg of the resulting dark red resin was repeatedly washed with dichloromethane/propan-2-ol (1:1, 10 ml) at 60 °C for 1 hour until no colour was seen in solution, followed by acetone (3 × 10 ml) for 1 hour, filtered and dried overnight in a vacuum oven (0.61 mmol Ir/g).

9.7.6 Synthesis of 7.11 (Immobilised 2.11)

Under an anhydrous nitrogen atmosphere, a solution of 2,6-di-tert-butylpyridine (0.16 ml, 0.07 mmol) in dichloromethane (0.34 ml) was added to trifluoromethanesulfonic anhydride (0.06 ml, 0.37 mmol) in dichloromethane (0.37 ml) at -10 °C. A solution of **2.10** (0.10 g, 0.09 mmol) in dichloromethane (0.43 ml)

was slowly added over an hour. After stirring for 1 hour, a small portion was transferred to an ampoule and the solvent was removed to leave a brown residue containing **7.5**.

^{1}H NMR (300 MHz, CDCl$_3$, 300 K) 4.54 (t, ^3J (^{1}H-^{1}H) = 6.2 Hz, 4H, 2 × CH_2OTf), 2.11 (t, ^3J (^{1}H-^{1}H) = 7.5 Hz, 4H, 2 × CH$_2$), 1.89-1.76 (m, 4H, 2 × CH$_2$), 1.72 (br. s, 12H, 4 × CH$_3$), 1.71 (br. s, 12H, 4 × CH$_3$) 1.35-1.50 (m, 8H, 4 × CH$_2$), 1.30 (br. s, 16H, 8 × CH$_2$).

The resulting solution of **7.5** was evaporated to dryness to remove excess trifluoromethanesulfonic anhydride, The residue was dissolved in dichloromethane (1.0 ml) and transferred to Wang resin, pre-swelled in dichloromethane (0.06 g, 0.09 mmol) and agitated. After 22 hours the suspension was filtered and washed with dichloromethane until the filtrate was colourless. The residue was added to water (10 ml) and the slurry filtered. This was repeated with 1M hydrochloric acid, water methanol, and the resulting dark red resin was repeatedly washed with propan-2-ol (10 ml) at 60 °C for 1 hour until no colour was seen in solution, filtered and dried overnight in a vacuum oven (0.07 g).

9.7.7 Synthesis of 7.12 (Immobilised 2.12)

Under an anhydrous nitrogen atmosphere, a solution of ditertiarybutylpyridine (5.28 ml, 24.8 mmol) in dichloromethane (11.22 ml) was added to trifluoromethanesulfonic anhydride (2.07 ml, 12.3 mmol) in dichloromethane (12.25 ml) at -10 °C. A solution of **2.12** (3.81 g, 3.19 mmol) in dichloromethane (14.5 ml) was slowly added over an hour. After stirring for an hour, the solution was evaporated to dryness to remove excess trifluoromethanesulfonic anhydride, leaving a brown residue containing **7.6**. The residue was redissolved in 14.5 ml dichloromethane and 0.24 ml was transferred to an ampoule and re-evaporated for an NMR sample to confirm triflation.

^{1}H NMR (300 MHz, CDCl$_3$, 300 K) 4.52 (t, ^3J (^{1}H-^{1}H) = 6.4 Hz, 4H, 2 × CH_2OTf), 2.26 (t, ^3J (^{1}H-^{1}H) = 7.5 Hz, 4H, 2 × CH$_2$), 1.86-1.75 (m, 4H, 2 × CH$_2$), 1.69 (s, 12H, 4 × CH$_3$), 1.68 (s, 12H, 4 × CH$_3$)1.35-1.50 (m, 8H, 4 × CH$_2$), 1.24 (br. s, 36H, 18 × CH$_2$).

The resulting solution containing **7.6** was transferred to Wang resin (4.0 g, 6.0 mmol) and agitated. After 22 hours the suspension was filtered and washed with

dichloromethane until the filtrate was colourless. The residue was added to water (200 ml) and the slurry filtered. This was repeated with 1M hydrochloric acid, water and methanol. The resulting dark red resin was repeatedly washed with propan-2-ol (200 ml) at 60 °C for 1 hour until no colour was seen in solution, filtered and dried overnight in a vacuum oven (5.6 g, 0.48 mmol Ir/g, 2.7 mmol Ir). A small portion of the resulting dark red resin was repeatedly washed with dichloromethane/propan-2-ol (1:1, 10 ml) at 60 °C for 1 hour until no colour was seen in solution, followed by acetone (3 × 10 ml) for 1 hour, filtered and dried overnight in a vacuum oven (0.47 mmol Ir/g)

9.7.8 Synthesis of [IrCp*$_2$Cl$_3$]OSO$_2$CF$_3$ (7.13)

AgOTf (0.14 g, 0.55 mmol) was added to [IrCp*Cl$_2$]$_2$ (0.44 g, 0.55 mmol) in dichloromethane (25 ml) and the solution was stirred for 24 hours. The resulting mixture was filtered and the filtrate evaporated to dryness. The crude product was recrystallised by vapour diffusion with a dichloromethane/pentane solvent system to give **7.13** as yellow crystals (0.43 g, 0.47 mmol, 86%)

Anal. Found: C: 27.8, H: 3.3, Cl: 11.5% **Anal. Calculated**: C: 27.7, H: 3.3, Cl: 11.7%

^{1}H NMR (300 MHz, CDCl$_3$, 300 K) 1.70 (CC$\underline{H}_3$). ^{13}C{^{1}H} NMR (75 MHz, CDCl$_3$, 300 K) 120.9 (q, ^1J (^{13}C-^{19}F) = 321.0 Hz,, 88.2 ($\underline{C}$CH$_3$), 9.6 (C$\underline{C}$H$_3$).

^{19}F NMR (300 MHz, CDCl$_3$, 282 MHz, -78.3 (C$\underline{F}_3$)

9.7.9 Reaction of 7.13 with 1M HCl

[IrCp*$_2$Cl$_3$]OTf (0.05 g, 0.05 mmol) was added to 1M HCl (10 ml) and stirred overnight. The resulting suspension was filtered, washed with water, dissolved in dichloromethane (50 ml), dried over sodium sulfate, filtered and the solvent evaporated to give [IrCp*Cl$_2$]$_2$ as an orange powder (0.02 g, 0.03 mmol, 46%).

9.7.10 General catalytic reduction of benzaldehyde/acetophenone with immobilised complexes

To the selected immobilised resin (57.0 mg) in a carousel tube was added potassium *tert*-butoxide (0.50 mg, 0.004 mmol) and propan-2-ol (5 ml). The mixture was stirred at 60 °C for one hour, then the substrate (0.5 mmol) was added. The

mixture was stirred at 60 °C and the reaction was monitored by GC at intervals of 0, 2, 4, 24 and 48h. Further runs were conducted by decanting the solution, and recharging the resin with potassium *tert*-butoxide (0.5 mg, 0.004 mmol), propan-2-ol (5 ml) and benzaldehyde (0.05 ml, 0.5 mmol) immediately.

After 35 runs resin **7.10** was recovered by filtering, washing with dichloromethane and dried using a vacuum oven (35.0 mg, 0.034 mmol Ir).

After eight runs resin **7.12** was filtered from the reaction solution, stirred in 1M HCl/ethanol (10 ml) overnight, and washed with water (10 ml), acetone (10 ml), dichloromethane (10 ml) and dried overnight in the vacuum oven before its ninth run.

9.7.11 Reduction of benzaldehyde by 7.12 in flow

The immobilised complex **7.12** (0.93 g, 0.44 mmol Ir), encased in a HPLC column, was washed with a 1:1 mixture of dichloromethane/propan-2-ol (400 ml) at 60 °C, followed by an acetone wash (150 ml) at room temperature.

Run one

A solution of potassium *tert*-butoxide (39 mg, 0.35 mmol) and benzaldehyde (0.89 ml, 8.70 mmol) was dissolved in propan-2-ol (100 ml) and pumped through the column at 60 °C at a flow rate of 1.45 ml/min for 60 minutes. The eluted solution was poured back into the starting material solution and recycled through the column for 24 hours (98% conversion of benzaldehyde to benzyl alcohol).

Run two

Benzaldehyde (3.56 ml, 34.9 mmol) in propan-2-ol (4.00 L) was pumped through the column over 79 hours, with variable flow rates in the range of 0.49-1.54 ml/min (58% conversion of benzaldehyde to benzyl alcohol). Due to an inconsistent flow rate, all of the reservoir was pumped through the column leaving the catalyst exposed to air. The solution was recycled through the column for a week, but the catalyst was inactive.

9.7.12 Control Reaction One

Under an anhydrous nitrogen atmosphere, a solution of 2,6-di-tert-butylpyridine (0.39 ml, 1.80 mmol) in dichloromethane (0.83 ml) was added to trifluoromethanesulfonic anhydride (0.15 ml, 0.89 mmol) in dichloromethane (0.91

ml) at -10 °C. A solution of [IrCp*Cl$_2$]$_2$ (0.17 g, 0.22 mmol) in dichloromethane (1.00 ml) was slowly added over 30 minutes. After stirring for an hour, the solution was evaporated to dryness to remove excess trifluoromethanesulfonic anhydride. The residue was dissolved in dichloromethane (1.00 ml), and transferred to Wang resin (0.28 g, 0.42 mmol) and agitated. After 22 hours the suspension was filtered and washed with dichloromethane until the filtrate was colourless. The residue was added to water (10 ml) and the slurry filtered. This was repeated with 1M hydrochloric acid, water and methanol respectively. The resulting resin was repeatedly washed with dichloromethane/propan-2-ol (1:1, 10 ml) at 60 °C for 1 hour until no colour was seen in solution, followed by acetone (3 × 10 ml) for 1 hour, filtered and dried overnight in a vacuum oven (0.25g).

9.7.13 Control Reaction Two

Under an anhydrous nitrogen atmosphere, a solution of **2.10** (0.20 g, 0.21 mmol) in dichloromethane (1.0 ml) was slowly added to of 2,6-di-tert-butylpyridine (0.37 ml, 0.17 mmol) in dichloromethane (0.78 ml) at -10 °C. over 30 minutes. After stirring for 1 hour the resulting solution was evaporated to dryness. The residue was dissolved in dichloromethane (1.0 ml) and transferred to Wang resin, pre-swelled in dichloromethane (0.28 g, 0.42 mmol) and agitated. After 22 hours the suspension was filtered and washed with dichloromethane until the filtrate was colourless. The residue was added to water (10 ml) and the slurry filtered. This was repeated with 1M hydrochloric acid, water and methanol respectively. The resulting resin was repeatedly washed with dichloromethane/propan-2-ol (1:1, 10 ml) at 60 °C for 1 hour until no colour was seen in solution, followed by acetone (3 × 10 ml) for 1 hour, filtered and dried overnight in a vacuum oven (0.26 g).

9.7.14 Control Reaction Three

Under an anhydrous nitrogen atmosphere, a solution of 2,6-di-tert-butylpyridine (0.37 ml, 0.17 mmol) in dichloromethane (0.78 ml) was added to **2.10** (0.20 g, 0.21 mmol) in dichloromethane (1.0 ml). The solution was cooled to -10 °C, and trifluoromethanesulfonic anhydride (0.14 ml, 0.86 mmol) in dichloromethane (0.86 ml) was slowly added over 30 minutes. After stirring for 1 hour, the solvent was evaporated and the crude product recrystallised using layer diffusion with a

dichloromethane/hexane solvent system. The resulting brown oily solid was stirred in hexane, and filtered to leave a brown solid (0.19 g). ^{1}H NMR (300 MHz, CDCl$_3$, 300 K) 3.54 (t, ^{3}J (^{1}H-^{1}H) = 6.4 Hz, 4H, 2 × CH$_2$OR), 2.08-2.17 (m, 4H, 2 × CH$_2$), 1.75-1.96 (m, 4H, 2 × CH$_2$), 1.71 (s, 24H, 8 × CH$_3$), 1.45-1.56 (m, 8H, 2 × CH$_2$).

The solid was dissolved in dichloromethane (1 ml) and added to Wang resin (0.28 g, 0.42 mmol) and agitated. After 22 hours the suspension was filtered and washed with dichloromethane until the filtrate was colourless. The residue was added to water (10 ml) and the slurry filtered. This was repeated with 1M hydrochloric acid, water and methanol. The resulting yellow resin was repeatedly washed with dichloromethane/propan-2-ol (1:1, 10 ml) at 60 °C for 1 hour until no colour was seen in solution, followed by acetone (3 × 10 ml) for 1 hour, filtered and dried overnight in a vacuum oven (0.24 g).

9.8 References

(1)   J. Cosier; A. M. Glazer *J. Appl. Crystallogr.* **1986**, *19*, 105-107.
(2)   Z. Otwinowski; W. Minor *Methods Enzymol.* **1997**, *276*, 307-326.
(3)   G. M. Sheldrick; T. R. Schneider *Methods Enzymol.* **1997**, *277*, 319-343.
(4)   A. Altomare; G. Cascarano; C. Giacovazzo; A. Guagliardi *J. Appl. Crystallogr.* **1993**, *26*, 343-350.
(5)   A. Altomare; M. C. Burla; M. Camalli; G. Cascarano; C. Giacovazzo; A. Guagliardi; A. G. G. Moliterni; G. Polidori; R. Spagna *J. Appl. Crystallogr.* **1999**, *32*, 115-119.
(6)   L. J. Barbour, in 'XSeed', **1999**
(7)   M. Thornton-Pett, in 'WC-A Windows CIF Processor', **2000**
(8)   A. L. Spek *J. Appl. Crystallogr.* **2003**, *36*, 7-13.
(9)   A. J. Blacker; S. Brown; B. Clique; B. Gourlay; C. E. Headley; S. Ingham; D. Ritson; T. Screen; M. J. Stirling; D. Taylor; G. Thompson *Org. Process Res. Dev.* **2009**, *13*, 1370-1378.
(10)   J. Blacker; K. Treacher; T. Screen, patent number WO 2009/093059 A2, 2009